Using modeling to assess CO2 sequestration, engineering, environmental and economic issues related to a proposed coal-to-liquids plant in Interior Alaska

Prepared for the U.S. Air Force Office of Scientific Research

Award no. FA9550-11-1-0006

by

Geophysical Institute
University of Alaska Fairbanks

and the

Alaska Center for Energy and Power
University of Alaska

February 2013

To cite this report:

Hanks, C., and Holdmann, G. (Eds.). 2013. Using modeling to assess CO2 sequestration, engineering, environmental and economic issues related to a proposed coal-to-liquids plant in Interior Alaska: Prepared for the U.S. Air Force by the Geophysical Institute and the Alaska Center for Energy and Power, University of Alaska Fairbanks, 222 pp.

For information about this report:

Catherine Hanks, Principal Investigator
Geophysical Institute
University of Alaska Fairbanks
Box 757320
Fairbanks, AK 99775-7320
Phone: (907) 474-5562 Fax: (907) 474-5912
chanks@gi.alaska.edu

Gwen Holdmann, Director
Alaska Center for Energy and Power
University of Alaska
814 Alumni Drive, Box 755910
Fairbanks, AK 99775-5910
Phone: (907) 474-5402 Fax: (907) 474-5475
gwen.holdmann@alaska.edu

Using modeling to assess CO2 sequestration, engineering, environmental and economic issues related to a proposed coal-to-liquids plant in Interior Alaska

Prepared for the U.S. Air Force Office of Scientific Research

Award no. FA9550-11-1-0006

by

Geophysical Institute
University of Alaska Fairbanks

and the

Alaska Center for Energy and Power
University of Alaska

Edited by

Catherine Hanks and Gwen Holdmann

Contributing authors:

Vahid Nourpour Aghbash	**Chang Ki Kim**	**William Schnabel**
Mohabbat Ahmadi	**Edward King**	**Antony Scott**
Amanda Byrd	**Kaveh Madani**	**Brent Sheets**
Nilesh Dixit	**Mousa Maimoun**	**Martin Stuefer**
Rajive Ganguli	**Soroush Mokhtari**	**Stephen Sparrow**
Catherine Hanks	**Art Nash**	**Carla S. Tomsich**
Gwen Holdmann	**Laura Read**	**Dan Walsh**
Daisy Huang	**Carl Schmitt**	**Dennis Witmer**

February 2013

EXECUTIVE SUMMARY

This study used a variety of approaches to augment our understanding of how specific geologic, engineering, environmental and economic factors in Interior Alaska may impact decisions regarding implementation of alternative energy sources available to the community. The specific alternative energy source under investigation, a coal-to-liquids plant proposed for Eielson Air Force base outside of Fairbanks, drove the direction of the detailed studies, but the overall methodology and results are applicable to any isolated community where multiple decision makers are trying to reach a consensus on an alternative energy solution.

Two major environmental concerns related to the proposed CTL plant are CO2 emissions and the creation of ice fog due to water emissions during Interior winter conditions. Hypothetically, there is sufficient capacity to sequester the emitted CO2 by using the CO2 for enhanced oil recovery in known North Slope oil fields or injection in deep coal seams in the nearby Nenana basin. However, while CO2 sequestration using EOR is a known technology, sequestration using this method on the North Slope would require construction of a ~400 mile pipeline. Sequestration in deep coal seams in the Nenana basin is also not a short term solution as this technique is still being developed as a technology, and there is not sufficient known about the Nenana basin that allows identification of where in this basin one could safely inject and store CO2.

Co-firing a CTL plant with locally grown biomass has the potential to reduce CO2 emissions while regrowth of the biomass could sequester the CO2. While small scale biomass power plants that use existing, unmanaged biomass are being developed in Interior Alaska, this study indicates that over 10 million acres would have to be cultivated to compensate for the yearly CO2 emitted by a large coal-fired plant such as the proposed CTL plant.

CO2 emissions and other pollutants from the proposed CTL plant could possibly be reduced by ultra-cleaning the coal and optimizing the gasification technology. Ash levels can be brought down to very low levels if necessary but would require significant effort and additional costs. Using entrained flow gasification would yield a much cleaner product gas with a lower CO2 content, but would gas product would include other pollutants, including mercury and arsenic.

The proposed CTL facility will generate significant additional water vapor, leading to the generation of ice fog during severe winter conditions and related visibility and air quality issues. This project developed an ice fog forecasting tool in order to better predict the impact water vapor emissions from the proposed CTL facility. This tool confirmed that additional water vapor from the proposed CTL plant will lead to additional visibility restrictions due to ice fog during the arctic winter.

This study also evaluated the economics of a proposed CTL facility along with a range of other proposed projects being considered, including several gas pipelines from gas fields on the North Slope or Cook Inlet, a large hydropower project and a HVDC line from the

North Slope. The study first developed a cost analysis of all the projects using the same assumptions for construction costs, etc and then compare the effect of the scale of the project, changing commodity prices, 100% private ownership vs 100% state ownership and implementation time on the overall cost of the produced product. The results indicated that some form of state subsidy would be necessary in order for any project to be economically viable.

These studies highlight that, in order to be implemented, any project will require a consensus between what is economically best, what is technically feasible, and what is socially and politically desirable. This makes the decision-making process potentially complex and contentious. To address this, the project developed a stochastic multi-attribute assessment methodology that first ranked the competing energy projects based only on environmental, economic, political or social criteria. Multicriteria multidecision maker (MCDM) and game theory methods were then used to determine overall project rankings. While these final project rankings did not identify the 'right' project, it did provide insights into the likelihood of the ‘success’ of a particular project in meeting the criteria of the various stakeholders and thus the likelihood that a consensus can be reached regarding which project should move forward.

This study, while focused on one particular community, highlights the complex issues surrounding development of alternative energy resources. A need to satisfy technical, environmental, social, economic and political needs and concerns makes the decision making process complex and often contentious. The stochastic multi-criteria, multi-decision maker analysis developed in this study helps decision makers understand the level of risk associated with individual projects and identifies what conditions may need to change in order for a previously nonviable project to become attractive to a broad cross section of stakeholders.

ACKNOWLEDGMENTS

This project was funded by USAF Office of Scientific Research, award no. FA9550-11-1-0006. We wish to thank our program manager, Dr. Robert Bonneau, for his encouragement and suggestions.

We also gratefully acknowledge the many scientists, companies, federal and state agencies and companies that provided access to data and software during the course of this project, specifically: Douglas Moore and ConocoPhillips for kindly providing seismic data; Kenneth Papp and the Alaska Geological and Geophysical Surveys GMC for sharing well information; Michelle Hayhurst from Platte River Associates for providing BasinMod software; and Usibelli Coal Mine for providing coal samples.

The authors also wish to thank the various faculty, undergraduate and graduate students that contributed to the project, including Mandar Kulkarni, Bernard Coakley, Paul McCarthy and Jeff Benowitz for timely help and suggestions. The project would also like to thank the Hydro-Environmental and Energy Systems Analysis (HEESA) group members at the University of Central Florida who helped with the multicriteria decision making part of this study.

TABLE OF CONTENTS

CHAPTER 1: INTRODUCTION

by Catherine L. Hanks

Providing energy in remote locations is a complex and expensive task. Remote communities and military installations are frequently far from established power grids, requiring local generation of electricity by diesel generators or, in larger, well-established communities, oil, gas or coal-fired power plants. The cost of transporting fossil fuels into these remote communities has a significant impact on the economic health and viability of the community. Finding an alternative, local source of energy is an obvious solution to this problem. However, each community has a unique set of circumstances that constrains the nature of that alternative energy source, how economically viable it is, and the environmental and social impacts it has on the community. Key to finding the right alternative energy resource for each community is understanding the local geographic, geologic and environmental setting and how those variables impact the economic and political viability of the resource. Evaluation of all of these various factors is necessary to determine the most appropriate alternative energy source for a remote location. Multi-criteria, multi-decision maker and game theory models can aid in the decision-making process once viable energy options are identified.

Fairbanks and the other communities in Interior Alaska provide textbook examples of the difficulties and costs associated with providing energy in remote locations. The Fairbanks North Star Borough has a total population of nearly 100,000 (U.S. Census Bureau, 2010) and is home to the University of Alaska, two military bases and several state and federal agencies. Homes and businesses are generally heated with fuel oil; electricity is provided by a coal-fired electric plant located 125 miles to the southwest that is augmented by oil during peak load conditions. Diesel and jet fuel are refined locally at a small refinery using North Slope crude oil tapped from the TransAlaska pipeline.

Fairbanks also serves as a regional hub for outlying communities with populations <500. Many of these small communities are only accessible by air. Electricity in many of these smaller communities is provided by diesel-powered generators, with fuel brought in during the summer months by barges up the Yukon River. Development of local resources in these communities is restricted by a lack of affordable energy.

The reliance of Interior Alaska on oil, a volatile energy resource, was highlighted during the summer of 2008 when the crude oil reached $145/barrel. Homeowners in the Fairbanks area were faced with the possibility of paying $6/gallon for heating fuel. Outlying villages purchasing their annual fuel at this time paid over $10/gallon. Fairbanks community leaders met to explore alternative energy options for Interior Alaska. Because of the abundant availability of local coal, the task force recommended construction of a Fischer-Tropsch coal-to-liquids facility at the nearby Eielson Air Force base. Preliminary engineering analysis suggested that the plant could be economically viable, but failed to address the sequestration options needed for the CO2 that would be emitted.

Prior phases of this study focused on how CO2 could either be reduced or sequestered, and other environmental impacts related to the proposed CTL plant. In the past 2 years, community focus has turned from a coal-to-liquids plant to more conventional options, including accessing stranded North Slope gas either as either natural gas or LNG and development of hydropower resources. However, all of the proposed projects face environmental, economic, social and political obstacles.

This project used a variety of approaches to augment our understanding of how the geology, environmental factors and economics of Interior Alaska constrained the alternative energy available to the community. The results of individual studies were then used as input into a stochastic multi-attribute assessment of energy options for Fairbanks, Alaska. This assessment provides one mechanism that can aid decision-makers in determining which energy alternatives best fulfill the needs and criteria of the community.

This report presents a summary of project findings, organized as follows:

- Geologic CO2 sequestration potential of early Tertiary coal seams of the southern Nenana basin, Interior Alaska (Chapter 2--N.C. Dixit, C. L. Hanks and C.S. Tomsich)

- Modeling and simulation of an Alaska North Slope field to determine actual CO2 storage capacity (Chapter 3--V. Nourpour Aghbash, M. Ahmadi)

- Biomass Production and Carbon Sequestration of Short Rotation Coppice Crops in Alaska (Chapter 4--W. Schnabel, A. Byrd, S. Sparrow)

- Analysis of biomass usage in Alaska (Chapter 5--A. Nash, D. Huang)

- Gasification simulations to study the gasification performance of different ultraclean coal products (Chapter 6--R. Ganguli, D. Walsh)

- Refining a plume model to predict ice fog development associated with a CTL facility (Chapter 7--M. Stuefer, C. K. Kim, and C. Schmitt)

- Energy project options for Fairbanks--a comparative economic analysis (Chapter 8--A. Scott, D. Witmer, E. King and B. Sheets)

- A Stochastic Multi-Attribute Assessment of Energy Options for Fairbanks, Alaska (Chapter 9--L. Read, S. Mokhtari, K. Madani, M. Maimoun, C. Hanks)

CHAPTER 2
GEOLOGIC CO_2 SEQUESTRATION POTENTIAL OF EARLY TERTIARY COALS SEAMS OF THE SOUTHERN NENANA BASIN, INTERIOR ALASKA

by Nilesh C. Dixit, Catherine L. Hanks and Carla S. Tomsich

INTRODUCTION

Carbon dioxide (CO_2) is a primary green house gas emitted from stationary point sources such as coal-fired power plants and coal-to-liquids plant (CTL). The effect of increasing carbon dioxide concentrations from the proposed CTL plant on the Eielson Air Base, near the city of Fairbanks, is a major environmental issue facing residents and businesses in Interior Alaska. Similar to a conventional coal-fired power plant, the CTL plant could release up to 1.5 million metric tons of CO2 per year (Hand et al., 2011). Geologic sequestration of carbon dioxide in deeply buried, unmineable coal seams is one of most promising ways to stabilize these increased levels of greenhouse gas concentrations in the atmosphere due to the relatively high adsorption capacity of coal seams to CO_2. This would have the additional benefit of simultaneous recovery of coal bed methane (CBM).

The Nenana coal province of Interior Alaska has up to 8 billion short tons of identified Tertiary coal resources (Merritt, 1986). Significant volumes of these coal deposits are located in a series of structurally similar, isolated major subbasins of the Nenana coal province (Figure 1; Table 1).

Table 1. Tertiary age coal resources in Interior Alaska- Nenana Coal Province. Estimates are in millions of short tons.

Coalfield	Classification	Estimate	Source of data
Healy Creek	Identified	1,300	Wahrhaftig and others (1994)
Lignite Creek	Identified	4,900	Wahrhaftig and others (1994)
Jarvis Creek	Hypothetical	63	Wahrhaftig and Hickcox (1955)
Wood River	Inferred	241	Barnes (1967)
Rex Creek	Identified	70	Merritt and Hawley (1986)
Tatlanika Creek	Identified	290	Merritt and Hawley (1986)
Nenana Basin	Estimated	120,000	Tomsich et al. (2012)

The most promising area for coal seam sequestration in Nenana coal province are in deep (up to 21000 ft), unmineable coal seams of the Tertiary Usibelli Group and older non-marine clastic rocks of the Nenana Basin. (Kooten et al., 2012; Tomsich et al., 2012). Recent seismic, drilling and outcrop studies in suggest that these coal seams also hold large volumes of coal bed methane, making the Nenana Basin an attractive prospect not only for geologic sequestration of carbon dioxide but also for enhanced coal bed methane recovery (Doyon, 2012).

Nenana Basin is one of the several basins located near the northern foothills of the Central Alaska Range (Figure 2). The basin is an NNW-SSW oriented elongated Tertiary half graben located between the Denali Fault to the south and the Tintina Fault to the north (Figure 2; Johnsson et al., 1993; Ridgway et al., 2007; and Kooten et al., 2012). Non-marine sedimentary

fill of the basin reaches thicknesses in excess of 21000 ft and include recent alluvial and glacial deposits, a synorogenic alluvial fan sequence (Nenana Gravel), a fluvio-lacustrine sequence (Usibelli Group) and early Tertiary non-marine strata (Figure 3; Merritt, 1986; Kooten et al., 2012). Coal bearing sequences mainly occur in the Tertiary Usibelli Group and in early Tertiary clastic rocks located in the deepest part of the basin. Two exploration wells, ARCO Totek Hills #1 (TD: 3590 ft.) and Unocal Nenana # 1 (TD: 3052 ft.), were drilled along the flanks of the basin breaching anticlines whereas Nunivak # 1 well (TD: 11,140 ft) was drilled into the deepest area targeting a horst structure between two major depocenters of the Nenana Basin (Figure 2).

For this report, our research is mainly confined to the southern depocenter of the Nenana Basin (hereafter called as southern Nenana Basin) that has been tested by the only exploration wells drilled in the basin as has the only available seismic data. In the absence of seismic and well data, the thickness and distribution of the coal bearing sediments remain unknown in northern part of the Nenana Basin.

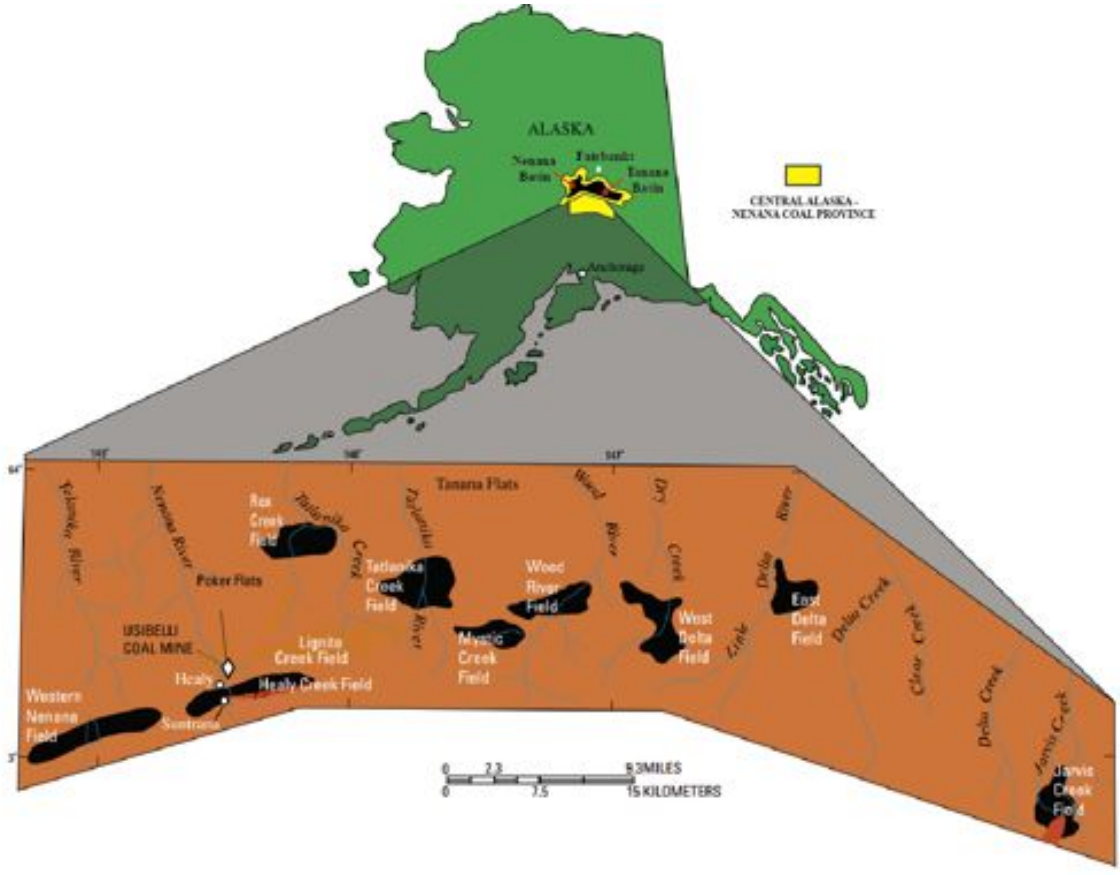

Figure 1. Map showing the major coal-fields in the Nenana coal province, Central Alaska. Nenana coal province is situated in the northern foothills of the Alaska Range and is made up of several coal-bearing synclinal basins (modified from Flores et al., 2004). These coalfields include Healy Creek, Lignite Creek, Jaris Creek, Wood River, Rex Creek, Tatlanika Creek, and Nenana and Tanana basins.

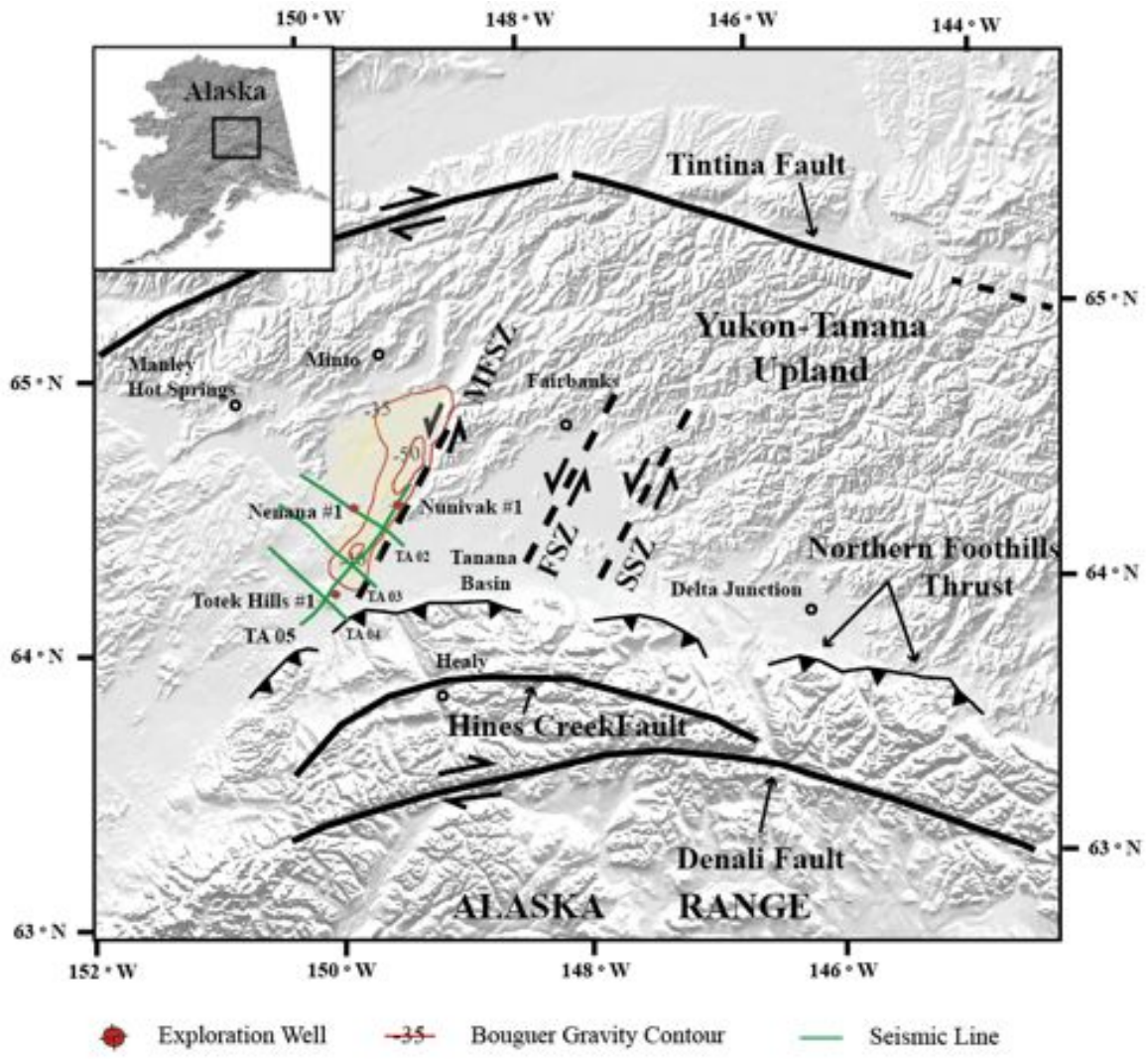

Figure 2. Shaded relief topographic map and tectonic features of Interior Alaska (modified from Riehle et al., 1997). Three north-northeast trending seismic zones, Minto Flats Seismic Zone (MFSZ), Fairbanks Seismic Zone (FSZ) and Salcha Seismic Zone (SSZ), represent deformed crustal blocks rotating clockwise in a major dextral shear zone between the Denali and Tintina fault systems (Ratchkovski and Hansen, 2002). This shear zone causes substantial crustal seismicity in the interior in response to the compressive stresses from plate convergence in southern Alaska. The Nenana Basin (marked in light yellow) is located in north of foothills of Central Alaska Range.

Due to the active seismicity, the Nenana Basin is considered to be tectonically active. However, very little is known about its structural features and subsurface geology. Carbon dioxide storage in such a basin may pose environmental risk, with gas leakage back to the atmosphere along fractures and faults within the basin. A well-constrained structural model for the basin is thus essential in order to identift active basin scale structures (faults and folds), predict fluid flow within the basin, and to examine distribution and volumes of candidate coal seams capable for long term geologic sequestration of carbon dioxide. In this report, 2-D reflection seismic and well data have been used together with potential field data (gravity and magnetic anomaly data) to constrain the basin structure and subsurface distribution of the coal bearing sequences within the southern Nenana basin.

BACKGROUND

Geography of the study area

Most of the study area is covered mainly by a broad, low-land floodplain with an average elevation of 575 ft. Elevation ranges from 400 ft to 2000 ft in the highland areas of the Alaska Range that border southern margin of the subbasin. Non-marine sedimentary fill of the southern Nenana Basin derives sediments from two source terranes: Yukon-Tanana Terrane to the north and north-east and Central Alaska Range to the south. The basement rocks from Lower Paleozoic and Precambrian schist sequence crop out along the George Parks Highway and are exposed, weathered and highly fractured at the surface by erosion of coal-bearing strata around the structural highs.The study area can be accessed along its eastern margin by mile 412 of Alaska Railroad and by George Parks Highway near the town of Nenana. Electricity grid for future power management and Trans Alaska Pipeline System runs near the city of Fairbanks, about 40 miles east of the study area. The Nenana Basin is a current target for natural gas exploration in Interior Alaska.

Tectonic setting of the Nenana Basin

The tectonic framework of Central Alaska is characterized by two continental-scale, dextral strike-slip fault systems: the Denali and Tintina fault systems (Figure 2). The Denali fault system arcs through the Alaska Range and has been active during Quaternary time as evident by 2002 Mw 7.9 Denali earthquake (Matmon et al., 2006). Tintina Fault curves along the southern margin of Yukon Flats basin and connects with the Kaltag fault systems in west-central Alaska. Since Early Tertiary, slip on the Tintina fault system is minimal than that of Denali Fault system (Brogan et al., 1975). Geologic evidence suggests that a zone of distributed dextral shear exists between the two, dextral strike-slip Denali and Tintina fault systems deforming Paleozoic and older basement rocks of the Yukon-Tanana Terrane in a brittle fashion. Presence of active faults and numerous active seismic zones (Minto Flats Seismic Zone, Fairbanks Seismic Zone and Salcha Seismic Zone) across the Denali-Tintina shear zone indicate clockwise rotation of the deformed crustal blocks in this region (Figure 2) (Page et al., 1995).

As the Alaska Range deformation front migrated northward in response to the plate convergence in Early Tertiary, several synclinal non-marine basins were developed in a foreland basin setting along northern foothills of the Alaska Range. Nenana Basin represents one of these synclinal basins and is located within the dextral shear zone between the Denali and Tintina fault systems. Recent geologic studies suggest that the basin is extensional in origin and is superimposed on the deformed crustal blocks of Yukon-Tanana Terrane rotating clockwise in dextral shear zone (Lesh and Ridgway, 2007; Kooten et al., 2012) . Active Minto Flats Seismic Zone runs along the eastern margin of the Nenana Basin (Figure 2). A north-northeast directed, sinistral, strike-slip Minto Fault defines this seismic zone and represents a surface contact between basement schist rocks and Quaternary deposits of the basin with down-to-west motion along fault plane (Ratchkovski and Hansen, 2002). Along southern flank of the basin, a complex system of active thrust faults and fault-related folds exist as a part of northern foothills fold and thrust belt of the Alaska Range. To the north of Denali Fault, the thrust front propagates into the Nenana Basin.

Recent seismicity (1947 Mw 7.2 Minto Flats earthquake) in the Minto Flats Seismic Zone implies that the eastern margin of the Nenana Basin is tectonically active (Ratchkovski and Hansen, 2002). Set of fractures parallel to the Minto Fault confirm an extensional regime with a strike-slip motion across the fault in this area of the basin (Rizzo and Hanks, 2012). Along the southern margin of the basin in Healy area, fracture are oriented perpendicular to the foothills fold and thrust belt of the Alaska Range that indicates active thrusting in the area. South-dipping thrust faults of the northern foothills transfer compressive stresses due to plate convergence into the Nenana Basin and resulting stress-partitioning occurs along the active faults of Minto Flats Seismic Zone.

Further studies by Kooten et al. (2012) imply that the Nenana Basin experienced three phases of tectonic subsidence and two uplift events since Late Cretaceous. Observed angular unconformities and the differential sediment thicknesses in the Nenana Basin support their conclusion (Doyon, 2012). Recent strike-slip faulting and thrusting along the basin margins suggest that the region is characterized by transpressional tectonics driven by shortening in response to the north-northwest directed plate convergence along the Gulf of Alaska.

Generalized stratigraphy

The southern Nenana Basin is filled with Tertiary-age non-marine sedimentary rocks that rest directly on an unconformity marked by an erosional surface of the Precambrian to Paleozoic metamorphic rocks (Merritt, 1986; Frost et al., 2002; Kooten et al., 2012) (Figure 3). The major coal-bearing formation, the Usibelli Group, is up to 3000 m thick and ranges in age from Late Oligocene to Late Miocene (Wahrhaftig, 1987). The Usibelli Group is further subdivided into five different formations--the Healy Creek, Sanctuary, Suntrana, Lignite Creek and Grubstake Formations. These coal bearing rocks are underlain by Late Paleocene lacustrine and fluvial deposits and overlain by Pliocene Nenana Gravel.

Overall, coal-bearing deposits of the southern Nenana Basin are result of the continental fluvial depositional environment, mostly sandy to gravelly braided river systems. Some of the sedimentary successions also reflect lacustrine as well as an alluvial fan and flood-plain deposition (Table 2).

METHODS

The main aim of this study is to develop geophysical models for the southern Nenana Basin that would constrain the basin geometry, fault and fold kinematics and subsurface distribution of candidate coal seams within the basin. Geophysical data used for this study include:

- Borehole data from three exploratory wells (Nunivak # 1, ARCO Totek Hills # 1 and Unocal Nenana # 1). This data consists primarily of well cuttings, sonic and density logs, all archived and publically available at Alaska Geologic Materials Center, Eagle River.
- Four 2-D reflection seismic profiles (TA02, TA03, TA04 and TA05) provided by ConocoPhillips.
- State of Alaska (DNR) Complete Bouguer Anomaly and Total Magnetic Intensity survey maps (Meyer, 2008)
- Local and regional geologic maps (Wahrhaftig, 1970; Athey, 2006; Bemis, 2010)

- Outcrop field data from Nenana coal province (Ridgway et al., 2007; Stanley and Lillis, 2011; Kooten et al., 2012)

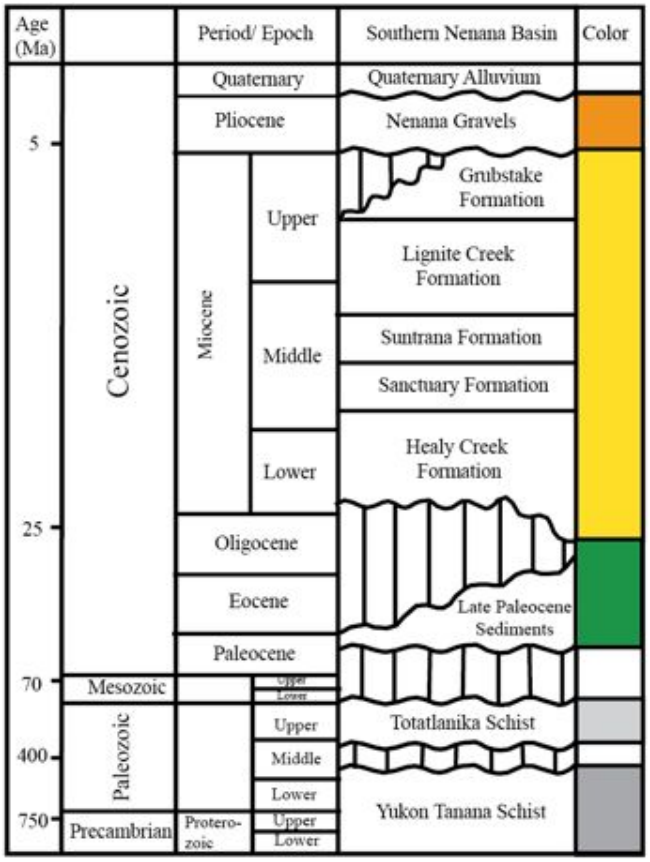

Figure 3. Generalized stratigraphic nomenclature, age and lithology of coal-bearing formations of the Nenana Basin- Nenana Coal Province (modified from Merritt (1986)). Note that along flanks of the basin the Usibelli Group overlies metamorphic rocks of the Yukon –Tanana terrane whereas in the deeper areas of the basin, the Usibelli Group overlies the Late Paleocene sediments.

Geologic basin modeling is necessary to assess the carbon dioxide sequestration potential of the unmineable coal seams of the southern Nenana Basin and how fluids such as water, CO_2 and coal bed methane will behave during and after CO_2 injection. The workflow for building a structural model is hierarchical, given the data is collected at variable scales. We followed the following workflow sequence in this study:

- Evaluated lithostratigraphy of the southern Nenana Basin from borehole data and calculate thicknesses and depths of major coal-bearing formations;
- Established well-to-seismic tie to identify and map coal horizons on depth migrated 2-D seismic profiles;
- Interpreted 2-D seismic data for basin scale structures and simulated the basement profile using interpolation techniques

Basin profiles were constructed using electric logs (such as sonic and density logs) from the existing wells, 2-D reflection seismic, high resolution gravity and magnetic anomaly data collected from the regional surveys and field studies of the local outcrops.

Table 2. Summary of stratigraphy and lithofacies of the Nenana Basin, Interior Alaska. Age data from Ridgway et al. (1999) and Frost et al. (2002). Lithostratigraphy and depositional environment data from Ridgway et al. (2002) and this study. Assigned densities and susceptibilities data from this study.

Period/ Epoch	Formation	Major Lithology	Depositional Environment	Assigned Density (kg/m³)	Assigned Susceptibility (SI x 10^{-03})	Color Code
Quaternary	Surficial Deposits	Unconsolidated gravel, sand, silt and clay	Alluvial fan/ flood-plain/ lacustrine/ swamp	1800-1900	0.02	o o o o - - - - - o o o o
Pliocene to Miocene	Nenana Gravel	Coarse-grained conglomerate and sandstone	Alluvial fan/ braided fluvial systems	2100-2250	0.22	
Miocene to Late Eocene	Grubstake Formation	Laminated mudstone and sandstone	Lacustrine	2300-2450	0.25	
	Lignite Creek Formation	Conglomerate, sandstone, mudstone and coal	High-sinuosity mixed-load fluvial systems			
	Suntrana Formation	Coarse grained sandstone and coal	Distal sandy braided fluvial systems			
	Sanctuary Formation	Laminated mudstone	Lacustrine			
	Healy Creek Formation	Conglomerate, sandstone, mudstone and coal	Proximal, gravelly braided stream systems			
Early Eocene to Late Paleocene	Late Paleocene Sediments	Siltstone, mudstone and coal	Fluvial/lacustrine/swamp/ alluvial fan	2450-2500	0.29	
Early Mississippian-Middle Devonian	Totatlanika Schist	Metavolcaniclastic schist and gneiss with phyllite	-	2550-2620	0.4	
Proterozoic to early Paleozoic	Yukon-Tanana Schist	Greenschist facies sequence with quartzite, phyllite and muscovite	-	2650-2670	0.5	
Paleocene to Late Cretaceous	Plutonic Intrusions	Granitic rocks with diorite, monzonite, syenite and dikes	-	2750-2900	9	+ + + + + + + + +

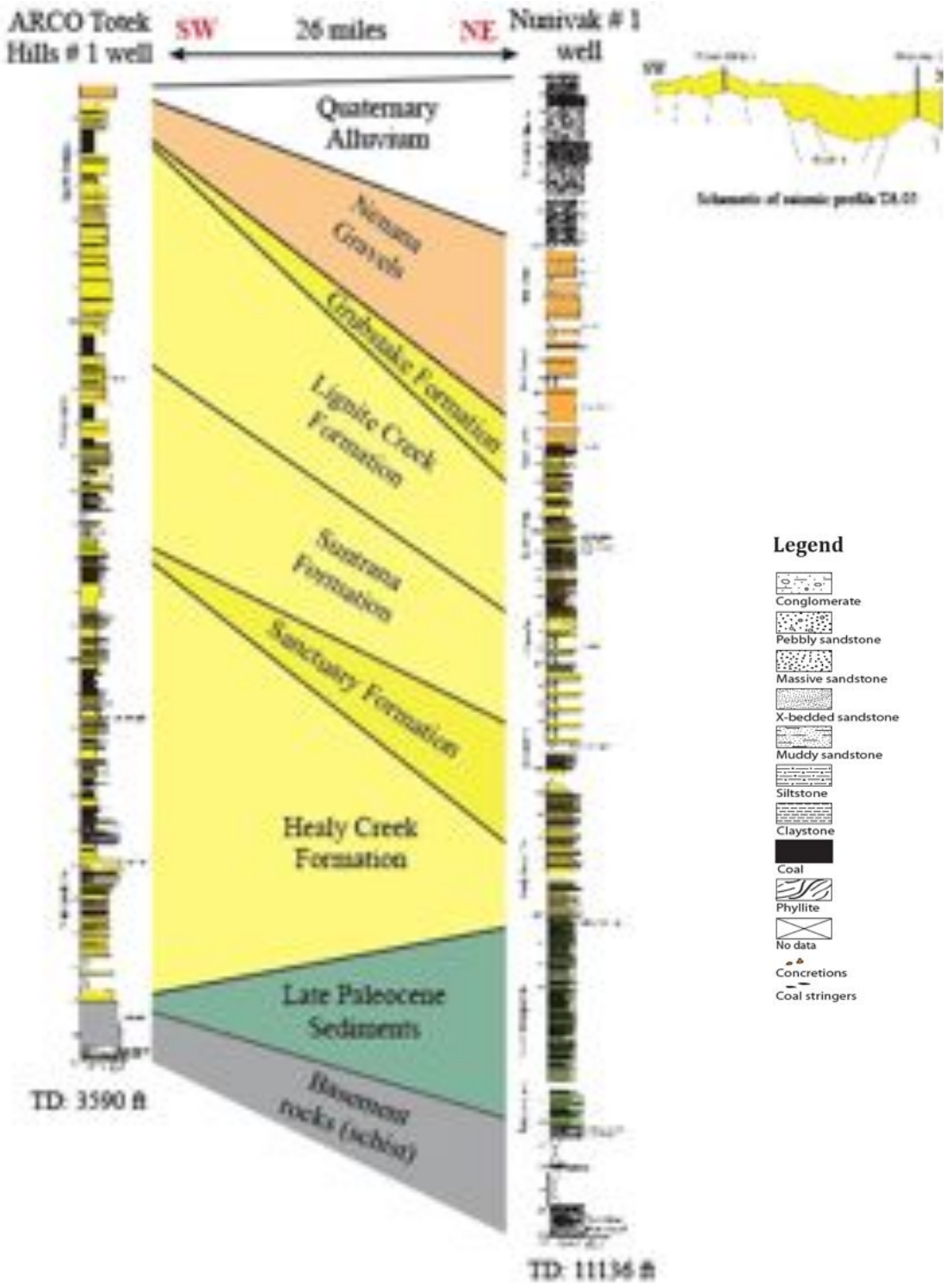

Figure 4. North-east to south-west stratigraphic cross section showing variations of the coal-bearing sequences in the southern Nenana Basin. Nunivak # 1 well was drilled into the deepest zone of the subb whereas Totek Hills # 1 well was drilled at the flank of an anticline. Pinching of sedimentary layers to south-west suggests uplifted basement along the southern margin of the basin.

(1) Well log analysis:
Sonic, density and lithologic logs from the three exploration wells drilled into the southern Nenana Basin were used as control points to determine the subsurface geology of the basin (Figure 2). Sonic logs from Unocal Nenana # 1 well (TD: 3052 ft.), ARCO Totek Hills #1 well (TD: 3590 ft.) and Nunivak # 1 well (TD: 11140 ft.) were further used to establish well-to-seismic ties using a Ricker based (15Hz) wavelet extracted from available seismic data. Using density and time-travel calculations, time-to-depth charts were created for the key horizons and the basement profile of the southern Nenana Basin.

(2) 2-D reflection seismic:
Land seismic data allow detailed analysis of the basin-scale structures along with geometry of the basin and delimits the different layers of the sedimentary fill based on their seismic attributes. This study incorporates four time-migrated seismic profiles (TA02, TA03, TA04 and TA05) acquired by ConocoPhillips in 2005 as part of land seismic survey in the southern Nenana Basin (Figure 2). Resulting from the collaboration between ConocoPhillips and UAF, these seismic lines were first made available for basin modeling in 2011. All of these seismic lines are of good quality and displayed up to 5 s two way time (TWT). Seismic data has been referenced to the NAD 83 datum.

All three wells were used as control points to constrain the time-to-depth calibration: Unocal Nenana # 1 well located along seismic profile TA02 and ARCO Totek Hills # 1 and Nunivak # 1 wells located along seismic profile TA05. All seismic lines were depth-migrated using interval velocities from sedimentary formations derived from sonic logs. Constant velocity was assumed per seismic unit. The derived synthetic seismograms were tested for best fit between the well sonic logs and seismic traces. The finalized time-to-depth chart was further extrapolated for the subbasin depth up to 25000 ft using depth-migrated seismic line 5004 published in Kooten et al. (2012). Interpreted seismic profiles were further applied to geophysical models from the potential field data (gravity and magnetic anomaly data) to constrain the basement profile and subbasin geometry.

(3) Gravity and magnetic data:
State of Alaska (DNR) Complete Bouguer Gravity and Total Intensity Magnetic Anomaly maps (Meyer, 208 a & b) were used to calculate residual gravity data points along four combined gravity and magnetic profiles across the southern Nenana Basin. The observed gravity was subtracted from smooth fitting regional gravity signal to obtain residual gravity data for the southern Nenana Basin. Sediment and crustal densities along with magnetic susceptibilities were derived from available well data (well cuttings, density and sonic logs) and from basement rocks exposed on the basin margin. Table 2 summarizes physical properties used for each lithologic unit in the geophysical model.

Profiles along the southern Nenana Basin were modeled for 2D gravity using Geosoft GM-SYS software. GM-SYS is a 2 ½ D computer modeling program that uses a flat-Earth model and calculates hypothetical gravity and magnetic response from a geological model constrained by well, seismic, local and regional outcrop data. The program presumes that the bodies and surfaces of the geological model extend to infinity along the strike of the profile to remove edge effects (NGA, 2004).

(4) Sample analysis and modeling

Magnetic susceptibility and density

One hundred and thirty three samples from Nunivak # 1 well and six samples from Nenana # 1 well were collected from the Alaska Geologic Materials Center (GMC) and analyzed for magnetic susceptibility and density. A Bartington MS2 magnetic susceptibility meter was used for the discrete measurements of magnetic susceptibility. Mass density for each sample was derived by the calculating mass and approximate volume for every sample. Table 2 summarizes observed and averaged magnetic susceptibility values for all the formations present in both wells.

One hundred and seven additional magnetic susceptibility measurements were taken from the sediment outcrops at the Suntrana Creek field area and along the George Parks Highway near the town of Nenana using a Terraplus KT-10 handheld magnetic susceptibility meter. However, surface weathering, roughness and uneven sample size made these surface measurements unreliable and they were not used. Densities of outcrop samples were measured in the laboratory and incorporated into the data.

Vitrinite reflectance

Vitrinite reflectance is a well established standard to evaluate basin thermal history by determining sediment's state of thermal maturity at specific depth intervals (Thomas, 2002). For this study, ten samples of coal were collected from Nunivak # 1 well cuttings (interval depths ranging from 4450 to 6940 ft) at the GMC. Samples were then submitted to Weatherford Laboratories (Houston) for vitrinite reflectance analysis. Resulting data was used to build thermal history models for the southern Nenana Basin.

Apatite fission track

Apatite fission track (AFT) analysis is a method which determines the time and rate of cooling of a body of rock though a range of temperatures (140° F to 248 ° F) (Donelick et al., 2005). In this study, AFT analysis data will be used to constrain the cooling history of the sediments in the southern Nenana Basin. Two samples from the Nunivak # 1 well were taken over depth intervals 4450 ft- 5770 ft and 9250 ft- 11136 ft. The samples were sent to Apatitie to Zircon Inc. (Idaho) for AFT analysis. Results were not available at the time of this report.

Tectonic subsidence modeling

2-D modeling for tectonic subsidence history of the southern Nenana Basin was performed on selected wells based on the conditions that: 1) they show good tectonic history (unconformities and subsidence); 2) they represent different stratigraphic settings well constrained by well-data; 3) they are drilled at geographic locations which cover different tectonic setting within the basin; and 4) they have reasonable petrophysical data for sedimentary fill to well calibrate subsidence history models.

Two of the three exploration wells drilled in the Nenana Basin (Nunivak # 1 and ARCO Totek Hills # 1; Figure 1) were used to generate basin subsidence history models. ARCO Totek Hills # 1 well (TD= 3590 ft) is located at the south-eastern flank of the basin, breaching the Totek Hills anticline whereas Nunivak # 1 well (TD = 11140 ft) was drilled deeper into the basin targeting a

saddle between two deep subbasins of the Nenana Basin. Subsidence history models were generated using BasinMod software, a windows based basin modeling software developed by Platte River Associates Inc. BasinMod software uses decompaction and subsequent backstripping techniques based on the tectonic subsidence equation of Steckler and Watts (1978) to calculate cumulative basin subsidence.

Gravity and magnetic models

In this study, we developed four 2D geophysical models to investigate different aspects of gravity and magnetic data. By using GM-SYS, polygonal rock bodies with an infinite strike in a direction perpendicular to the profile were incorporated as the building blocks of 2D models. Table 2 summarizes the physical properties of the rock bodies in the model and associated geologic units. Average errors in the geophysical models are approximately 1 % for gravity anomaly data and 10 % for magnetic anomaly data. Seismic depth picks were used as a general guide to locate the base of the modeled gravity and magnetic profiles of the southern Nenana Basin.

RESULTS

Gravity and magnetic models

(A) Model TA02--Southern Nenana Basin

Gravity and magnetic profile TA02 is 53 miles long and oriented NW-SE across the southern Nenana Basin. The profile starts from Bean Ridge, passes through Unocal Nenana # 1 well, and stops near Totatlanika River on the east side of the George Parks Highway (Figure 2). Profile TA02 crosses the deepest part of the southern Nenana Basin, characterized by gravity low of 41 mGal and magnetic low of 6 nT. (Figure 5A). The basement profile is consistent with interpreted seismic and has been adjusted for a good fit between the observed and calculated gravity and magnetic profile beyond seismic limit (Figure 5B).

Our model indicates that the major gravity low on the profile can be modeled as a basin ~ 21300 ft deep. The sudden change in the gravity values observed in the eastern part of the profile supports presence of a major, NE-SW trending Fault 1 (hereafter called as “Minto Fault”) (Figure 5A). Linear increase in the total magnetic intensity accompanied by gravity high on the eastern side of the Minto Fault is resolved by incorporating an uplifted basement block having average basement density of 2.67 g/cc. Short wavelength gravity low on the eastern side of Minto Fault, near Julius Creek indicate a basement depth of up to 5200 ft.

In the vicinity of Unocal Nenana # 1 well, on the western part of the profile TA02, a noticeable magnetic high (~36 nT) and higher gravity values imply a basement high. This high is visible on the seismic profile. This uplifted basement block forms the footwall of Fault 2 that bounds the western margin of the southern Nenana Basin (Figure 5B). A low gravity (-16 mGal) and low magnetic (-15 nT) anomaly on the western side of Fault 2 is compensated by basement depth of 5900 ft.

Three intrusive bodies have been incorporated into the model in order to resolve short wavelength magnetic and gravity anomalies. Intrusive bodies have densities ranging from 2.75 g/cc to 2.82 g/cc (typical of plutonic rocks). Modeled intrusive bodies represent Late Cretaceous to Early Tertiary intrusions into the basement rocks.

This model shows that the basin is about 21300 ft deep in this area and could accommodate coal-bearing strata thicker than 10000 ft (Figure 5A and 5B). Tectonic burial of coal seams at deeper depths could significantly improve thermal maturity and coal bed methane potential of the sub-bituminous coals encountered in the basin. The Minto Fault as modeled on this profile has significant dip slip and fanning of the strata along its hanging wall, suggesting active subsidence in this part of the basin (Figure 5B).

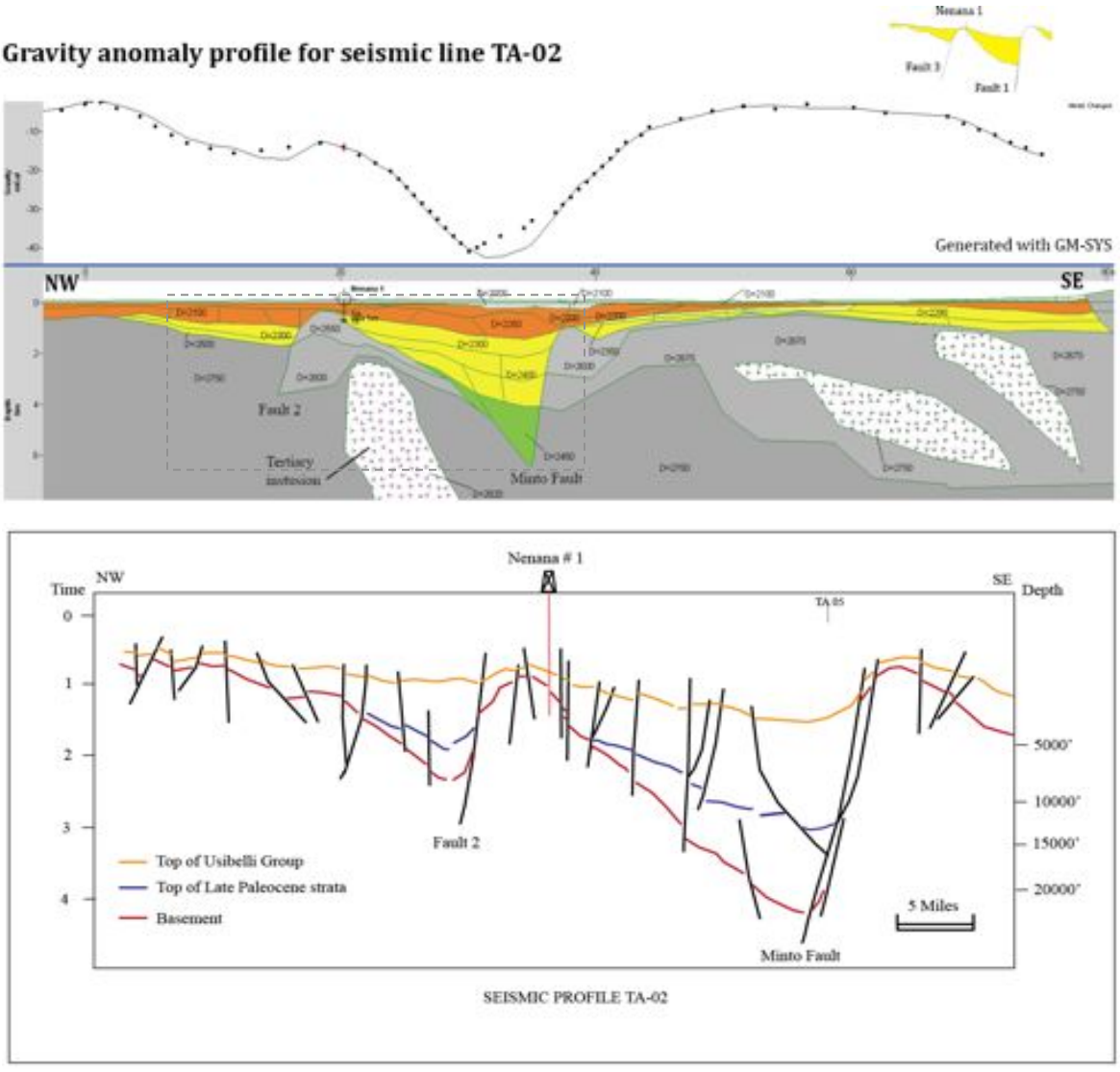

Figure 5. (A) Geophysical Model TA 02: Gravity profile TA02 is 53 miles long and oriented NW-SE across the southern Nenana Basin (as shown in Figure 1). Area outlined by the dashed line is constrained by available seismic profile TA-02. (B) Interpreted seismic profile TA-02 shows presence of two major faults, Fault 2 and Minto Fault.

In the western part of the profile, coal bearing strata thins to 650 ft, suggesting that the basin gradually shallows up from the east towards its western margin.
These observations are critical to evaluating the migration pathways of hydrocarbons and fluid flow in the basin and developing accurate estimates of paleo-heat flows and geothermal gradients in the area.

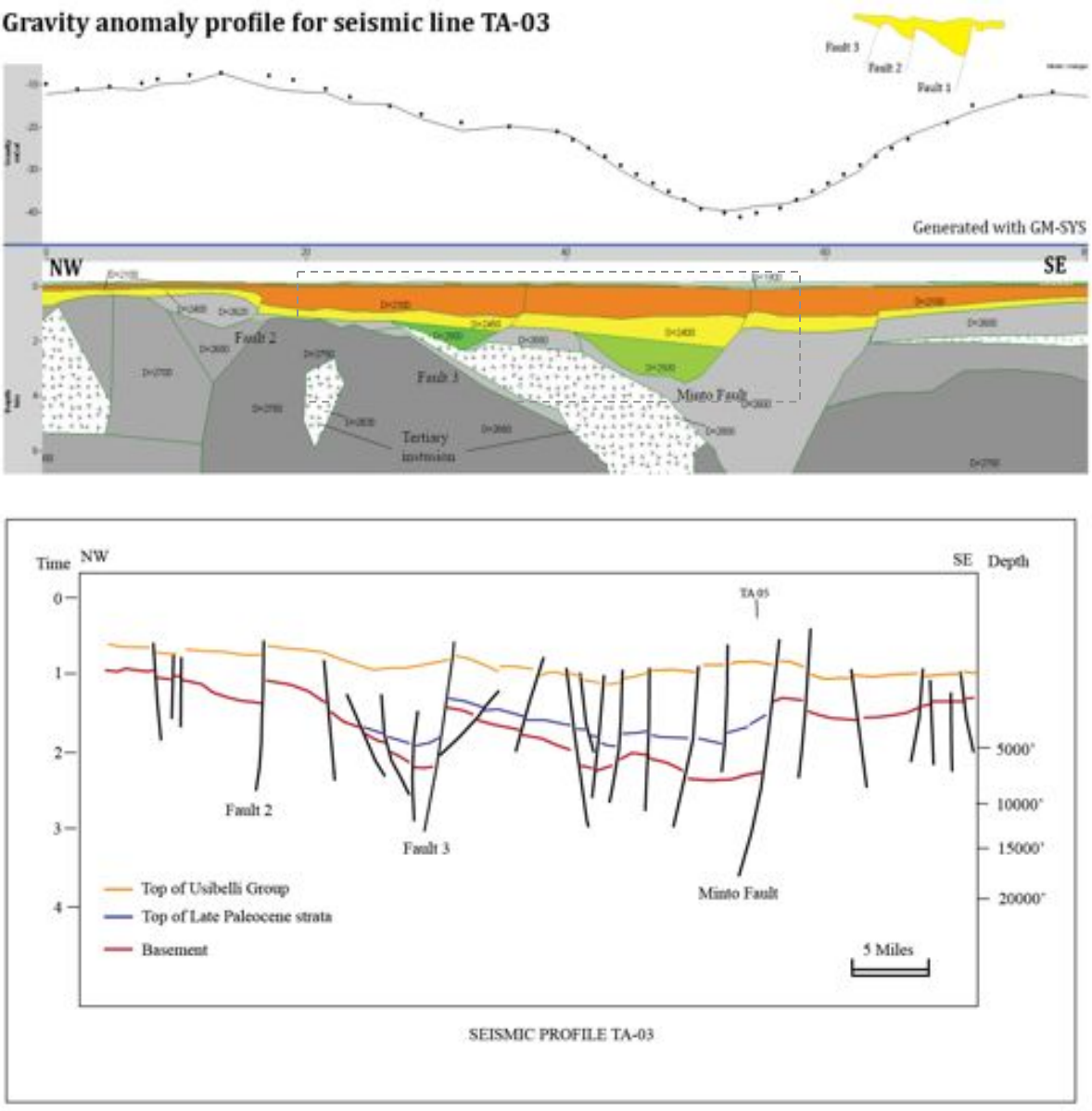

Figure 6. (A) Geophysical Model TA 03: Gravity and magnetic profile TA03 is 64 miles long and oriented NW-SE across the southern Nenana Basin (as shown in Figure 1). Area outlined by the dashed line is constrained by available seismic profile TA-03 (B) Interpreted seismic profile TA-03 confirm presence two sub-basins bounded along their eastern margins by Fault 3 and Minto Fault respectively.

(B) Model TA03

Gravity and magnetic profile TA03 is 64 miles long and runs south of and parallel to profile TA02 (Figure 2). In the absence of any well control in this part of the basin, Model TA02 is constrained mainly by seismic profiles TA03 and TA 05 and geologic maps of the region (Figure 2 and 6B).

A prominent, long wavelength gravity low (41 mGal) marks the main part of the basin (Figure 6A). A shorter wavelength gravity low (20 mGal) occurs to the west of Fault 3 and is interpreted as a shallower subbasin. Basement rocks of Totatlanika schist with a density of 2.6 g/cc underlie both basins. Another prominent feature of this transect is the gravity low of 41 mGal which marks the footwall of the Minto Fault (Figure 6A).

In Model TA03, we modeled two intrusive bodies with density of 2.8 g/cc to fit the observed and calculated gravity and magnetic anomaly response. These Late Cretaceous to Early Tertiary intrusions may represent the same plutonic bodies observed in the Model TA 02 or could be two discrete plutonic bodies intruded along Fault 3 and Minto Fault planes.

This model predicts the maximum sediment thicknesses along these two gravity lows are up to 11400 ft and 8200 ft respectively (Figure 6A and 6B). A steep increase in the magnetic and gravity anomaly towards the western flank of the deepest basin reflects uplifted basement blocks, possibly indicating the presence of new fault (Fault 3) in the area, which could represent a fault splay of the Minto fault system. Down-to-the-west motion along the Minto Fault has resulted into low magnetic and gravity anomalies (Figure 6A).These anomaly effects could be due to sediment warping in the hanging wall of the Minto Fault. Presence of folds in the hanging wall of the Minto Fault as interpreted from seismic profile TA 03 supports this observation (Figure 6B). These folds could reflect reverse motion on the Minto Fault on this profile, suggesting some minor basin inversion in this area.

(C) Model TA04

Profile TA 04 runs NE-SW across the southern portion of the basin, is 49 miles in length and is parallel to and south of profiles TA02 and TA03. This is an important profile as it crosses though all major faults and show significant basin inversion across Minto Fault. This profile is constrained by ARCO TotekHills # 1 well, seismic line TA04 and TA 05 and geologic maps from the area (Figure 2 and 7B).

Compared to previous models (Model TA02 and TA03), profile TA04 is characterized by a long-wavelength gravity low with an average gravity anomaly value of -29 mGal and distinct, short-wavelength magnetic highs with a magnetic anomaly value ranging from 6 nT to 35 nT (Figure 7A). The increase in the magnetic anomaly values across the profile defines footwalls of the identified faults. Our model indicates the presence of three major faults (Minto Fault, Fault 2 and Fault 3) along the profile (Figure 7A and 7B). The Minto Fault appears on the eastern end of the Totek Hills and is expressed by long wavelength gravity and magnetic anomaly high above the footwall. In contrast, the hanging wall of Minto Fault is characterized by decreasing gravity and magnetic anomaly.

ARCO Totek Hills # 1 well (TD: 3590 ft) was used to constrain physical properties of sedimentary fill along the Totek Hills anticline. In the absence of any well and seismic data control in the westernmost part of the profile, plutonic block of density 2.9 g/cc has been added to resolve the long-wavelength gravity and magnetic anomaly in this region. No intrusive bodies have been included on to the eastern end of the profile.

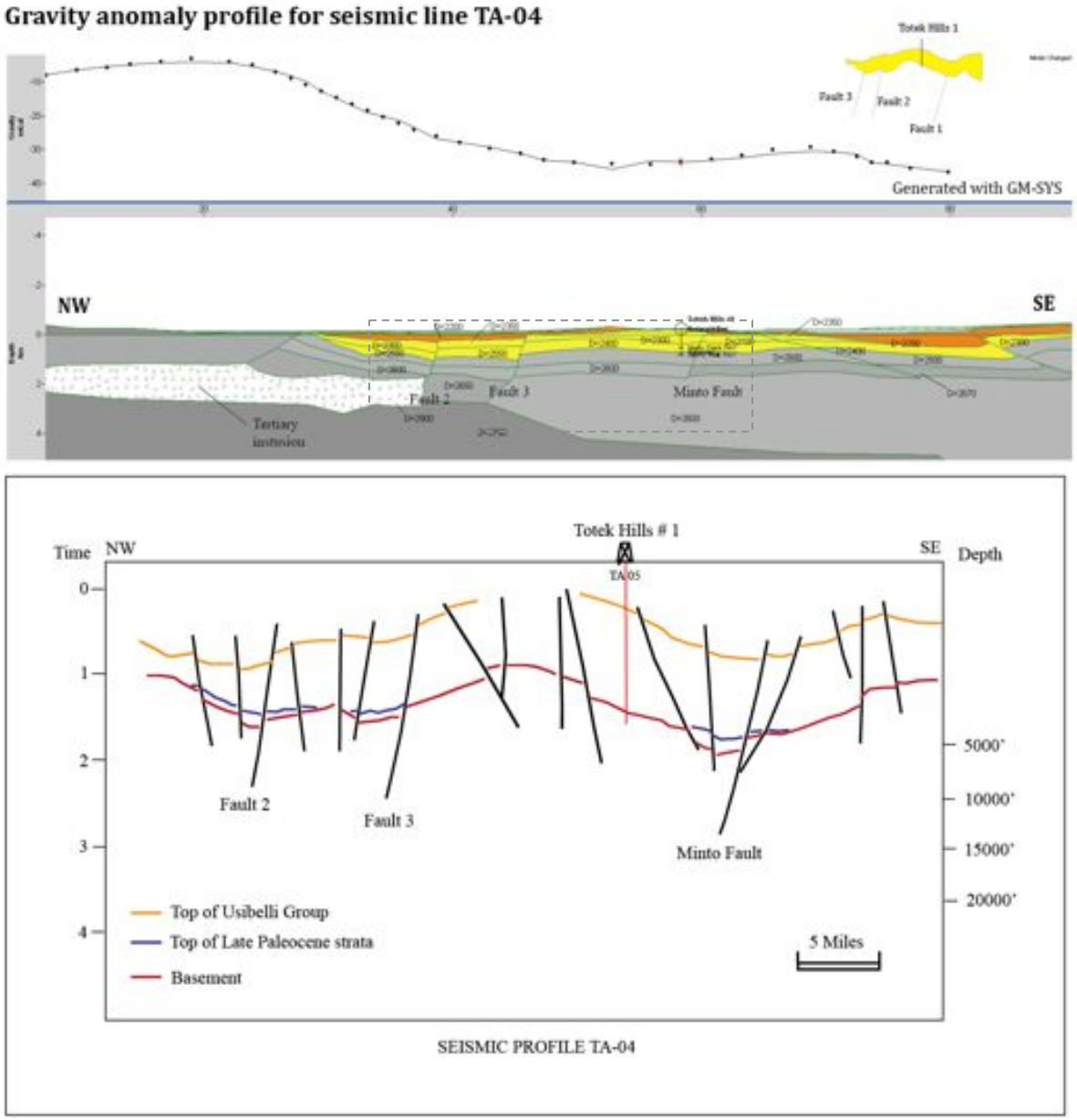

Figure 7. (A) Geophysical Model TA 04: Gravity and magnetic profile TA04 is 49 miles long and oriented NW-SE across the southern Nenana Basin (as shown in Figure 1). Note that Totek Hills # 1 breaches anticline structure present in this area. Area outlined by the dashed line is constrained by available seismic profile TA-04 (B) Folding of strata as observed from the seismic profile TA-04 suggests recent basin inversion along the southern margin of the southern Nenana Basin.

Our model suggests that the maximum depth of basin in this part of the southern Nenana Basin is up to 4200 ft (Figure 7B). Calculated uniform gravity anomaly (-24 mGal to -34 mGal) along the profile suggest that the thickness of coal-bearing strata in this region could be up to 3500 ft. On the western side of Totek Hills, steep variations in the magnetic and gravity anomaly values are interpreted to be the result of the footwall basement blocks of Fault 2 and Fault 3 respectively (Figure 7A).

Sediment warping along the Totek Hills, absence of younger formations in the well, shallow basement depth and formation of fold structures in the downthrown side of Minto Fault (Figure 7B) all can be interpreted as due to recent uplift and inversion along the southern margin of the southern Nenana Basin.

(D) Model TA05

Model TA 05 strikes NE-SW, parallel to the strike of the eastern Nenana basin (Figure 1). Nunivak # 1 and ARCO Totek Hills # 1 constrain the depth, densities and lithologic units of the profile; depth-to-basement is constrained by seismic line TA 05 (Figure 2 and 8B).

The long wavelength gravity low of 40 mGal at the northeastern part of the profile reflects basement depths of up to 21300 ft (Figure 8A and 8B). Short wavelength gravity highs (-14 mGal and -24 mGal) define normally faulted basement blocks along Fault 5 and Fault 6 respectively. In contrast, along the southwestern part of the profile, short- wavelength gravity high of -29 mGal suggests presence of a low angle thrust (?) fault, Fault 4. The southwest dip of Fault 4 is constrained by seismic profile TA 05 (Figure 8B).

Our model TA 05 implies that the basement of the southern Nenana Basin is fairly steep along its northeastern margin (basement depth: ~21300 ft) whereas basement shallows up gradually towards its southern margin near the Totek Hills (basement depth: ~ 4200 ft; Figure 8B). Coal-bearing strata in the northeastern part of the subbasin could be more than 10000 ft thick as discussed with Model TA02. Late Paleocene coal seams occur at maximum depth and temperatures in this part of the southern Nenana Basin. Though no well or seismic data are available to constrain the northern part of the profile, the model suggests that the northern part of the Nenana basin is very deep with depths up to 30000 ft (Figure 8A).

Figure 9 outlines the observed fault orientations and basement profiles as constrained by the geophysical models (TA 02, TA 03, TA 04 and TA 05) of the southern Nenana Basin.

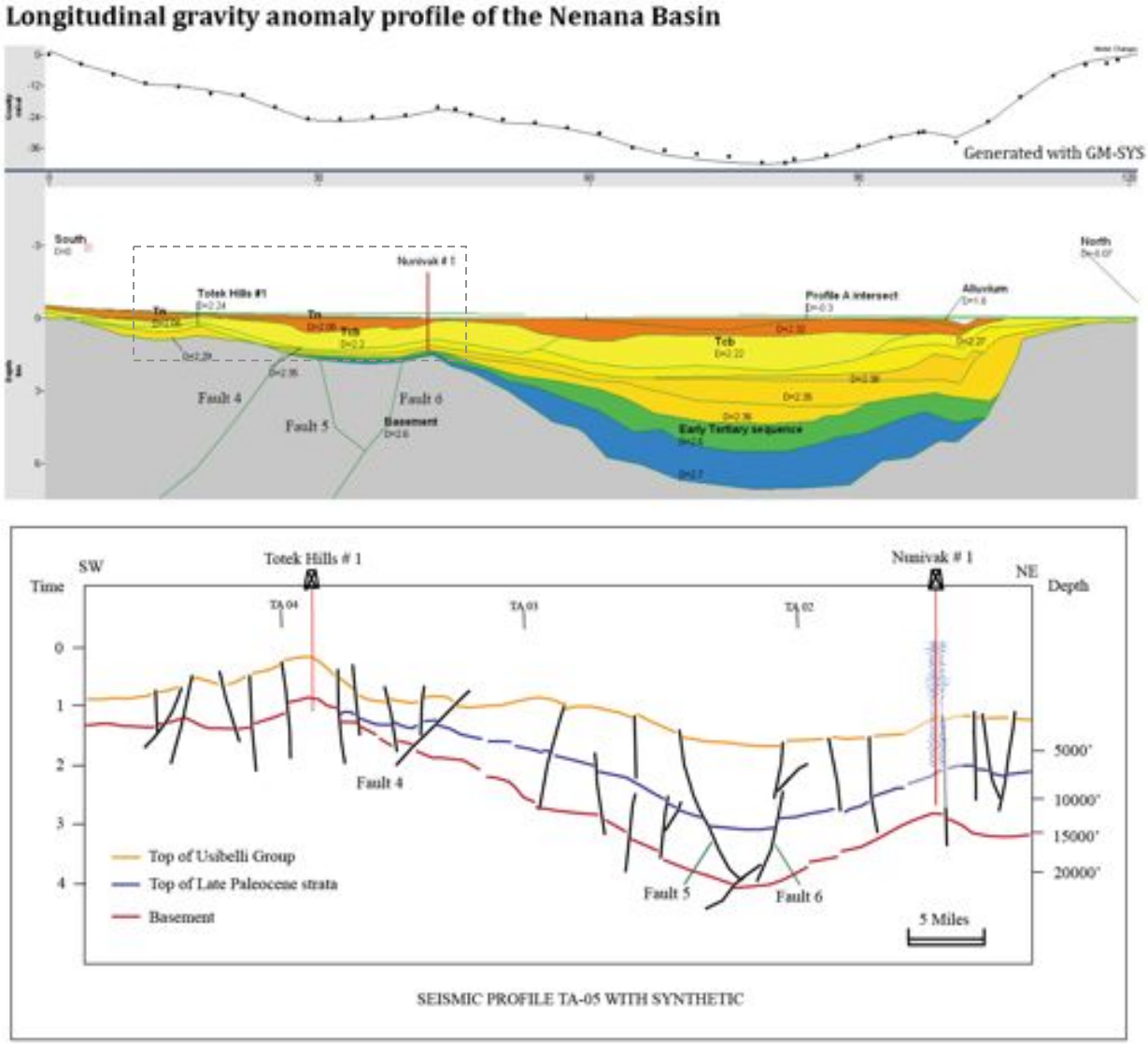

Figure 8. (A) Geophysical Model TA 05: Gravity and magnetic profile TA05 is 51 miles long and oriented NE-SW across the southern Nenana Basin (as shown in Figure 1). Note that Fault 4 is a thrust fault associated with Totek Hills anticline. Area outlined by the dashed line is constrained by available seismic profile TA-05 (B) Fault 5 and 6 are steep normal faults which form a negative flower structure in subsiding area of the profile TA-05.

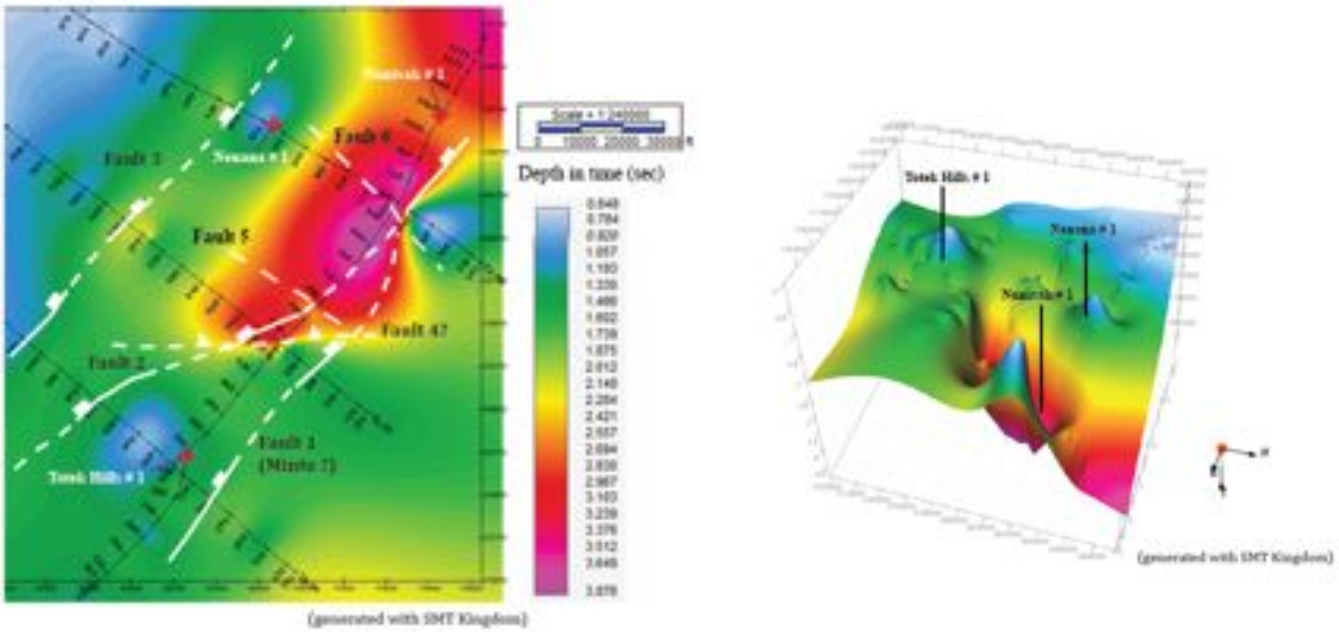

Figure 9. Map Basement depths and 3-D basement profile of the southern Nenana Basin Simulated 3-D basement profile of the southern Nenana Basin (to the right). Basement depths were populated using Flex Gridding technique.

Basin Subsidence and Burial History

A. Vitrinite reflectance

Vitrinite reflectance values of ten samples collected from coal-bearing intervals of the Usibelli Group from Nunivak # 1 well cuttings are summarized in Table 3. Maximum recorded vitrinite reflectance value at depth of 6940 ft is R_0= 0.44 indicating that the coal-bearing rocks of the Usibelli Group at this depth are immature. Published vitrinite reflectance data from deeper in Nunivak #1 (8170 ft to 10420 ft) ranges from R_0= 0.46 to R_0= 0.62 (Kooten et al., 2012). As vitrinite reflectance varies uniformly with basin depth, depth of sediment burial and local geothermal gradient seem to be most dominant controlling factors of coal rank in Nunivak # 1 well.

Present day geothermal gradient in Nunivak # 1 well along the northeastern edge of the southern Nenana Basin is calculated to be 1.5° F/ 100 ft (assuming a surface temperature of 35° F and 205° F at depth of 11, 075 ft.) (Kooten et al., 2012). At ARCO Totek Hills # 1 well along the southwestern edge of the subbasin, the estimated geothermal gradient is 2.92° F/ 100 ft (assuming a surface temperature of 65° F and 169° F at 3560 ft; ConocoPhillips, 2004).

This suggests that the geothermal gradients across the southern Nenana Basin may be highly variable. The mechanism responsible for northeastward decline of geothermal gradient is not clear. However, we speculate that low geothermal gradient in Nunivak # 1 well could be related to the rapid subsidence in this part of the southern Nenana Basin. Sediments usually have low

thermal conductivity. Increased subsidence causes more sediment accumulation which further allows slow dissipation of heat. As a result, for a constant heat flow, increased thickness of sedimentary fill causes a reduction in the geothermal gradient. At ARCO Totek Hills # 1 well, uplifted basement has resulted into comparatively thinner sediment fill causing relatively high geothermal gradient at shallow depth. Other possible factors which may influence geothermal gradient in the subsurface include lithology and physical properties of rocks, variable heat flow, groundwater dynamics and the rate of consolidation and compaction of the sediments.

B. Subsidence history

The amount of coal-bed methane (CBM) that is stored in the subsurface coals depends mainly on depth of burial and its related pressure, rank of coal and a time vs depth-of-burial relationship (Ozdemir, 2009). Better understanding of the basin subsidence history is thus essential to evaluate both the coal-bed methane and CO2 sequestration potential of deeply buried coal seams of the southern Nenana Basin. Two subsidence history models of representative stratigraphic sequences encountered in ARCO Totek Hills # 1 well and Nunivak # 1 well were plotted with the depths of rock units against their respective geologic ages (Figure 10A and 10B). Based on the geochemical analyses from Nunivak # 1 well, we have assigned differential heat flows (48 – 59 mW/m²) and geothermal gradients (1.5 – 2.92 ° F / 100 ft) to construct thermal maturity models for both the wells (Table 4) (Kooten et al., 2012).

Table 3. Vitrinite reflectance data and sample depths for Nunivak # 1 well cuttings, southern Nenana Basin

Sample	Depth (ft)	% Ro	Stage of coalification	Present day temperature (°F)
1	4450	0.27	lignite	105.5
2	5020	0.34	lignite	114
3	5110	0.41	subbituminous	115.5
4	5380	0.40	subbituminous	119.5
5	5560	0.41	subbituminous	122.3
6	5740	0.40	subbituminous	125
7	5830	0.41	subbituminous	126.3
8	6010	0.43	subbituminous	129
9	6910	0.44	subbituminous	142.5
10	6910	0.43	subbituminous	142.5

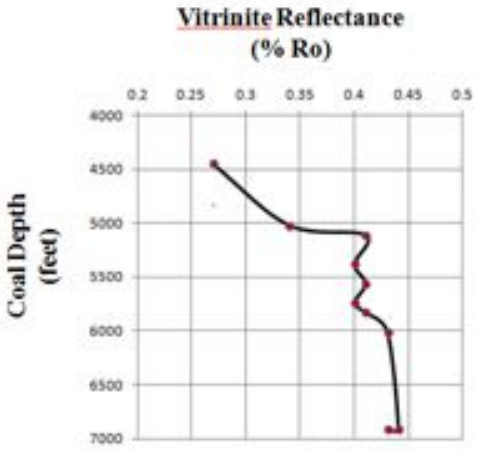

Model A: Nunivak # 1 Well

Nunivak # 1 was drilled in a major depocenter located at the northeast margin of the southern Nenana Basin that accommodates more than 21000 ft sedimentary fill (Figure 8B). Early Tertiary sediments of Nunivak # 1 record three distinct phases of tectonic subsidence and two phases of uplift in this region (Figure 10A).

The first phase of tectonic burial occurred between 37 to 68 Ma ago and placed coals from Late Paleocene strata in a temperature window of 77 ° F to 221 ° F, ideal for biogenic and thermogenic methane generation (Figure 10A). The basin was then uplifted and erosion of Late Paleocene sediments took place about 24 to 37 Ma ago. This exhumation event was responsible

for the removal of about 200 ft of Late Paleocene strata by erosion and is evident on the seismic profiles in the form of an angular conformity at the base of Healy Creek Formation (Figure 8B). Basin uplift led to the cooling of Late Paleocene coals to temperatures of about 212° F.

A second phase of subsidence took place between 8 to 24 Ma ago and is recorded by deposition of Usibelli Group strata. Coal beds from the Usibelli Group and Late Paleocene strata were buried up to depths of 7000 ft in the deepest areas of the basin and were subjected to the temperatures up to the 302 ° F.

A final phase of basin uplift and erosion occurred between 3 to 8 Ma ago and is evident on seismic profile with the generation of an angular unconformity at the base of the Nenana Gravels (Figure 8A and 8B). Compared to the first phase of uplift, the effects of the second phase were minimal in the deepest areas of the southern Nenana Basin.

Onset of final phase of subsidence took place about 3 Ma ago and the basin is still subsiding along its deeper areas. The Nenana Gravels were deposited during this phase of tectonic subsidence and provides overburden for deeply buried coals of the basin. At present day, coals of the southern Nenana Basin are at maximum depths and temperature. The modeled temperature at 11140 ft in Nunivak # 1 well is 338 ° F.

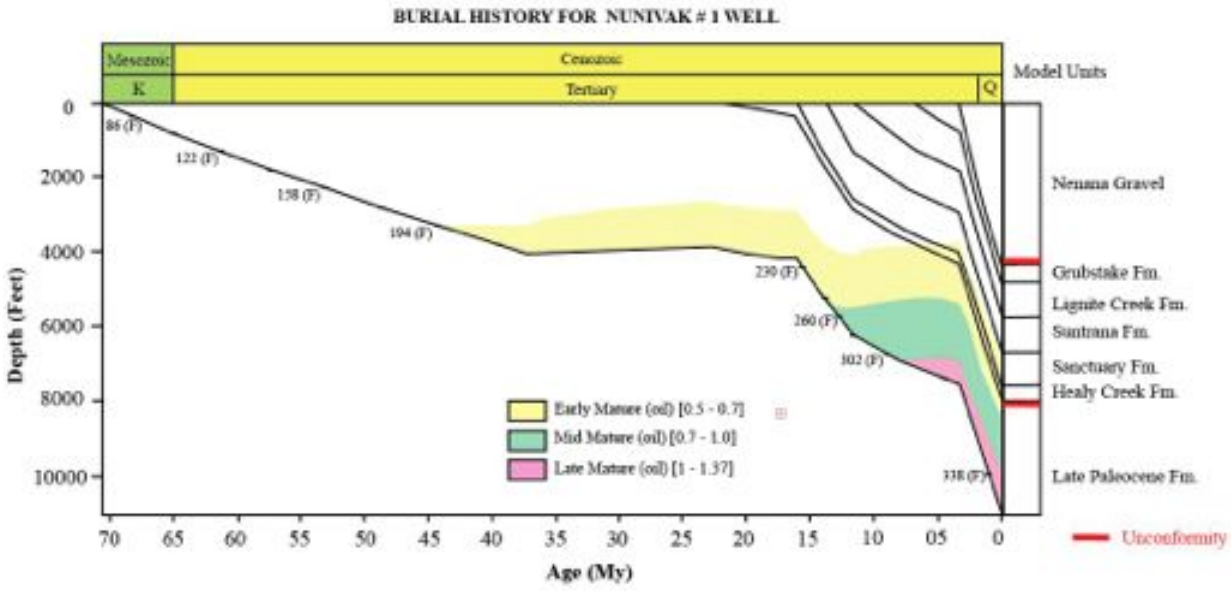

Figure 10 (A) Burial depths of representative formations through time are shown for Nunivak # 1. Three distinct episodes of tectonic subsidence and two phases of basin uplift characterize the deeper areas of the southern Nenana Basin. Colored bands indicate coal maturity levels modeled using BasidMod software and are based on the vitrinite reflectance data, in percent.

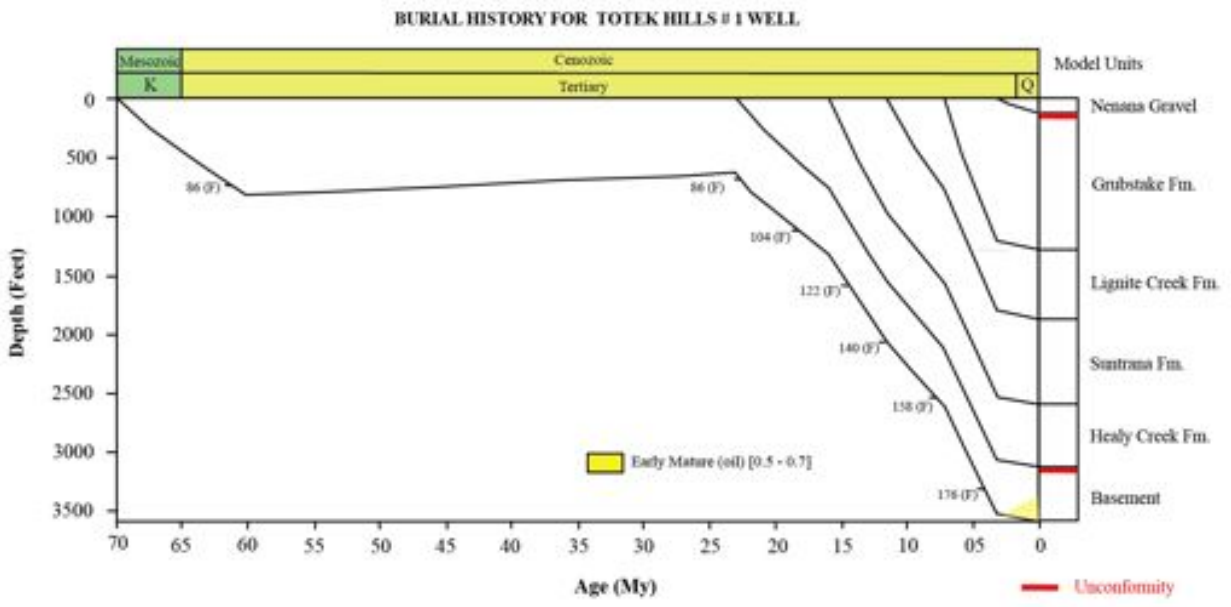

Figure 10 (B) Burial history curve for Totek Hills # 1 drilled into the Totek Hills anticline located at southern margin of the Nenana Basin. This area is marked by two distinct phases of subsidence and two episodes of basin uplift. Coals present at deeper depths in this area appear to be of very low coal rank and immature to generate any thermogenic methane at deeper depths.

Implications

Observed vitrinite reflectance values of about 0.34 % Ro at 5000 ft imply that the coal rank increases with increasing depths, which may have enhanced the CBM generation capacity of deeper coal seams (Table 3). However, the first phase of uplift and erosion, with related removal of overburden and decrease in pressure could have resulted in expulsion of early-formed gas from low-ranked coal beds. In the absence of laterally continuous, thick and impervious layers of caprock (shale or claystone from overlying formations) during this time, CBM generated prior to the first phase of uplift might not be preserved in the basin and should not be included in the CBM reserve estimates of the southern Nenana Basin.

Thermogenic methane gas generation takes place at temperatures above 122 ° F. Consequently, during the second phase of basin subsidence deeper coal beds of the southern Nenana Basin were within range of ideal bacterial methane generation. This interpretation is supported by increased coal maturity (from lignite to sub-bituminious stage) as observed from vitrinite reflectance values (0.43 % Ro at depth of 6910 ft; Table 3).

The second episode of basin uplift and erosion in the late Miocene/early Pliocene resulted in additional sediment cooling and pressure reduction. This could have lowered ground-water levels resulting in degassing of CBM from the coal beds to overlying sandstone reservoirs of the Usibelli Group and Late Paleocene strata. This basin exhumation may also have formed

additional migration pathways for biogenic and thermogenic CBM to migrate towards the flanks of the basin, especially to the western and northern basin margins.

According to this model, coals currently located at depths greater than 7500 ft (with a vitrinite reflectance value of 0. 62 %) fall into the early-gas zone of conventional gas window and are generating hydrocarbons in this area of the basin (Table 3; Figure 8B and 9A).

Model B: ARCO Totek Hills # 1

Along the southwestern margin of the southern Nenana Basin, ARCO Totek Hills # 1 was drilled into the Totek Hills anticline, encountering basement rocks at a depth of 3128 ft (Figure 7B). No data is available to evaluate the thermal maturity of coals from this well. A subsidence model of the sediments preserved in the well suggests that the basin experienced two distinct episodes of tectonic subsidence and two phases of basin uplift and erosion (Figure 10B).

The first phase of tectonic subsidence in this part of the southern Nenana Basin occurred between 61 to 68 Ma ago (Figure 10B). Compared to Nunivak # 1 well, this episode of tectonic subsidence was short-lived and created accommodation for 620 ft of Late Paleocene strata. Modeled temperatures suggest that the temperatures at the base of the Paleocene strata at this time was about 91° F.

This short episode of tectonic subsidence was then followed by a long-lived phase of basin uplift and erosion which lasted from 61 to 24 Ma. This uplift and erosion led to sediment cooling from 91 ° F to 82 ° F. This uplift and erosion is associated with the regional angular unconformity at the base of Healy Creek Formation (Figure 7B).

A second phase of rapid basin subsidence was initiated 24 Ma ago and continued until 3Ma. During this phase of basin subsidence, up to 3000 ft of Usibelli Group sediments were deposited over the remnant Late Paleocene deposits in this part of the basin. Coal-bearing strata of the Usibelli Group may have reached maximum temperatures of 169 ° F at a depth of 3500 ft.

Since the Late Miocene, the basin in this area has been undergoing inversion along its south-western margin at the Totek Hills anticline (Figure 7B).

Implications

During first phase of tectonic subsidence in this part of the Nenana basin, any coals deposited during Late Paleocene time were probably immature and did not generate any thermogenic CBM. Basin uplift during Early Eocene to Early Oligocene time may have further reduced biogenic methane production in these very low ranked coals (Figure 10B). During Late Miocene, increased temperatures and pressures during basin subsidence may have resulted in increased production of biogenic and thermogenic CBM in coals of the Usibelli Group and Late Paleocene strata.

This, combined with the absence of thick, deeply buried, laterally continuous coal beds in this part of the Nenana basin, suggests that CBM production in this area is significantly less when

compared to the deeper areas of the basin. In the absence of any gas shows in Totek Hills # 1 well, the southwestern margin of the southern Nenana Basin appears to be either CBM starved or the coals are still too immature to generate any thermogenic gas in this area.

DISCUSSION

Physical properties and geothermal regime

Our study shows that the coal beds of the Usibelli Group and Late Paleocene strata that are capable of thermogenic methane production are located at the depths greater than 5110 ft in the deeper parts of the basin and are sub-bituminous in stage (Table 3 and 4). Along the basin flanks, coal attains an approximate rank of lignite and is in the late phase of biogenic methane generation. Coal beds located at the depths greater than 5110 ft are considered to be good candidates for geologic CO_2 sequestration via enhanced CBM reserve estimates.

Thermal maturity models of the southern Nenana Basin (Figure 10A and 10 B) show that the temperatures attained by candidate coal reservoirs fall into the early to late oil window and are favorable for thermogenic coal bed methane generation. Sub-bituminous coal beds are as thick as 40 ft and could hold significant volumes of coal bed methane. Lacustrine claystones and coaly shales in overlying formations (Grubstake and Sanctuary Formations) have good potential to act as seals, further preserving generated coal bed methane in the candidate coal reservoirs of the basin (Table 2).

Table 4. Summary of geological data for coal reservoirs identified in Nunivak # 1 well.

Property	Decription	Source
Reservoir	Mid Miocene to Late Paleocene coal beds	Well Logs/ Geologic Studies
Reservoir Depth	> 5110 ft(Usibelli Group coal), > 8110 ft ((Late Paleocene coal)	Well Logs/ Seismic
Caprock	Coaly shale/ Mudstone	Well Logs/ Seismic
Coal Rank	Sub-bituminous	Sample Analysis
Coal Seam Thickness	5 ft. to 40 ft.	Well Logs/ Seismic
Average Coal Thickness	800 ft	Well Logs/ Seismic
Vitrinite Reflectance (% Ro)	0.43 % to 0.62 %	Sample Analysis
Burial Temperatures	200 ° F (at 5110 ft) to 338 ° F (at 11140 ft.)	Well Logs/ Geologic Studies
Geothermal Gradient	1.5 – 2.92 ° F / 100 ft	Well Logs/ Geologic Studies
Heat flow (mW/m²)	48 (65 Ma to 13 Ma) 59 (13 Ma to present)	Kooten et al. (2012)

Tectonic implications

The geophysical modelling, tectonic burial history and geochemical studies from wells in this study confirm previous interpretations of geologic structures in the southern Nenana Basin region and provide new insights.

The geometry of the southern Nenana Basin resembles a pull-apart structure overprinted by compressive features (Figure 11). The prominent gravity and magnetic gradients reflect the boundary between dense basement rocks and low-density sedimentary fill of the Nenana Basin and clearly define six major faults in the southern Nenana Basin (Figure 5A, 6A, 7A and 8A). The Minto Fault forms the eastern margin of the basin and consistently shows down-to-west motion, except in the far southeastern part of the basin, where reverse offset along a splay is observed. This could be the result of inversion on the otherwise normal fault in response to recent thrusting in the vicinity of northern foothills of the Alaska Range (Figure 6A and 7A).

Fault 3 is a normal, down-to-the west fault as observed on transects TA-03 and TA-04. However, associated splays show reverse offset with gentle folding of basement and sediments between the splays (Figure 6B and 7B). We propose that the Fault 3 and associated splays are part of a negative flower structure, possibly related to movement along the sinistral Minto fault system.

Fault 2 shows normal offset with a minimal down-to-west motion along its single fault plane. Fault plane solutions obtained using regional broadband data (Ratchkovski and Hansen, 2002) suggest sinistral strike-slip displacement along Fault 2. Strike-slip component of motion across Fault 2 has not been evaluated in the absence of seismic or fracture data making interpretation subjective.

Faults 4, 5 and 6 are observed on transect TA-05 that parallels the strike of the Nenana basin. Fault 4 is a thrust fault with an associated anticline, Totek Hills anticline (Figure 8B). This thrust fault could be an extension of thrust system characterizing northern foothills of the Alaska Range. Faults 5 and 6 are north of Fault 4 and are steep faults showing a considerable normal-slip components. Fault 5 and 6 mark a depressed area which is indicative of active subsidence in the area.

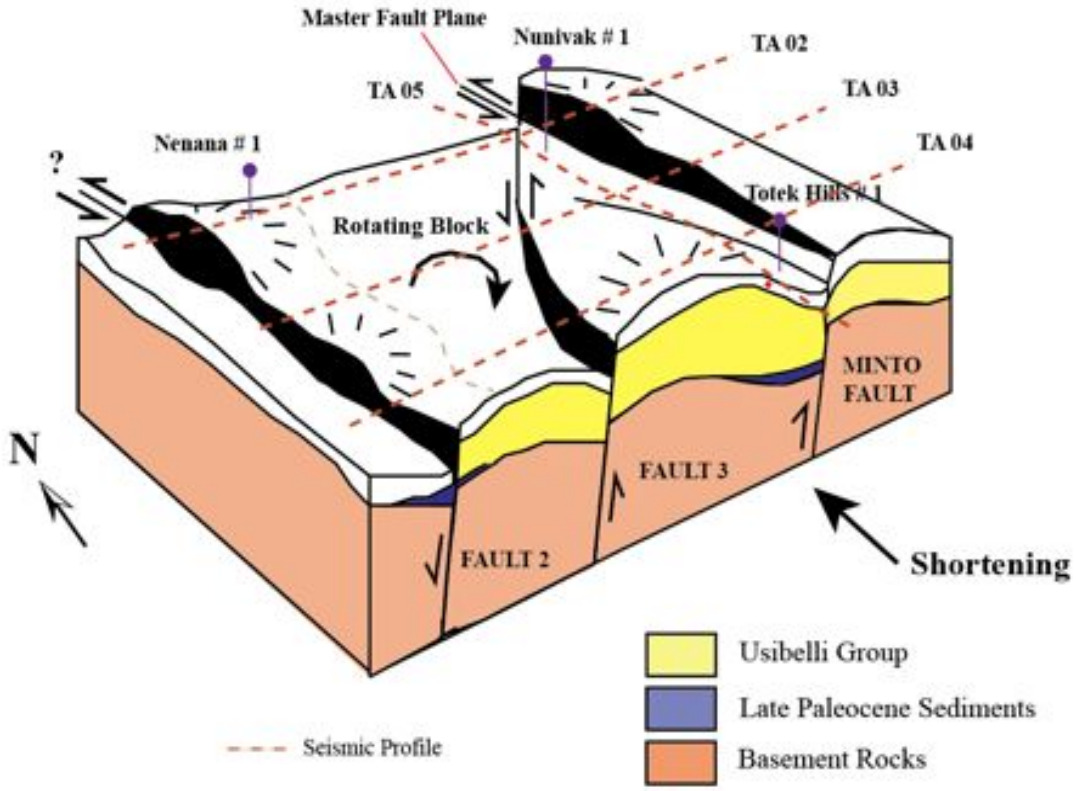

Figure 11. Structural model of the southern Nenana Basin as inferred from the seismic and geophysical data.. Sinistral Minto fault system forms the eastern margin of the basin and may be associated with Fault 3 and an intervening strike-slip duplex. Fault 2 is interpreted as strike-slip fault with a normal component of motion..

Tectonic controls on Nenana basin evolution

Southern Alaska is tectonically complex, with a variety of tectonic drivers during Tertiary time that may have influenced the initiation and growth of the Nenana basin (Figure 12; Brogan et al., 1975; Packer et al., 1975; Cole et al., 1999). Different episodes of tectonic subsidence observed in the basin burial history could be the result of Early Tertiary strike-slip faulting along the Denali and Tintina Fault systems and subsequence strike-slip tectonics in Interior Alaska (Figure 10A and 10B). Other far-field driving mechanisms that may have controlled basin subsidence to lesser degrees include subduction of a spreading center along the former coast of southern Alaska (61 Ma- 50 Ma) and resulting oroclinal bending of western Alaska in response to the northwestward shift in plate convergence (60 Ma– 42 Ma). Different phases of basin uplift and erosion may have resulted in response to increased northward compressive stresses due to Kula-Pacific plates reorganization (42 Ma – 23 Ma) and/or ongoing flab-slab subduction of Yakutat block beneath south-central Alaska (26 Ma to present day) (Trop and Ridgway, 1997; Cole et al., 1999, Ridgway et al., 2007).

The different local stress regimes associated with these far-field tectonic driving mechanisms undoubtedly influenced strike-slip motion along the major faults in the Nenana Basin and controlled the geometry of the basin over time. However, there is not sufficient data on the

timing and extent of these strike-slip events to link any one driver to particular uplift or subsidence events.

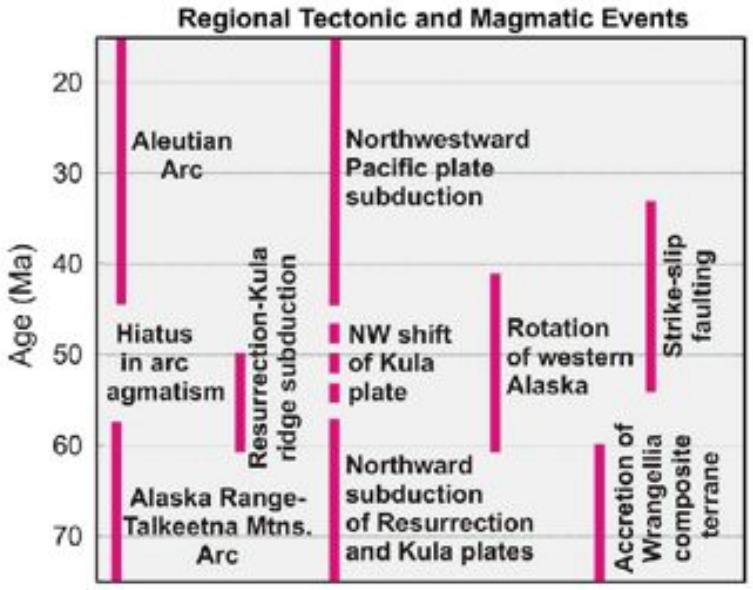

Figure 12. Age-event diagram showing distinct regional tectonic events which directly and indirectly influenced the tectonics of Interior Alaska through time. They provide an important link between differential stress regimes and the tectonic features that shaped the southern Nenana Basin since Late Cretaceous time (modified from Cole et al. 2006).

Carbon dioxide sequestration potential

The Nenana basin has two different coal-bearing intervals that could potentially serve to sequester CO_2--Late Paleocene sediments and the Miocene-age Usibelli Group. This study helped define the areal extent and thickness of these intervals.

The geophysical models, well and seismic data revealed the lateral extent of a regional angular unconformity which is located at the base of Healy Creek Formation and overlies Paleozoic to Precambrian basement rocks of Yukon-Tanana Terrane (Figure 8B) and, in some locations, Early Tertiary coal-bearing strata. This angular unconformity is ~17 to 26 m.y. in age and is defined by the truncation of Early Tertiary folds and onlapping of Usibelli Group sediment strata against it (Kooten et al., 2012). The subsurface distribution of this angular uniformity indicates the location and volumes of the underlying Early Tertiary coal-bearing rocks. Geophysical models further indicate that the Early Tertiary coal-bearing strata is thickest (> 3000 ft) and laterally continuous in the deeper parts of the sub-basin along the Minto Fault (Figure 5 to 8). Nunivak # 1 well data shows that coal beds are up to 40 ft thick in this region and become thinner near the southern and eastern flanks of the sub-basin as observed from seismic profiles TA 02 and TA 05 (Figure 5B and 8B).

The potential volume of CO_2 that could be sequestered in these Late Paleocene coal deposits can be estimated based on the basement profile and the extent of Late Paleocene sediments in both seismic data and the geophysical profiles. Based on the basement profile of the southern Nenana Basin , Late Paleocene coal deposits covers an area of approximately 216 km² (24 km in NE-SW direction and 9 km in NW-SE direction) (Figures 5B, 8B and 9). Observed total thickness of coal seams contained within Late Paleocene sediments is on an average 0.244 km (approx 800 ft). Coal seams would therefore have a total volume of 53×10^9 m^3. Considering an average density

of 1.3 g/cc for sub-bituminous coal (Wood et al., 1983), total mass of coal available in Late Paleocene sedimentary rocks is calculated to be 68.5 x 10^9 metric tons.

Under given set of temperature and pressure, coal seam sequestration of CO_2 is a function of CO_2 adsorption capacity. From the available published data (Tamon et al., 2003; Ryan and Richardson, 2004), we have assumed a CO_2 adsorption capacity of sub-bituminous coal at depths greater than 2000 m to be around 20 cc/g. A detailed fracture model for coal reservoirs is necessary to explicitly evaluate fracture-matrix interaction and estimate net volume of solid matrix of coal capable of a CO_2 adsoption. For given value of CO_2 adsorption capacity, total volume of CO_2 that could be sequestered in estimated mass of coal seams would be 137 x 10^{16} cm^3. At standard temperature (298°K), the density of carbon dioxide is 1.98 x 10^{-3} g/cc. Total mass of carbon dioxide that could be sequestered in Late Paleocene coal seams is estimated to be 2.708 billion metric tons of CO_2.

Oliocene to Miocene coals of the Usibelli Group in the subsurface of the southern Nenana Basin extend over an approximate area of 366 km^2 with an average thickness of 400 ft. To calculate CO_2 uptake potential of Usibelli Group coals, we have considered the coal beds located at depths greater than 5110 ft in the southern Nenana Basin (Table 3 and 4). Candidate coal reservoirs from the Usibelli Group therefore have a gross volume of 40.9 x 10^9 m^3. The total mass of coal in the Usibelli Group which is available to adsorb injected CO_2 is estimated to be 53.3 x 10^9 metric tons. The CO_2 adsorption capacity of sub-bituminous coal in the Usibelli Group at depths greater than 5110 ft and temperatures of up to 115° F is 15 cc/g (Ryan and Richardson, 2004). The total volume of injected CO2 that could be sequestered completely within this calculated mass of coal is calculated to be 79 x 10^{16} cm^3. Assuming the density of carbon dioxide at standard temperature, the total mass of CO2 that could be sequestered geologically in Tertiary coals of the Usibelli Group in the southern Nenana Basin is 1.66 billion metric tons of CO_2.

Based on these preliminary estimates, the combined CO2 adsorbtion capacity of the Late Paleocene coal-bearing rocks and the Usibelli Group in the southern part of the Nenana basin could be as high as 4.368 billion metric tons. This far exceeds the projected 315 million tons of CO2 generated by the proposed CTL plant over a 30-year design life (Dover, 2008).

These estimates are for the southern part of the Nenana basin. To the north of our study area, the entire Nenana Basin deepens gradually and basement rocks reach depths of up to 30000 ft (Figure 8A; Tomsich and others, 2012). Modeled thicknesses of the Tertiary coal-bearing strata in the northern Nenana Basin indicate the presence of significant amounts of coal reserves in both the Usibelli Group and Late Paleocene sediments, with average total thicknesses potentially greater than 10000 ft. Further studies are needed to evaluate the subsurface volumes of coal, thermal maturity of coal, distribution and sealing capacities of cap rock and CO_2 uptake potential of the coal in this northern part of the Nenana Basin.

CONCLUSION AND FUTURE SCOPE

Our preliminary work offers new insights into the structural geometry and tectonic subsidence history of the southern Nenana Basin. 2.5 D modeling of magnetic and gravity data along four profiles was carried out to define the internal architecture of the southern Nenana Basin. All the

geophysical models were constrained by seismic data, well logs and regional geologic maps to obtain more realistic approximation of basin geometry relative to local surface geology.

Our models reveal a pull-apart structure for the southern Nenana Basin which is probably driven by a complex transpressional regime related to a dextral shear zone between the Denali Fault to the south and the Tintina fault to the north. The rift geometry of the sub-basin is mainly controlled by a series of north-northeast trending steep normal faults and thrust faults. The fault system forming the eastern margin of the basin, the Minto fault system, is interpreted to be a strike-slip duplex where the Minto Fault is a master left lateral strike-slip fault and subsidiary faults form an associated horsetail splay fault. The models further show that the internal geometry of the sub-basin varies greatly towards the flanks of the sub-basin, possibly in response to the deformation across other north-northeast trending sinistral strike-slip faults, some of which show inversion structures.

Complex convergent tectonics in southern Alaska leading to compressive stresses and active strike-slip faulting across basin-bounding fault systems probably resulted in distinct episodes of subsidence and uplift of basement block in the southern Nenana Basin.

Low gravity anomalies and high magnetic response suggest that the Paleozoic to Precambrian metamorphosed basement rocks include Late Cenozoic to Early Tertiary mafic intrusive bodies which may have further complicated the thermal regime of the southern Nenana Basin since Late Cretaceous time.

Our preliminary investigations have identified two stratigraphic intervals at depths greater than 5100 ft with the potential for CO2 sequestration via enhanced CBM production. Coal beds of the Miocene Usibelli Group are sub-bituminous in rank and have an average total thickness of 600 ft. Distinct phases of tectonic subsidence in the basin since Early Paleocene may have exposed the Usibelli Group coal beds to the temperatures above 200 °F favorable for late phase of biogenic methane and early phase of thermogenic methane production. Intermittent episodes of basin uplift may have formed migration pathways for generated methane to migrate into adjacent shallower coal reservoirs in the basin. Overlying lacustrine claystones from the Grubstake and Sanctuary Formations have the potential to provide seals.

Late Paleocene coal beds appear to have higher thermal maturity than the Miocene coals. These coals are exposed to the temperatures above 260 °F at the depths greater than 8110 ft and thus fall into the early gas window. Late Paleocene coal seams are thicker than those observed in the Usibelli Group, with a total average thickness of about 800 ft. These coals are sealed by Late Paleocene lacustrine claystones and shales. Large volumes of Late Paleocene coals at depth in the southern Nenana Basin could thus hold significant amounts of thermogenic coal bed methane.

Preliminary analyses suggest that the Late Paleocene coals of the southern Nenana Basin could sequester up to 2.708 billion metric tons of carbon dioxide; Oligocene to Miocene coals of the Usibelli Group could sequester 1.66 billion metric tons of carbon dioxide, with an overall capacity in the southern Nenana basin to sequester about 4.368 billion metric tons of CO_2. Note that this is just an estimate for the southern part of the basin; including the northern Nenana

basin, which is significantly deeper, would significantly increase this amount. The CO2 sequestration potential of the Nenana basin is thus significant, and could make a significant contribution to reducing green house gases emissions from a coal-to-liquids plant (CTL) or coal-fired power plant near Fairbanks, Interior Alaska.

Future work will focus on to refining geophysical and petrophysical models of the identified coal reservoirs of the southern Nenana Basin to accurately quantity their geologic CO_2 sequestration and coal bed methane generation potential. Future scope of this project includes:

- Examining different thermal history scenarios, uplift rates and timing of tectonic processes using geochronological techniques such as AFT and Ar-Ar analysis which would provide important constraints on the stages of evolution of the southern Nenana Basin through time.
- Refining existing geophysical models with newly obtained geochronological data and building a static reservoir model for coal reservoirs and cap rocks incorporating laboratory tested petrophysical properties of candidate coals, cap rocks, ground-water samples, carbon dioxide and coal bed methane.
- Conducting a sensitivity analysis on various reservoir modeling parameters to determine how each petrophysical parameter would most affect the CO_2 adsorption capacity of individual coal seams and flow of fluids such as CO_2, ground-water and coal bed methane in the subsurface
- Establishing an effective strategy for carbon dioxide injection and coal bed methane recovery from candidate coal seams to determine realistic estimate of total volumes of CO_2 that could be sequestered economically and total volumes of coal bed methane that could be recovered economically.

CHAPTER 3: EVALUATION OF CO2 SEQUESTRATION IN ALASKA WEST SAK RESERVOIR

by Vahid Nourpour Aghbash and Mohabbat Ahmadi

INTRODUCTION

Concentration of greenhouse gases in the atmosphere has increased since the industrial revolution (Inventory of U.S. Greenhouse Gas Emissions and Sink, 2012). This increase has amplified the greenhouse effect and is known to be responsible for global warming. Carbon Dioxide (CO_2) is one of the major greenhouse gases and is responsible for 83.6% of US greenhouse gas emission in 2012 (Inventory of U.S. Greenhouse Gas Emissions and Sink, 2012). Reducing the CO_2 sources and increasing the sinks are the possible CO_2 mitigation options. CO_2 sequestration is capturing CO_2 from the source/atmosphere and disposing it permanently (Bachu, 2000). Geological sequestration is the safest and the most attractive method for the long term sequestration due to the understood mechanism and developed technology. Following are the main geological basins which are known to be the most suitable for this purpose (Bachu, 2000):

- Storage in deep saline aquifers
- Injection into the mature oil field as enhanced oil recovery (EOR) agent
- Storage in depleted oil and gas reservoirs
- Storage in coal beds to recover Methane
- Storage in salt caverns

Among all these options, injecting CO_2 as an EOR agent has many advantages over the others (Bachu, 2000):

1. Increased oil recovery due to injecting CO_2 into the mature oil fields can compensate the CO_2 capture and sequestration costs.
2. Mechanisms of the enhanced oil recovery by CO_2 have been studied and field results have been reported in literature.
3. Existence of oil in the reservoir for millions of year demonstrates existence of a reliable and integrated cap rock, insuring no future leak.
4. Produced oil demonstrates existence of connected permeable pore volume for the CO_2 injection/sequestration.
5. Reservoir characterization data have been gathered during the reservoir development and can be used to manage the sequestration operations.
6. Injection wells, pipes and other infrastructures are available in the field site and can be used for CO_2 injection/sequestration.

CO_2 EOR AND SEQUESTRATION

Application of CO_2 as an EOR agent has been known for decades (Beeson and Ortloff, 1959; Holm, 1976; Wang and Locke, 1980; Goodrich, 1980; Brock and Bryan, 1989). Depending on the reservoir pressure, temperature and the oil composition, CO_2 – oil displacement can be miscible or immiscible. For specific oil at reservoir condition, when the pressure is above minimum miscibility pressure (MMP), CO_2 develops miscibility with oil upon multiple contacts. The residual oil saturation is decreased due to considerable reduction in interfacial tension

between oil and injectant. If the pressure is below MMP, miscibility is not developed, but CO_2 dissolves in the oil phase to some extent, depending on the pressure, temperature and oil composition. This dissolution decreases the oil viscosity and causes the oil swelling. The oil recovery is increased consequently (Beeson and Ortloff, 1959; Simon and Graue, 1965). In addition to increased oil recovery, CO_2 is also sequestered through this process. The sequestered CO_2 occupies the space previously filled with oil and also is partially dissolved in residual oil and water.

Because of low gas viscosity, mobility ratio is unfavorable resulting in low sweep efficiency and oil recovery. In practice, water slugs are injected alternatively with the CO_2 slugs to control the gas mobility and reduce viscous fingering and channeling (Caudle and Dyes, 1958). This is called water-alternating-gas (WAG) injection. The CO_2 dissolution in aqueous phase can be significant when the water saturation is high, e.g. WAG flooding (Enick and Klara, 1992; Chang et al. 1998; Yan and Stenby, 2009, 2010). Therefore, if CO_2 is injected through WAG process, a portion of CO_2 will also be dissolved and trapped in the water phase.

WEST SAK RESERVOIR

It is estimated that 15 to 25 billion barrels of viscous and heavy oil is accumulated in the shallow pools of Alaska North Slope (ANS) (Panda et al. 1989). Majority of this oil has deposited in West Sak and Schrader Bluff formations in the Kuparuk River Unit (KRU), Milne Point Unit (MPU), Nikaitchuq and the western Prudhoe Bay Unit. The West Sak reservoir in KPU, shown in Fig. 1, contains 7 to 9 billion barrels of original oil in place (OOIP) (McGuire et al., 2005). The reservoir layers are stratigraphic equivalent of Schrader Bluff formation, deposited in MPU, Nikaitchuq and the western Prudhoe Bay. It consists of inner shelf to shallow-marine or delta-front, late-cretaceous aged deposits. Reservoir interval consists of very fine- to fine-grain sized unconsolidated sandstones separated by layers of siltstone and mudstones (Werner, 1987). The poor consolidation causes large amount of sand production challenging the efficiency of the oil production. The West Sak interval is divided into two distinctive members, Upper and Lower West Sak. The Upper West Sak consists of two sand packages, sands D and B, each having 25 to 40 ft thickness. The Lower West Sak, sand A, consists mainly of thin-bedded sand layers (0.2-5 ft) with interbedded siltstone and mudstone forming amalgamated sand units of 10 ft thick. Gross thickness of the West Sak reservoir is about 700 ft in southwest area of KPU and it decreases to 350 ft in northeast area, making the average gross thickness of 450 ft (Werner, 1987). Net thickness of the reservoir interval is about 90 ft (Targac et al., 2005). Reservoir interval lies between 2400 ft subsea true vertical depth (SSTVD) in western areas of KPU to 3800 ft SSTVD in eastern areas. The permafrost is extended to about 1600 ft SSTVD in ANS area. Due to proximity of the permafrost, the reservoir temperature is relatively low, 45 to 100 °F depending on depth. Low reservoir temperature and oil degradation, in shallow parts of the reservoir, have made the oil very viscous (>300 cp). This high viscosity increases the difficulties associated with the oil production. Therefore, operators have determined the eastern and deeper part of the reservoir as West Sak Core Area (WSCA), shown in Fig. 2. It is estimated that the core area contains 2.5 billion barrels of OOIP with the viscosity of 20 to 100 cp in reservoir initial pressure and temperature of 1600 psia and 75 °F.

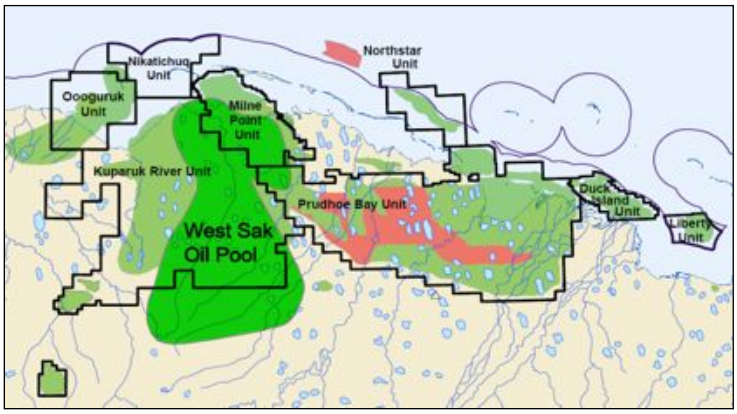

Fig. 1- Map of West Sak Oil Pool in Alaska North Slope
(Source: http://doa.alaska.gov/ogc/annual/current/annindex_current.html)

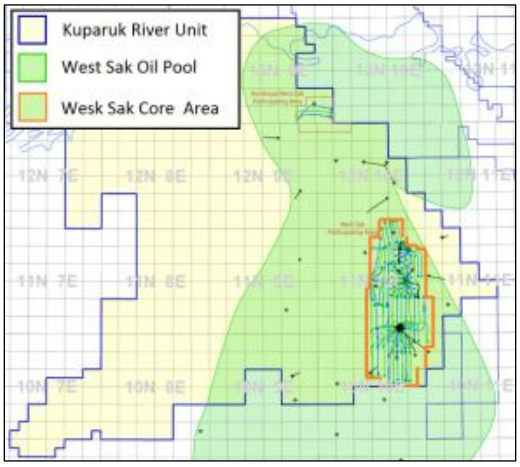

Fig. 2- Location of West Sak Core Area
(Source: http://doa.alaska.gov/ogc/annual/current/annindex_current.html)

WEST SAK DEVELOPMENT

The pilot project in West Sak KRU reservoir started in 1980's a decade after its discovery in 1971 (Targac et al., 2005). The project was implemented in DS-1J area due to better reservoir oil quality. 15 vertical wells were drilled in inverted nine spot pattern with five acre well spacing to inject water and produce oil from all three major West Sak sand packages, A, B and D. During the first two years, considerable amount of rock and fluid information was gathered and 900,000 barrels of oil was produced. Pilot project confirmed that the oil production is practical using tightly spaced waterflooding. After a decade, second phase of development started in 1997. DS-1D area was chosen considering availability of in site infrastructure which decreases the project cost. The project used similar well pattern; however, the well spacing increased from 5 to 40 acres. Because of low oil production rate, economic results were marginal. Horizontal and multi-lateral production wells were implemented in 1999 to boost the oil production rate. Lateral length of horizontal and multi-lateral wells increased to over 6000 ft. This increased oil recovery per well and decreased the cost of production. Horizontal injectors were also drilled in 2002. Initially, development was limited to sands D and B. Sand A was added to the development plan, but sand production problem initiated afterward. After evaluating different well designs,

dedicated laterals to sands D and B and undulating lateral in sand A2 were determined to be the optimum well design (Fig. 3).

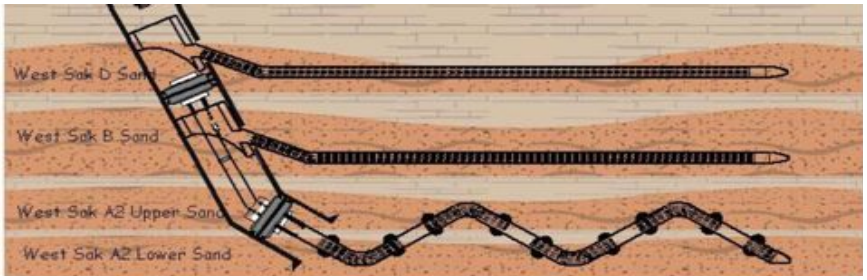

Fig. 3- Optimum Well Design in West Sak Reservoir (Targac et al., 2005)

McGuire et al. (2005) reported that estimated oil recovery from the West Sak is about 21% OOIP, after 30 year of waterflooding. This leaves a considerable amount of oil for the tertiary production phase. Injection of CO_2 into the reservoir is one of the options to increase the oil recovery. Khataniar et al. (1999) conducted slim tube and coreflood experiments using CO_2, Prudhoe Bay gas (PBG) and NGL enriched mixtures, to displace the Schrader Bluff oil. They reported that the CO_2 injection is an efficient method to increase the oil recovery. McGuire et al. (2005) evaluated the injection of enriched Methane, known as West Sak Viscosity Reduction Immiscible (VRI), into the reservoir and reported 3.5% OOIP increase in oil recovery. They also evaluated the injection of other VRI agents into the other viscous reservoirs, Schrader Bluff in MPU and Orion and Polaris in Prudhoe Bay. Ning et al. (2011) evaluated the injection of CO_2 and enriched CO_2 into a sample ANS viscous oil reservoir. They reported that injecting 30% hydrocarbon pore volume (HCPV) CO_2 into the reservoir increases the oil recovery by 10% OOIP. In this process oil viscosity decreases by 85%, from 122 cp to 18 cp. Injection of CO_2 into the West Sak can similarly increase the recovery over the waterflood recovery while a considerable amount of CO_2 is sequestered permanently.

Due to shallow depth of the reservoir and proximity to permafrost, reservoir temperature in WSCA is about 75 °F. Critical temperature of CO_2 is 87.9 °F; therefore, at reservoir temperature of 75 °F and initial reservoir pressure of 1600 psia, pure CO_2 will condense into liquid. Formation of three hydrocarbon phases, two liquid and one vapor, and even a solid phase, asphaltene, is reported in literature (Shelton and Yarborough, 1977; Orr et al., 1981; Henry and Metcalfe, 1983). Sharma (1990) reported that the mixture of 20 mol% West Sak oil and 80 mol% pure CO_2 forms three hydrocarbon (HC) phases, oil, CO_2-rich liquid and CO_2-rich vapor, in 1119.7 to 1214.7 psia pressure range. Different studies have evaluated the significance of accurate modeling of this complex phase behavior (Khan et al., 1992; Lim et al., 1992; Wang and Strycker, 2000; Guler et al., 2001). They reported that ignoring the second non-aqueous liquid phase, the CO_2-rich liquid, and including it in the gas phase can underestimate the oil recovery by up to 5% OOIP.

FLUID CHARACTERIZATION

Accurate modeling of the reservoir fluids is the most important factor in any compositional simulation study. The composition and properties of each phase is determined using an equation

of state (EOS). Due to uncertainties in the properties of the heavy components and interaction between different components, the property calculation of each phase using EOS bears some degree of uncertainty. Therefore, the properties of the heavy components and interaction parameters are regressed to tune the EOS by matching the laboratory results. Al-Meshari and McCain (2005) recommended a routine procedure to tune EOS. Sharma (1990) reported formation of L/L/V equilibrium for the CO_2 and West Sak oil mixtures. Therefore, the tuned EOS should be able to capture the phase boundaries. Khan et al. (1992) suggested a comprehensive procedure to tune the EOS capable of modeling L/L/V equilibriums. They verified the efficiency of the procedure by tuning EOS for different reservoir oils.

SIMULATOR DESCRIPTION

Currently the commercially available simulators are incapable of modeling the L/L/V equilibrium and four-phase flow simulation. UTCOMP, a three dimensional compositional simulator, is used for this study. UTCOMP is capable of handling four phases including: water, oil, gas and second hydrocarbon liquid phase. Chang (1990) provided a comprehensive description of the simulator. Here is a brief introduction.

UTCOMP conducts the Gibbs free energy test to determine the number of the phases. The flash calculations are then conducted to determine the composition of each phase. The Peng-Robinson (Peng and Robinson 1976) or modified version of the Redlich-Kwong (RKES) (Turek et al. 1984) are available as EOS options. Viscosity of the water is assigned as constant in input file and remains constant through the simulation. The viscosity values of oil, gas and second HC liquid phase are calculated using the Lohrenz correlation (Lohrenz et al. 1964). UTCOMP provides vertical and horizontal well options in which wells can be control by constant rate or constant bottom hole pressure.

METHODOLOGY

Porosity, permeability and water saturation data of the well WS1-01 was obtained from the well file Image database of Alaska Oil and Gas Conservation Commission (AOGCC). Stratigraphic Modified Lorenz (SML) plot of the West Sak was generated using the core data (Fig. 4). The results were used to define the flow units, the reservoir quality sand packs of D, B and A, and flow barriers, interbedded shale layers. 13 flow and barrier units and their corresponding thickness and average porosity values were calculated (Table 1). The porosity-permeability and porosity-water saturation cross plots were also generated (Figs. 5 and 6). The exponential trend lines were fitted to the data and the fitting equations were obtained.

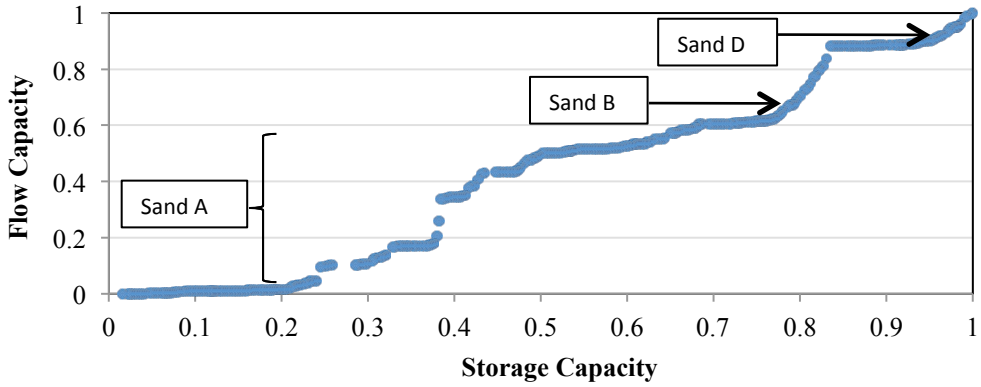

Fig. 4- SML of West Sak Well WS 1-01

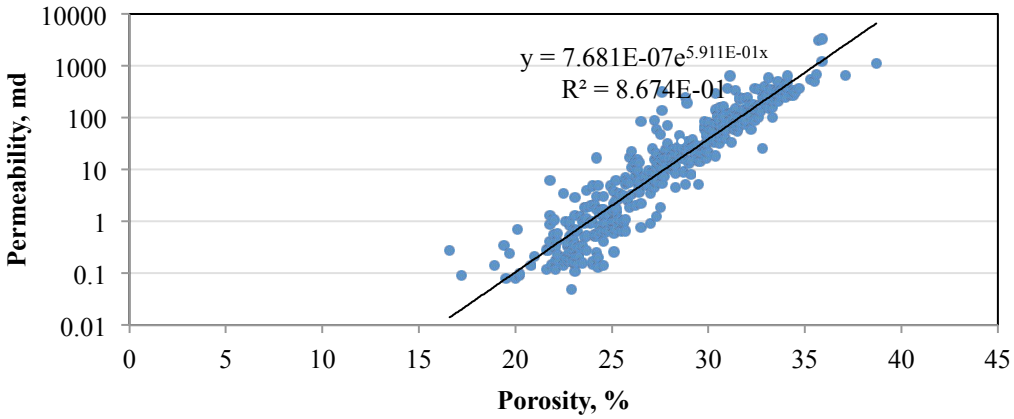

Fig. 5- Porosity – Permeability Cross Plot of Well WS1-01

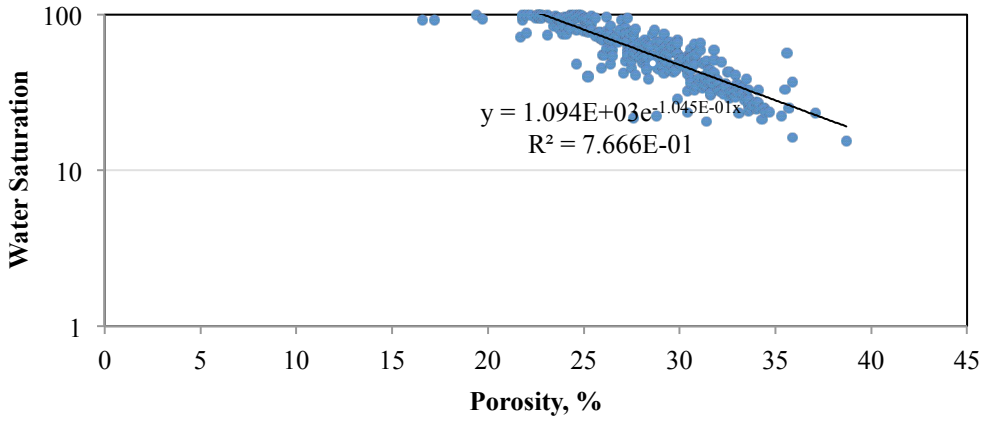

Fig. 6- Porosity – Water Saturation Cross Plot of Well WS1-01

TABLE 1: WEST SAK RESERVOIR PROPERTIES			
Layer Number	Thickness (ft)	Average Porosity	Sand Package
1	13	0.31	D
2	35	0.23	D
3	18	0.33	B
4	24.8	0.27	B
5	25.2	0.28	A
6	34.5	0.26	A
7	7	0.31	A
8	12.6	0.28	A
9	7.9	0.31	A
10	4	0.23	A
11	10	0.30	A
12	12	0.23	A
13	9.1	0.30	A

A homogenous model is not a good representative of the real reservoir and would also cause numerical anomalies in certain cases (NourpourAghbash and Ahmadi, 2012). Current heterogeneous model captures the variations in reservoir properties. The model is 1000, 1000, 213.1 ft in x, y and z directions. The grid size in x and y direction are assigned to be 50 ft so that it would be small enough to prevent numerical dispersion and large enough to decrease the total grid numbers and computational time. The porosity of each layer is populated using the normal random distribution function. Having the 3D porosity model built (Fig. 7), the obtained exponential equations are used to calculate the permeability and water saturation values for each grid (Figs. 8 and 9). The model does not necessarily capture all the real reservoir heterogeneity; however, it as representative as possible and prevents the possible numerical anomalies.

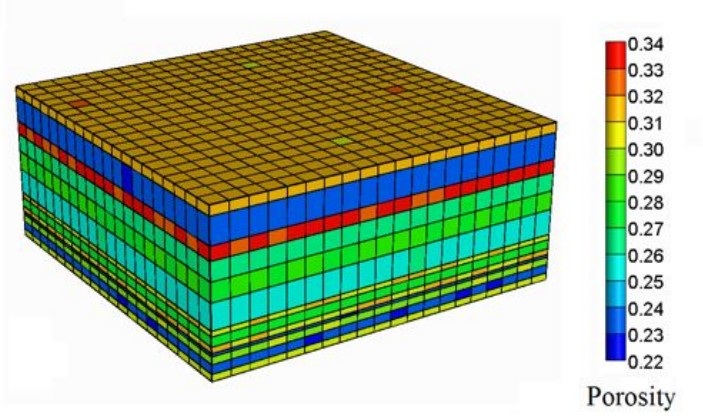

Fig. 7- Porosity Distribution of the Pattern Model

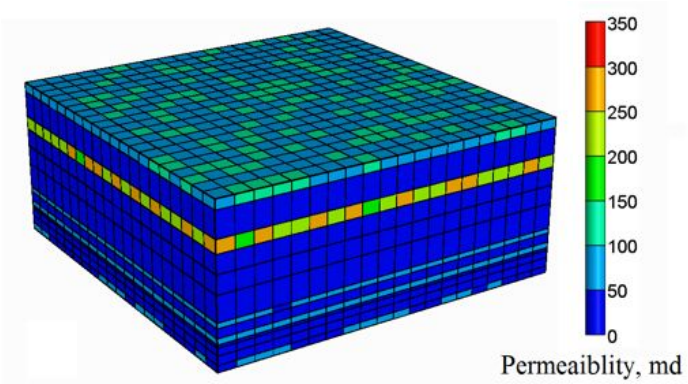

Fig. 8- Permeability Distribution of the Pattern Model

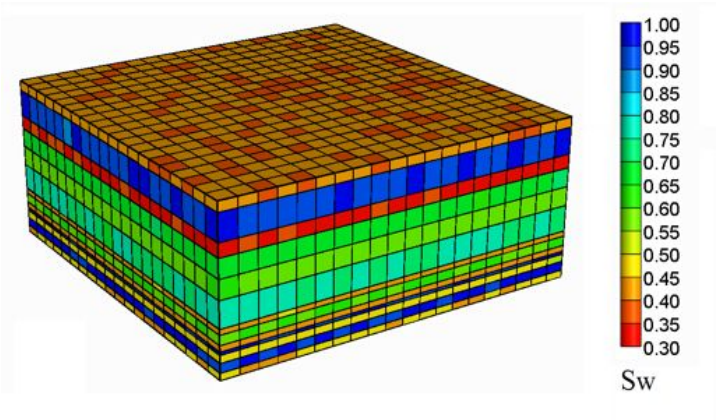

Fig. 9- Water Saturation Distribution of the Pattern Model

TUNING OF EOS

WinProp, the PVT package of CMG suite, was used to tune the EOS and build the reservoir fluid model. West Sak oil composition (Table 2) and the PVT tests results, including differential liberation (DL), constant composition expansion (CCE) and swelling test, were obtained from a previous study (Sharma, 1990). The computational time of the compositional simulation studies increases with increasing the number of components; therefore, it is always recommended to use the minimum number of the components. Since the West Sak oil contains very low amount (0.03 mol%) of N_2, it was neglected in favor of decreasing the computational time. CO_2 and intermediate components were kept to be used in evaluation of the injection of different mixtures. Peng-Robinson EOS was selected. C_{21+} fraction was split up to C_{45+} using gamma

splitting function. Twu correlation (Twu, 1984) option was used for calculation of the critical properties. Khan et al. (1992) recommended using three pseudo-components, when C_{7+} mole fraction is 0.4 to 0.6, to model the L/L/V equilibriums accurately. Therefore, C_7-C_{45+} components were lumped into three pseudo-components. DL test was simulated and results were compared to experimental values. P_c, T_c and acentric factor of pseudo components were selected as regression parameters to match the experimental oil saturation pressure, oil density, gas oil ratio, gas specific gravity and gas compressibility factor. In regression process, higher weight was assigned for the saturation pressure considering the significance of correct phase identification.

Sharma (1990) conducted swelling tests with 60 mol% and 80 mol% of CO_2. He reported that when 80 mol% of CO_2 is mixed with 20 mol% West Sak oil, L/L/V equilibrium forms in 1119.7 to 1214.7 psia pressure range. Binary interaction coefficients between CO_2 and other components were changed to match the experimental values for swelling test and L/L/V phase boundaries.

V_c of pseudo-components and Lohrenz correlation parameters were then selected as regression parameters to match the experimental values for oil and gas viscosities. Higher weight was given to oil viscosity due to its significance in simulation results. Considering the importance of the injected gas viscosity and density, the experimental values for the pure CO_2 were obtained from the National Institute of Standards and Technology database. V_c value of CO_2 was regressed to match the experimental viscosity values for pure CO_2 and CO_2 – oil mixtures.

Tables 3 - 5 show the tuned EOS parameters and coefficients of Lohrenz viscosity correlation. These parameters were used throughout this study. Figs. 10 – 13 show the results of DL test after the tuning. The EOS accurately simulates the experimental value for all oil and gas properties. However, predicted oil viscosity values at pressures below 500 psia deviate significantly from the experimental values. Since the pressure range of simulation model is 600 – 2500 psia, this poor match can be safely ignored. The simulated and experimental oil relative volumes for 80 mol% CO_2 and 20 mol% West Sak oil mixtures is shown in Fig. 14. The results show that the EOS is capable of modeling the oil swelling test. Fig. 15 shows the phase equilibriums for CO_2 and West Sak oil mixture at different pressures and CO_2 concentrations. The tuned EOS could be able to capture the reported L/L/V boundaries accurately. Fig. 15 shows that in operating pressure range of West Sak there are four different phase equilibrium conditions. The experimental and simulated values of CO_2 density and viscosity are plotted in Figs. 16 and 17.

TABLE 2: COMPOSITION OF THE WEST SAK OIL	
Component	Mol%
CO2	0.02
N2	0.03
C1	38.25
C2	0.86
C3	0.36
NC4	0.18
NC5	0.06
C6	0.20
C7	0.02
C8	0.01
C9	0.82
C10	1.50
C11	1.72
C12	1.35
C13	1.50
C14	1.80
C15	1.94
C16	1.80
C17	1.57
C18	1.80
C19	2.46
C20	2.83
C21+ (MW=455, SG=0.875)	38.95

TABLE 3: WEST SAK FLUID DESCRIPTION								
Component	Z	Pc (psia)	Tc (K)	Vc	MW	Acc Factor	Parachor	Vol Shift
CO2	0.000	1069.865	547.560	1.506	44.010	0.225	78.000	0.000
C1	0.382	667.196	343.080	1.586	16.043	0.008	77.000	0.000
C2	0.009	708.345	549.720	2.371	30.070	0.098	108.000	0.000
C3	0.004	615.760	665.640	3.252	44.097	0.152	150.300	0.000
NC4	0.002	551.098	765.360	4.085	58.124	0.193	189.900	0.000
NC5	0.001	489.375	845.280	4.870	72.151	0.251	231.500	0.000
FC6	0.002	477.030	913.500	5.510	86.000	0.275	250.100	0.000
C7-C17	0.140	333.875	1199.185	25.348	181.699	0.339	499.971	0.000
C18-C30	0.291	216.307	1307.185	31.999	326.686	0.639	803.632	0.000
C31+	0.170	128.131	1451.185	38.867	595.260	0.925	1088.620	0.000

TABLE 4: BINARY INTERACTION COEFFICIONTS										
	CO2	C1	C2	C3	NC4	NC5	FC6	C7-C17	C18-C30	C31+
CO2	0.0000									
C1	0.0500	0.0000								
C2	0.0700	0.0027	0.0000							
C3	0.0700	0.0085	0.0017	0.0000						
NC4	0.0700	0.0147	0.0049	0.0009	0.0000					
NC5	0.0700	0.0206	0.0086	0.0027	0.0005	0.0000				
FC6	0.0700	0.0253	0.0117	0.0046	0.0015	0.0003	0.0000			
C7-C17	0.1100	0.0598	0.0382	0.0244	0.0163	0.0111	0.0080	0.0000		
C18-C30	0.1100	0.0952	0.0684	0.0500	0.0382	0.0302	0.0251	0.0049	0.0000	
C31+	0.1500	0.1303	0.0998	0.0780	0.0636	0.0534	0.0467	0.0168	0.0036	0.0000

TABLE 5: COEFFICIENTS OF LOHRENZ VISCOSITY CORRELATION				
Coefficient 1	Coefficient 2	Coefficient 3	Coefficient 4	Coefficient 5
0.1006	0.0127	0.0588	-0.0277	0.0047

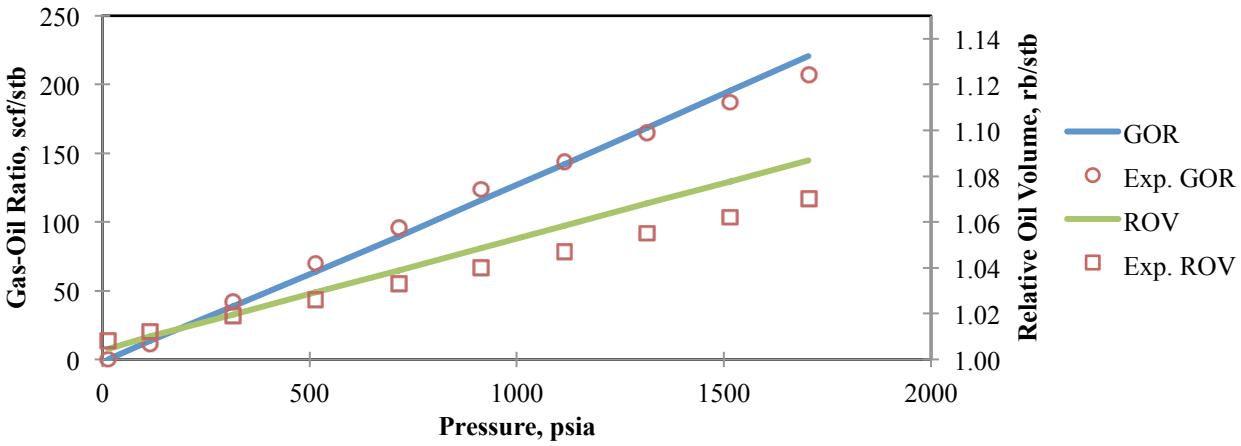

Fig. 10- Simulated and Experimental Gas Oil Ratio and Relative Oil Volume

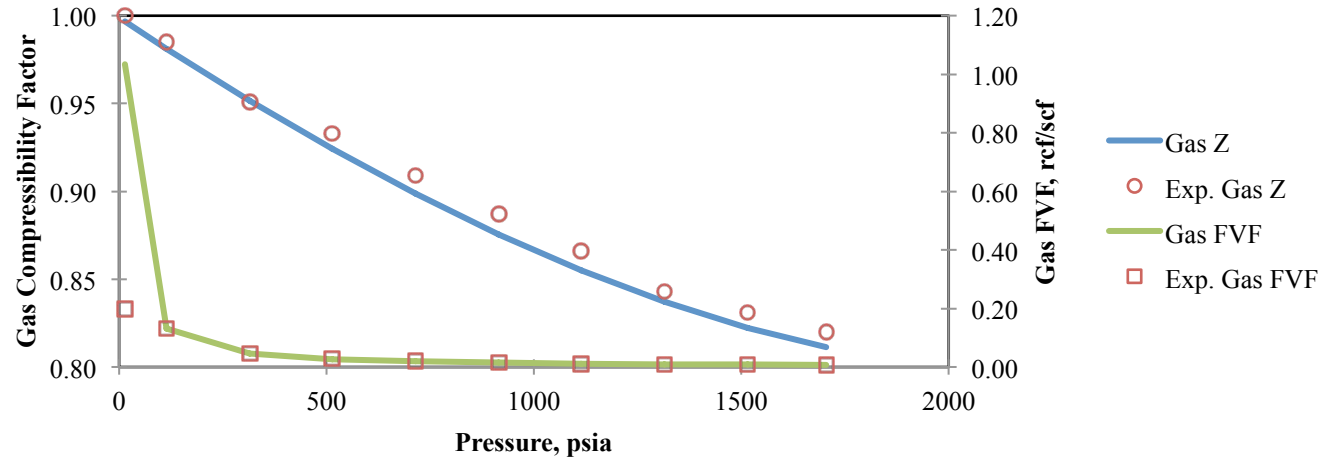

Fig. 11- Simulated and Experimental Gas Compressibility Factor and Gas Formation Volume Factor

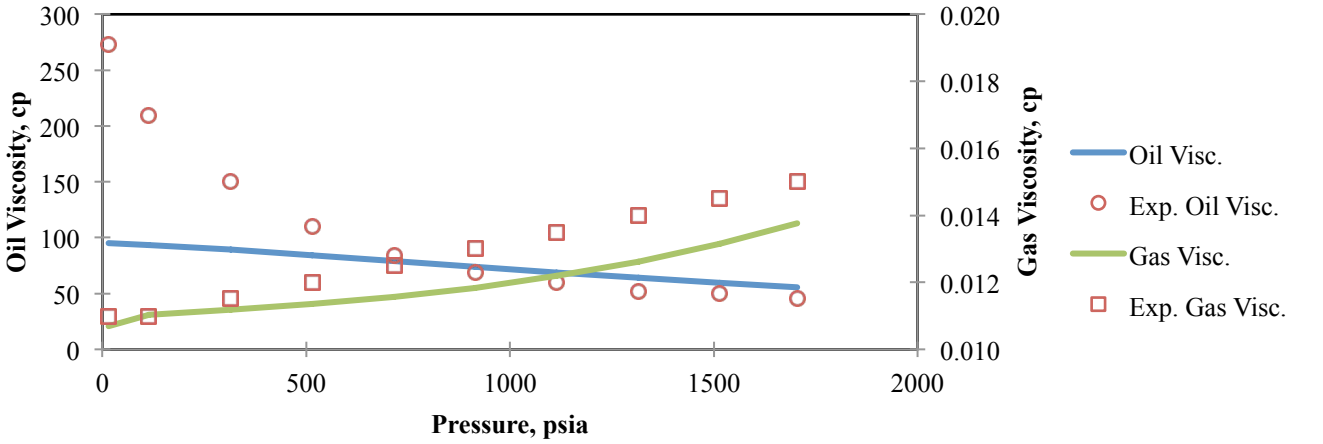

Fig. 12- Simulated and Experimental Oil and Gas Viscosity

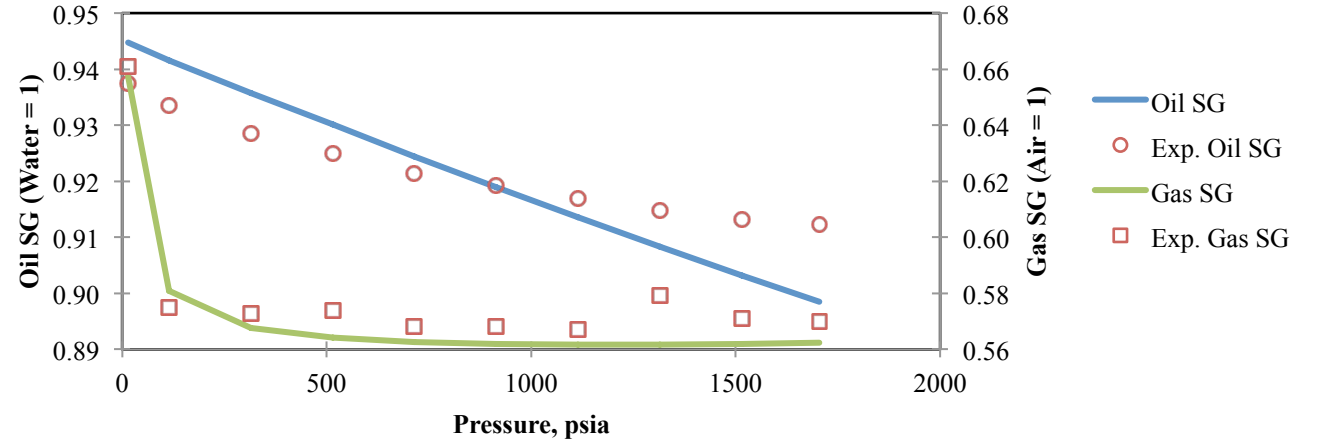

Fig. 13- Simulated and Experimental Oil and Gas Specific Gravity

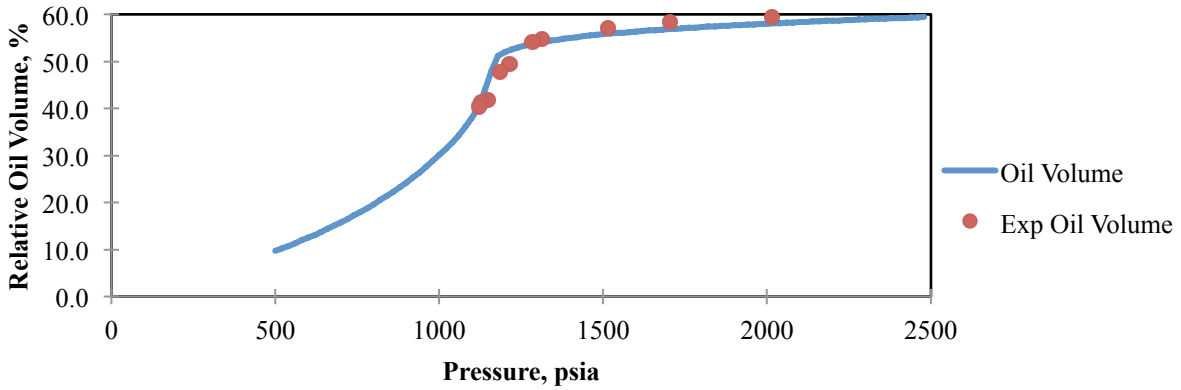

Fig. 14- Relative Oil Volume for 80 mol% CO_2 and 20 mol% West Sak Oil Mixture

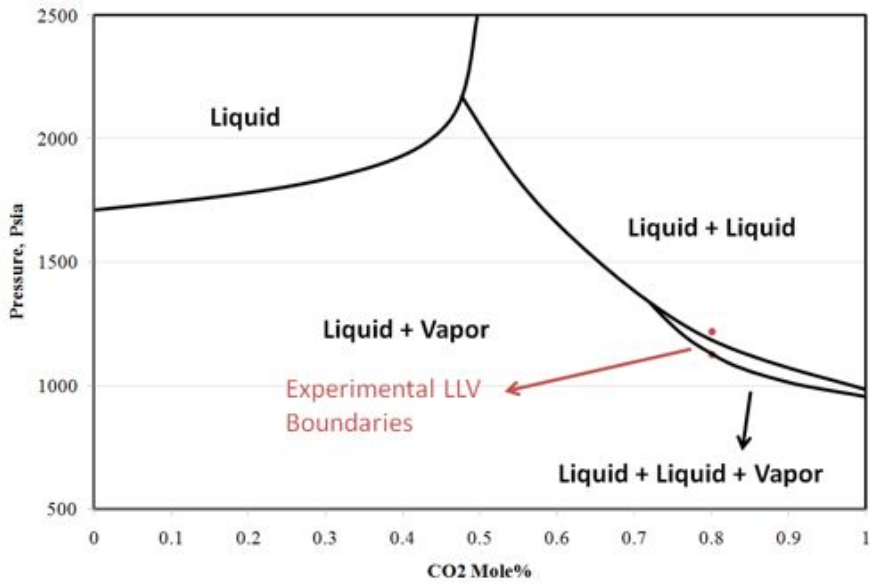

Fig. 15- Simulated and Experimental Phase Equilibriums

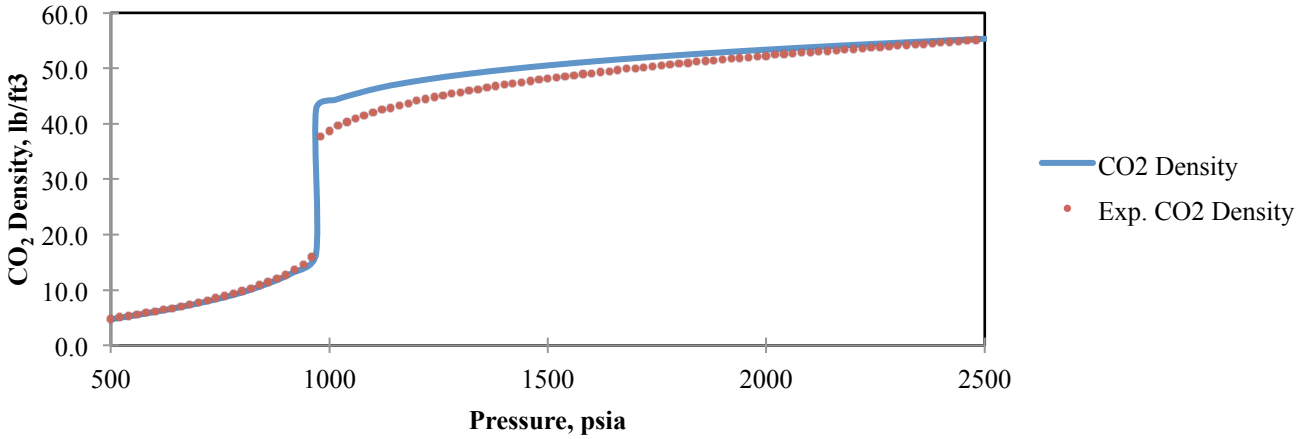

Fig. 16- Simulated and Experimental Density of Pure CO_2

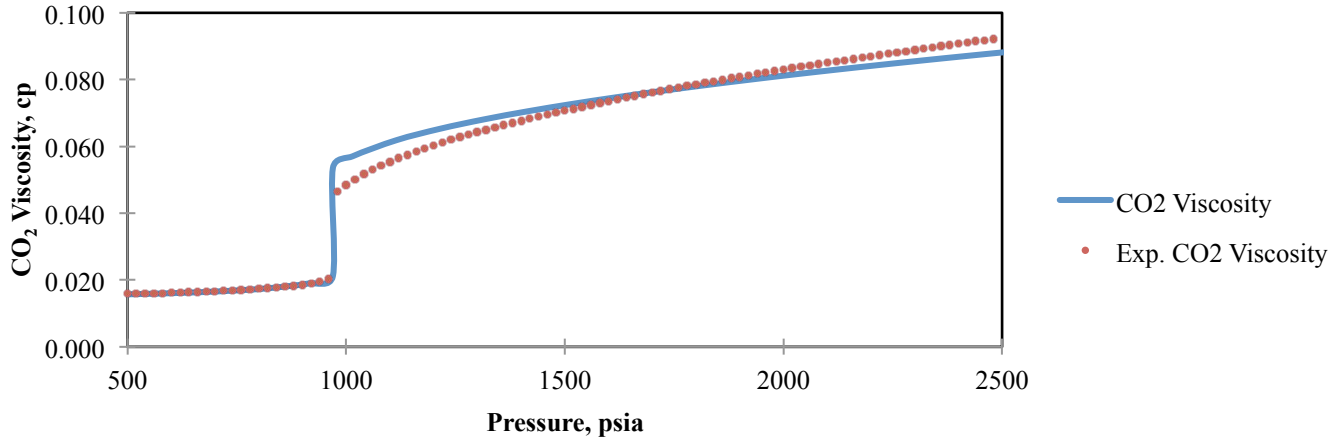

Fig. 17- Simulated and Experimental Viscosity of Pure CO_2

Sharma (1990) reported that mixing CO_2 with oil decreases oil viscosity by 75%. The EOS model could successfully capture this viscosity reduction (Fig. 18).

Comparing the experimental and simulated values verifies the accuracy and the efficiency of the tuning procedure in this study.

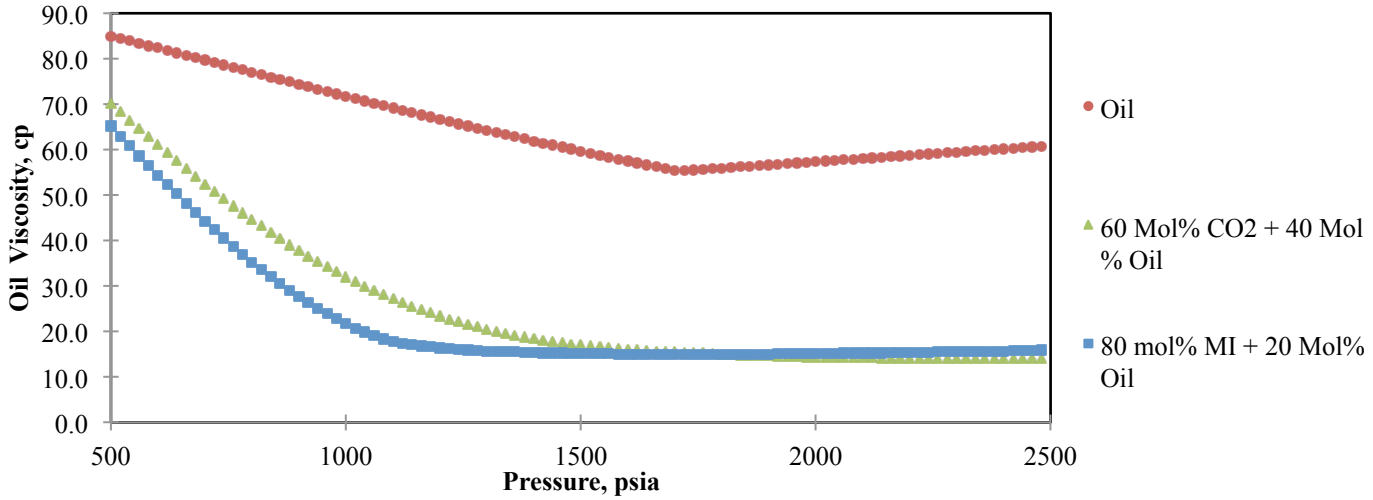

Fig. 18- Viscosity of Oil and CO_2-Oil mixtures

RELATIVE PERMEABILITY

Similar to West Sak oil, mixing Schrader Bluff oil and CO_2 forms three HC phases in certain pressures and CO_2 concentrations. Wang and Strycker (2000) conducted a slim tube test by flooding the Schrader Bluff oil with pure CO_2. They used different relative permeability models and compared the simulation results. They reported that modified Corey model gives the best match between experimental and simulated oil recovery. Therefore, modified Corey model was chosen in this study. The relative permeability parameters for water, oil and gas were obtained

from a previous study (Bakshi, 1991). Benson (2006) conducted a drainage test with liquid CO_2 and water in a sandstone (K=300md). Due to similar characteristics of this sandstone and West Sak sand packages, the Benson's test results were matched to obtain relative permeability parameters of second HC liquid phase. Table 6 includes all the relative permeability parameters used in this study.

TABLE 6 - RELATIVE PERMEABILITY SPECIFICATION			
Parameters of the Relative Permeability Model	Sand D	Sand B	Sand A
Residual Water Saturation (S_{wr})	0.35	0.33	0.44
Residual Oil Saturation for Water-Oil Flow(S_{orw})	0.4	0.37	0.24
Residual Oil Saturation for Gas-Oil Flow(S_{org})	0.4	0.33	0.28
Residual Gas Saturation (S_{gr})	0.1	0.1	0.1
Residual Second HC liquid Saturation for Water-2nd HC Liquid Flow (S_{4rw})	0.15	0.15	0.15
Residual Second HC liquid Saturation for Gas-2nd HC Liquid Flow (S_{4rg})	0.15	0.15	0.15
Water End-point Relative Permeability (K^0_{rw})	0.145	0.057	0.19
Oil End-point Relative Permeability (K^0_{ro})	1	1	1
Gas End-point Relative Permeability (K^0_{rg})	1	1	1
Second HC liquid End-point Relative Permeability (K^0_{r4})	0.4	0.4	0.4
Water Relative Permeability Exponent (e_w)	1.3	2	1.8
Oil Relative Permeability Exponent for Water-Oil Flow (e_{ow})	2	2.5	2
Oil Relative Permeability Exponent for Gas-Oil Flow (e_{og})	3	3	2.5
Gas Relative Permeability Exponent (e_g)	1.3	1	1.5
Second HC Liquid Relative Permeability Exponent for Water-2nd HC Liquid Flow (e_4)	3	3	3
Second HC Liquid Relative Permeability Exponent for Gas-2nd HC Liquid Flow (e_4)	3	3	3

One tri-lateral injection and one tri-lateral production well were defined. The laterals in sands D and B were defined to be horizontal, but the laterals in sand A2 were undulating. Fracture parting pressure was calculated by multiplying the depth, 3500 ft by assumed fracture parting gradient, 0.75 psi/ft. The injector was assigned to operate with constant bottom-hole pressure of 2500 psia, slightly below fracture parting pressure. Targac et al. (2005) reported that in West Sak the production wells operate with 1000 psi pressure drawdown. Therefore, in this study, production well was assigned to operate in constant bottom-hole pressure of 600 psia. In waterflooding case, 1 HCPV of water was injected. In base WAG case, first, 0.06 HPCV of CO_2 was injected with WAG ratio of 1 and slug sizes of 0.02 HCPV. Water is then injected for the total injection of 1 HCPV.

RESULTS AND DISCUSSION

CO_2 EOR and Sequestration

Waterflooding was simulated on the prepared pattern model. The oil recovery reached 14.1% OOIP after injecting 1 HCPV (Fig. 19). McGuire et al. (2005) reported that oil recovery due to waterflood will be about 21% OOIP after 30 years of water injection, but they did not report the total injected water volume. CO_2 WAG injection is then simulated on the model. CO_2 was dissolved into the oil and reduced the oil viscosity (Fig. 20). It decreased the residual oil saturation (Fig. 21) and improved the oil recovery by about 4.5% OOIP (equal to 112 million

barrels of oil in WSCA) (Fig. 19). In addition to increased oil recovery, 1300 MMSCF of CO_2 was also sequestered in the pattern model (Fig. 22). This corresponds to 0.104 tonnes of sequestered CO_2 per barrel of produced oil. On this basis, if the results of the pattern model are upscaled, it is estimated that 48 Megatonnes of CO_2 can be sequestered in the WSCA. The CO_2 – oil mixture formed L/V equilibriums in low pressure areas around the production well and formed L/L equilibrium in high pressure areas near the injection well. This mixture was then flooded with water, left the trapped gas phase near production well (Fig. 23) and trapped second HC liquid phase near injection well (Fig. 24).

Fig. 25 shows the CO_2 concentration in reservoir after injecting 1 HCPV of gas and water. It is clear that most of CO_2 is trapped in Sand D and B, due to better reservoir quality rocks. Some CO_2 is also sequestered in Sand A2. Figs. 26 – 28 show the CO_2 concentration in oil, gas and second HC liquid phases. More than half of the CO_2 is sequestered in trapped liquid form. 32% is trapped as dissolved CO_2 in the residual oil (Fig. 29). Very small amount, 3%, is sequestered as trapped gaseous CO_2. Dissolution of CO_2 was ignored in this case; therefore, no CO_2 was dissolved in the aqueous phase.

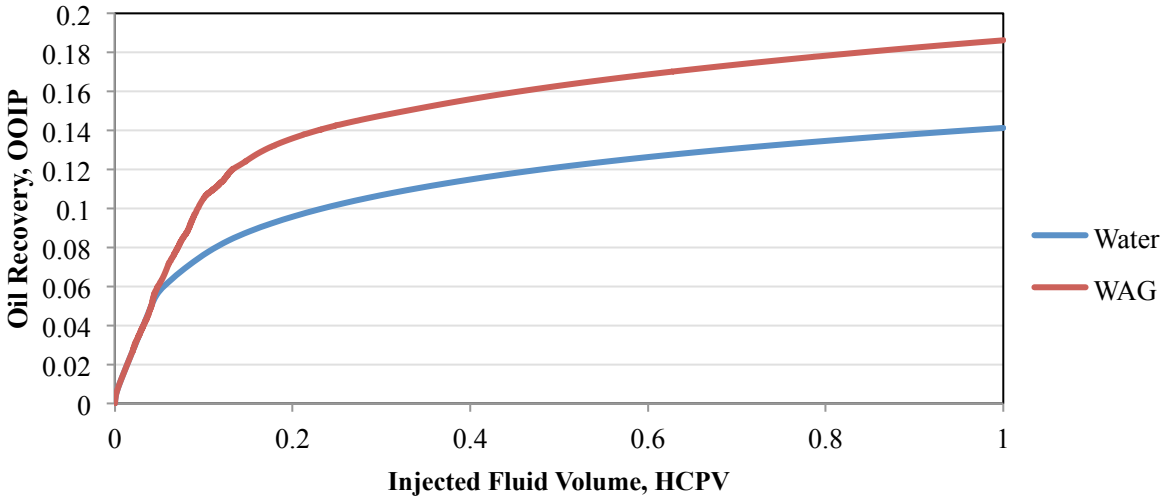

Fig. 19- Oil Recovery Due to Waterflooding and CO_2 Injection

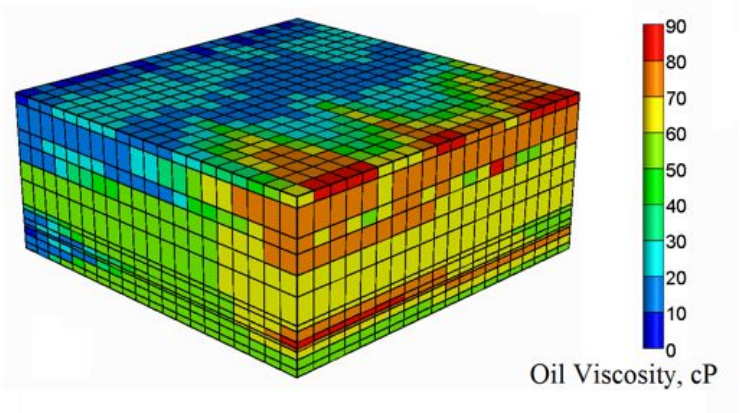

Fig. 20- Oil Viscosity after 1 HCPV CO_2 and Water Injection

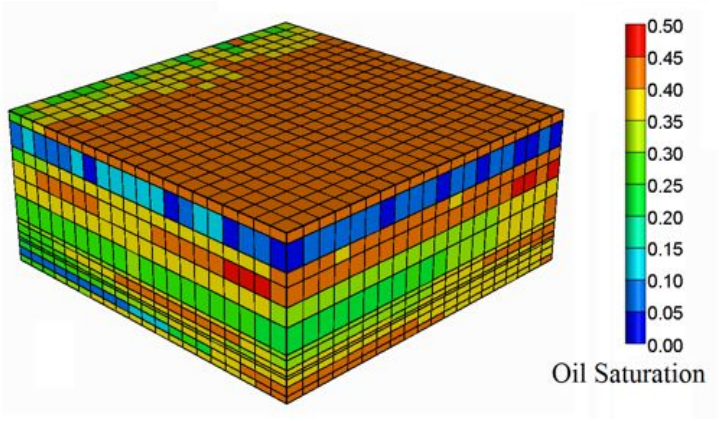

Fig. 21- Oil Saturation after 1 HCPV CO_2 and Water Injection

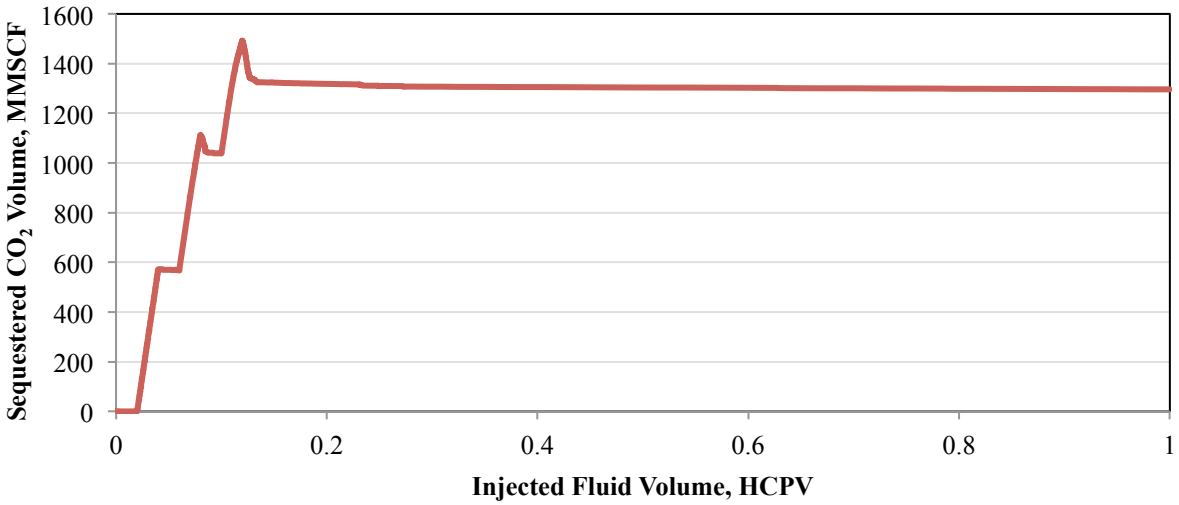

Fig. 22- Sequestered CO_2 Volume in the Pattern Model

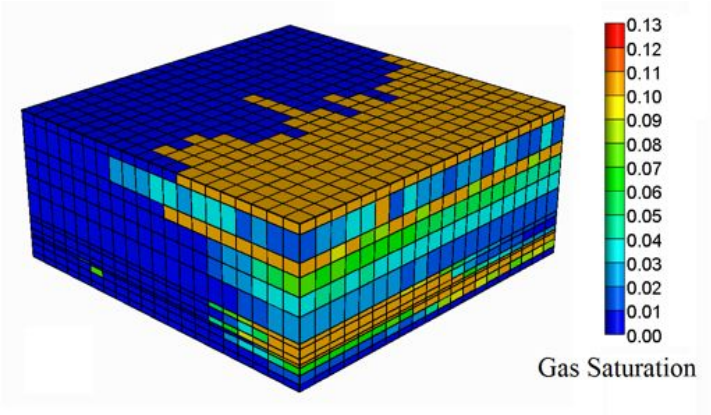

Fig. 23- Gas Saturation after 1 HCPV CO_2 and Water Injection

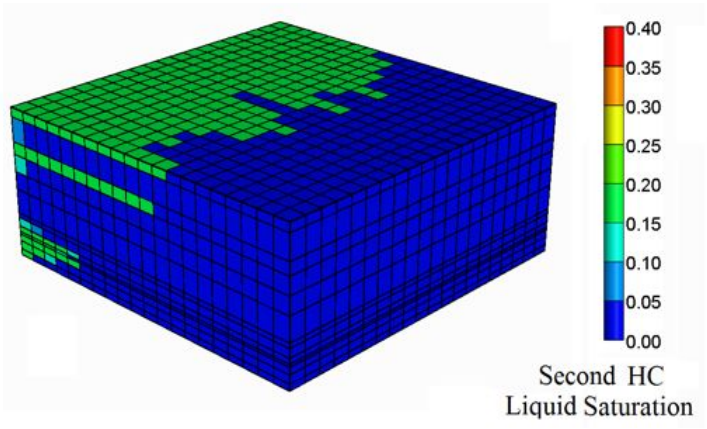

Fig. 24- Second HC Liquid Saturation after 1 HCPV CO_2 and Water Injection

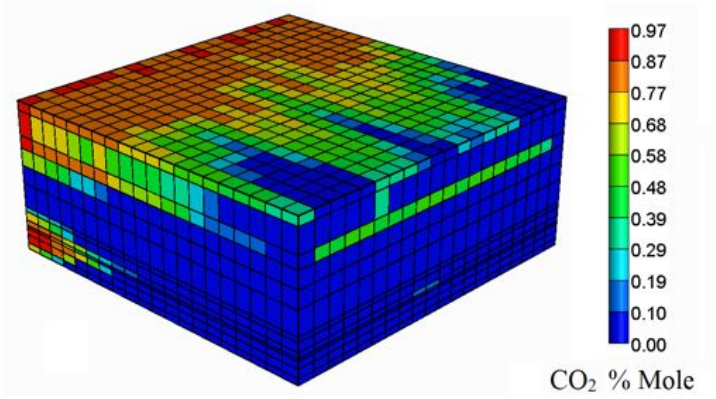

Fig. 25- CO_2 Concentration after 1 HCPV CO_2 and Water Injection

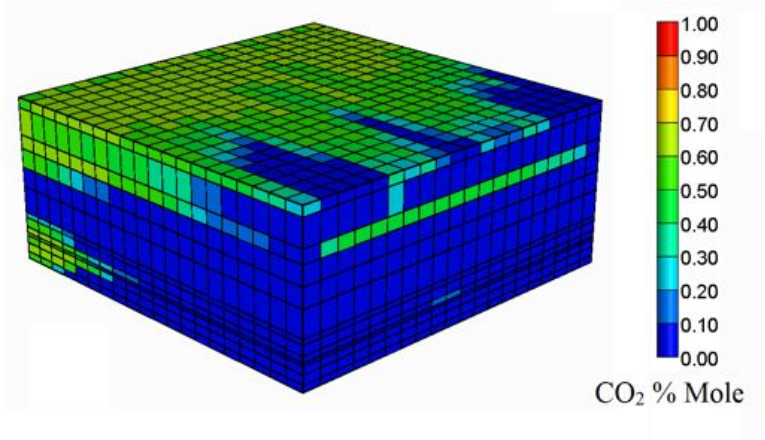

Fig. 26- CO_2 Concentration in Oil Phase after 1 HCPV CO_2 and Water Injection

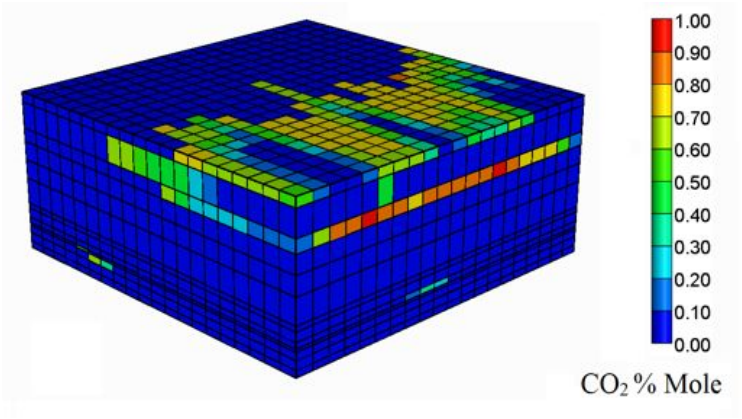

Fig. 27- CO_2 Concentration in Gas Phase after 1 HCPV CO_2 and Water

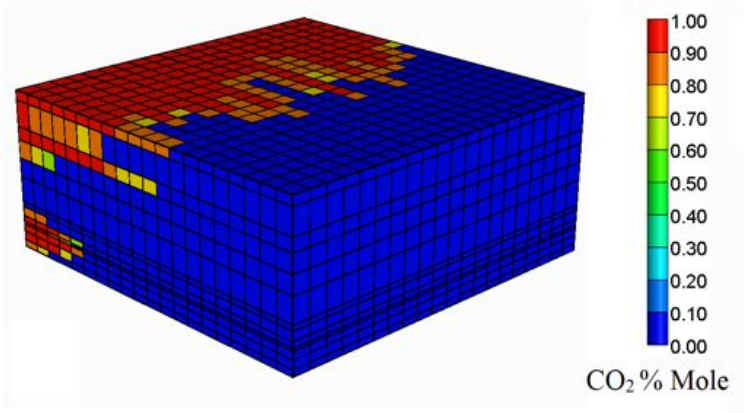

Fig. 28- CO_2 Concentration in Second HC Liquid Phase after 1 HCPV CO_2 and Water Injection

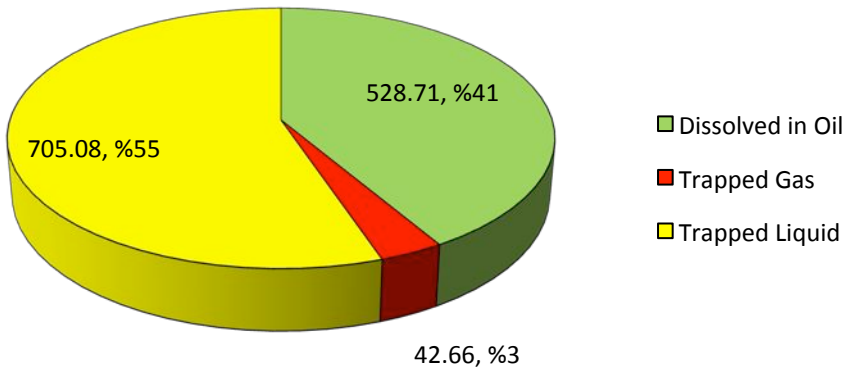

Fig. 29- Sequestered CO_2 Distribution in Different Reservoir Fluids

One of the major questions in this project was the significance of accurate modeling of L/L/V phase equilibrium. To address this question, another CO_2 WAG case was defined. In this case, two-phase flash calculation option was used instead of three-phase flash calculation. Total number of phases decreased to three by ignoring the second HC liquid phase. Fig. 30 shows that this simplification underestimates the oil recovery by about 0.8% OOIP. Sequestered CO_2 volume is also underestimated by 17% (Fig. 31). These results show that using the simulators that are unable to handle four phase flow, e.g. commercial simulators, can yield erroneous results while evaluation of CO_2 injection into low temperature viscous and heavy oil reservoirs.

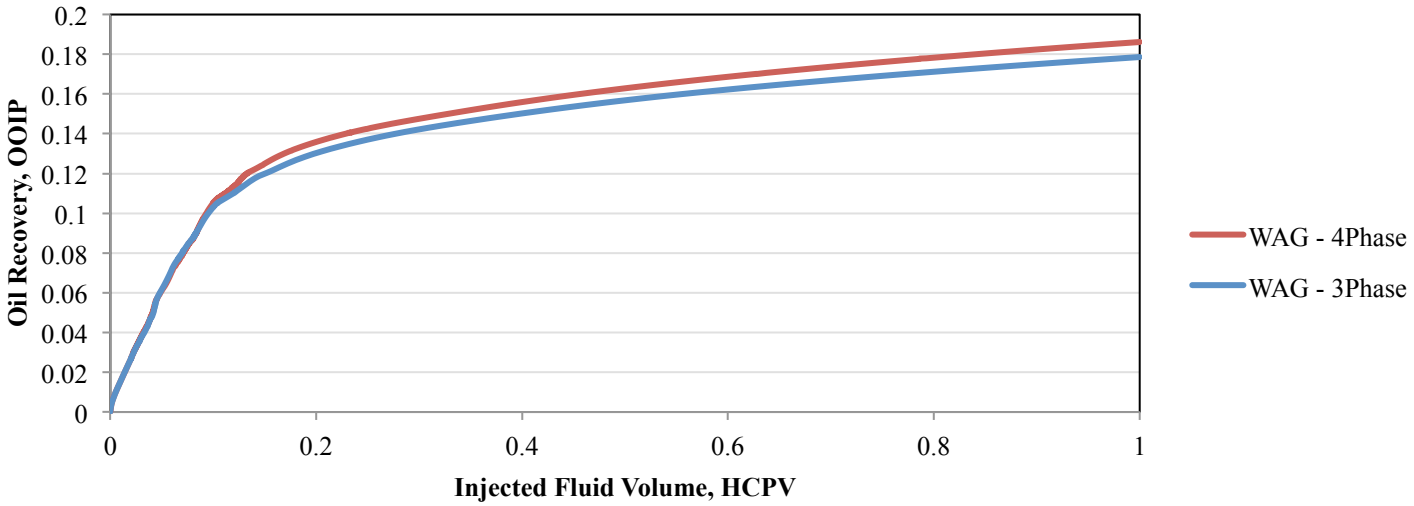

Fig. 30- Oil Recovery for Three and Four Phase Flow Simulation Cases

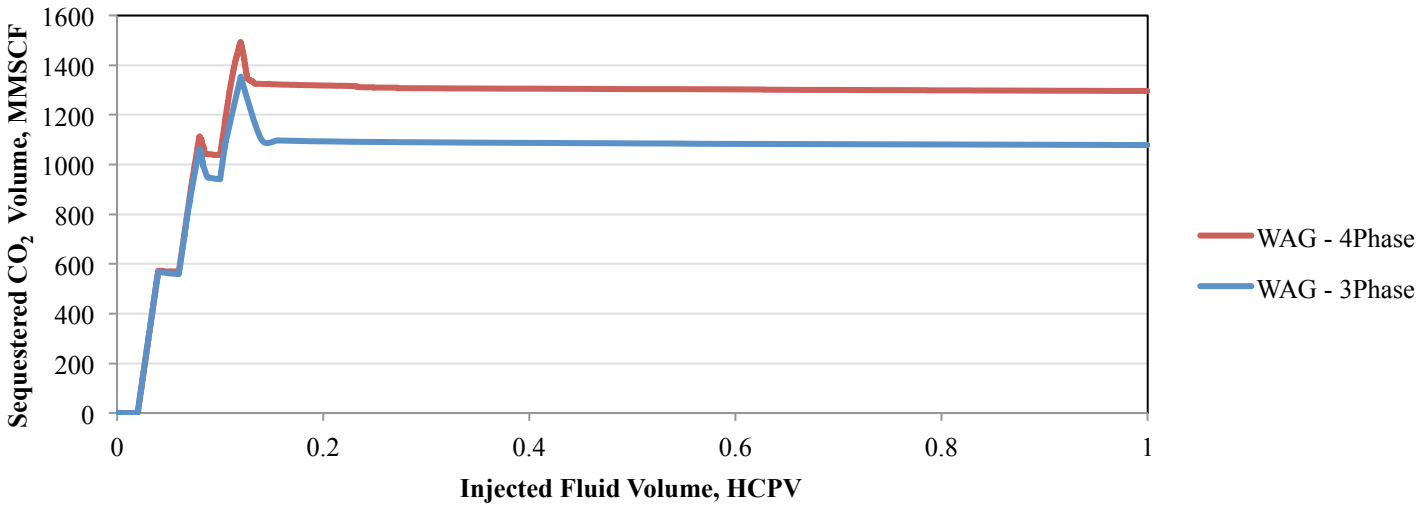

Fig. 31- Sequestered CO_2 Volume for Three and Four Phase Flow Simulation Cases

The effect of CO_2 dissolution in aqueous phase was evaluated. When the CO_2 dissolution keyword was included in the data file, computational time of simulation increased significantly. Therefore, it was decided to use a 2D Y-Z cross section model. CO_2 WAG process was simulated by injecting one CO_2 slug (0.02) HCPV followed by 0.08 HCPC water. A similar case was defined and CO_2 dissolution option was included in data file. Minimal change was observed in the oil recovery and sequestered CO_2 volume in the model (Figs. 32 and 33). The distribution of the sequestered CO_2 in different reservoir fluids, however, changed significantly after considering CO_2 dissolution in aqueous phase (Fig. 34). The results show that this option can be safely ignored as we are interested in the oil recovery and sequestered CO_2 volumes.

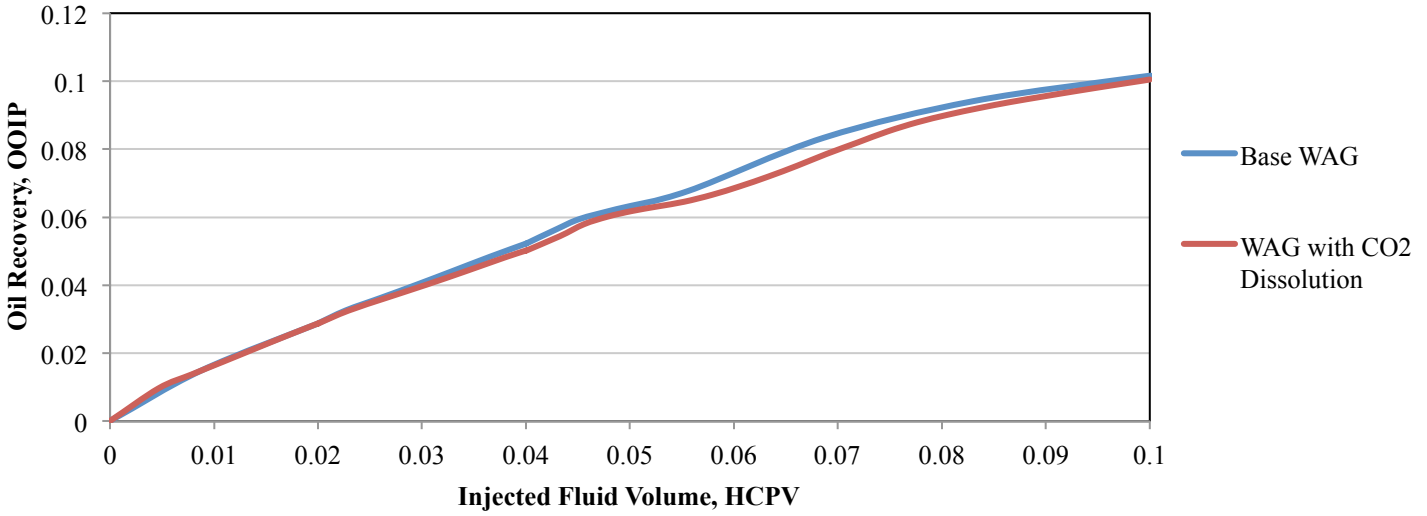

Fig. 32- Effect of CO_2 Aqueous Dissolution Option on Oil Recovery

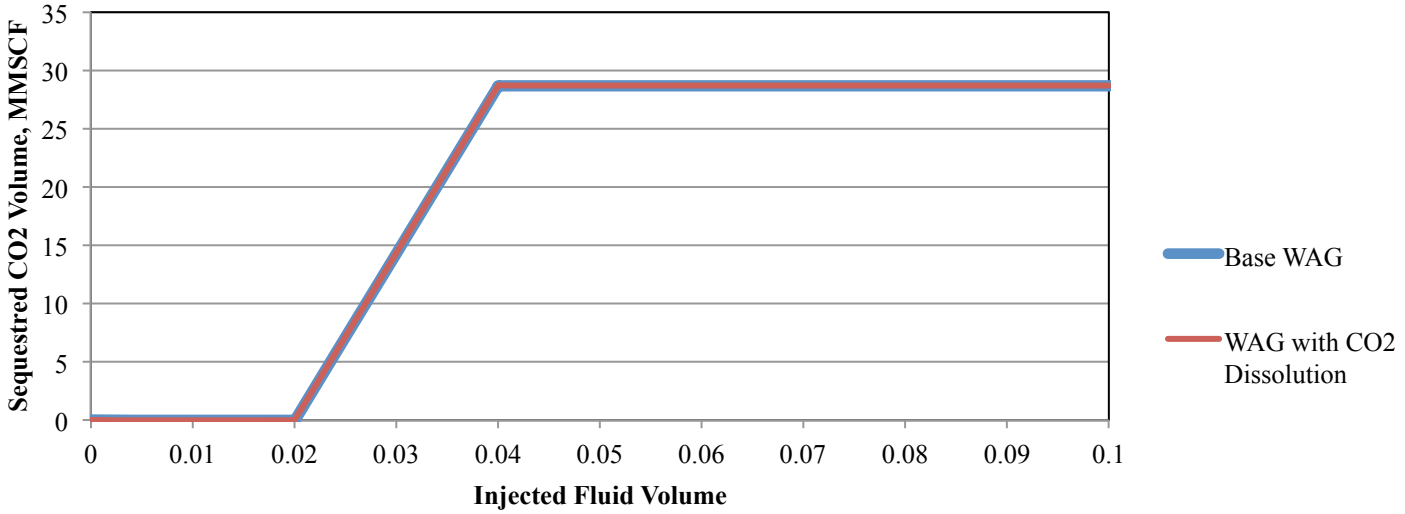

Fig. 33- Effect of CO_2 Aqueous Dissolution on Sequestered CO_2 Volume

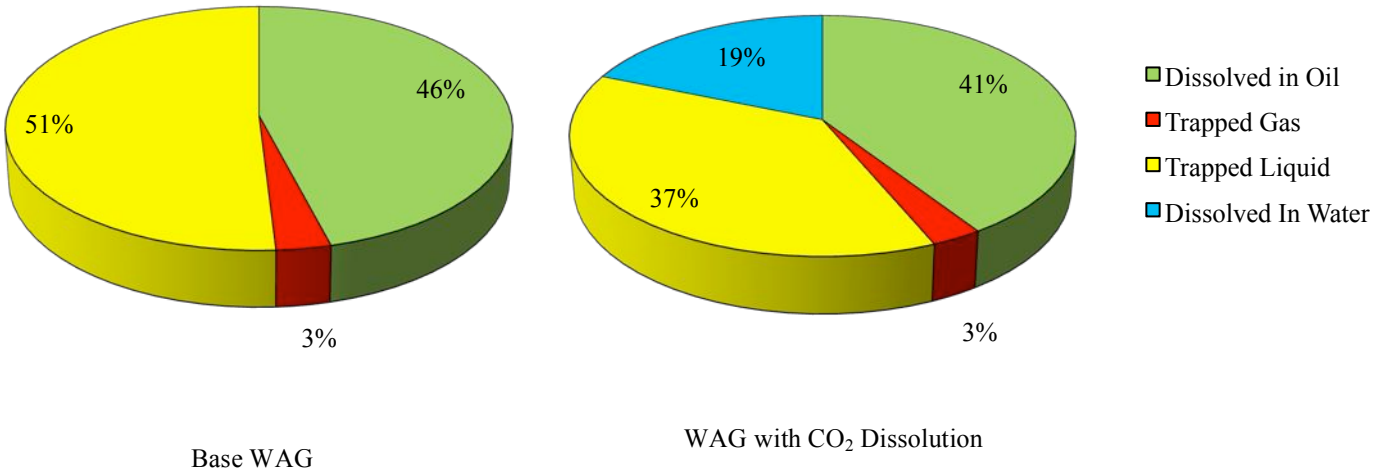

Fig. 34- Effect of CO_2 Aqueous Dissolution on Sequestered CO_2 Distribution

It is a common practice to mix methane or CO_2 with NGL to enrich them with intermediate components. This can enhance the viscosity reduction and oil swelling mechanisms leading to increasing the oil recovery. However, the NGL mixtures are expensive and the cost of the enrichment should be considered. It also can decrease the sequestered CO_2 volume as trapped gas/liquid will include other components. The average composition of Prudhoe Bay MI (McGuire and Morits, 1992) (Table 7) was used to mix with CO_2. The enrichment changed the boundaries of phase equilibrium for the MI and oil mixture (Fig. 35). 10%, 25%, and 50% of the MI and CO_2 mixtures are injected into the 3D pattern model. Slight changes in oil recovery were observed, but sequestered CO_2 volume decreased significantly (Figs. 36 and 37). The results show that enrichment of CO_2 is not an efficient option in the West Sak reservoir. It decreases the sequestered CO_2 volume without significant increase in oil recovery. It also increases the cost.

Table 7- AVERAGE CENTRAL GAS FACILITY MI COMPOSITION

Components	CO2	C1	C2	C3	NC4
Z	0.2115	0.3344	0.1978	0.2152	0.0404

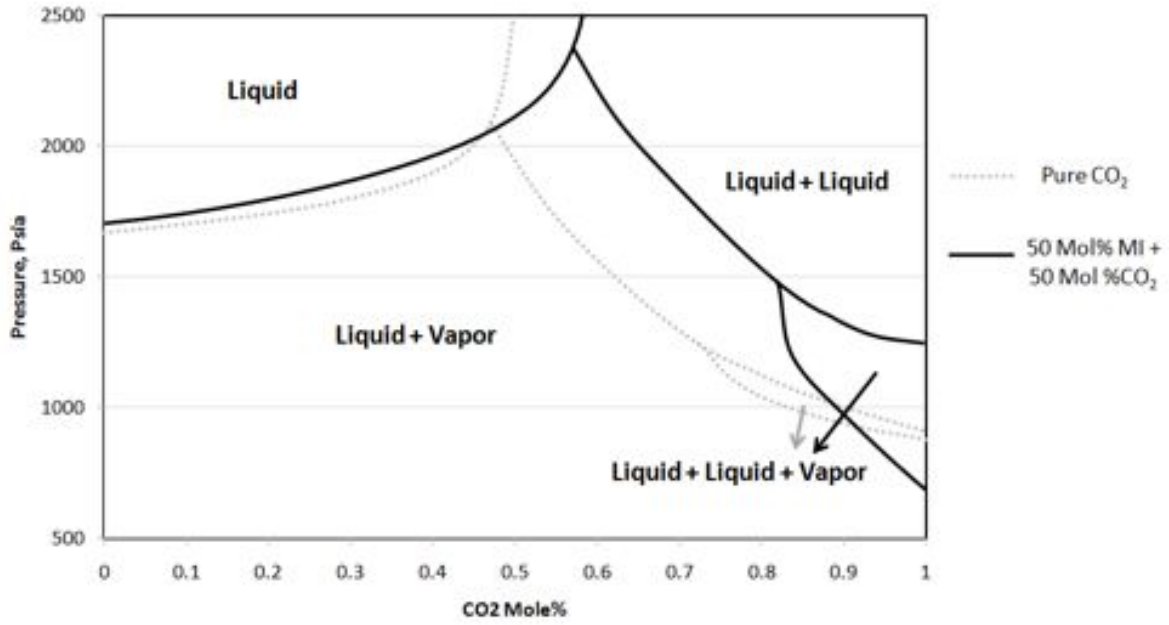

Fig. 35- Effect of Enrichment on the Phase Equilibrium Boundaries

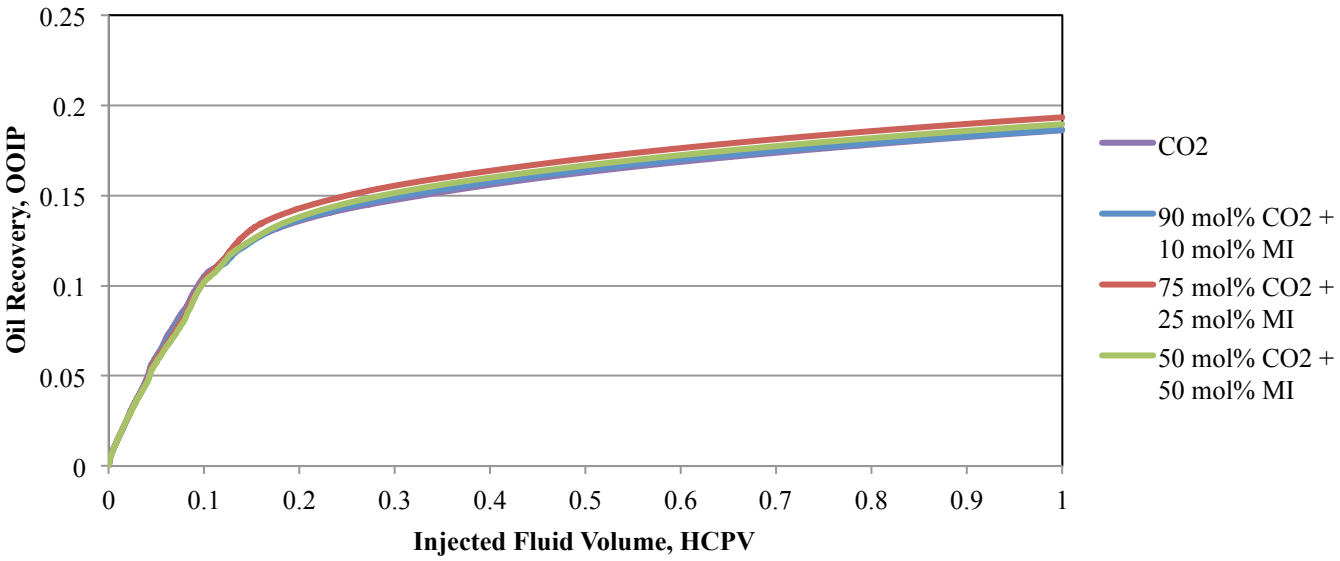

Fig. 36- Effect of Enrichment on the Oil Recovery

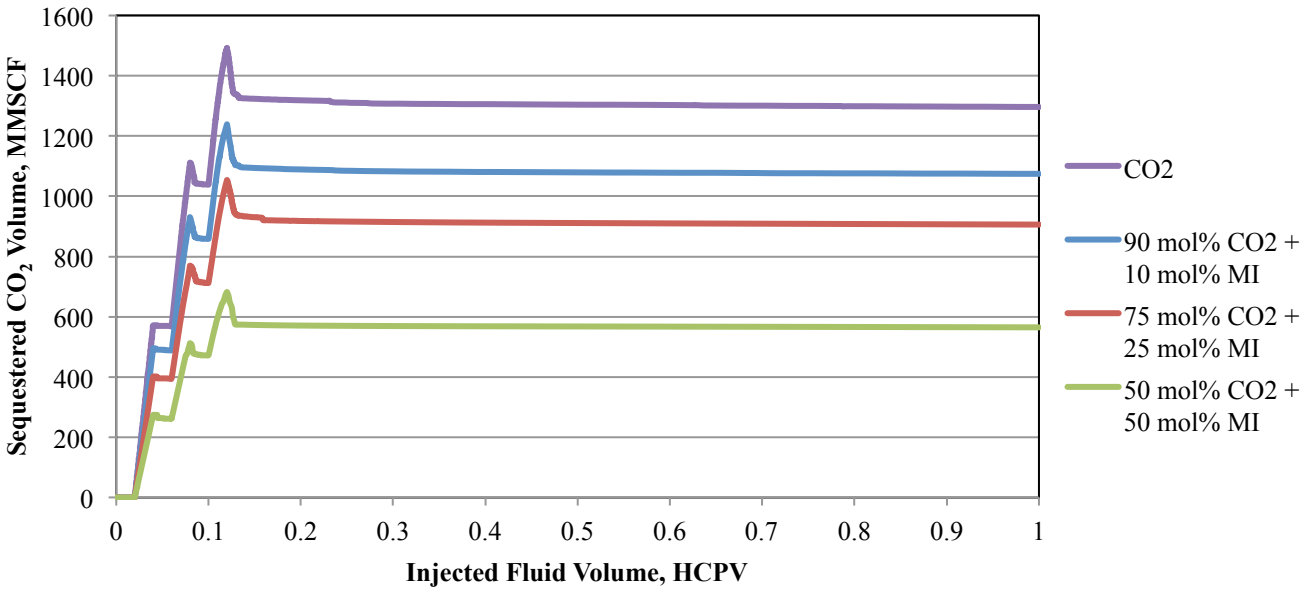

Fig. 37- Effect of Enrichment on the Sequestered CO_2 Volume

The sensitivity of the simulation results to the WAG ratio and slug size was also evaluated. Table 8 shows the WAG parameters for the defined cases. The oil recovery values were affected slightly by changing these parameters (Fig. 38). Sequestered CO_2 volumes are slightly higher for the cases with 0.02 HCPV (Fig. 39) and showing that small slugs can increase sequestered CO_2 volume slightly.

Table 8- WAG FLOODING PARAMETERS

Case Number	WAG ratio	Slug size (HCPV)
1	0.5	0.02
2	1	0.02
3	2	0.02
4	0.5	0.03
5	1	0.03
6	2	0.03

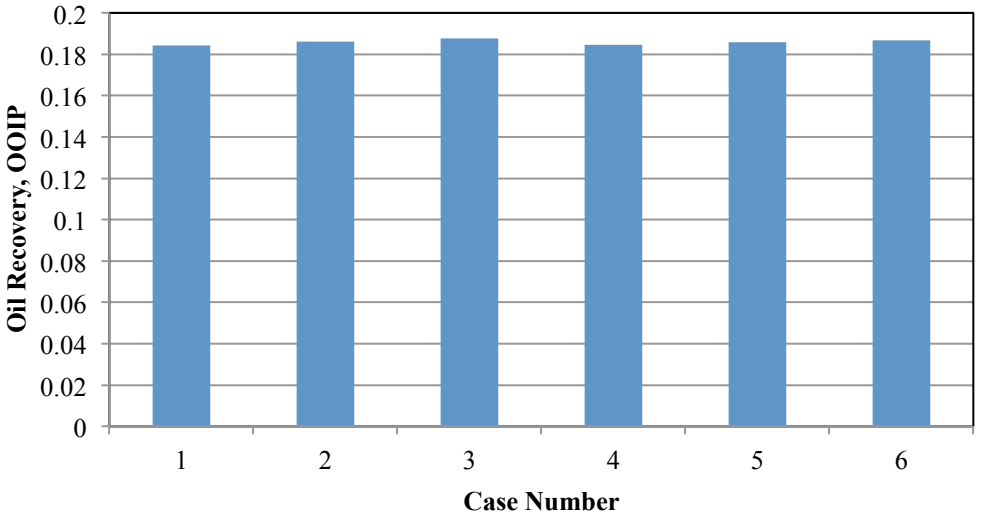

Fig. 38- Effect of WAG Parameters on the Oil Recovery

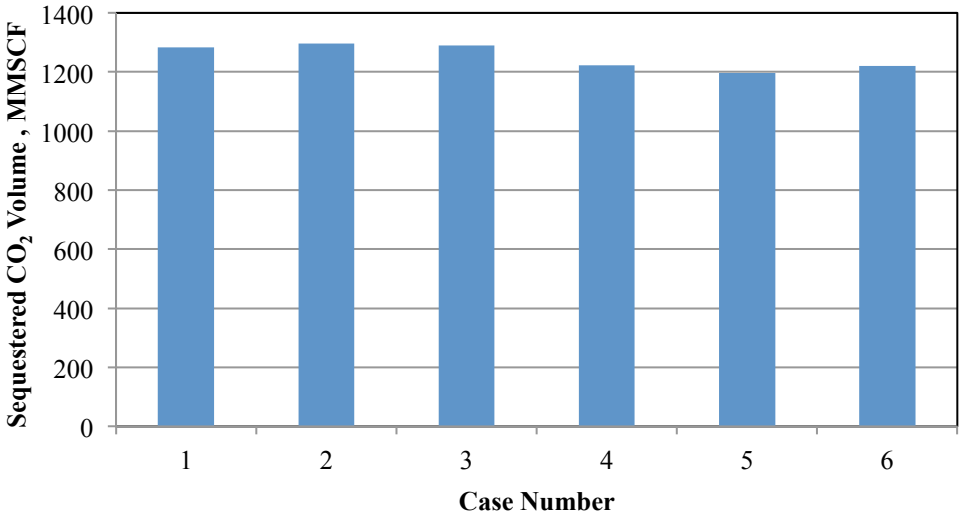

Fig. 39- Effect of WAG Parameters on the Sequestered CO_2 Volume

CONCLUSIONS

- Waterflood recovers 14.1% OOIP in West Sak and CO_2 injection increases it by 4.5% OOIP (112 million barrels).
- It is estimated that the 48 megatonnes of CO_2 can be sequestered in the West Sak Core area
- A simulator capable of handling four-phase flow is required for accurate evaluation of CO_2 sequestration in West Sak. Using commercial simulators which are incapable of handling four-phase flow can yield to erroneous results for oil recovery and sequestered CO_2 volumes.
- Ignoring the CO_2 dissolution in aqueous phase does not change the oil recovery and sequestered CO_2 volume. However, it changes the distribution of sequestered CO_2 in different phases.
- Enrichment of CO_2 by NGL is not an efficient option in West Sak reservoir. It decreases sequestered CO_2 volume without significant increase in oil recovery.
- Slug size and WAG ratio have minimal effect on the oil recovery. Sequestered CO_2 volume, however, slightly increases with decreasing slug sizes.

CHAPTER 4: BIOMASS PRODUCTION AND CARBON SEQUESTRATION OF SHORT ROTATION COPPICE CROPS IN ALASKA[1].

by W. Schnabel, A Byrd and S. Sparrow

INTRODUCTION

The use of biomass as a feedstock has been identified as a means to reduce gross CO_2 emissions from power plants. In states where trials have been conducted on the use of biomass as a fuel feedstock alongside coal, growth rates of short rotation woody biomass have been studied and quantified. In Alaska, scant data exist on the growth rates of biomass as a sustainable fuel source. The goal of this project was to collect growth rate and, where possible, carbon sequestration data on existing plots of Alaskan tree species considered to be promising as short rotation biomass crops. Such data would benefit not only the planners of large co-fired power facilities, but also residents of small Alaskan communities seeking alternatives to fuel oil as a heat source.

Many Alaskan energy planners seek to offset the rising monetary and environmental costs of fossil fuels for heat and power. In remote off-road communities, the monetary costs are rising particularly quickly due not only to the price of the fuel itself, but also to the costs associated with transportation of the fuel (Alaska Department of Commerce Community and Economic Development, 2012; Alaska Energy Authority, 2010). In larger communities, there is an interest in utilizing biomass as a way to mitigate the environmental costs of fossil fuels in large power facilities. Thus, there is interest throughout a broad range of Alaska communities to evaluate the feasibility of biomass as a feedstock. For communities with a local and sustainable source of wood, biomass may be a feasible option as an alternative or supplementary source. While standing forest biomass has been extensively studied in Alaska, yields of Alaskan woody species grown as short rotation coppice (SRC) crops have not been well studied (Garber-Slaght et al., 2009). However, in some instances, SRC may be a better option than forest biomass due to the proximity of available cropping space or lack of proximal forest biomass. In order to evaluate the potential of SRC in a given area, planners need to understand the growth rates of the woody species, optimum harvesting frequencies, and the annual energy yield of an SRC stand.

Trees belonging to the genus *Populus* (e.g., poplar, cottonwood) represent promising Alaskan SRC species due to their relative high growth rates, ease of propagation, distribution throughout the state, and successful use as SRC crops in other locations. Studies describing the SRC potential of poplar are abundant in the scientific literature, including reports of successful plantations in Sweden, Belgium, USA, Canada, and India (Karacic et al., 2003, Laureysens et al., 2005b, Felix et al., 2008, Ajit et al., 2011, Peichl et al., 2006). While there has not been extensive research in Alaska, biomass estimation models have been undertaken in Scandinavia at latitudes similar to those in Alaska (Telenius, 1999, Johansson and Karacic, 2011).

[1] *This chapter is based upon data presented in the MS thesis currently in the final phases of completion by University of Alaska Fairbanks graduate student Amanda Byrd. The data will serve as the basis for a peer-reviewed publication to be completed following submission of the thesis*

Allometric equations are frequently used to determine tree biomass from easily-measured parameters such as diameter at 30cm (D30) and diameter at breast height (DBH). These equations are derived by correlating a readily-measured parameter (e.g., DBH) to the dry weight of the same sampled tree or stem (Yarie and Mead, 1988, Arevalo et al., 2007). A strong allometric relationship (ie, r^2 values approaching 1.0), can result in a cost effective measurement technique for estimating standing biomass (Ballard et al., 2000). Thus, allometric equations can be a useful tool for estimating growth rates of a woody crop being actively managed, and provide information necessary for determining harvest rotations (Tahvanainen, 1996). Published allometric equations for poplars and other short rotation species have historically been developed for different species and hybrids at lower latitudes e.g. (Zianis and Mencuccini, 2004, Felix et al., 2008). While allometric equations for Alaskan poplars grown as SRC crops are not currently available, such equations have been developed for natural stands of Alaskan poplars (Yarie et al, 2007).

OBJECTIVES

As indicated above, the overall goal of the study was to collect data to inform consideration of SRC crops as a biomass fuel source in Alaska. In order to achieve this goal, we performed an intensive study on an existing research plantation in Southcentral Alaska. In so doing, we were able to leverage existing infrastructure and published data to the project's advantage. The specific objectives of the project were:

1) Measure the aboveground biomass and develop allometric equations specific to an existing stand of *P. balsamifera* (balsam poplar) grown over a seven-year period in a managed Southcentral Alaska plantation.
2) Measure the biomass accumulation of *P. balsamifera* managed as an SRC under a two-year rotation.
3) Test the impact of fertilization on the growth of *P. balsamifera* over a two-year SRC rotation.
4) Evaluate the ability of *P. balsamifera* to sequester carbon in an SRC cropping scheme.

While these objectives were intended to provide data relevant to SRC practices in Southcentral Alaska, they were not intended to be directly applicable to other regions of Alaska due to the wide range of climatic conditions observed throughout the state. Nonetheless, we designed the study to serve as a guide for future studies to be performed in various regions throughout the state.

MATERIALS AND METHODS

Study Site

The study site was an experimental 10m x 20m lysimeter located on Joint Base Elmendorf Richardson (JBER) in Anchorage, Alaska (Figure 1). The lysimeter was previously utilized for a study designed to test the efficacy of poplar plantations used as landfill covers in Southcentral

Alaska (Schnabel et al, 2012). The soil materials were obtained from local forest areas being cleared for housing. The bottom soil layer (1.4m) was a mixture of sand, gravel, and silt loam. The top soil layer (0.6m) was locally derived silt loam soil, with woodchips and forest organic matter mixed in (Schnabel et al., 2012).

Figure 1 *Populus balsamifera* saplings ready to plant at the JBER site, Spring 2004

Sapling poplar trees, locally acquired from nearby forests, were harvested with roots intact and planted in pots in fall 2003, then transplanted to the JBER site in spring 2004. The planting mixture included Populus balsamifera (80%), P. tremuloides (10%), and Salix sp. (10%). The trees were planted at 1.2m intervals, equivalent to 7330 trees ha^{-1}. In addition to these trees, four rows of trees were planted on the perimeter of the site to minimize edge effects (Schnabel et al., 2012).

Estimate of Aboveground Biomass

In Summer 2010, each stem of the 128 poplar and aspen trees within the study area were measured for DBH and D30 using digital calipers. In March 2011, while the trees were still in winter dormancy, the entire aboveground biomass on the site was harvested at 30cm above ground level using a chainsaw. The harvested biomass was measured for total height using a tape measure, wet weight was taken using a field scale, and diameter measurements were taken at DBH and D30 using digital calipers. One P. balsamifera was retained from each row (sixteen total) and stored in Hessian sacks, dried at 60°C and re-weighed for dry weight biomass estimations. Measurements taken on the harvested material were used to correlate the standing biomass measurements with the dry weights, and create allometric equations.

Following the initial harvest, the trees were allowed to regrow from the cut stems or root suckers for a period of two years to simulate an SRC rotation. After the first harvest, the plot was divided into four quadrants. Fertilizer was added to two diagonally adjacent quadrants, and two diagonally adjacent quadrants were left as controls. The slow-release fertilizer was added in a single application at a rate of 112 Kg N ha^{-1}, and 56 Kg P ha^{-1}, and 70.00 Kg K ha^{-1}. In Fall 2012, the regrowth was harvested and measured as described above. Pictures of the poplar plantation at various periods during the project are presented in Figures 2 – 5.

Allometric equations were created for relationships between D30, DBH, and total height against dry weight using the scatter plot feature in Microsoft Excel. Logarithmic or non-linear trend lines were applied to the scatter plots as a best fit relationship, and from the relationship, an allometric equation was derived.

Figure 2: Poplar plantation in Summer 2010, during the seventh season of growth.

Figure 3: Poplar plantation following harvest of first rotation crops in March 2011.

Figure 4: Poplar plantation regrowth observed in August 2011.

Figure 5: Poplar plantation prior to second rotation harvest in September 2012.

Biomass Composition and Energy Analysis

Harvested trees were chipped through a Steinmax 1800 wood chipper. Chipped trees and roots were stored in cotton bags for further processing. Chipped trees and roots were subsampled via four grab samples of chips from four different areas of each bag. The subsamples of each tree were then combined and passed through a 1mm mesh in a Wiley Mill Standard Model #3 grinder. Carbon and nitrogen content analyses were performed on a LECO TruSpec CN analyzer. The samples were combusted at 950°C, and the combusted gases were analyzed for CO_2 by an infrared detector, and for nitrogen by a thermal conductivity cell.

Ash free dry mass (AFDM) was determined gravimetrically on an analytical balance by drying the samples at 60^{o}C for 24 hours, 105^{o}C for 24 hours, and ash at 550^{o}C for 420 minutes using a Thermolyne Type 30400 muffle furnace. Energy content of ground tree samples was analyzed in a Parr Plain Jacket bomb calorimeter (model number 1341). Samples were processed for total combusted energy expressed as BTU/lb.

Estimate of Belowground Biomass

In the buffer zone outside of the study site, three poplars were harvested for total above and belowground biomass to be used in a carbon balance model. The entire belowground material, to

a depth of 30cm and halfway between adjacent trees, was removed from the basal area of the three trees. Roots were cleaned manually and dried to 60^{o}C for 24 hours, and weighed for total dry weight prior to chipping. Root samples were included with the aboveground tree samples tested for carbon, nitrogen, Ash free dry mass (AFDM), and energy content.

Soils Analysis

Soil samples (ten randomly throughout each quadrant) were obtained at depths of 0 - 15.25 cm, and 15.25 cm - 30.50 cm below the surface in the fertilized and unfertilized quadrants of the study site. The soil samples were passed through a 2 mm screen, analyzed for total carbon and nitrogen, inorganic nitrogen, extractable phosphorous, and extractable potassium.

RESULTS AND DISCUSSION

Aboveground Biomass Production

The aboveground biomass accumulated at the time of the first harvest measured 21,600 kg ha^{-1} (Table 1). However, we could not precisely quantify the biomass accumulation rate during this first rotation because the tree mass was not measured at the time of planting. Nonetheless, the maximum theoretical rate, based upon the total biomass measured after seven years, was 3,086 kg ha^{-1} yr^{-1}. Assuming that the mass of the trees at planting was minimal compared to the mass of the trees at harvest, the biomass accumulation rate over the seven-year first rotation was slightly less than that. Consequently, the first rotation biomass accumulation rate was lower than the rate observed during the two-year second rotation (5,530 kg ha^{-1} yr^{-1}). This result is unsurprising, as the trees growing in the second rotation had the advantage of a well-developed root system at the beginning of the rotation. An additional difference between the first and second rotation relates to the number of stems per tree. While the first rotation trees were generally limited to one or two relatively large diameter stems, the second rotation trees had from 10 to 38 small diameter stems.

Table 1: Measured biomass accumulation of *P. balsamifera* at first and second harvest

Tree age (Years)	Average D30 (mm)	Average DBH (mm)	Average Tree Total Height (cm)	Average Tree Dry Weight (Kg)	Average Biomass per Hectare (Kg)	Average Annual Biomass per Hectare (Kg)
7+	34.0	27.0	449	2.93	21,550	< 3,086 (estimated)
1 (Regrowth)	9.4	7.6				
2 (Regrowth)	13.7	11.5	166	1.54	11,060	5,530

Allometric Equations for Aboveground Biomass

The measured relationships between tree diameter and biomass are plotted in Figures 6 – 8. The allometric equation in Figure 6 illustrates a moderately strong relationship between D30 and dry

weight of the aboveground biomass (R^2= 0.8736) for the first rotation trees. The relationship between DBH and dry weight (Figure 7) is very similar to that of D30 (R^2 = 0.8653). Both of these R^2 values suggest a moderately strong relationship between diameter of the tree at both DBH and D30 and total tree biomass. Most poplar studies employ diameter at breast height (DBH) for their biomass estimations due to the large size of the main stem (Felix et al., 2008, Zalesny et al., 2007). Unpublished preliminary growth data indicate that diameter at breast height (DBH) in Alaska tends to be smaller than those in data from studies published elsewhere around the world, and experience under this project revealed that D30 measurements were approximately equal in their ability to predict biomass. The relationship between total height and dry weight was not as strong as D30 and DBH (R^2 = 0.7699), data not shown. This suggests that height was not the best predictor of aboveground biomass in this study.

The allometric relationship for the second rotation is best described by a polynomial equation with an R^2 of 0.8304 (Figure 8). Ballard et al. (2000) noted that different transformations may need to be applied to data to achieve an allometric equation that effectively describes the data, and that young stems often have a different equation than older stems. While Yarie et al. (2007) reported R^2 values of 0.96 and greater using best-fit polynomials based upon DBH of Alaskan poplars, it is unlikely that the equations generated from the large trees used for that study would be applicable to the SRC trees evaluated here.

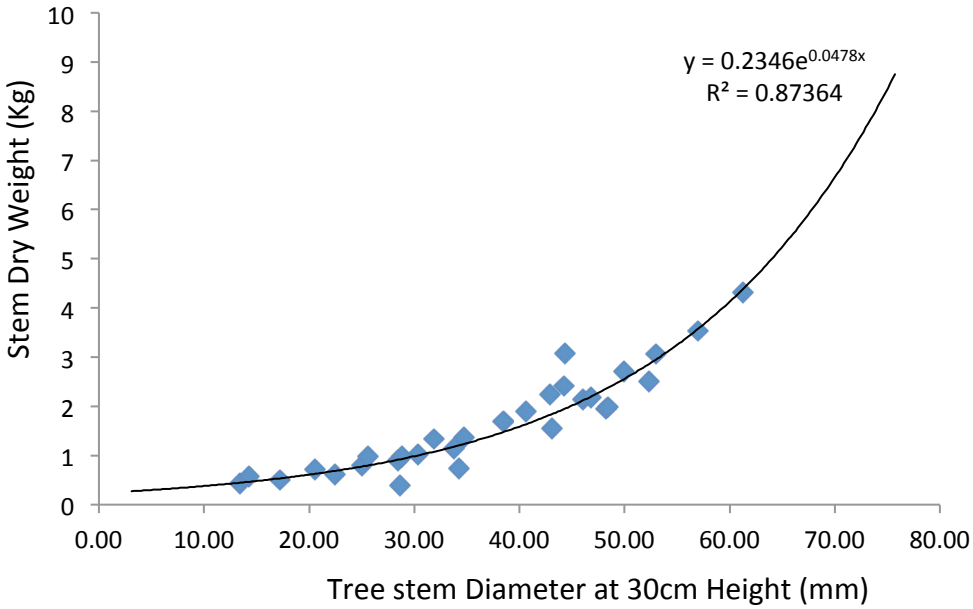

Figure 6: An exponential allometric relationship between diameter at 30cm (D30) above ground and dry weight for first-rotation *P. balsamisfera*.

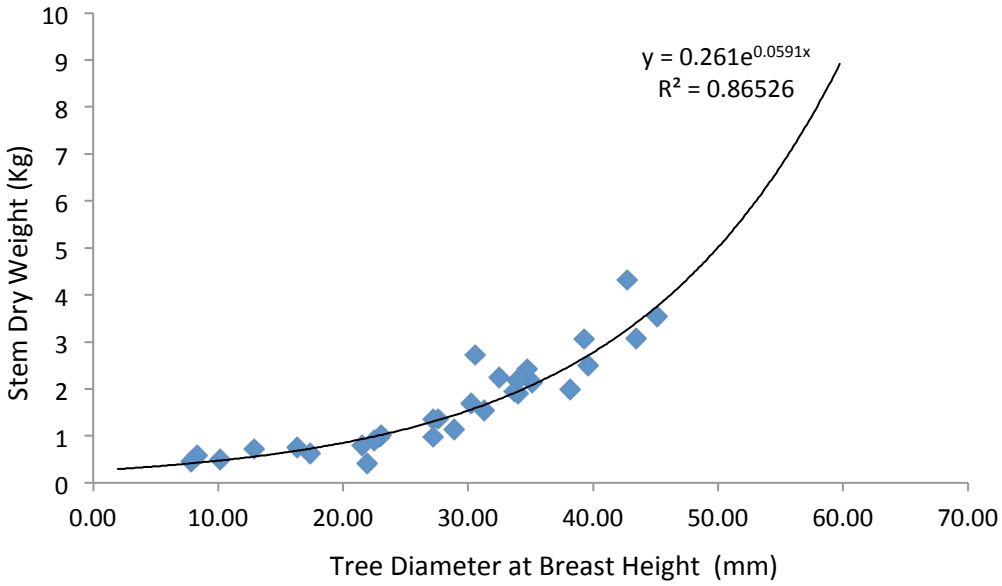

Figure 7: An exponential allometric relationship between diameter at breast height (DBH) and dry weight for first-rotation *P. balsamisfera*.

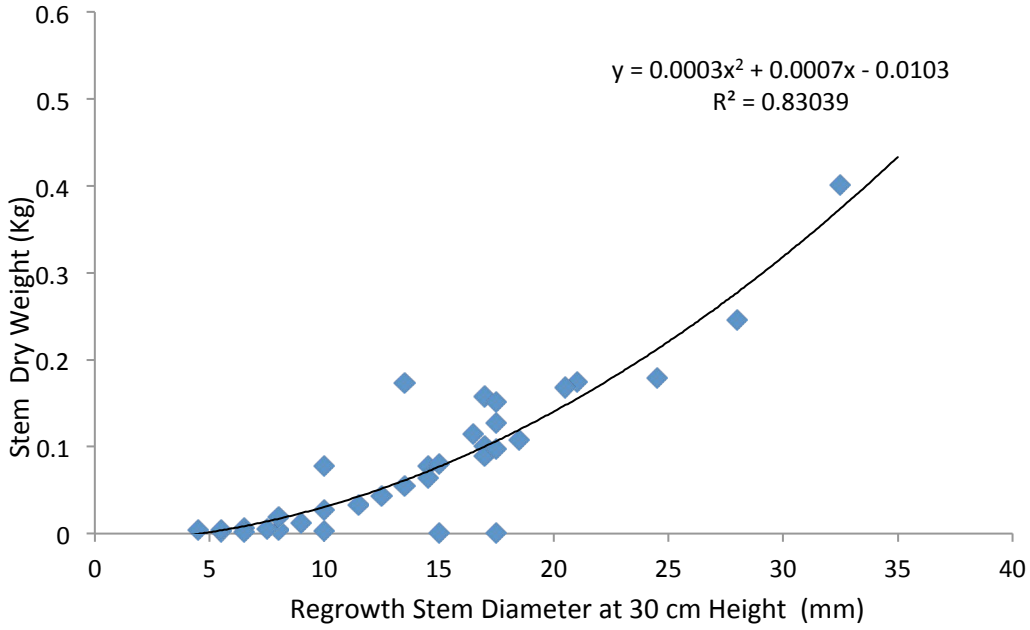

Figure 8: A polynomial allometric relationship between D30 and dry weight of second rotation *P. balsamifera*

The allometric equations produced by plotting the dry weight of poplar stems with their diameters at 30cm, breast height, and total height are presented in Table 2. After the first harvest, the equations that best fit the data were exponential, whereas in the second harvest, the stems were fit with a polynomial equation. This agrees with previous findings suggesting that the

small diameter of the regrown stems don't often fit well into an exponential model for biomass (Abrahamson et al., 2002, Ballard et al., 2000).

Table 2: Summary of allometric equations and R^2 values for first and second harvest trees

Measurement	a	b	Equation	R^2
First harvest D30	0.2346	0.0478	$W=ae^{bD}$	0.8736
First harvest DBH	0.261	0.0591	$W=ae^{bD}$	0.8653
First harvest Height	0.1121	0.7699	$W=ae^{bD}$	0.7699
Regrowth D30	0.0003	0.0007	$W=aD^2+bD-a$	0.8304

Biomass Composition and Energy Content

Biomass composition and energy content are presented in Table 3. As illustrated in the table, nitrogen concentration in the aboveground biomass was similar between the two harvest intervals. Carbon concentration, likewise, resulted in only a 1% difference between the two rotations. The percent of ash free dry mass was also very similar between the two harvests. While the energy content per dry mass was slightly higher in the second rotation trees compared to the first rotation, it is not clear whether that difference is statistically significant. Additional evaluation is required to make this determination.

In Table 3, the energy produced per hectare is strikingly different between the first and second rotations. Biomass energy measured for the first rotation was 404,100 MJ/ha, compared to 217,700 MJ/ha for the second rotation. However, the first rotation trees had seven years to produce that amount of biomass energy, while the second rotation trees had two years. Consequently, the annual production rate for the second rotation trees was significantly higher. Please note that the annual energy produced for the first rotation crops are reported as "less than" due to the unknown dry mass of the trees at the project startup. However, this mass is assumed to be very small compared to the final mass of the trees, so the actual annual biomass produced was likely close to the number reported.

Table 3: Total nitrogen, carbon, ash free dry mass, and energy content of aboveground biomass

Tree age	Nitrogen %	Carbon %	Ash Free Dry Mass %	Energy content KJ/Kg	Energy per hectare MJ/ha	Annual Energy per hectare MJ/ha-yr
7+ years (first rotation)	0.62	48.7	94.9	18,750	404,100	<57,730
2 years (second rotation)	0.63	49.7	95.1	19,680	217,700	108,900

The values presented in Table 3 can be used to estimate the amount of heating oil that might be offset through the use of an SRC energy crop. For example, the energy content of heating oil is approximately 131,750 KJ/Kg. After seven years of growth for the first rotation, one hectare of

poplars with energy content of 404,100 MJ/ha would offset approximately 3000 gallons of diesel fuel, assuming a 100% burning efficiency. Since modern high-efficiency burners attain approximately 70 – 90% efficiency (Truax et al., 2012), the actual amount of fuel oil offset would likely be in the 2,100 to 2,700 gallon range. If an entity required between 2,100 and 2,700 gallons of heating oil per year, then seven 1 hectare plots managed at a staggered rotation would provide the equivalent amount of biomass energy. However, if the rotation length was decreased, the annual observed fuel offset may be higher due to the higher annual energy production rate observed for the shorter rotation.

Fertilizer Effects

Fertilization effects upon biomass production and site soils for the second rotation crops are presented in Tables 4 and 5, respectively. As indicated in these tables, the fertilization effort had little measurable impact in this study. There were no statistically significant differences in biomass production or vegetation characteristics between the fertilized versus unfertilized plots. Similarly, the soils analysis revealed only a slight increase in soil carbon content for the fertilized plot. These results were surprising, as previous studies indicated that fertilization can increase the biomass production rates (Guillemette and DesRochers, 2008). While these results do not provide much guidance for those hoping to evaluate fertilization requirements for similar plantations, they do serve to indicate that fertilization does not always produce the desired or anticipated effect. More research is necessary to better understand the relationship between soil characteristics and nutrient requirements for Alaskan SRC crops.

Table 4: Fertilizer effects upon second rotation biomass

Treatment	Unfertilized (mean)	Fertilized (mean)	DF	P-Value (0.05) *significant
Mean Dry weight (Kg)	1.55	1.5	1	0.48
D30 (mm)	14	14	1	0.41
DBH (mm)	11	14	1	0.092
Height (cm)	194	139	1	0.173
AFDM %	95	95	1	0.49
KJ/Kg	19608	19761	1	0.08

Table 5: Compositional analysis of fertilized and unfertilized second rotation soils

Measurement	Depth (cm)	Fertilized / Unfertilized (mean)	DF	P-Value (0.05) *significant
Total Soil Carbon (%)	0-15 15-30	3.2 / 2.4 2.7 / 2.7	1	0.003* 0.484
Total Soil Nitrogen (%)	0-15 15-30	0.2 / 0.2 0.2 / 0.2	1	0.590 0.439
Available NO3- (PPM)	0-15 15-30	0.4 / 0.1 1.3 / 1.1	1	0.293 0.273
Available NH4- (PPM)	0-15 15-30	1.6 / 2.1 2.7 / 1.6	1	0.111 0.230

Root Development / Carbon Sequestration

As described in the Methods section, three trees were destructively harvested above and below ground in order to quantify root growth relative to aboveground biomass. Results are presented in Table 6. In the table, the total carbon column represents the carbon recovered from the roots, 30cm stump, and stem/branches. The harvested carbon column represents only the portion of the tree that would be removed during a typical harvest process (i.e., the portion above the 30cm stump). The stored carbon column represents the root plus stump carbon, or the amount that may be considered sequestered on the site.

Based on the data presented in Table 6, approximately 31% - 36% of the total biomass produced in the first rotation crops remained at the site following harvest. However, this value does not reflect carbon added to the soil through leaf litter, fine (unobserved) roots, or root exudates. Consequently, the actual proportion of the carbon remaining on site was likely somewhat higher than this. With respect to sequestration, the carbon remaining onsite following harvest might be considered to be sequestered over a short period of time. However, much of it would likely return to the atmosphere at some point as a result of natural soil carbon cycling processes.

Table 6: Carbon content in above and belowground compartments of three harvested trees

Tree Sample	Total Carbon (Kg)	Aboveground Carbon (Kg)	Root Carbon (Kg)	Harvested Carbon (Kg)	Carbon Stored (Kg)
Tree 1	1.09	0.80	0.29	0.70	0.39
Tree 2	2.81	2.15	0.66	1.92	0.89
Tree 3	2.59	2.00	0.62	1.80	0.79

One way to evaluate carbon sequestration from these results would be to evaluate the amount of carbon stored in an SRC system, assuming growth rates similar to those we observed during the

first rotation. In this instance, the first rotation produced approximately 21,550 kg/ha dry biomass over a period of seven years (Table 1). As the measured carbon content was 48.7% (Table 3), the plot produced approximately 10,490 kg/ha of harvested carbon. Assuming the same harvested carbon to total carbon ratios as those presented in Table 6, the total carbon sequestered at the site during the first rotation was approximately 15,000 to 16,000 kg/ha. Thus, installation of the SRC plantation resulted in the sequestration of approximately 2,100 to 2,300 kg/ha of carbon per year over the first seven years of growth.

CONCLUSIONS

This study yielded important data that will be used to help evaluate the feasibility of SRC crops as a sustainable source of biomass energy in Southcentral Alaska. Data presented here will be leveraged with existing and future data to provide researchers with the information necessary to make planning decisions about Alaska's future energy needs. While the study represents only a single step, it can serve as a guide for evaluation of SRC cropping practices in other areas of the state.

The biomass production rates provided in Table 1 can give planners an indication of the amount of harvestable poplar biomass that may be produced under shorter or longer rotations in Southcentral Alaska. The allometric equations listed in Table 2 can help managers to estimate the amount of harvestable biomass available in a standing SRC crop. This study indicated that fertilization had insignificant impact upon production of biomass under a two-year rotation scheme, indicating that managers may at times be able to reduce production costs by more carefully assessing their fertilization needs. Finally, the estimated amount of carbon remaining on site after harvest of a seven-year SRC rotation was found to be approximately 31%-36% of the total carbon produced. Prior to harvest, it was estimated that approximately 2,100 to 2,300 kg/ha of carbon were removed from the atmosphere per year during the first seven years of growth. These numbers may assist planners in evaluating the carbon sequestration potential of SRC practices.

CHAPTER 5: ANALYSIS OF BIOMASS USAGE IN ALASKA

by Art Nash and Daisy Huang

INTRODUCTION

Woody biomass is considered one solution to the high cost of energy in Alaska, especially rural Alaska. At the end of this past decade, Alaska was ranked second in the nation in energy consumption per capita, at nearly three times the national average (eia Beta, 2012). Approximately three quarters of Alaska's energy is used by the transportation sector, and the other quarter is almost evenly divided between the residential and commercial/industrial sectors (Alaska Energy Wiki, 2012). Within the residential and commercial/industrial sectors, the number one demand for energy in Alaska is for heat. Eighty percent (80%) of residential energy and 51% of nonresidential energy is used for heating. In rural areas, those amounts are 89% and 72%, respectively (WHPacific, 2012). Therefore, it is reasonable to focus on economical solutions for heating, with other uses of energy being secondary. Burning biomass to obtain heat directly is simple and intuitive and requires no advanced technical knowledge or skills.

Some biomass resources available in Alaska are:

- Fish processing byproduct
- Farmed agricultural biomass products, such as grain
- Naturally-occurring woody biomass, including:
    - Wood that is purposely harvested
    - Woody byproducts of the lumber industry
    - Wood that is cut for fire remediation
    - Wind-felled or beetle-killed trees

A recent example of the last bullet point is that September 2012's wind storms brought down 70% to 90% of the trees around Tanacross and Dry Creek. In Alaska, woody biomass dominates the supply of overall biomass in quantity, distribution, and ability to be preserved, but needs to be deliberately managed to provide a long term, sustainable, supply if it is to be used in large quantities. Therefore, this report is focused on woody biomass, and is an effort to obtain a general overview of its use as a heating source in rural Alaska communities. Information was obtained from a combination of official reports from the Alaska Energy Authority, from conferences and presentations, and from interviews of key participants in woody biomass projects throughout Alaska.

SOURCES OF WOODY BIOMASS

Woody biomass is most commonly harvested local to where it's consumed. Yet woody biomass could be commoditized and barged from initial supply locations to usage locations. It has been suggested that as demand and supply grow together at complementary rates, one day pellet barges could deliver fuel pellets to non-wooded areas just as oil barges deliver heating oil to isolated villages today. That market vision is not currently being realized on a large scale, and thus this report has focused on projects that utilize locally obtained wood fuel.

The three common forms of woody biomass are cordwood, wood chips, and pellets. Of these three, only pellets are regularly obtained from outside of the local community where it is used. Pellets are typically used in residential and business heating systems and are procured from local vendors. Cordwood is typically harvested on local land or pulled out of nearby rivers by community members. The splitting and handling of large quantities of cordwood can be tedious and labor-intensive. Chips are generally produced locally and are used to heat large facilities. Also, lower quality wood not used as cordwood or pellets may be made into chips. Chips and pellets have a main advantage over cordwood in their ability to be automatically fed into a boiler by an auger.

In Alaska, users of cordwood are typically in smaller communities that have smaller heating requirements. A typical village school in a remote location can be heated by one cordwood-fired boiler, and the labor required to stoke the boiler would be about half an hour, one to four times per day (thus creating a job for a single person). Fig. 1 shows the pile of cordwood for the boiler that heats the Howard Valentine School in Coffman Cove.

Figure 1. Pile of Cordwood in Coffman Cove for heating the local school.

Yet a larger school or a boiler serving multiple buildings via a district heating system would require too much manpower to burn cordwood; thus chips or pellets work best.

Southeast Alaska has a nontrivial lumber industry, so scrap and byproduct is available to be processed into both chips and pellets. The mountainous geography of Southeast Alaska tends to lead to more densely located buildings in communities because of the availability of relatively flat land upon which to build. In the Interior, Arctic, and Western areas of Alaska, villages are more spread out relative to many Southeastern communities. Therefore, Southeast Alaskan woody biomass usage tends toward higher volume due to the density of buildings, thus there are more opportunities for district heating systems. Additionally, access to ferries and more frequent barges also provide better access for products, such as wood pellets, to be imported into the community.

Fig. 2 is a photo of the pile of chips made from scrap lumber from Viking Lumber in Craig. These chips are sold to the school which burns them to provide heat.

Figure 2. Pile of Chips at Viking Lumber.

Fig. 3 and Fig. 4 show the amount of scrap and erstwhile waste at Tongass Forest Products outside of Ketchikan.

Figure 3. Scrap pile at Tongass Forest Products

Figure 4. **Erstwhile waste product at Tongass Forest Products**

Tongass Forest Products processes this into pellets for use in several city buildings, shown in Fig. 5

Figure 5. **Pellets at two stages of production at Tongass Forest Products**

Larger facilities benefit by using chipped wood. An example of this is found in Tok, located in Interior Alaska. The high school has a dedicated large chip-fired boiler with a Combined Heat and Power (CHP) system, and takes advantage of the Department of Forestry clearing wood locally for fire remediation. The wood is chipped using a chipper purchased specifically for the school. Because Tok is on the road system, the chipper's use may be shared by other communities. Currently Delta Junction (110 miles west of Tok) does so. Delta Junction modeled the biomass-fired heating system of its high school after Tok's, thus leveraging the knowledge and experience of its neighbor. Delta Junction has its wood delivered from Dry Creek Lumber,

which chips its scraps using Tok's chipper. The situation in Delta Junction is discussed further in section 3.1.

Smaller communities that use cordwood acquire it locally. Unique and productive situations sometimes arise. For example, the city of Tanana has installed nine cordwood-fired boilers to heat various buildings around the city. To secure a wood supply and create jobs, the city of Tanana began a program to purchase wood at $250 per cord to heat various facilities. This has encouraged local residents to either pull driftwood from the Yukon River or cut wood to earn money, thus stimulating the local economy. The situation in Tanana is discussed in greater detail in section 3.1.

OVERVIEW OF BIOMASS BOILERS

There are many manufacturers producing good wood-fired boilers. This report highlights those most commonly used to heat community buildings in Alaska: Garn, Messersmith, TARM, and Chiptec.

All of them- whether burning chips, pellets, or cordwood- heat the buildings by circulating a heat-carrying fluid (generally either water or glycol) in a closed loop between the boiler and the building to be heated. The quantity of heat delivered to the building is controlled by the flow rate of the water or the glycol, rather than by the air flow to or from the boiler's fire box, as is done with wood stoves. When the boiler's fire is always at maximum heat with maximum air flow, it ensures clean burns with very little soot or creosote buildup. Moreover, most of the wood-fired boilers of this type have a system to reclaim some of the exhaust products and combust them a second time, thus extracting more heat and further reducing pollutant output.

A Garn boiler is shown in Fig. 6. This is the type used in Tanana, Coffman Cove, Kasilof, and Thorne Bay, among other communities.

Figure 6. **Garn Boiler. From Garn.com**

A Chiptec boiler is shown in Fig. 7. This photo was taken in Craig. This boiler heats the school and municipal pool, with chips locally purchased from Viking Lumber.

Figure 7. Chiptec Boiler

Fig. 8 shows the pellet-fired boiler used to heat the Ketchikan library. This boiler is manufactured by ACT Bioenergy.

Figure 8. ACT Bioenergy Pellet Boiler

Two views of a Messersmith chip-fired boiler are shown in Fig. 9. These are the boilers used at the Tok and the Delta Junction schools. The chips are fed from a hopper into the boiler using a screw auger.

Figure 9. Messersmith chip-fired boiler

Water is heated, and the water is run through heat exchanger plates to heat a separate glycol loop, that circulates around the school to heat it. An in-depth look at the Delta Junction Messersmith boiler is presented in section 3.1.

A TARM boiler installation is shown in Fig. 10.

Figure 10. TARM installation in Tetlin

These are cordwood-fired boilers that heat a closed loop of glycol. The contractor who designed and built the Tetlin system ran the glycol loop through a series of copper coils that are immersed in water. The water then circulates throughout the school to heat it. The copper coils are shown in Fig. 11.

Figure 11. **Heat exchanger system in Tetlin school**

SUMMARY OF BIOMASS PROJECTS SUBSIDIZED BY THE ALASKA ENERGY AUTHORITY

Overview

The Alaska Wood Energy Development Task Group (AWEDTG) was established by the Alaska Energy Authority as "a coalition of federal and state agencies and not-for-profit organizations… to explore opportunities to increase the utilization of wood for energy and biofuels production in Alaska." (Akenergyauthority.org, 20112). AWEDTG has solicited applications for community heating projects that would use biomass in high-efficiency, low-emissions heating systems. From 2002 to 2012, over 60 communities applied for grants under this program. In 2012, sixteen (16) communities with 24 projects had prefeasibility assessments performed.

The Alaska Center for Energy and Power has used the list of communities that have applied for AWEDTG grants as a springboard for its biomass data collection effort. The applicants in the communities were contacted in an attempt to gather information about whether the project was a technical, economic, and social success. Fiscal, operational, and mechanical data were all collected, and the current statuses of the projects were noted.
Key community members, such as tribal leaders, school administrators, building construction managers, and city government officials, were interviewed to get an idea of what it takes to make a biomass program succeed.

Among the questions asked were:

1) What was the fuel type and quantity used for heat before and after biomass boiler installation?
2) How much money was saved?
3) Was reliability of diesel fuel delivery a problem?
4) Is wood availability a problem now?
5) Was the new biomass burner intended to replace an oil-fired burner? If so, how was the performance of the old oil-fired boiler? Was it reliable?
6) How is the performance of your biomass-fired boiler? Is it reliable?
7) Have there been any labor issues associated with delivering biomass fuel or opeating the device?
8) Is the community happy with the installation and operation of the device?
9) When was the biomass device installed? Is it still in operation? If not, when did it cease to operate and for what reason?

In a typical situation, a community would have a woody biomass-fired boiler installed to heat a main building, such as a school or a tribal hall. If the installation and implementation are successful, the next step would be to extend biomass heating to other community buildings, such as a clinic or washeteria, either via a district heating loop from the first boiler (if there is excess heating capacity), or via installation of additional boilers.

Usually the existing diesel heater is left in place as a backup heat source, and when the wood-fired boiler is not in use, the diesel fires up automatically. This is convenient for when no one is available to stoke the wood-fired boiler; however, it also disincentivizes use of the wood-fired boiler if the person whose responsibility to keep the fire going does not benefit from the money saved by the community.

Fuel oil prices in villages can range from $5-$9 per gallon, with price spike up to $12 per gallon as occurred in the crisis year of 2008. A typical range of oil usage for a school in mid-sized community of several hundred residents would be about 10,000 – 50,000 gallons per year, and a typical community saves $80,000-$150,000 per year on fuel costs after installation of the wood-fired boiler.

Fig. 12 shows all of the communities that have applied for prefeasibility studies. Attempts were made to contact all communities; meaningful data was gathered from most of them.

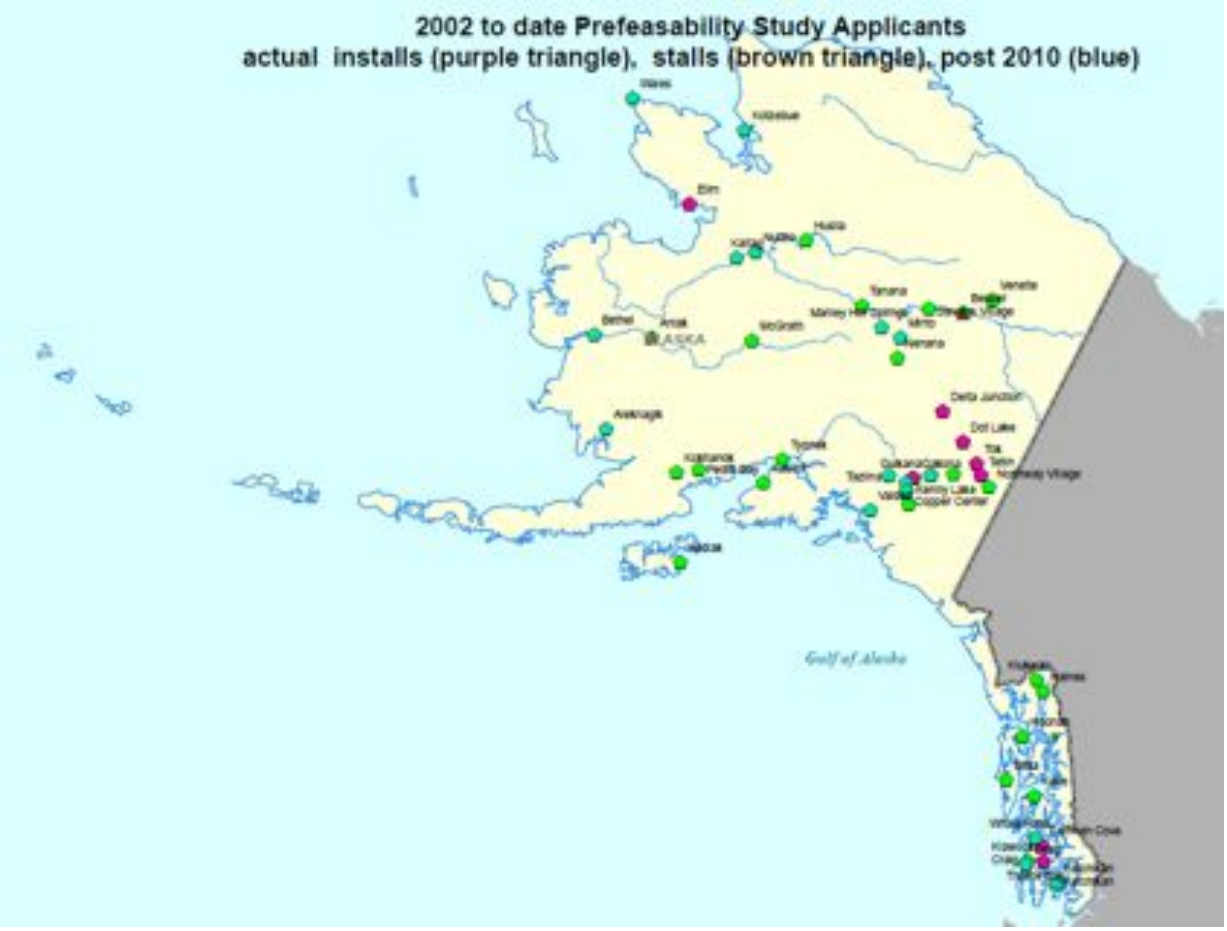

Figure 12. Communities that have performed prefeasibility studies since 2002, funded by the Alaska Energy Authority.

Results of the Data Collection Effort

Of the 101 proposed community projects that completed prefeasibility studies between 2002 and 2012, 19 have had wood-fired boilers installed. Of the 101 communities, nine of them completed prefeasibility studies in summer of 2012; and of these, four were recommended as "good candidates" for detailed feasibility assessments. The remaining five projects were either not recommended as good candidates, the community lost interest, or the projects stalled for other reasons. What detailed results are available are given in Microsoft Access relational database that is being released concurrently with this report, and are summarized in Table 1.

Table 1. Biomass-fired boilers that are in operation and have seen one winter as of 2012.

Community	Heating Degree Days, 65 deg F*	Facility	Year Installed	Project Cost*	Boiler Type	Wood Fuel Type	Previous Fuel Type	Annual Wood Fuel Usage	Previous Annual Oil Usage (gallons/ year)	Displaced Fuel Oil (gallons/ year)
Coffman Cove	7593	Coffman Cove school	2010	$369, 056 (CDF)	2 Garn	cordwood	oil	unknown	10,000	2,000
Coffman Cove	7593	Multi-purpose municipal complex	2010	$35,000 (CDF)	Econoburn	local chips	oil	24 cords	3,000	3,000
Craig	7593	Craig municipal pool and school	2008	$1,710,000 (CDF)	Chiptec	chips	oil and propane	750 tons	14,000 oil and 39,000 propane	14,000 and 33,150 propane
Delta Junction	13429	High school	2011	$2,868,000 (CDF)	Messersmith	chips + trivial amounts of waste paper	oil	1,000 tons	24,000	15,000
Gulkana	13763	Tribal office	2010	$898,000 (C&D)	2 Garn and 1 Tarn	cordwood	oil	50 cords	13,100	8,800
Kasilof	11290	Long House community hall	2008	$307,623 (C)	2 Garn	cordwood	oil and propane	32 cords	8,200	1,500 and (8,200 propane)
Ketchikan	7081	Tongass National Forest visitor center	2012	unknown	Operational	pellets	oil	182 tons	20,000	12,000
Tanana	14790	Washeteria, City Shop, Teacher Housing	2007, 2010, 2011	$644,375 (CDF)	2 Garn, 4 Econoburn	cordwood	oil	80 cords	30,000	15,000
Tok**	15131	Tok High School	2010	$3,950,000 (CDF)	Messersmith	chips	oil	3000 tons	60,000	60,000

*C=contruction, D=design, F= feasability

**Toks also burns wood to run a 60 kW Combined Heat and Power generator, which provides 75% of its electricity.

A successful project saves the community money or stabilizes the cost of heat while utilizing wood resources at a sustainable rate. In order to achieve this, a wood-fired boiler must be actively and consistently used. Although wood-fired boilers are added to provide heat to community buildings, the old oil--fired boiler is frequently left in place as a backup heat source. Since the failure to use the wood-fired boiler has no safety or usability consequences, the community must be motivated either by economic or emotional reasons to use the biomass boiler. This is especially true in the case of cordwood-fired boilers, whose usage is the least automated and therefore the most labor-intensive of the technologies considered in this report.

General trends that have been observed during the data collection effort:

- Prior to installation of the wood-fired boiler, annual fuel usage for typical school was several hundred gallons for small, well insulated, schools; and up to the tens of thousands of gallons for large schools.
- Heating requirements depend on the building size, layout, and insulation, as well as the local climate. For example, the Ahtna tribal hall in Glenallen is 18,000 square feet and burns 19,000 gallons of fuel oil annually (1.05 gallons per square foot). The Delta Junction high school is 77,000 square feet and used to burn 24,000 gallons of fuel oil annually (0.31 gallons per square foot), when it burned oil alone.

- The capacity of the boiler, how often it is fired, and the quality of the wood fuel are also factors in determining the savings to be realized from a wood boiler. Typically, a wood-fired boiler displaces about a quarter to half of the oil burned. In Tanana, two Garn boilers in the washeteria displace about 9,000 gallons per year, or 30% of the oil burned. In Craig, a chip-fired boiler saves the school about $100,000 annually in fuel costs. In the Tok school, almost no oil is burned. Tok is an exceptional case because the school burns more wood than is needed for heat alone, in order to run the combined heat and power generator. In fact, the system produces so much excess heat that the building housing the boiler has had holes bored into its exterior walls, and the school opens its windows to vent excess heat even when it's -40 degrees outside.

Technical Factors that lead to project success

In order for a project to be funded by the Alaska Energy Authority (AEA), certain criteria must be met. The AEA has prefeasibility and feasibility assessments performed first. Among the factors considered are the size and insulation of the building, and the cost and availability of biomass fuel.

Additional factors to make a project succeed come from the community itself, which must ensure the following:

- The wood sources must be either local or reliably delivered.
- The wood must be dry (ideally under 30% moisture content) which means it is either delivered dry or stored for an adequate length of time with adequate air exposure to ensure proper seasoning.
- A chipper, if chips are used, must be reliably available (for example, deliverable via the road system).
- Sufficient local labor must be available to maintain the boiler.
- Sufficient training of local operators and maintenance workers must occur.

Wood quality affects performance of the boilers, as well as the regular maintenance requirements. For example, because one of Tanana's wood sources is driftwood pulled from the Yukon River, their wood supply contains silt, and they must clean the boilers more frequently than other Garn users do. Another example is in Tok, where the wood used has been cut for fire remediation and is mostly small and spindly. Moreover, the trees are fed into the chipper whole—"branches, roots, and all" as said by a local operator. This means that the resulting chips are not that clean, and that the boiler must be scraped clean daily as there is slag in the ashes from vitrified rock. A piece of this is shown in Fig. 13.

Figure 13. **Vitrified material scraped from Tok boiler**

In Delta Junction, the same boiler and the same chipper are used. However, the chips are waste scraps from a local lumber mill, Dry Creek Lumber Mill, and so they are much cleaner and do not generate this slag.

Nontechnical factors that lead to project success

As mentioned earlier, even after technical and numerical feasibility has been determined, social factors can play an important role in determining the success of a biomass project. It was found that in addition to general community support, there must be a local champion who is enthusiastic about biomass. Furthermore, the enthusiasm of both this local champion and of the community must not be motivated by economics alone, although the amount of money saved is definitely a large motivating factor. Other motivations that may drive a community biomass project forward are:

- pride in the community
- a more general wish for self-reliance within the community such as energy independence from Outside suppliers
- creation of local jobs
- concerns about for environmental ethics and stewardship

EXAMPLES OF BIOMASS USAGE

Tanana

The City of Tanana has population 300 and is situated at the confluence of the Tanana and Yukon Rivers. In November 2007, the City Manager, Bear Ketzler, kicked off Tanana's now burgeoning biomass program with the installation of two 425,000 Btu/hour cordwood-fired Garn boilers in its city washeteria. The cost of installation of that first project, which included a new boiler building, was under $100,000. It has displaced annually about 6000 gallons of diesel with 50 cords of wood. The first project has reduced oil consumption in the washeteria by about 50%.

Bolstered by the success of that first project, Ketzler has since had two Garn boilers installed to heat the city office, two more installed in the senior center, and four wood-fired boilers manufactured by Econoburn to heat the city shop and the teachers' housing. Three more Garns are slated to be installed into various city buildings within the next year.

Figure 14. **Tanana City Hall (source: Nicholas School of the Environment, Duke University)**

Ketzler's goals were to reduce reliance on diesel fuel (which costs about $6.50 per gallon in Tanana), as well as create a healthy local economy around biomass. In order to achieve this, he set the price of wood at $250 per cord (which has since been raised to $275 per cord), and informed the locals that the city would purchase wood from anyone who cared to harvest it, either by pulling driftwood from the river, or by harvesting it in legal lands.

By setting a wood price, Ketzler has effectively raised the price of lower-quality wood that otherwise would have sold for less on the open market, and lowered the price of higher-quality wood that would have sold for more. The effects of this on the local population, many of whom burn wood for private use and now purchase commoditized wood at $275 per cord, are not known at this time.

Delta Junction

The Delta Junction high school is a single 77,000 square foot building, shown in Fig. 15. It used to be heated entirely with oil.

Figure 15. Delta Junction High School, with oil tank visible on right

In the summer of 2011, a 5.5 million Btu chip-fired Messersmith boiler, shown in Fig. 16, was obtained for the school using a $2 million grant from the Alaska Energy Authority, and $800,000 from the State of Alaska. The boiler is housed in its own building (pictured in Fig. 17) approximately 200 feet from the school. The boiler was selected and installed by leveraging knowledge gained from the same model of boiler that had been installed in Tok in 2010.

Before installation of the biomass boiler, Delta Junction High school consumed 24,000 gallons of fuel oil annually. In its first year of service, the wood-fired boiler consumed about 500 tons of chips, which were purchased at $60 per ton, and 15,000 gallons of oil. It was noted that when the wood-fired boiler was running, no oil was burned. In future years, the wood-fired boiler is projected to burn continuously, bringing the annual chip usage to approximately 1000 tons and displacing almost all of the oil. It is notable that before installation of the boiler, projection of chip usage was estimated to be 2000 tons per year versus the more current estimate of 1000 tons per year. Delta Junction has been a more extreme example of how the feasibility studies have been very conservative with their initial estimates; almost all of the installed boilers are saving more oil than anticipated. These numbers could not have been known beforehand, because most of the boiler manufacturers had not deployed boilers in such extremely cold regions before. The price of oil in Delta Junction is close to that in Fairbanks, around $4 per gallon.

Using these numbers, the annual heating cost before installation of the wood-fired boiler was $96,000. In the first year of intermittent service of the wood-fired boiler, the heating bill was reduced to $90,000. With the wood-fired boiler in continuous service, the heating costs are expected to be about $60,000 annually.

Figure 16. Delta Junction High School Boiler

Figure 17. Boiler building at Delta Junction High School

The Messersmith boiler heats the high school with chips.. The chips are delivered to the front of the building and dumped directly into the storage area from the truck. From the storage area, they are fed into the boiler using an automated feed via an auger, shown in Fig. 18 . The only manual work is in shoveling out the ash, which takes about 4 hours per week. The ash accumulation is shown in Fig. 19.

Figure 18. Screw auger feeding chips

Figure 19. Ash from Messersmith boiler

The chips are purchased from the Dry Creek Lumber mill, which makes them out of scrap using a wood chipper rented from Tok, about 110 road miles away. Contrary to the chips in Tok that have dirt and sand in them from the trees, these chips are very clean, since they are from lumber scrap. Delta Junction also adds to the boiler scrap paper, cardboard, and other combustible refuse from the school. This contributes a negligible amount of heat; their primary motivation for doing this is that they are "trying to be green".

The boiler heats water, and heat is transferred from the water to a separate glycol loop, which distributes heat to the school. The heat exchange is accomplished using two mating plates, with grooves to maximize contact surface area. These are shown in Fig. 20. The glycol loop was in

place before the installation of the wood-fired boiler, and is used by the oil-fired boiler. That boiler is still in place, and provides heat when heat from the wood-fired boiler is insufficient.

Figure 20. **Delta Junction school heat exchanger**

Anonymous Community

This section discusses a local community whose biomass project did not succeed. It is a small community with fewer than 30 people, located on the road system. The community installed a cordwood boiler to provide heat for a community building under AWEDTG funded by the Alaska Energy Authority. In 2011, there was a fire in the building in which the boiler was housed, and the boiler was damaged. Emergency management funds were provided by the Alaska Native Tribal Health Consortium to repair and rebuild the boiler and building, but the community leaders elected to purchase instead a modern oil-fired boiler and give up on biomass.

When a community leader was interviewed, he stated that the cordwood boiler was tedious to keep stoked, and that he had a difficult time motivating anyone to stoke the boiler three to four times per day. Other users of the same boiler model have only had to stoke the boiler one to two times per day, so it seems a reasonable conjecture that inadequate training was provided to this community, leading to frustration.

Additionally, the community has had a factious local government, and no localized champion to push the merits of biomass. It has been demonstrated that when a community does not have a local champion for a biomass project, then it seldom succeeds.

CONCLUSIONS

In the ten years since the Alaska Wood Energy Development Task Group started subsidizing woody biomass-fired boilers in communities, nineteen have been installed and are saving money by displacing oil. A twentieth unit was installed, but the community abandoned the biomass effort after a fire in the facility prompted them to replace it with a modern oil-fired boiler. Of the nineteen success stories, several common factors were identified that make a community a good

candidate for a woody biomass project. The first is a local champion, who is excited about biomass and inspires the local population to support him. Secondly, the local population needs to be engaged as well as the champion, because biomass requires more labor than oil. Thirdly, the biomass fuel should come from the local community. In theory, wood pellets could be delivered from outside the community the same as oil is today, but this vision has not yet been realized.

It is noteworthy that most of these criteria are "soft" criteria. It is very difficult to quantify how enthusiastic a community or a community leader will be. However, it has been found that even once all of the "hard" criteria are in place that indicate that a project will succeed, i.e., that there is local fuel available, that the construction of the building is adequate, etc., it is no guarantee of a project's realization or success.

Most successes have come from communities where the local population is very enthusiastic, not only about saving money and about energy independence from outside the community, but also about environmental stewardship. More than one community member has mentioned that they would use their biomass-fired boiler even if it saved no money at all, simply out of a wish to be more sustainable.

CHAPTER 6: ULTRA CLEANING AND GASIFICATION OF LOW RANK ALASKA COAL

by Rajive Ganguli and Daniel Walsh

INTRODUCTION

Ganguli and Walsh (2010) had previously examined the use of acid leaching in ash removal to determine if low rank Alaska coal could be ultra-cleaned prior to gasification. The intent of ultra-cleaning was to prevent the entry of coal contaminants into the high temperature (and possibly high pressure) environment of a coal gasifier. Contaminants present in coal are extremely harmful not only to the gasification unit, but also to the various downstream process units in a coal-to-liquids (CTL) plant. As the reader may be aware, these studies were conducted to study the feasibility of locating a CTL plant in Fairbanks.

Ganguli and Walsh (2010) used nitric acid, sulfuric acid and hydrochloric acid in their leaches. However, acid leaching of raw coal could bring down the ash content to only about 8.2% from the raw coal ash content of 12.4%. Unless specified otherwise, all ash content reported here is in dry basis. The kinetics of the leach reactions, however, was very hopeful, with most of the reductions needing only 5 to 30 minutes. Short reaction times result in small reactor sizes, resulting in reduced physical footprint and improved process economics. When the coal was pre-cleaned using gravity methods, more ash could be removed, though at 6.2%, it was still higher than the goal of 0.5% ash.

As a result, in this phase, the authors suggested exploring hydrofluoric acid for leaching, as the acid is well known for dissolving silicates. Silicates are a major component of ash in the coal being studied. Additionally, the investigators proposed conducting gasification simulations to understand how ultracleaning of coal would impact its eventual gasification, especially product gas composition. Given how trace elements can be harmful to processes downstream of gasification, simulations were also suggested to examine if the trace elements were emitted into the gas product streams. Therefore, the following tasks were conducted in this project:

1. Coal leaching experiments (using hydrofluoric acid) to investigate ash removal from low rank Alaska coal
2. Gasification simulation to determine product gas composition for two competing technologies, moving bed gasifier and entrained flow gasifiers
3. Simulation to determine trace element emission phases

LEACHING STUDIES

Methodology

A preliminary series of HF leaching tests were conducted to establish a reliable laboratory protocol and leached coal neutralization/rinse procedure. Ten preliminary tests were conducted using 25 gram samples of raw or HNO_3pre-leached coal. Based on the analytical results of these 10 tests, the following test procedure was established. HF leach tests were done using 100 gram samples of coal. Prior to acid leaching experiments, the 100 grams of raw coal was pre-wet in 200 mL of Aerosol OT solution (0.5% by weight). The coal was thoroughly mixed and then allowed to sit overnight. 4 L Nalgene beakers were used for acid leaching experiments.

All pre-wet coal samples were pre-leached with HNO_3 for 5 minutes. This pre-leach step was conducted to remove the majority of Ca, Mg, Na and K from the raw coal. Research by others (Steel, et al., 2001 and Ganguli and Walsh, 2010) and the preliminary HF leach tests at the Mineral Industry Research Laboratory (MIRL) noted above, indicated this would be an important consideration, due to the precipitation of Ca, Mg, Na and K fluorides during HF leaching.

Whereas HF leach residence times ranging from 5 minutes to 4 hours were studied by MIRL in its preliminary HF leach tests, only 4 residence times were investigated in a final series of HF leach tests. These residence times were 2 hours, 4 hours, 8 hours and 16 hours. Preliminary HF leaching results indicated much slower kinetics for silicate mineral dissolution, compared to the rapid leach kinetics for cation exchange reactions noted for HNO_3, HCl and H_2SO_4 (Ganguli and Walsh, 2010).

For the HF leaching tests, each 4 L beaker was given a Teflon coated magnetic stir bar and the tare mass recorded. A thoroughly rinsed and filtered, well mixed, HNO_3leached coal sample was then poured into the beaker. The coal slurry was then brought to a specified mass with the addition of reverse osmosis water and the beaker was placed on a magnetic stirrer in a fume hood. Once the slurry was brought to a desirable agitation, a specified volume of concentrated HF was added to the slurry, in order to bring the acid concentration of the aqueous phase of the slurry to 2 M. From preliminary HF leach studies, an acid concentration and aqueous volume was chosen to approximate a [F^- (in solution):Si + Al (in coal)] ratio of 40:1. The measurement of residence time was initiated when the concentrated acid was added to the slurry sample.

When the desired residence time was reached, the beaker was removed from the magnetic stirrer and the magnetic stir bar was removed. The leach slurry was then filtered through a 32 cm vacuum filter. The coal filter cake was rinsed with reverse osmosis water 10 times, with a 15 minute standing time during each rinse. After the final vacuum filtration, the filter paper and filter cake were transferred to a drying pan, where the sample was allowed to air dry. After drying, the filter cake was pulverized by hand using a mortar and pestle to -300 um and prepared for analysis.

Results and Discussion

Chemical and physical properties of typical low-rank coal (LRC) ash are significantly different than bituminous coal ash. With the exception of extraneous ash, which is incorporated during mining, or is due to ash partings within or between coal seams, LRC ash consists primarily of inherent ash, which is bonded into the organic molecular structure of the coal or is present as finely disseminated mineral matter.

Since much of the ash in Usibelli coal is inherent ash rather than extraneous ash, ash reduction using low cost, wet gravity cleaning processes are rather ineffective. This is true in general for LRCs, where the added cost of cleaning and yield loss makes LRC cleaning unattractive ahead of most utilization applications. Ganguli and Walsh (2010) showed that Usibelli coal could be physically cleaned from 12.4% (dry basis) to 10.0% (dry basis) with a 76% clean coal yield, emphasizing the ineffectiveness of physical cleaning. However, Rao, et al. (1999) showed selective mining of Usibelli coal (No. 3 seam) could produce a low ash coal ranging from 4-6% ash (dry basis); approximately 50-60% of this ash would be attributable to the exchangeable cations of Ca, Mg, Na and K, with the majority of the remaining ash attributable to finely disseminated clay minerals.

It has been well established by others (Rao, et al., 1999; Potas, et al., 1989; and Couch, 1990; and Ganguli and Walsh, 2010) that acids and other proton donors serve as effective ion exchange agents for cationic exchange reactions in LRCs. Ganguli and Walsh (2010), suggested that nitric acid seems the best candidate for low-rank coal leaching, since it does not have potential to leave residual chlorine atoms from hydrochloric acid (HCl) or sulfur atoms from sulfuric acid (H_2SO_4) in the clean coal product.

Further, Ganguli and Walsh (2010) noted that sulfuric acid leaching showed the probable precipitation of calcium sulfate (gypsum), a mineral known to be insoluble in sulfuric acid. They proposed that as the abundant calcium cations present in the coal were exchanged into solution by the sulfuric acid protons, these calcium cations combined with the sulfate ions present in the acid solution and precipitated as gypsum, which reported to the clean coal product by filtration.

However, leach kinetics for nitric, hydrochloric and sulfuric acid are all very rapid. Ganguli and Walsh (2010) demonstrated that the ion exchange reactions were completed in under 5 minutes, when these acids were reacted with pulverized (-150 micron) Usibelli LRC. Such rapid exchange kinetics highlight an important design implication for possible, future industrial applications of acid leaching of LRCs; cation exchange reactor volumes could be relatively small, even for large feed rates of coal. From a plant design point of view, cation exchange reactions using dilute nitric acid ($\leq$ 1 M) solutions might be carried out using horizontal belt filters fitted for acid application and rinsing cycles.

The present research targeted the finely dispersed silicate minerals, which nitric acid does not dissolve. Based on the earlier results of Ganguli and Walsh (2010), this study proposed the use of hydrofluoric acid to dissolve the finely dispersed silicate minerals. HF is commonly used for dissolving silicates and Steel, et al. (2001) demonstrated the characteristics and effectiveness of hydrofluoric acid leaching of coal based minerals isolated using a low temperature ashing technique. Based on this information, Usibelli LRC samples were first leached with nitric acid for 5 minutes, to rapidly remove exchangeable cations, and then leached with hydrofluoric acid for various residence times, in order to remove silicate minerals. The combined ash reduction results using this strategy are shown in Table 1. On a dry basis, nitric acid leaching reduced ash content of the coal from 12.4% to 8.3%. Complete HF ash reduction results are shown in Figure 1, with selected results shown in Table 1 for comparison. A combination of nitric and hydrofluoric acids would result in a highly significant reduction in ash reporting to the gasifier, which should result in a longer gasifier refractory liner life. The final ash content of 0.49% ash is very good, though it comes with significant leaching effort.

Trace element analyses (Tables 2 and 3) demonstrate that either (1) most trace elements are associated with minerals that are resistant to dissolution by 1M nitric and 2M hydrofluoric acid solutions, or (2) these trace elements are intimately associated with the organic structure of the coal, relatively tightly bonded, and not subject to removal by these acid solutions. In any case, acid leaching, except in the case of vanadium, does not significantly affect trace element concentrations for those elements considered. As trace elements are a component of ash, significant reduction in ash content implies significant reduction in trace elements.

It was previously noted that due to the very favorable kinetics of nitric acid leaching and the associated cation exchange reactions, the nitric acid leaching would require low reactor volume and might be accomplished using a horizontal belt filter. These options would lead to very low capital investment, when treating coal prepared for gasifier feed, especially for a gasifier designed to receive a coal slurry feed. The longer residence times required for effective hydrofluoric acid leaching, 2-16 hours, would require significant agitated reactor volume. However, similar reactor volumes are familiar to the mining industry. For example, the Fort Knox Gold Mine near Fairbanks, Alaska, uses agitated leaching to recover gold from ground, minus 150 micron ore. The mine's agitated reactor volume was designed to provide a 24 hour leach residence time to approximately 30,000 tons per day ore. The ore is fed to the agitated leach tanks as a 60% (w/w) slurry.

What is not familiar to the mining industry is the use of 2M HF on an industrial scale. This would pose significant regulatory and health and safety investment, not to mention the cost of the acid itself. There is also the question regarding rinsing of the HF leached coal and to what levels residual F^- could be reduced; would they be acceptable levels achieved economically?

Any cleaning technology will likely have impacts on ash chemistry. Slag chemistry during gasification will be impacted in terms of whether the slag is 'acid' or 'basic'. Gilchrist (1989) summarizes ash chemistry: "In terms of the ionic theory a "basic" slag is one in which there are free O2- ions and an "acid" slag one in which there are no free O2- ions but which have a high capacity for incorporating them into their more complex structures. Thus acid slags attack refractories made from basic oxides and vice versa." Gilchrist (1989) further notes that quantitatively the simplest molecular ratio to describe the degree of basicity of the slag is CaO/SiO2. Using this ratio (Table 1), it is apparent that the combined acid cleaning of Usibelli LRC demonstrated by this study will produce a clean coal product with more acid ash characteristics. Gasifier refractory design/selection would need to consider such ash composition and its pros and cons.

Table 1. Raw Coal and Acid Cleaned Coals Ash Characteristics

Property		Raw Coal	HNO_3 Cleaned Coal	HF Cleaned Coal (2 hr RT)	HF Cleaned Coal (8 hr RT)
Ash, wt. % (dry basis)		12.4	8.3	1.9	0.8
Ash Composition (wt. %)	SiO_2	41.3	64.2	50.9	52.4
	Al_2O_3	18.3	25.8	10.6	10.1
	CaO	19.1	0.5	7.9	3.7
	MgO	3.1	0.7	2.6	0.9
	Na_2O	1.1	1.6	0.8	0.3
	K_2O	0.2	0.2	2.2	1.9

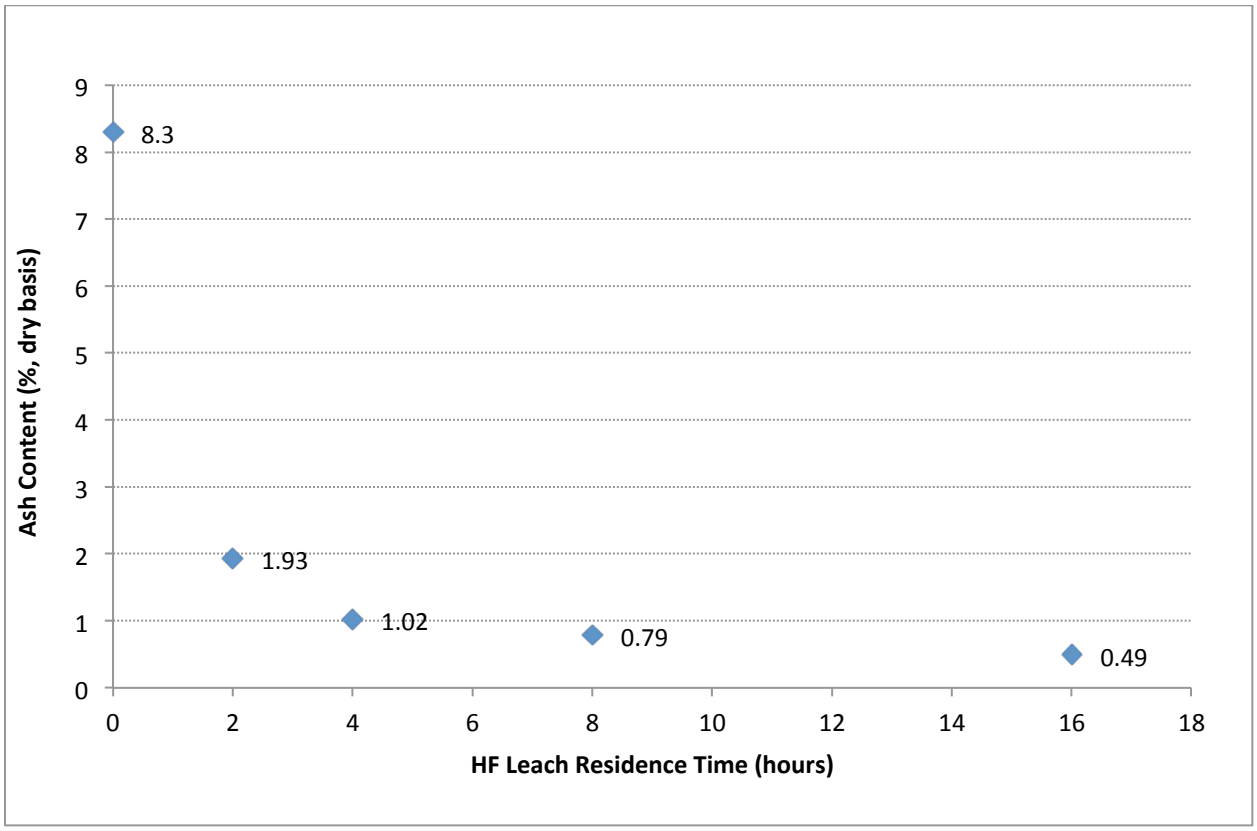

Figure 1. Results of Ash Reduction Using HF Leaching at Various Residence Times.

Table 2: Coal and ash characterization

Sample*		C070	C071	C072	C073	C074
Test	Unit					
AS RECEIVED BASIS						
Total Moisture	% wt	8.84	8.97	10.06	9.42	27.98
Ash	% wt	1.76	0.93	0.71	0.44	8.50
Volatile Matter	% wt	48.63	48.89	48.47	49.02	35.34
Fixed Carbon	% wt	40.77	41.21	40.76	41.12	28.18
Sulphur	% wt	0.26	0.26	0.26	0.26	0.09
DRY BASIS						
Ash	% wt	1.93	1.02	0.79	0.49	11.80
Volatile Matter	% wt	53.34	53.71	53.89	54.12	49.07
Fixed Carbon	% wt	44.73	45.27	45.32	45.39	39.13
Sulphur	% wt	0.29	0.28	0.29	0.29	0.13
Calorific Value - Gross (as received)	BTU/lb	10378	10444	10350	10461	7489
Calorific Value - Gross (dry basis)	BTU/lb	11384	11474	11508	11549	10399
Calorific Value - Net (as received)	BTU/lb	9852	9923	9818	9936	6887
Calorific Value - Net (dry basis)	BTU/lb	10908	11003	11032	11077	9966
ULTIMATE ANALYSIS (dry basis)						
Carbon	% wt	66.44	67.36	67.19	67.46	59.15
Hydrogen	% wt	5.14	5.08	5.13	5.09	4.67
Nitrogen	% wt	0.77	0.78	0.78	0.78	0.65
Sulphur	% wt	0.29	0.28	0.29	0.29	0.13
Ash	% wt	1.93	1.02	0.79	0.49	11.80
Oxygen (diff)	% wt	25.43	25.48	25.82	25.89	23.60

*C070 – Nitric Acid Leach (5 mins), followed by 2 hour HF leach (2Molar);
C071 – Nitric Acid Leach (5 mins), followed by 4 hour HF leach (2Molar);
C072 – Nitric Acid Leach (5 mins), followed by 8 hour HF leach (2Molar);
C073 – Nitric Acid Leach (5 mins), followed by 16 hour HF leach (2Molar);
C074 – Raw Coal

Table 2: Coal and ash characterization (continued)

Sample*		C070	C071	C072	C073	C074
MINERALS OF ASH						
Alumina, Al203	%	10.55	12.36	10.09		16.96
Barium Oxide, Ba0	%	0.26	0.39	1.01		0.46
Lime, Ca0	%	7.89	2.83	3.74		20.52
Ferric Oxide, Fe203	%	5.88	9.08	11.13		7.10
Potassium Oxide, K20	%	2.24	2.35	1.94		1.05
Magnesia,Mg0	%	2.60	0.93	0.92		3.26
Manganese Oxide, Mn0	%	0.04	0.06	0.08		0.14
Sodium Oxide, Na20	%	0.80	0.29	0.30		0.17
Phos. Pentoxide, P205	%	0.14	0.25	0.30		0.09
Silica, Si02	%	50.88	58.41	52.43		39.21
StromiumOxide, Sr0	%	0.05	0.05	0.07		0.17
Titania, Ti02	%	3.05	5.47	6.67		0.71

*C070 – Nitric Acid Leach (5 mins), followed by 2 hour HF leach (2Molar);
C071 – Nitric Acid Leach (5 mins), followed by 4 hour HF leach (2Molar);
C072 – Nitric Acid Leach (5 mins), followed by 8 hour HF leach (2Molar);
C073 – Nitric Acid Leach (5 mins), followed by 16 hour HF leach (2Molar);
C074 – Raw Coal

Table 3: Trace Element Analysis

Sample ID:*		C070	C071	C072	C073	C074
TRACE ANALYSIS * (air dry basis)						
Vanadium	mg/kg	2.88	2.08	2.07	1.99	10.5
Chromium	mg/kg	13.4	12.6	12.3	11.8	8.36
Nickel	mg/kg	6.6	6.06	5.8	5.7	5.88
Zinc	mg/kg	9.2	4.86	4.02	3.29	3.10
Arsenic	mg/kg	2.31	1.32	2.57	2.46	1.15
Selenium	mg/kg	2.02	0.759	1.06	1.01	0.637
Cadmium	mg/kg	0.173	0.099	0.074	0.053	0.109
Mercury	mg/kg	0.051	0.102	0.115	0.099	0.067
Lead	mg/kg	1.89	1.92	1.83	1.70	2.02

*C070 – Nitric Acid Leach (5 mins), followed by 2 hour HF leach (2Molar);
C071 – Nitric Acid Leach (5 mins), followed by 4 hour HF leach (2Molar);
C072 – Nitric Acid Leach (5 mins), followed by 8 hour HF leach (2Molar);
C073 – Nitric Acid Leach (5 mins), followed by 16 hour HF leach (2Molar);
C074 – Raw Coal

Lang and Neavel (1982) studied the behavior of Ca and K as catalysts during steam gasification. Both were found to have significant catalytic benefits, especially when finely dispersed throughout the organic matrix of the coal, though K was found to be more mobile and less sensitive to fine dispersion than Ca. The abundant Ca and less K, present in Usibelli LRC as exchangeable cations, will catalyze the coal's gasification and these elements are a benefit to steam gasification. Thus, while acid leaching produces a lower ash product, it removes elements, Ca and K, known to catalyze the coal gasification process.

GASIFICATION SIMULATIONS

Process simulation software ASPEN PLUS[1] was used to model coal gasification. Two technologies were modeled, entrained flow and moving bed. While entrained flow gasifiers are preferred for their 'clean' product composition, moving bed gasifiers are considered an excellent choice for high moisture content low rank coal like the one being considered (Higman, and van der Burgt, 2003). Despite being popular, moving bed gasifiers have never been simulated for Alaska coal, unlike entrained flow gasifiers (Bibber et al, 2007; Chaney and Bibber, 2006; Dover, 2008).

Regardless of technology, coal goes through the following processes during gasification: drying, devolatilization, char decomposition, gasification, and combustion. Modeling of some these processes in ASPEN PLUS require fundamental data that can only be obtained from experiments conducted in a laboratory. Unfortunately, no such data exists for any Alaska coals, though char composition determined by Rao and Walsh (1991) for Alaska coal is somewhat relevant, and was thus used in the simulations. Note that laboratory experiments have to match not just the coal type, but also other factors such as the heating rate and environmental conditions, to be considered perfect data for simulations. Simulations also relied on data from Suuberg et al (1978) and Aspen Tech (2010).

Moving bed gasification simulation

The flowsheet, originally developed by Aspen Tech (2010) and used in the simulation, is shown in Figure 2. The following modifications were made to the Aspen Tech model to adapt it for this project:

1. Feed coal characteristics (proximate and ultimate analysis), as shown in Table 4
2. Char devolatilization models
3. Coal, oxygen, steam flowrates and other operational characteristics (Table 5)
4. Gasifier attributes such as height, diameter and pressure
5. Kinetics of reactions

[1] http://www.aspentech.com/

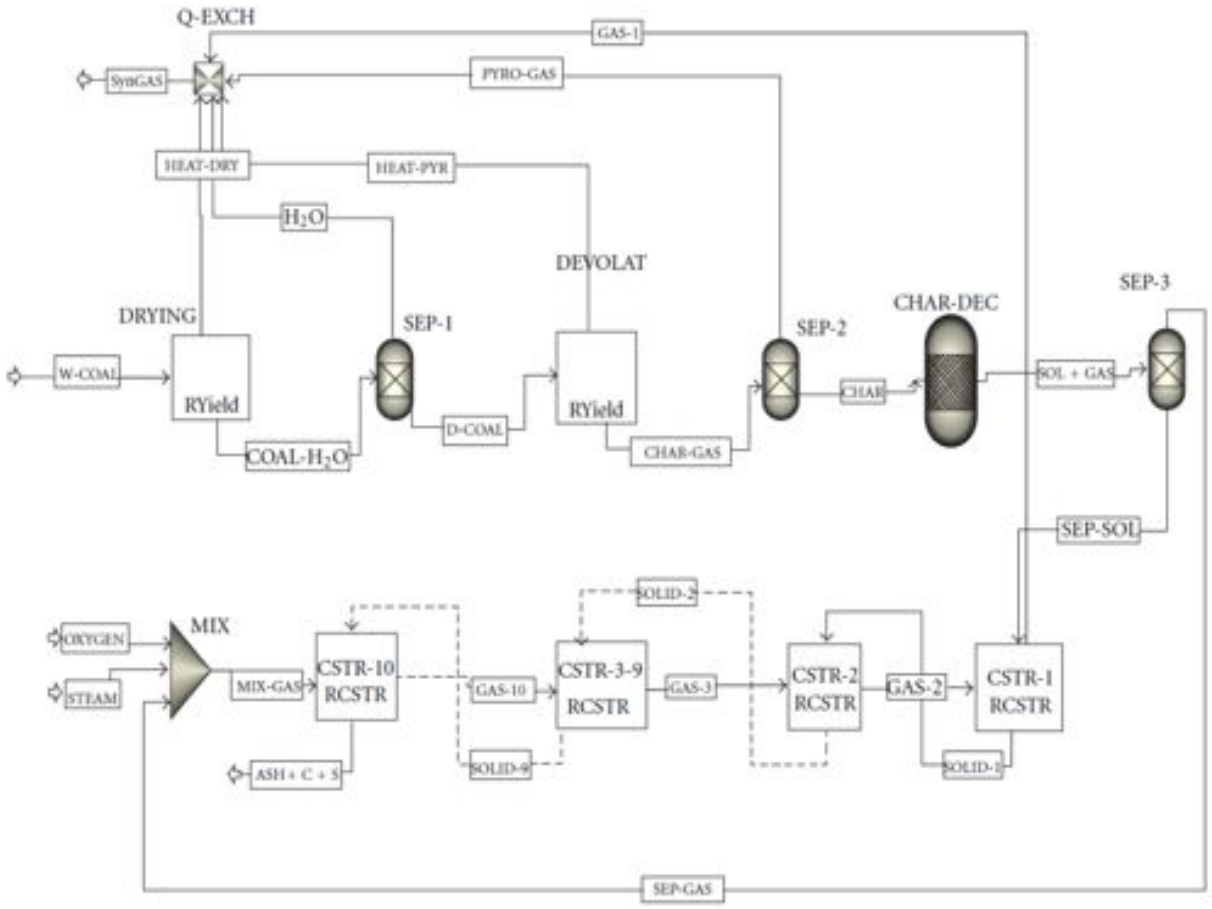

Figure 2. Moving bed gasifier flowsheet developed in ASPEN PLUS (Kulkarni and Ganguli, 2012)

The technical details of the simulation are reported in Kulkarni and Ganguli (2012). The model was tested against the experimental work of Wen and Onozaki (1982). Wen and Onozaki (1982) conducted gasification experiments on a coal that had very similar characteristics as the LRC coal used in the project.

The product gas composition obtained from moving bed gasification of Alaska coal is shown in Table 6. As expected, the product gas contains tars, which is not desirable. The product gas is characterized by low proportion of synthesis gas ($CO+H_2$), and high amounts of methane and carbon dioxide. Note that the simulation only considered raw coal feed (as evident from the 8% ash content of feed coal) as moving bed gasification would be inconvenient with ultraclean coal (UCC), as it requires coarse coal. UCC would be fine, as coal is ground to under 150 microns before it is ultra cleaned.

Table 4. Characteristics of feed coal used in moving bed gasification simulation.

Proximate analysis	As Received %
Moisture	27
Fixed carbon	29
Volatile Matter	36
Ash	8
Total	100.0
Ultimate Analysis	Dry Ash Free (DAF) %
Carbon	69.5
Hydrogen	4.5
Nitrogen	0.9
Chlorine	--
Oxygen	24.8
Sulfur	0.3
Total	100.0
Heating value	18143 KJ/Kg

Table 5. Operational parameters used in the moving bed gasification simulation.

Reactor Pressure (KN/m^2)	2473.15
Bed Diameter (m)	3.048
Bed Height (m)	3.048
Bed voidage (m)	0.122
Coal Feed rate (kg/hr)	6159.78
Steam feed rate (kg/hr)	6201.97
Oxygen Feed rate (kg/hr)	1513.18
Heat Transfer Coefficient, W/m^2K	170.34
Maximum temperature attained, ^0C	1182

Table 6. Moving bed gasifier product gas composition for low rank Alaska coal

Component	CO	H_2	CO_2	CH_4	H_2S	N_2	Tar
Simulation Results, mole%	20.3	40.2	28.8	8.4	0.2	1.13	114.21 (Kg/hr)

Entrained flow gasification simulation

Two competing approaches, thermodynamic equilibrium modeling and kinetics modeling, were explored for entrained flow gasifier modeling. Thermodynamic equilibrium (TE) modeling can provide a maximum limit to synthesis gas production. It is, however, not an effective tool for process optimization as reactor temperature is assumed to be independent of other gasification factors. It also tends to overestimate the synthesis gas component ($CO+H_2$), while underestimating the methane composition (Biagini et al, 2009). Kinetics modeling is more detailed, but requires a significant amount of fundamental data on reactions.

Figure 3 shows the flowsheet for the kinetics based model developed for this project. These models were founded on work done by Govind and Shah (1984); Serio et al (1986) and Lee et al (2011). The operational parameters used in the entrained bed models are shown in Table 7. Table 8 shows the simulation data for raw coal (12.3% ash on a dry basis), while Table 9 shows the same for sample C64 (7.7% ash on a dry basis). Sample C64 was HF leached coal, obtained by leaching raw coal directly with HF for 240 minutes. Similarly, Table 10 presents the data for sample C73 (0.49% ash on a dry basis). The sample C73 was leached coal that was first physically cleaned, then nitric acid leached (5 minutes) and finally HF leached (16 hours).

Gasification Results Discussion

A few things become evident from the simulations. There is very little impact of ultracleaning on the proportion of synthesis gas ($CO+H_2$) in the product gas. It remains at just over 90% of the product gas regardless of the amount of leaching. This is very high compared to what was obtained by moving bed gasifiers (60.5%). As is expected for entrained flow gasifiers, tar formation and CO_2 formation are absent or low. Overall, the product from entrained flow gasification is cleaner, having much less problematic components such as H_2S and tar.

Ultracleaning did impact the temperature needed to achieve high carbon conversion in entrained flow gasification. In the raw coal, carbon conversion was 97.8% at a temperature of 1750C. The carbon conversion was somewhat higher at a significantly lower temperature of 1475C, when the coal had less ash. This is not a surprise as ash would tend to increase the temperature needed for the coal to be fully consumed.

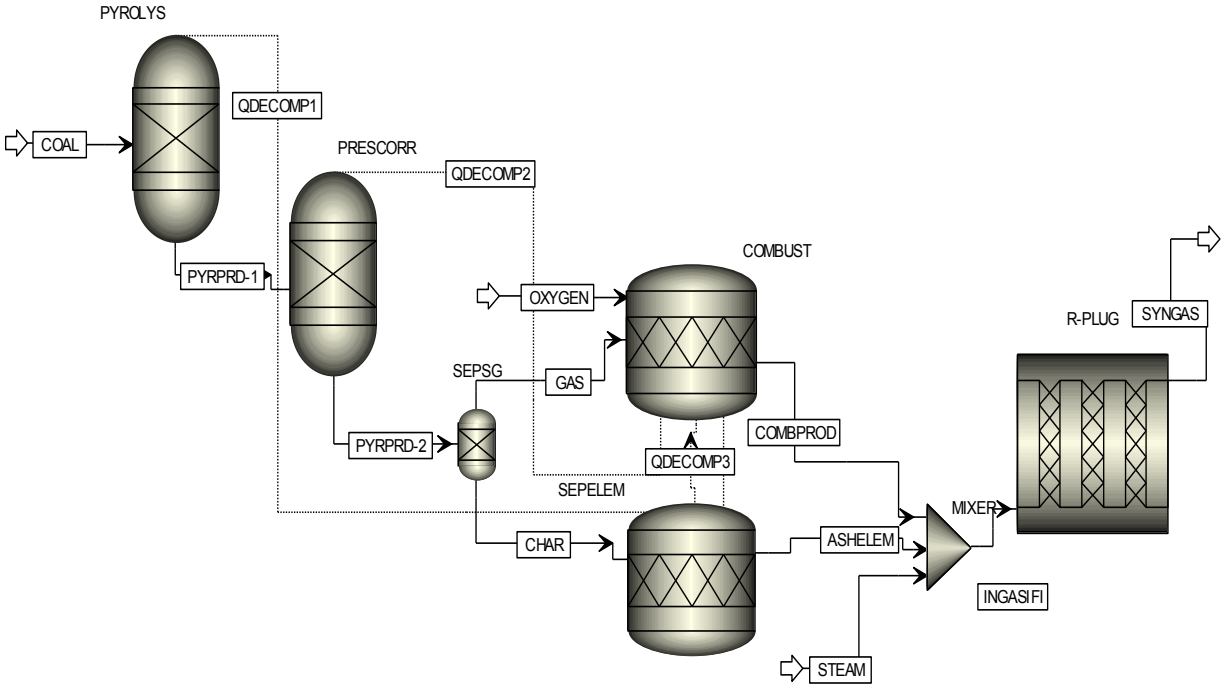

Figure 3. Kinetics model for entrained flow gasifier

Table 7. Operational parameters for the entrained flow model

	Operational parameters for Simulation
Reactor Pressure (atm)	
Reactor Length (m)	0.80
Diameter (m)	0.25
Coal Feed rate (gm/sec)	100
O_2 flow rate (gm/sec)	80
Steam flow rate (gm/sec)	30

Table 8. Raw coal feed quality and product gas composition.

Sample ID:			COAL-RAW#1
Test	Method	Unit	
Moisture	ASTM D3173	% wt	10.50
Ash (dry)	ASTM D3174	% wt	12.33
Calorific Value - Gross (as received)	ASTM D5865	BTU/lb	9111
Calorific Value - Gross (dry)	ASTM D5865	BTU/lb	10179
Calorific Value - Gross (as received)	ASTM D5865	Kcal/kg	5061
Calorific Value - Gross (dry)	ASTM D5865	Kcal/kg	5655
ULTIMATE ANALYSIS (dry)	ASTM D3176		
Carbon		% wt	60.48
Hydrogen		% wt	4.48
Nitrogen		% wt	0.70
Sulphur		% wt	0.21
Ash		% wt	12.33
Oxygen (diff)		% wt	21.80

Product Gas Composition (moisture free basis) for raw coal

	%
CO	55.6
H2	35.4
CO2	8.2
H2S	0.3
N2	0.4
CH4	0.1
Tar	0.0

Carbon conversion	97.8%
Final temperature	1750 C

Table 9. Feed quality and product gas composition for sample C64.

Sample ID:		C64
DRY BASIS		
Ash (dry basis)	% wt	7.71
Volatile Matter (dry basis)	% wt	49.33
Fixed Carbon (dry basis)	% wt	42.96
Calorific Value - Gross (as received)	BTU/lb	
Calorific Value - Gross (dry basis)	BTU/lb	10725
Calorific Value - Gross (as received)	Kcal/kg	
Calorific Value - Gross (dry basis)	Kcal/kg	5958
Calorific Value - Net (as received)	BTU/lb	
Calorific Value - Net (dry basis)	BTU/lb	10276
Calorific Value - Net (as received)	Kcal/kg	
Calorific Value - Net (dry basis)	Kcal/kg	5709
ULTIMATE ANALYSIS (dry basis)		
Carbon	% wt	62.74
Hydrogen	% wt	4.84
Nitrogen	% wt	0.73
Sulphur	% wt	0.25
Ash	% wt	7.71
Oxygen (diff)	% wt	23.73

Product Gas Composition (moisture free basis) for C64

	%
CO	54.2
H2	37.7
CO2	7.4
H2S	0.2
N2	0.4
CH4	0.1
Tar	0.0

Carbon conversion	97.3%
Final temperature	1665 C

Table 10. Feed quality and product gas composition for sample C73

Sample ID:		C073
Test	Unit	
DRY BASIS		
Ash	% wt	0.49
Volatile Matter	% wt	54.12
Fixed Carbon	% wt	45.39
Sulphur	% wt	0.29
Calorific Value - Gross (as received)	BTU/lb	10461
Calorific Value - Gross (dry basis)	BTU/lb	11549
Calorific Value - Gross (as received)	Kcal/kg	5812
Calorific Value - Gross (dry basis)	Kcal/kg	6416
Calorific Value - Net (as received)	BTU/lb	9936
Calorific Value - Net (dry basis)	BTU/lb	11077
Calorific Value - Net (as received)	Kcal/kg	5520
Calorific Value - Net (dry basis)	Kcal/kg	6154
ULTIMATE ANALYSIS (dry basis)		
Carbon	% wt	67.46
Hydrogen	% wt	5.09
Nitrogen	% wt	0.78
Sulphur	% wt	0.29
Ash	% wt	0.49
Oxygen (diff)	% wt	25.89

Product Gas Composition (moisture free basis) for C73

	%
CO	52.6
H2	40.7
CO2	5.9
H2S	0.2
N2	0.5
CH4	0.1
Tar	0.0

Carbon conversion	98.5 %
Final temperature	1475 C

TRACE ELEMENT EMISSION MODELING

Trace elements present within coal can depart the gasifier with slag/ash if they are in liquid or solid phase. In such cases, trace elements and their products do not cause much harm as they are discarded with the slag/ash, though in liquid phase they could stick to the liner and cause harm. If in gas phase, they will be part of the product gas stream, and depending on the products they form, they can harm downstream infrastructure and processes. For example, vanadium compounds cause corrosion in power plants. HSC CHEMISTRY[2] was used to model trace element behavior. This is similar to work done by Diaz-Somoano and Martinez-Tarazona (2003) who also used thermodynamic equilibrium modeling in HSC CHEMISTRY to understand trace element behavior during coal gasification.

Figures 4 to 6 show the various products formed from selected trace elements (Hg, V, As) when raw coal is gasified. The readers are instructed to disregard the units of the y-axis (kilo mole). The magnitude of emissions are based on the coal flow simulated (100 grams/sec). What is important are the implied relative proportions of various products shown in the plots.

The product species can change depending on temperature. The modeling approach does not distinguish between gasification technologies. However, since temperatures inside the gasifier are different for different technologies (900-1000C for moving bed, and 1300-1500C for entrained flow), one can distinguish between trace element products that would form for different gasification technologies.

The products of Hg are in gas phase at high temperatures and thus will leave primarily with the product gas stream, while Vanadium products are likely to leave with the slag. Arsenic products will almost entirely be in solid or liquid phase, with gaseous emissions being negligible compared to those in other phases. Figure 7 to 9 show the same when C64 was gasified. The sample C64 was coal leached directly by HF, i.e. it was not pre-leached with nitric acid. The products of Hg and V follow the same pattern as raw coal, whereas for arsenic, gasification of C64 results in mostly gaseous products. Thus, when leached coal C64 is gasified, whatever little arsenic is left in the coal will likely end up in processes downstream of gasification.

[2] http://www.outotec.com/

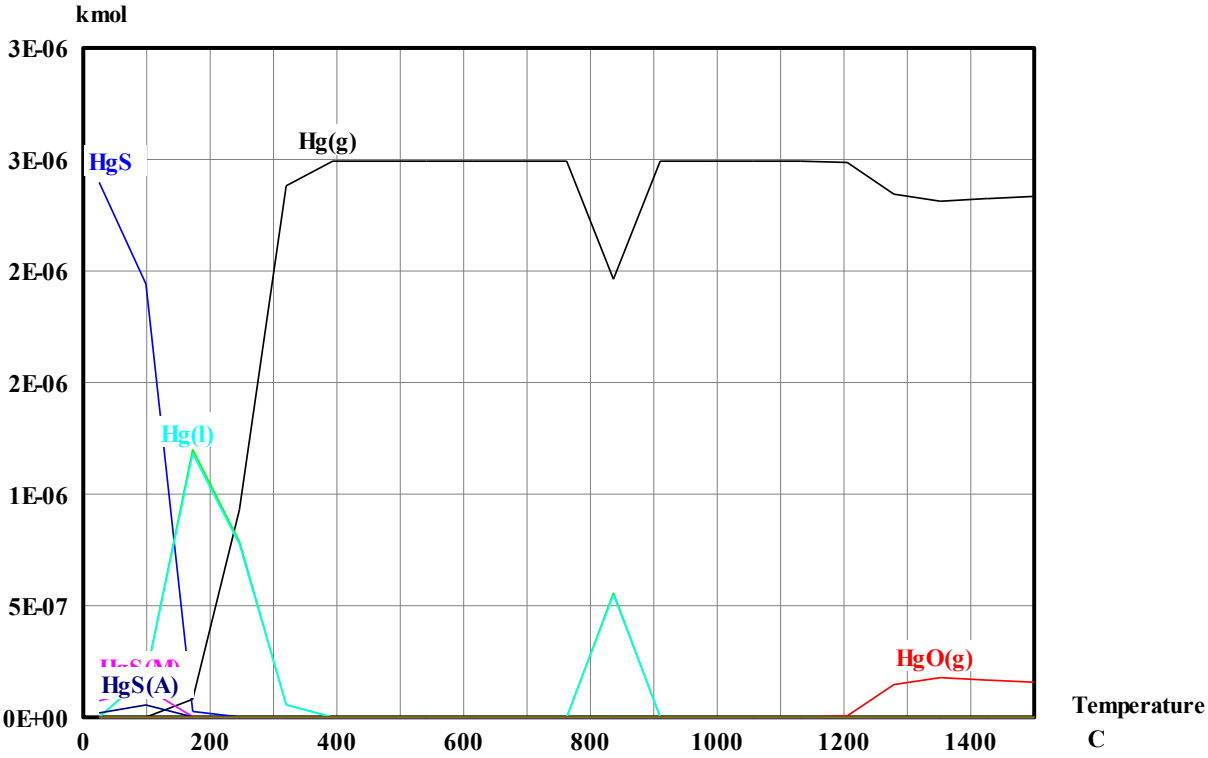

Figure 4. Plot shows the species and phases (g for gas, and A for amorphous) in which Hg and its products leave the gasifier.

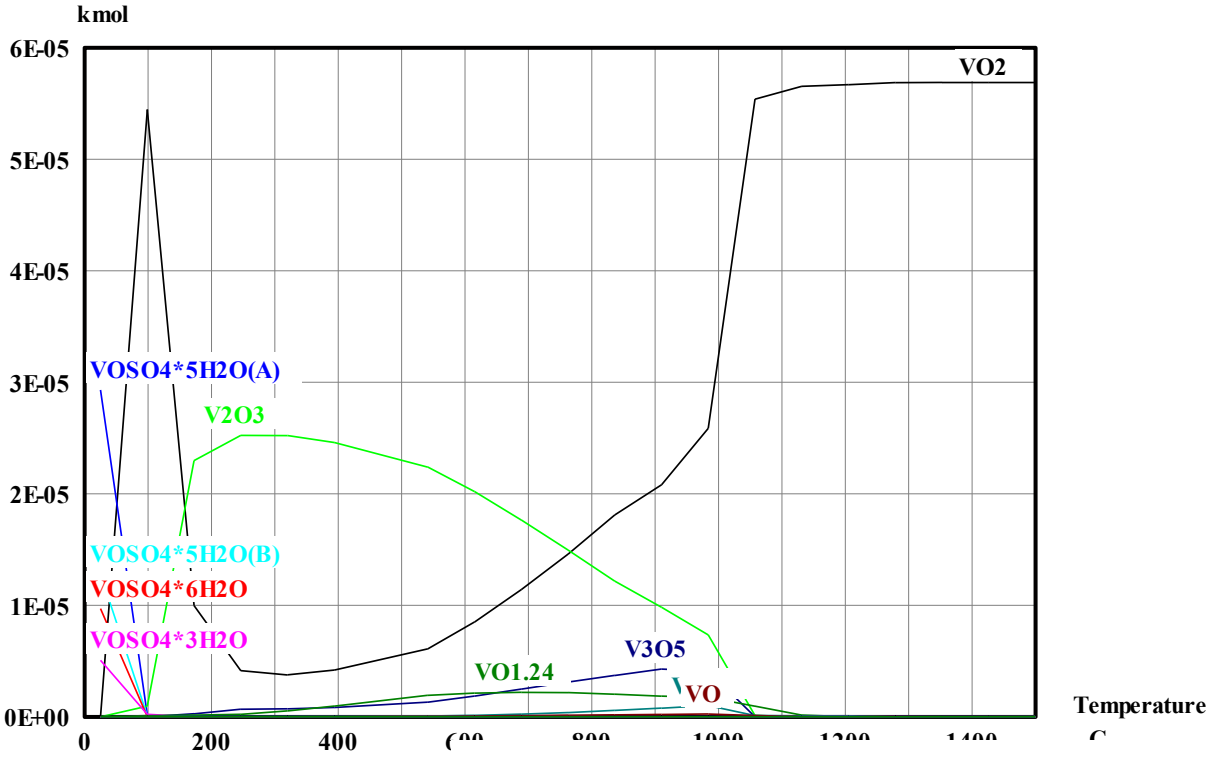

Figure 5. Plot shows the species of various Vanadium (V) products leaving the gasifier. Most will be in liquid phase.

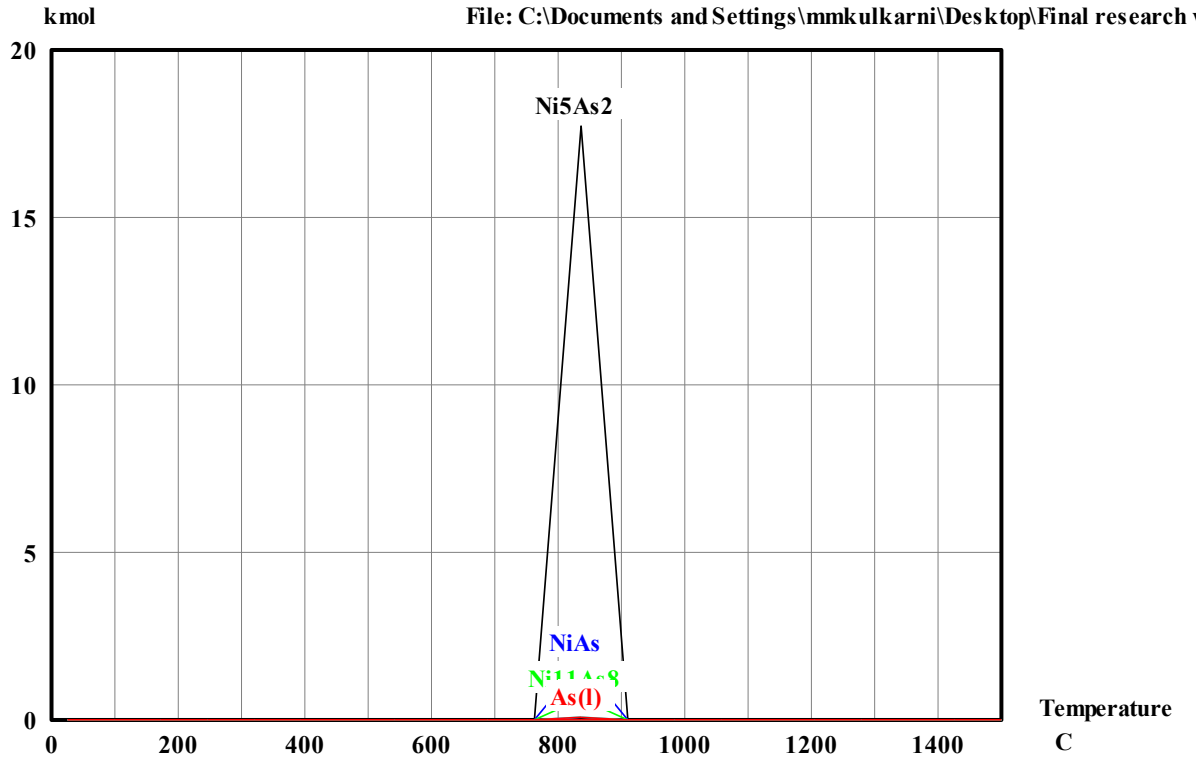

Figure 6. Arsenic products will almost entirely be in solid or liquid phases when raw coal is gasified.

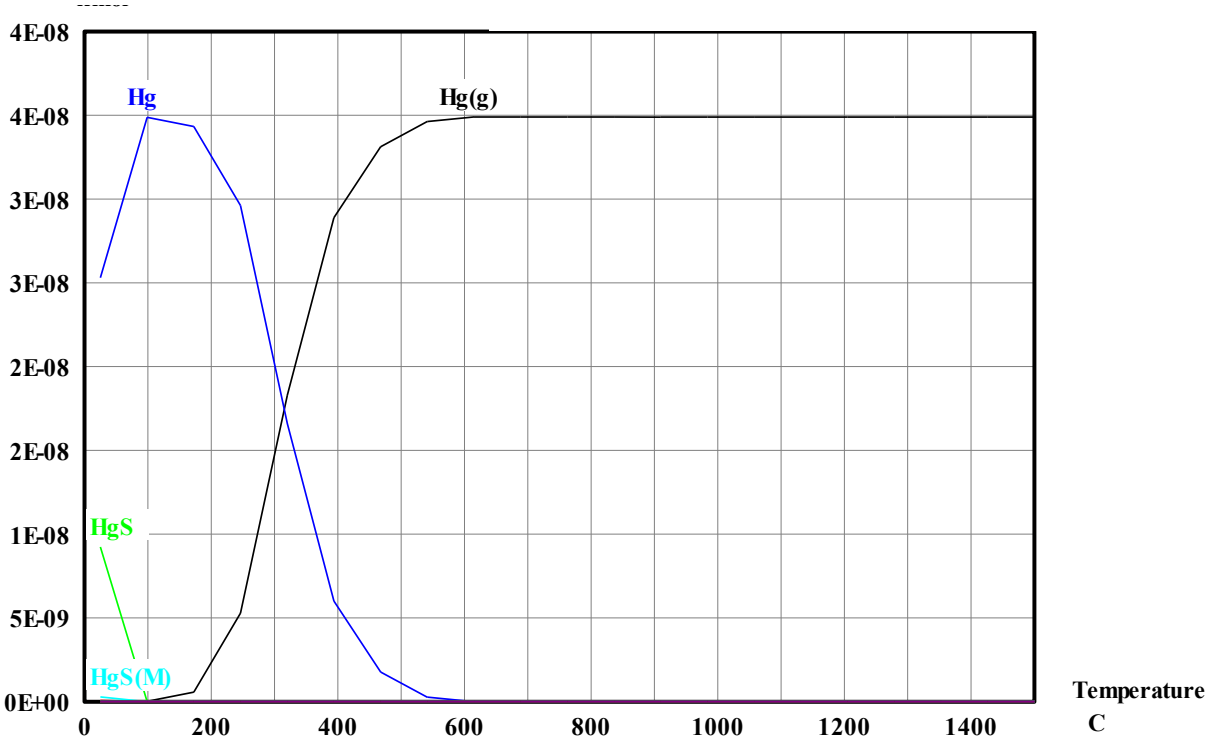

Figure 7. Mercury (Hg) emissions be in gaseous phase for leached coal (C64) gasification

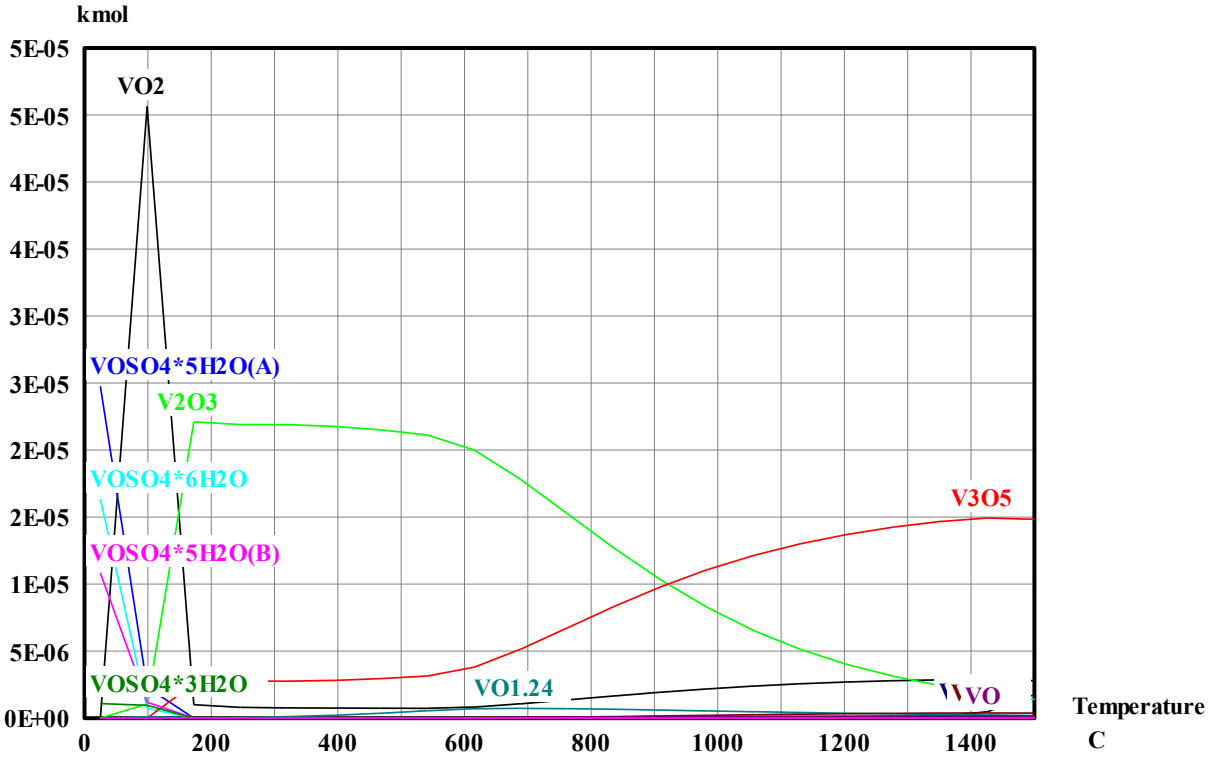

Figure 8. Vanadium products when C64 is gasified.

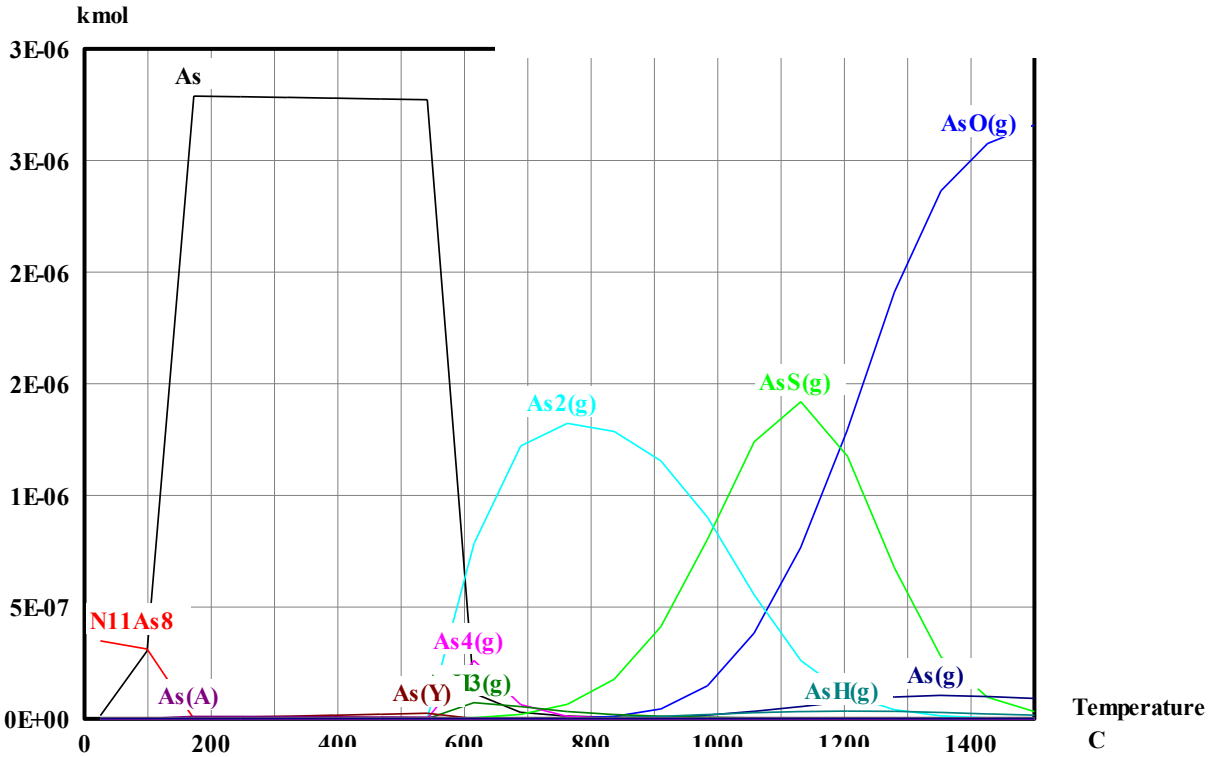

Figure 9. Arsenic products for C64

CONCLUSIONS

This project studied three important aspects of gasification of low rank Alaska coal (LRAC). The first aspect involved ultra cleaning of coal. The ash content in coal is extremely harmful to gasification units, especially in entrained flow gasification. Ultra cleaning of coal has the potential of bringing down the ash content to 0.5% or below, at which point, the coal is so pure that it can be burnt directly in a gas turbine. This project conducted leach tests on coal using hydrofluoric (HF) acid. When the raw coal was leached directly with HF, acid reduction was not significant. However, when it was cleaned by gravity methods, followed by nitric acid leaching (5 minutes) before being leached with HF, the results were excellent, as ash content was brought down from 12.4% to 0.49%. The leach kinetics with HF were slow, with ash reduction to 0.49% requiring a HF leach duration of 16 hours. The implications of the ultra cleaning tasks are:

- Ash levels of low rank Alaska coal can be brought down to very low levels if necessary. However, ultra cleaning to total ash levels of 0.5% or below will require significant effort including gravity cleaning, grinding (-150 microns), nitric acid leaching (5 minutes) and HF leaching (16 hours).

- When ash levels are so low--
    - Equipment life in CTL plants will increase significantly. This is especially true for the gasifying units.
    - Coal can even be burnt directly in gas turbines for electricity generation

The second aspect of gasification that was studied was the performance of two competing technologies, moving bed gasification and entrained flow gasification. The technologies were simulated using process modeling software ASPEN PLUS[3]. Moving bed gasification resulted in a product gas stream with a synthesis gas proportion ($CO+H_2$) of 60.5%. There was significant methane (8.4%) and CO_2 (28.8%) content. There was also some amount of tars. Entrained flow gasification yielded much cleaner product gas, with a synthesis gas proportion ($CO+H_2$) of 91-93%, low CO_2 and negligible tars and methane. Simulation studies also revealed a significant gap in fundamental laboratory data that is necessary to conduct accurate simulation of low rank Alaska coal.

The third aspect of gasification that was studied was the pathway taken by select trace elements, Hg, V and As, when LRAC is gasified. Thermodynamic equilibrium modeling in HSC Chemistry[4] showed that regardless of the type of coal gasified (raw coal or leached coal), mercury products would be in gas phase for both moving bed and entrained flow technologies. Thus, these would depart the gasifier along with product gases and, therefore, have the potential for causing harm downstream. Vanadium products on the other hand would be in solid/liquid phase and thus leave with ash/slag and thus, not be harmful to downstream processes. Unlike for arsenic, the phases of the products of Hg and V are the same in both raw coal gasification and leached coal gasification. For leached coal gasification, products of arsenic will be in gas phase and thus, end up in the product gas stream. For raw coal gasification on the other hand, products of arsenic will probably end up in the ash/slag.

[3] http://www.aspentech.com
[4] http://www.outotec.com

CHAPTER 7: REFINING A PLUME MODEL TO PREDICT ICE FOG DEVELOPMENT ASSOCIATED WITH A CTL FACILITY

by Martin Stuefer[1], Chang Ki Kim[1], and Carl Schmitt[2]

INTRODUCTION

Strong surface temperature inversions commonly form during Arctic winter months due to radiative cooling in combination with minimal solar radiation input. The cold stable boundary layer inhibits vertical aerosol exchange with the free atmosphere and can lead to continuous formation of atmospheric ice crystals. Exhaust from power plants and vehicle fuel combustion laden with pollution particles and excess water vapor is trapped below the inversion layers. Aerosol concentrations and vapor availability can both have a significant role in how optically thick ice fog can get. Ice fog microphysical properties have not been studied in Alaska in several decades. In the time since the previous measurements, the populations of the AFB, Northpole, and Fairbanks have significantly increased and the added pollution from more vehicles and power plants may have significantly altered the atmospheric conditions under which ice fog occurs. The occurrence of ice fog can have a serious impact on local populations by keeping daytime temperatures low as well as by decreasing visibility, affecting airport operations and vehicle travel. A better understanding of ice fog microphysical properties facilitates better modeling results leading to better forecasting. The purpose of this study was to provide high quality microphysical information on the ice fog particles and to improve model representation of ice fog.

Curry et al (1990) state that the main formation mechanism of ice fog and diamond dust is the advection of warmer air from the midlatitudes, which then radiatively cools on cloud free nights. Wendler (1969) suggested that additional moisture sources for ice fog included automobiles, power plants as well as household heating. Power plants with year round open water-cooling ponds add vapor as well as particle nuclei. Kumai (1966) showed that 90% of ice fog particles had nuclei, which were combustion products. Benson (1970) calculated that $4x10^6$ kg of water vapor per day was released into the atmosphere in the city of Fairbanks. As this study is more than 40 years old, it is safe to assume that vapor emissions are higher today. Moisture and pollution trapped below the inversion layer remains there until local meteorological conditions are perturbed. Figure 1 shows ice fog in the Fairbanks region during prime ice fog formation conditions. Exhaust plumes from vehicles and power plants do not appear to dissipate over time. The population of Fairbanks has increased substantially in the past 60 years. In the period between 1950 and 1970 the population of Fairbanks tripled, then doubled again by 2010. This significant increase in population has undoubtedly been accompanied by a significant increase in vehicular traffic as well as power plant activity in the Fairbanks area.

[1] Geophysical Institute, University of Alaska Fairbanks, Fairbanks, Alaska
[2] National Center for Atmospheric Research, Boulder, Colorado

Figure 1: Images of ice fog during measurement period on January 27, 2012 in Fairbanks, Alaska. The temperature was approximately -43C. A: Power plant in the background and vehicle exhaust plume. B: Ice fog near open water cooling pond at Eielson air force base. C: Ice fog over the city of Fairbanks.

The microphysical properties of ice fog have not been measured for many decades in the Fairbanks, Alaska region. Measurements of ice fog particles in the Fairbanks area by Thuman and Robinson (1954) showed that ice fog particles were often quasi-spherical 'droxtal' shaped particles with a mean diameter of 13 μm. Kumai (1966) observed ice fog particles to be between 2 μm and 15 μm in size with a sharp peak near 7 μm and concentrations between 100 cm^{-3} and 200 cm^{-3}. Ohtake and Huffman (1969) observed ice fog with median particle sizes between 3 μm and 8 μm and concentrations between 30 and 668 particles per cm^{-3}. These studies were generally conducted by collected particles on microscope slides coated with silicone oil. Slides were examined under a microscope and differential fall speed estimates were used to estimate size distributions and concentrations.

This report describes microphysical measurements of ice fog particles taken in the winter of 2012 in the Fairbanks region. During the observation period, the air temperature dropped to as low as -47ºC and dense ice fog decreased the visibility to as low as half a mile as measured at the Eielson AFB. We describe in the following the ice fog particle observation instrumentation and analysis techniques. We further will show results of the observations including particle size

distributions, particle habit information as well as time series showing the change in properties over time. The implementation and results of observations into the WRF microphysics scheme is described in the following paragraphs.

INSTRUMENTATION AND ANALYSIS TECHNIQUES

The microphysical properties of ice fog have been measured during the winter of 2012 in the vicinity of the Eielson AFB control tower. The National Center for Atmospheric Research (NCAR) Video Ice Particle Sampler (VIPS) probe was used to collect data continuously throughout several heavy ice fog events. Microscope slides with liquid formvar (polyvinyl formal) were also used to collect ice fog particles at the AFB and during an especially heavy ice fog event near the Fairbanks International Airport. Conditions in the Eielson AFB area were significantly influenced by the nearby power plant with the non-frozen cooling pond, which produced abundant particle nuclei as well as vapor for particle growth. Measurements showed that during heavier ice fog events, the particles were generally droxtal shaped (quasi-spherical) for sub 10-micrometer particles while plate shaped crystals were more frequently observed at larger sizes. The particles observed during optically thin ice fog periods were often larger hexagonal plates with abundant irregular shapes as well.

Instrumentation

The NCAR VIPS was deployed to Fairbanks for ground based particle sampling of ice fog. The VIPS is an electro-optical instrument used to collect and image a continuous sample of cloud particles down to sizes smaller than 5 μm. The VIPS has been used for airborne field campaigns as well as laboratory measurements for several years (Schmitt and Heymsfield, 2009, McFarquhar and Heymsfield 1997, Schoen et al, 2011). Particles are collected continuously on a looped clear plastic belt coated with silicone oil. The portion of the belt exposed to the atmosphere is imaged by a high-resolution video camera. The resulting video imagery is recorded onto a solid-state digital video recorder (DVR). For ground based and laboratory measurements the VIPS is housed in a sealed canister with a sampling inlet and an outlet equipped with an aspiration fan. To facilitate easy calibration, the canister used in Fairbanks was the same canister that is regularly used for laboratory experiments in the Aerosol Interaction and Dynamics in the Atmosphere (AIDA) cloud chamber in Karlsruhe, Germany. A variable speed fan drew air through the system at between 22 and 66 liters of per minute, which is comparable to values used in the AIDA cloud chamber.

The DVR recorded video at a rate of five frames per second. Software was used to extract individual frames from the video files. The resolution of the VIPS images is 1.12 microns per pixel making it possible to detect particles as small as 3 microns under ideal conditions. The collection efficiency of the VIPS has been estimated using calculations based on Ranz and Wong (1952) for particles larger than 10 micrometers. For the sub-10 micrometer size range, Ranz and Wong (1952) predicts that few particles would be collected and none smaller than 6 microns. As the VIPS did image particles in that size range, an empirical collection efficiency curve was determined. To do this, the particle size distribution measured with the VIPS was compared to particle size distributions calculated from the formvar slides (see below for discussion of formvar measurements). Empirical collection efficiency values for the VIPS were determined by looking at the relationship between particle concentrations in several of the smallest size bins. The

results of this comparison indicated that the VIPS was under-sampling the smallest particles (sub 5 μm) by a factor of 9 and the 5 to 10 μm range by a factor of 2. Figure 2 shows a VIPS particle size distribution before and after correction as well as a plot showing the correction factor applied to each size bin. Note that the median increase in total particle concentration resulting from the collection efficiency correction was 88%, while the median extinction increase was 27% and the median ice water content increase was 16.5%.

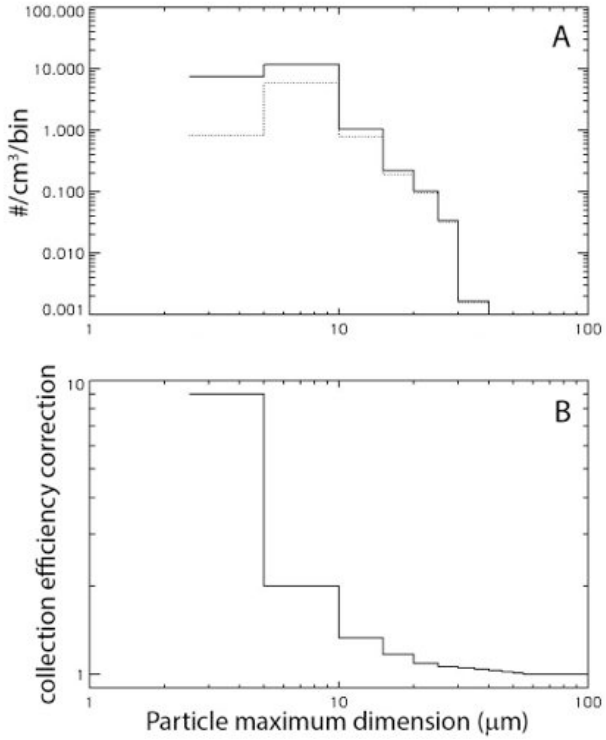

Figure 2: A: Measured particle size distribution from the VIPS (dotted line) corrected for collection efficiency uncertainties (solid line). B: Collection efficiency correction factor by size bin for VIPS data.

The VIPS aspiration fan speed as well as the belt movement rate could be varied depending on expected conditions. A faster belt speed and a slower fan speed would both result in fewer particles being in the field of view at once. Ideal settings led to approximately ten particles being in the field of view of each frame, though results varied significantly with fewer than one particle (on average) being in each frame to upwards of 500 particles being visible in a frame. The instrument was mounted on the side of a small trailer with the inlet approximately 1 meter above the snow surface. The data system was housed in a hard plastic case inside the trailer. The trailer was located in an infrequently used corner of a parking lot approximately 40 meters from the nearest road and 200 meters from the runway (see Figure 3 B). During operation the site was visited daily to change the memory card in the DVR as well as to check the data quality. If necessary, the instrument was returned to the lab for adjustments.

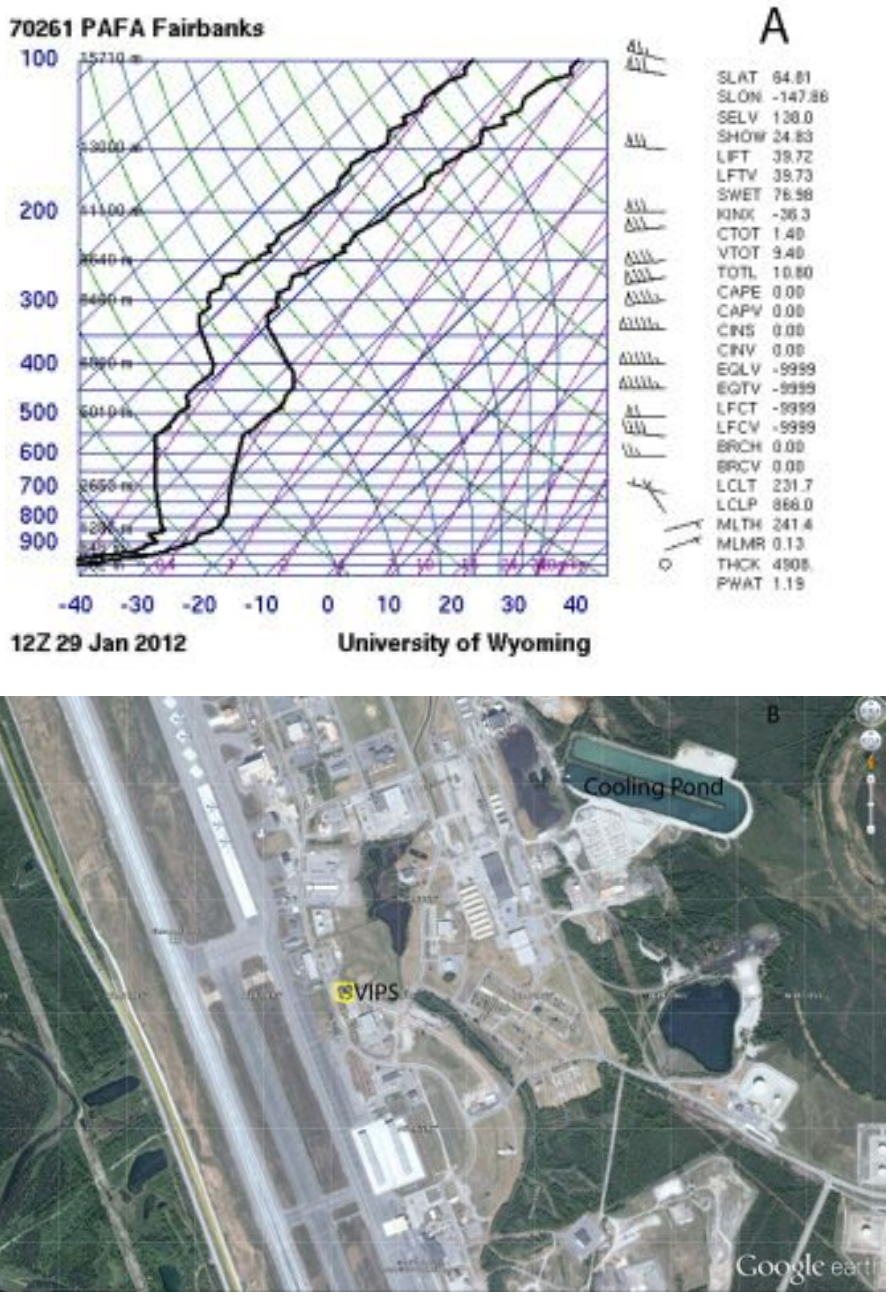

Figure 3: A: Sounding during heavy ice fog conditions. Note the extreme temperature difference near at the surface. B: Map showing the location of the VIPS, the power plant cooling pond, and the location of the NWS visibility measurement instrumentation at Eielson Air Force Base.

Formvar (polyvinyl formal mixed in a 7.5% by mass solution in Chloroform) coated microscope slides were also used to sample ice fog particles on several occasions. The slides were coated with liquefied formvar (see Takahashi and Fukuta, 1988) and placed on a flat surface to collect falling particles. Collected particles are encapsulated by formvar and when the formvar dries, perfect replicas of the particles remain. Particles replicas in the formvar were imaged using a Nikon Labofot-2 microscope with a Nikon D-80 DSLR camera attached. The DSLR photos had a resolution of approximately 0.42 microns per pixel enabling the measurement of particles as

small as 2 microns. Particle size distributions were calculated from ice fog particle replicas by scaling the number of observed particles by the estimated particle terminal velocity calculated using Heymsfield and Westbrook (2010). Ohtake and Huffman (1969) used this technique for scaling particle size distributions. Formvar coated microscope slides were used to collect particles if fog was present when the VIPS measurement site was visited as well as in the city of Fairbanks during a heavy ice fog event.

Analysis

Larger ice fog particles tend to be vapor grown and often have transparent parallel surfaces. Due to this fact, ice crystals impacted upon the oil coated belt often appeared similar in coloration to the surrounding oil with only the edges being obvious (see the large plates shown in Figure 4). Previous versions of VIPS analysis software have relied on the fact that aircraft observed ice crystals often appear much darker when immersed in oil due to their irregularity. Rather than re-write the software with improved edge finding capabilities, it was decided that the analysis could be done more quickly and accurately by hand. This also enabled the classification of particle shapes, which would have been less certain with automated software.

For each time period analyzed, individual particles were measured on the computer to determine the maximum dimension of the particle. This was done by using the line tool in Microsoft Paint software to determine the x and y extent in pixels of a line crossing the maximum dimension. For the most part, since plate shaped crystals dominated the larger sizes, the maximum dimension was equal to the dimension across the face of the plate (the a-axis). For each time period, the first 250 particles from the start of the time period were measured and used to determine the particle size distribution. In instances where the particle habit was non-uniform, the habit of each particle was also noted. The number of frames required to reach 250 was also tabulated which enabled the calculation of the sample volume. Images of irregular particles were also saved for later processing to determine the projected area to maximum dimension relationship.

For the analysis of the formvar slides, as with the VIPS data, 250 particles were measured and particle habits were tallied for each time period. Since formvar dries at different rates depending on the conditions as well as the application thickness, the particle size distributions could not be scaled without external information. Unscaled particle size distributions were scaled by the estimated particle fall speeds to determine the relative concentrations of each size bin. The NWS visibility measurements were used to scale the absolute values of the formvar size distributions, though significant uncertainty exists as the measurements were not collocated.

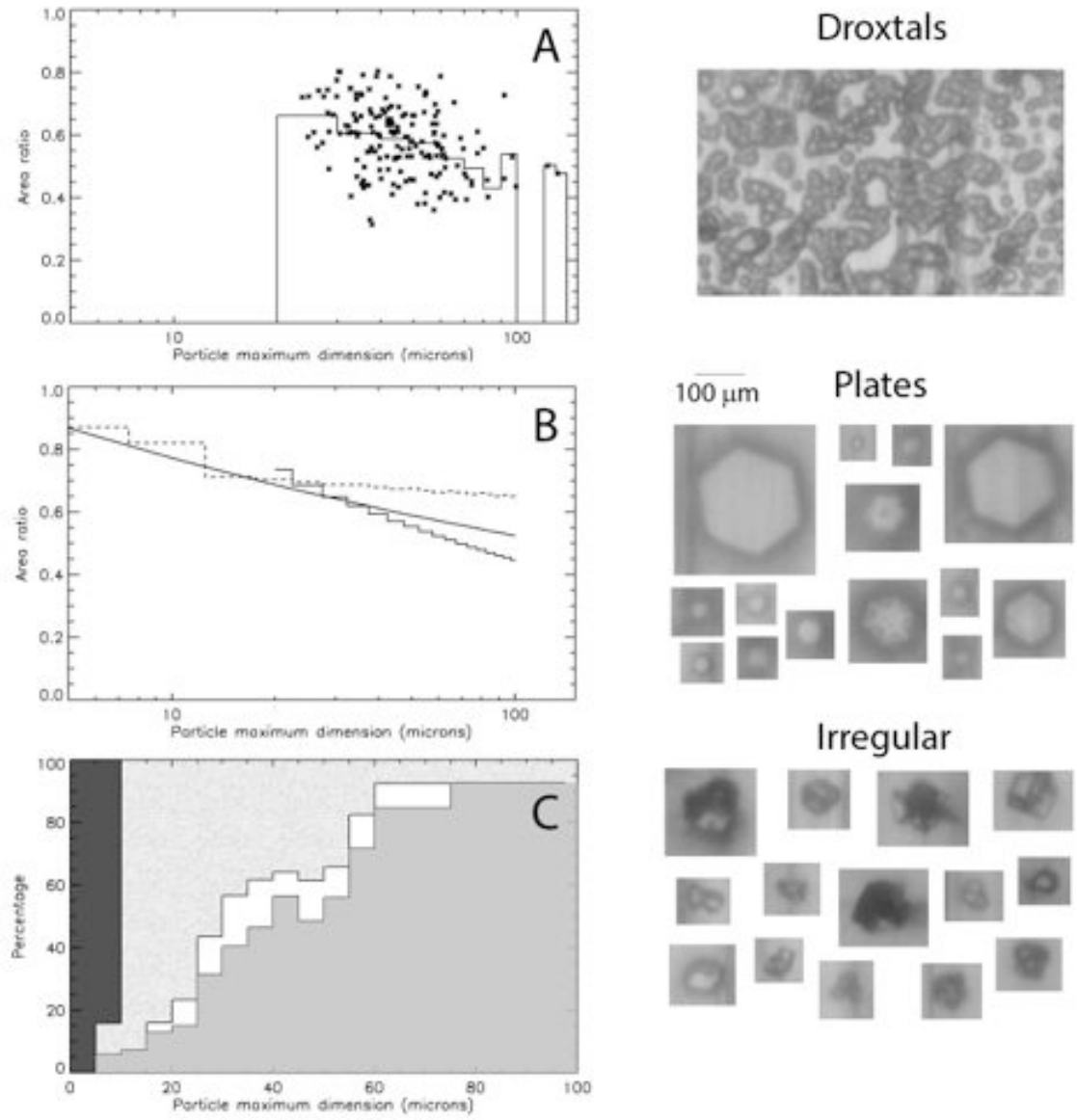

Figure 4: A: Measured area ratio for irregular particles. Individual particles are indicated with stars, and the median value per size bin is indicated by the solid line. B: Solid line with steps is a fit to the irregular area ratio values shown in A. Dashed line is the expected area ratio for randomly oriented plates of a given aspect ratio (see text). Solid smooth line: fit to average area ratio values based on percentage of each particle size present in each size bin. C: Particle habits observed by size: Dark gray: droxtals. Textured light gray: plate shaped crystals. White: column shaped crystals. Smooth light gray: irregular crystals. Example particle images from the more common habit types are also shown.

Measurements

During the January 26 to February 4, 2012 time period, there were several heavy ice fog events in the Fairbanks area. The ice fog developed on nights when the skies were clear and the surface was able to radiatively cool. A typical sounding from a particularly strong ice fog event is shown in figure 3. Note that the inversion at the surface was very strong and very thin. The temperature

150 meters above the surface was a full 10ºC warmer than at the surface. Figure 3 also shows a map with the location of the measurement site. The Eielson HPP with its open water-cooling pond was located near the measurement site. The location of the NWS visibility-monitoring site is also noted on the map.

The VIPS was operated at Eielson AFB nearly continuously during the January 26 – February 4 ice fog events. Only once was the ice fog so thick that the VIPS got completely clogged with ice particles. The probe operated successfully through several significant events where the NWS observed visibility dropped as low as 0.5 miles. Particle size distributions were determined from the VIPS measurements every 30 to 60 minutes throughout the events. Cloud extinction and ice water content were calculated based on the particle size distributions and the habit estimates. Particle shapes were categorized for all measurement periods. Figure 4 shows the breakdown of particle habits based on particle size for the entire dataset. Generally, particle habits were similar for all measurements when separated by particle size. Total percentages of observed habits changed dramatically as the properties of the particle size distributions changed. During the heaviest ice fog events, most of the observed particles were smaller than 10 microns and all were quasi-spherical droxtals, while during some lighter fog periods, the particles were all larger than 10 microns and the observed habits were mostly plate shaped crystals and irregulars.

The particle size distributions were integrated to get a bulk extinction value for visibility comparisons. To calculate accurate extinction estimates, it was necessary to estimate the projected area that would be blocked by individual particles which is not necessarily the projected area imaged by the VIPS. Breon and Dubrulle (2004) stated that particles with Reynolds numbers of less than 0.39 had no preferred orientation upon falling. Based on mass, maximum dimension, and area estimates, the 0.39 Reynolds number cutoff for the observed ice fog particles occurred at ~75 microns for the local temperature and pressure conditions. To calculate the average projected area of a randomly oriented hexagonal plate, a computer program developed by Schmitt and Heymsfield (2010) was used to create theoretical hexagonal crystals of known dimensions, which were rotated in three dimensions randomly. As it was impossible to measure both dimensions (the *a* and *c* axes) of plate shaped crystals from VIPS imagery, an equation derived by Schmitt and Arnott (1999) under similar conditions in the laboratory was used to estimate the thickness of plate shaped crystals. For column shaped crystals, both axes can be measured and it was determined that for the measured columns, the length was typically 1.5 times the width with no dependence on particle size which is also in agreement with the Schmitt and Arnott (1999) estimate for columns. For each set of crystal dimensions, the projected area was calculated for 5000 random orientations, which were then averaged to determine an average projected area for the crystal. For irregular shaped crystals, the area ratio of a selection of particles was determined and average values were calculated for each size bin. Figure 4 also shows the area ratio calculated for each of the different habit categories. As particle habits didn't vary much by size, this information was used to determine an area ratio relationship, which was used for all extinction calculations. For each size range, a weighted average was calculated of the area ratios based on the area ratio and percentage of each habit present in that size range.

The average mass of the observed ice fog particles was estimated in a similar way. The mass of droxtal shaped ice particles and hexagonal crystals was estimated by geometry. As it is not possible to determine the mass of irregular particles from two-dimensional images, we initially

assumed that irregular particles had the same mass as the hexagonal plates of the same maximum dimension. Uncertainty estimates were calculated by re-calculating the average particle mass while using different assumptions for the masses of the irregular particles. The area dimensional relationship and the mass dimensional relationship are shown in equations 1 and 2. Eqs. 1 and 2 are expressed in terms of particle area ratio and particle density (the three dimensional analogy of area ratio: the mass of the particle divided by the mass of a unit density sphere of equal maximum dimension). The principles of fractal geometry were applied to the particle area dimensional relationship and mass dimensional relationship to determine how synergistic the relationships are (Schmitt and Heymsfield, 2010). Fractal theory suggests that the projected area dimensional relationship and the mass dimensional relationship can be related if the particles grow in a random way. Following Schmitt and Heymsfield (2010), the three dimensional fractal dimension is 2.726 and the two dimensional fractal dimension is 1.832 (3.0+ the power in the density relationship and 2.0+ the power in the area dimensional relationship). The S factor (the ratio of the 3d fractal dimension and the 2d fractal dimension) is 1.49 which is very close to the 1.50 value that would be expected for particles that are single particles growing from vapor as opposed to aggregates. Equations 1 and 2 can each be used to determine the particle size, which should be spherical (or round in two dimensions). Both equations predict that particles would be spherical (and therefore have perfectly round cross sections) at between 1.0 and 1.5 microns, which, with the S=1.49 result, indicates that the equations make a good fractal pair. Though there is no known physical reason why the area and mass dimensional relationships should be a good fractal pair, it is convenient that they are.

$$A_r = 1.1386 * D^{-0.168} \quad (1)$$

$$\rho = 0.6626 * D^{-0.274} \quad (2)$$

With equations 1 and 2, it is possible to estimate particle terminal velocity using the Heymsfield and Westbrook (2010) formulations. Figure 5 shows the terminal velocity calculated for ice fog particles. Uncertainty estimates were made by recalculating particle terminal velocity with projected area and mass value perturbations at the upper and lower ranges that could be expected based on the observations. The resulting estimates show that the shaded uncertainty range is approximately +or- 30%. Stars on the figure represent mean values of terminal velocity measured by Kajikawa (1973) for differing particle shapes under slightly warmer atmospheric conditions. The dashed line shows the terminal velocity estimated for ice spheres for comparison. Given that the terminal velocity of 20-micron ice fog particles is less than 1 cm/s, it is not surprising that ice fog crystals remain airborne for a long time. A fit to the data is shown in equation 3.

$$V_t = 0.0027 * D^{1.73} \quad (3)$$

The data used to construct Figure 5, and equation 3 assumes a temperature of -40ºC and an atmospheric pressure of 1000 hPa. Equation 3 is similar to the equation reported by Heymsfield et al (2012) for particles smaller than 43 microns. Heymsfield et al (2012) presents an accurate method for adjusting terminal velocity estimates to different temperature and pressure regimes.

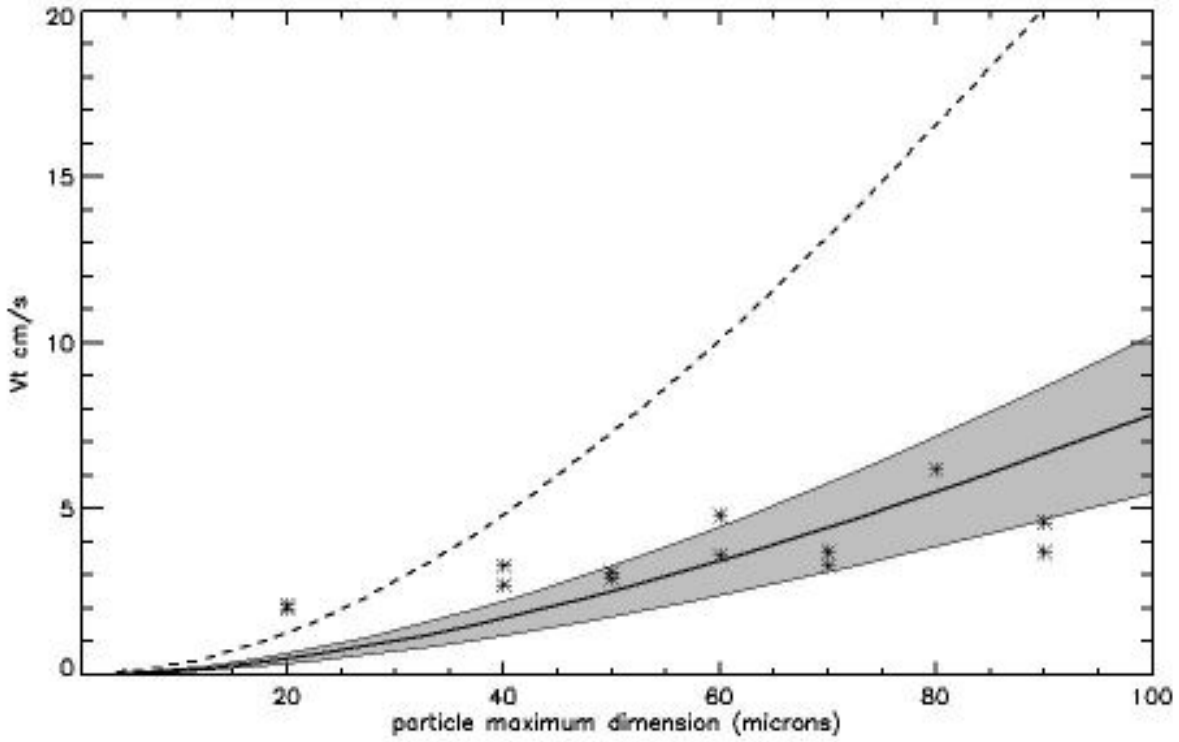

Figure 5: Particle terminal velocity calculated with area and mass assumptions described in text. Bold line is the value expected by particle size. The shaded area delineates a + or – 30% range based on applying minor perturbations to mass and area values. Dashed line is the calculated value for spherical particles. Stars represent direct measurements by Kajikawa (1973) under similar conditions.

Figure 6 shows several relationships for ice fog particle size distributions and bulk properties including ice water content and extinction. In all, values were derived from 36 particle size distributions, 30 from VIPS data, and six from formvar samples. Fog extinction was calculated by summing the projected area over the particle size distribution using equation 1, and then was converted to visibility using the Koschmieder equation (Koschmieder, 1924) $Vis = 3.912 / \sigma$ where σ is the extinction (the units of visibility depend on the units of σ). Figure 6a shows the relationship between the calculated visibility and the visibility measured by the NWS at the Eielson AFB site. Only data points shown for the VIPS are shown in 6a as the formvar measurements were scaled with by the visibility measurements. The scatter is likely due to the fact that the VIPS and the NWS instrumentation were not co-located and the plume from the power plant could easily impact one and not the other. Figure 6b shows fog extinction plotted versus fog ice water content with a fit (eq. 4). The relationship between extinction and ice water content does not compare well other relationships developed for ice clouds with particles in these size ranges. Typical parameterizations for ice clouds use mass and area dimensional relationships, which assume that the smallest particles are spherical. An exception to that rule is Schmitt and Heymsfield (2009) where they used exponential mass and area dimensional relationship. The ice water content to extinction relationship that they found implied a significantly higher mass as can be seen when comparing density relationships. This leads to a factor of three difference between their relationship and the relationship derived here for ice fog. Figure 6c shows the mass weighted fall speed plotted versus extinction (eq. 5). There is a lot of uncertainty in this relationship due to the fact that a small increase in the concentration of large

particles has a significant effect on the mass weighted fall speed. The points which appear to be outliers (very high extinction values) are the formvar measurements taken in Fairbanks, which were under much heavier conditions. The heaviest ice fog events were characterized by very small particles only, and as the fog lightened, larger particles became more prevalent. When visibility was lower, the mass weighted fall speed was quite variable. The plot appears to show two groupings. Further investigation shows that the low mass weighted fall speed times correspond to dissipating ice fog events while the higher mass weighted fall speed times correspond to times when there was diamond dust and little ice fog. The particle size distributions were fit to gamma distributions of the form $N(D) = N_o D^{\mu} e^{-\lambda_T \cdot D}$ where N_o is the intercept, λ_T is the slope, and μ is the dispersion. These parameters are plotted with respect to other more easily measured parameters in panels d, e, and f in figure 6. In general, the correlations are poor. Figure 6d shows the relationship between lambda and extinction. A poor trend is shown. The uncertainty is driven in part by the occasional large particle, which skews the distribution. Since the gamma fit is optimized to match the 2nd, 3rd, and 6th moment of the size distribution (Heymsfield et al, 2012), the occasional large particle causes a significant change in lambda. As these larger particles were likely in existence due to some other mechanism other than ice fog, it is reasonable to ignore them for strictly ice fog studies. Figure 6f shows the relationship between lambda and shape factor mu. As can be seen, there is a fairly good relationship (as has been found in previous research).

$$IWC = 0.0017 * \sigma^{0.74} \tag{4}$$

$$V_m = 0.3074 * \sigma^{-0.596} \tag{5}$$

$$\lambda_T = 1852 * \sigma^{0.16} \tag{6}$$

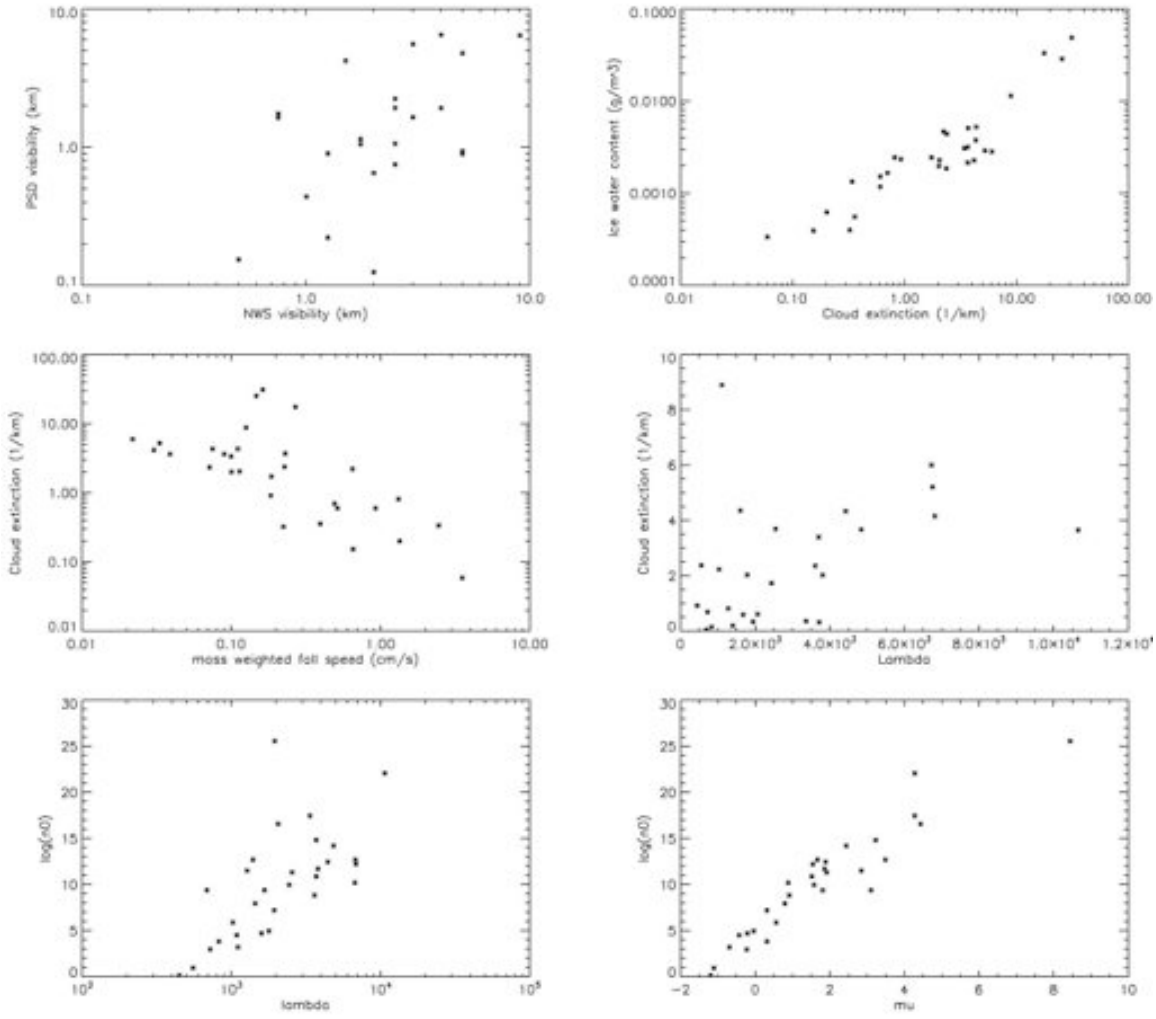

Figure 6: Particle size distribution properties from the measurements. 6a: The visibility calculated from the particle size distributions compared to the measured visibility. The comparison is reasonable, but significant uncertainty is due to the variability in the local conditions as apparent in the photo from the site (fig 1B).

As there no significant trends in ice fog microphysical properties with temperature for the entire dataset, the time evolution of ice properties for a thin and a thick ice fog event are shown in Figure 7. The specific conditions on the day dictate the onset of ice fog, and then ice fog generally develops similarly based on the temperature drop. The 1 February 2012 event (left side of figure) was significantly warmer and lighter than the 28-29 January 2012 event. The upper two plots show the evolution of the temperature for the two events. Note the different axes, as the 1 February event occurred under significantly warmer conditions and the temperature drop wasn't as significant. The second row of plots shows the evolution of the visibility measured by the NWS (dotted) and calculated from the VIPS measurements (solid). Note that the highest value recorded by the NWS instrument is 10 miles (~16 km), so the disagreement at the end of the 1 February case (7c) is due to the limits of the NWS reporting. The apparent shift in time of the peak in the 28 January case is likely due to the extreme variability of the ice fog over time due to the power plant plume. As seen in Figure 1B, the ice fog can be very thick and transition to much thinner fog nearby. As an example, when the photo

in 1B was taken, it was nearly perfectly clear approximately three kilometers to the east. The third row shows the time evolution of the calculated ice water content of the fog. Note that the highest ice water content values generally corresponded to times when the visibility was lowest. The bottom row of plots shows the slope of the particle size distributions from the VIPS measurements. While there is no significant trend, the slope values show that the particle size distributions were quite narrow.

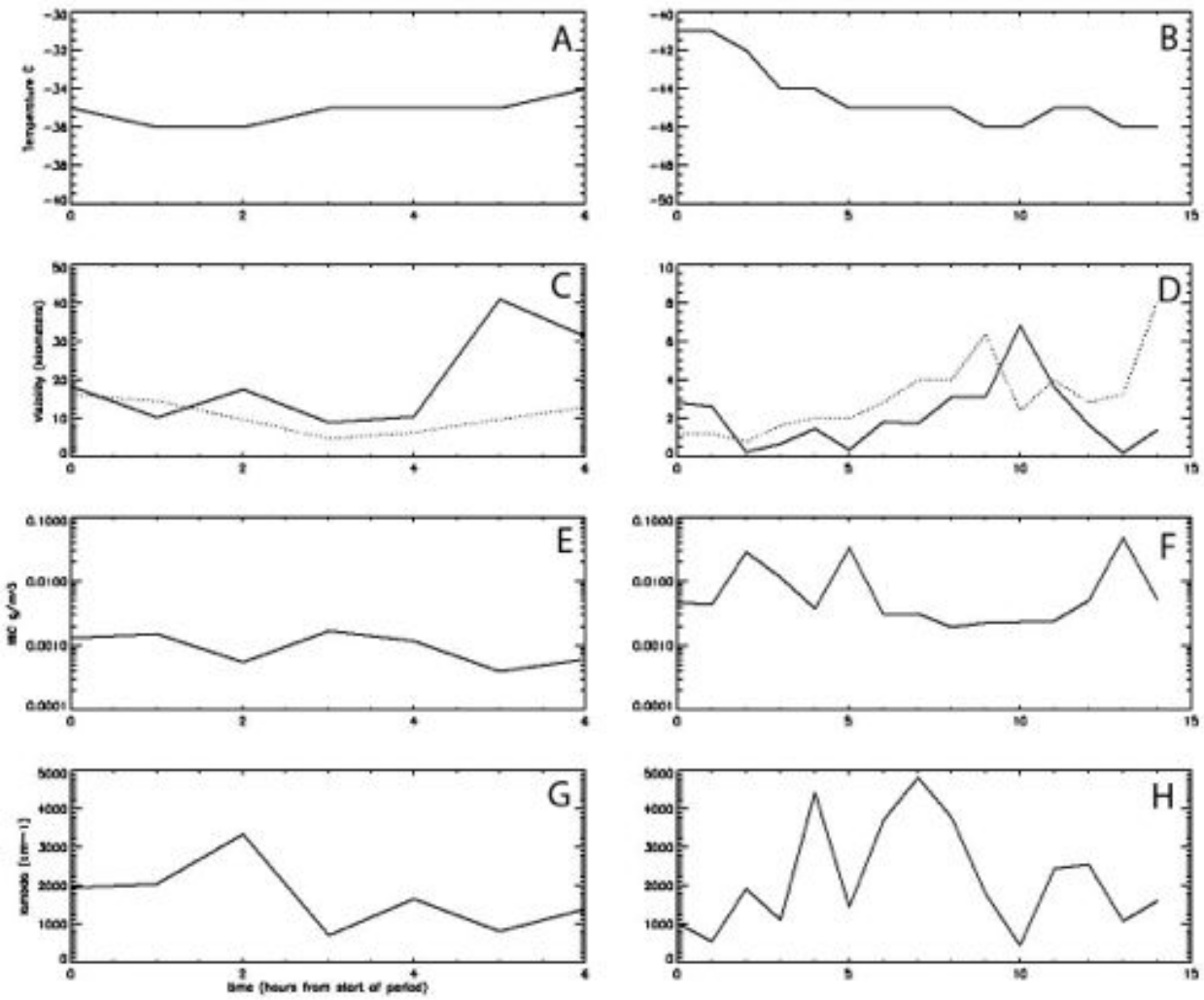

Figure 7: Time evolution of two ice fog events. A & B: Temperature during the ice fog events. Notice the different y axes values. C & D: Measured visibility (dotted lines) and visibility calculated from VIPS measurements (solid line). E & F: Ice water content calculated from VIPS particle size distributions. G & H: Slope of the particle size distribution.

Figure 8 shows particle size distributions from formvar measurements taken in Fairbanks during one of the most intense ice fog events. Formvar slides were used to collect ice fog particles near the Fairbanks International Airport. These data were notable because the visibility measured at the Fairbanks airport was significantly lower than at the Eielson AFB with values as low as 1/8th of a mile over night. As the particle size distributions were scaled by the estimated particle fall speed, and the formvar drying time was difficult to determine, the particle size distributions were scaled by the measured visibility. Slides were placed out every two hours through the night, but

only data from the evening and the following morning were usable as the liquid formvar mixture became too viscous for particle sampling during the coldest part of the night. Gamma fits to the particle size distributions are shown on the plots. The parameters for the gamma fits are displayed on each graph and some example particle images are shown as well. These measurements can be considered to be in a heavily polluted area as they were taken near an airport, a highway, and a major shopping area. Particle sizes were rarely larger than 20 or 30 microns and particles were mostly droxtal or plate shaped crystals. The occasional larger particles were plate shaped crystals and likely fell from above the ice fog layer.

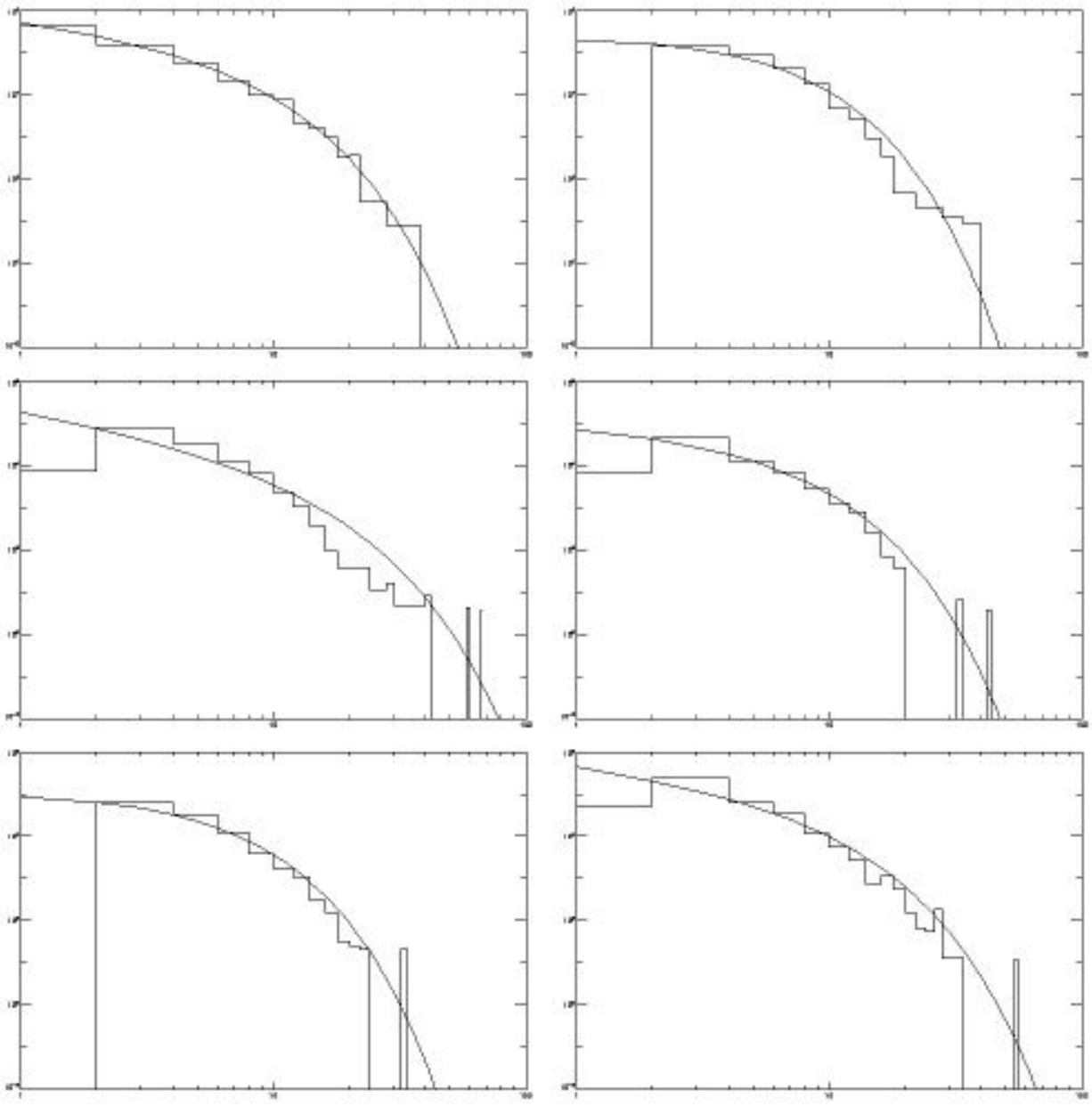

Figure 8: Particle size distributions and gamma fits for formvar measurements from Fairbanks. Gamma distribution parameters are printed on each plot and particle images are shown.

Microphysical characteristics

The following ice fog modeling experiments were developed with the data gained from the above measurements. Figure 9 is the time series of N_i and ice water content (L_i), measured at the Eielson AFB from 01 UTC to 15 UTC 29 January 2012. The mean N_i is 26.5 cm^{-3}, which is somewhat lower than N_i from the study by Kumai (1966). The other observation by Ohtake and Huffman (1969) showed that mean N_i ranges from 30 cm^{-3} and 668 cm^{-3} for eight ice fog cases. They mentioned that the ice crystal number concentration N_i is dependent on a given meteorological condition. In our observation, standard deviation and maximum value of N_i are 31.0 cm^{-3} and 99.4 cm^{-3}, respectively, and therefore the formation of ice fog particles is sensitive to the local meteorological characteristics. The ice water content L_i shows the larger fluctuation than N_i with mean L_i of 0.012 g m^{-3} (Fig. 9b). It is of interest to compare between L_i and N_i. L_i at 03 UTC 29 January is smaller than that at 06 UTC in same day whereas the opposite is true for N_i (96.9 cm^{-3} vs. 34.1 cm^{-3}). This is due to the difference of size distribution between two times. The size distribution of ice fog particles is given in Fig. 10. N_i for larger particles (larger than 25 μm) is 0.48 cm^{-3} and 3.4 cm^{-3} at 03 UTC and 06 UTC 29 January. It shows that the size distribution of ice fog particles is also a crucial factor determining the ice microphysical characteristics. For the ice habit, while the ice fog particles larger than 10 μm are mostly hexagonal plates, the smaller ice fog particles smaller than 10 μm are typically a mixture of plates and quasi-spherical ice. Kumai (1966) quantified the number of crystals with spherical shapes with 99 out of 105 crystals cm^{-3} collected during a case at –42°C.

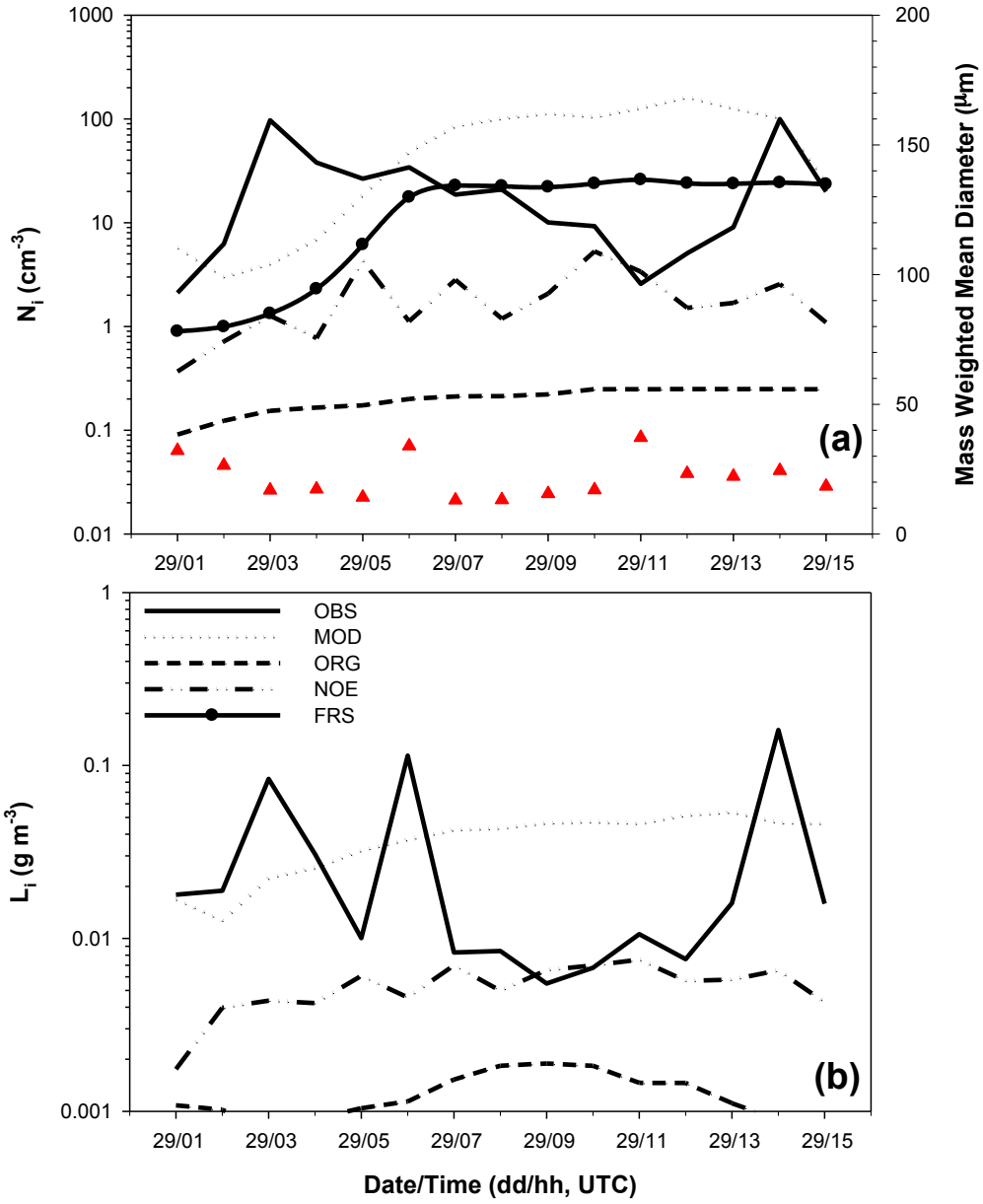

Figure 9. Time series of the number concentration (N_i) of ice fog particles (a) and ice water content (L_i) (b). The solid, dotted, dashed and dash-dot lines indicate the observation (OBS), the MOD, ORG, and NOE experiment, respectively. N_i from the FRS experiment is only illustrated in (a) as a solid line with closed circle.

Modification of ice microphysics process

We use the WRF version 3.2 to evaluate the performance for the formation of ice fog particles. Here, explained are the ice microphysics scheme, which is employed in the WRF for the purpose of this study. We employ the Thompson scheme (Thompson et al., 2004, 2008) as the cloud microphysics in the simulation. The Thompson scheme includes the five hydrometeors (cloud water, rain, ice crystal, snow and graupel) with water vapor and the number concentration of ice crystals and rain are treated as a prognostic variable. Microphysical processes for ice crystals are composed of ice crystal nucleation, freezing of water drops, ice multiplication, depositional growth, accretion, riming and aggregation. The first three processes are related to the formation of ice crystals. Depositional growth calculates the increase or decrease in the mixing ratio of ice crystal, based on the ambient concentration of water vapor. The last three processes contribute to the decrease in the mixing ratio and number concentration of ice crystals as a sink. As mentioned before, T was below –40°C during the observed ice fog episodes. At extremely low T, there is little supercooled liquid water in the cloud (Curry et al., 1990). Therefore the present study focuses on the ice crystal nucleation and depositional growth.

Ice Nucleation

In the original Thompson scheme, the ice crystal number concentration, which is the product from the heterogeneous nucleation and condensation freezing (Rogers and Yau, 1989), is determined by a formulation as a function of T. Most of mesoscale numerical models employ a simple formulation as a function of T since Fletcher (1962) presented the relationship between N_i and T. However, the method by Fletcher (1962) ignores the water vapor mixing ratio. As an alternative, Meyers et al. (1992) suggested the new formulation of N_i as a function of supersaturation. We tested the method by Meyers et al. (1992) to generate the ice fog particles in order to identify the influence of water vapor emission on the formation of ice for particles. However, this approach failed since the ice nucleation by Meyers et al. (1992) is valid for T between –5°C and –25°C.

Figure 10c represents the relationship between N_i and T, employed in the original Thompson scheme. N_i due to the heterogeneous nucleation exponentially increases as T decreases. For the lower T lower than –36°C, N_i is set as a maximum value of 250 L^{-1}. This value is much lower than mean N_i, 26.5 cm^{-3} (note the unit) as mentioned above. For the successful simulation of the ice fog episodes, we need to find the new formulation. Ohtake (1970) suggested N_i as a function of the ambient T. Ice fog particles, falling on the unit area at the unit time, are parameterized with the ambient T as follows:

$$N_H = \exp(-0.285 \times (T_0 - T) - 3.07), \quad (7)$$

where T_0 = 273.15 K and N_H is the number of ice crystals that fall on the unit area at the unit time (cm^{-2} min^{-1}). The precipitation method used by Ohtake (1970) is affected by the terminal velocity. In his report, terminal velocity is also given as a function of T as follows:

$$v_i = A + B \times T + C \times T^2 + D \times T^3, \quad (8)$$

where A = 26.83, B = 0.9143, C = –0.6845 x 10^{-3}, D = –0.1736 x 10^{-3} and v_i is the terminal velocity (cm s^{-1}). With above equations (7) and (8), N_i (m^{-3}) can be calculated:

$$N_i = \frac{N_H}{v_i} \times \frac{10^6}{60}. \quad (9)$$

Ice fog particles measured by Ohtake (1970) are not strictly newly formed ice fog particles. Nevertheless, we use equation (9) as an alternative for ice nucleation process in the model since ice fog particles, which are newly activated, only grow due to the vapor diffusion without the interaction with supercooled liquid water. Equation 9 is illustrated in Fig. 10c. Ohtake (1970) set the maximum value of N_H to 4500 $cm^{-2}min^{-1}$ at – 38°C to prevent to overestimate N_H at the extremely cold atmosphere. In our study, the maximal N_i is prescribed as 300 cm^{-3} at –40°C with the terminal velocity using the equation 8.

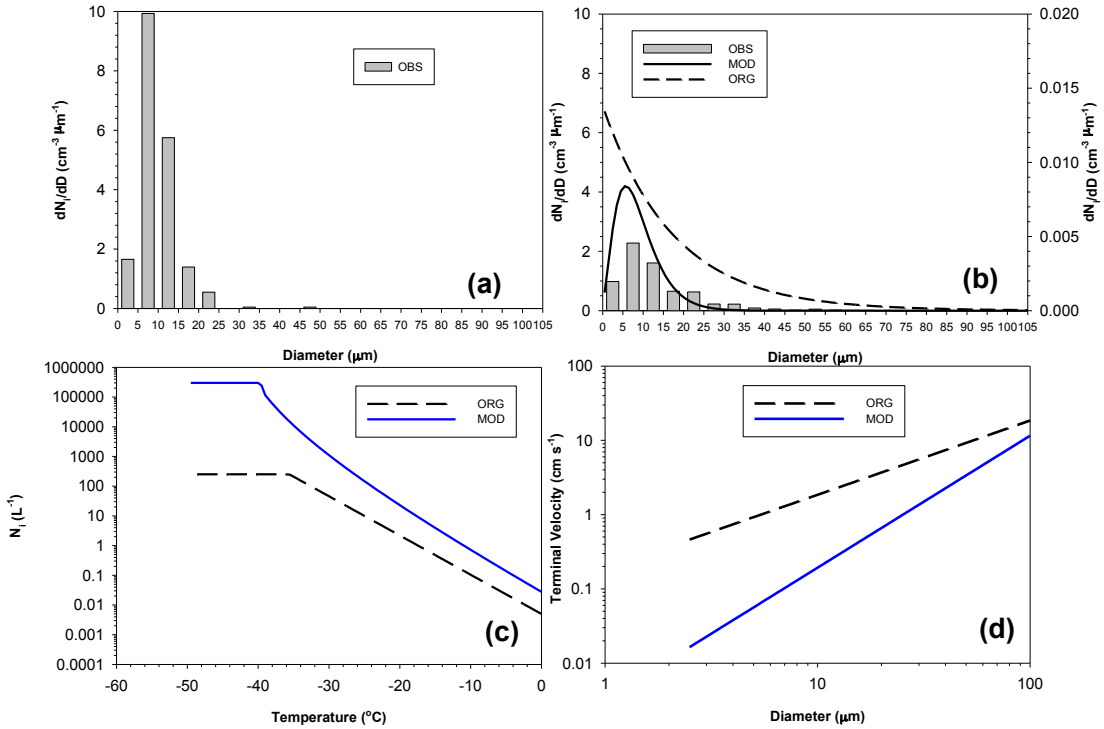

Figure 10. The size distribution of ice crystals observed at 03 UTC (a) and 06 UTC (b) 29 January 2012. The simulated size distributions of ice crystals from the MOD and ORG experiment are illustrated in (b). The number concentration of ice crystals (N_i) as a function of air temperature (T) and terminal velocity as a function of diameter from the MOD and ORG experiment is given in (c) and (d), respectively. In each plot, the solid and dashed lines indicate the MOD and ORG experiment, respectively.

Size distribution of ice crystals

As introduced above, low L_i with high N_i indicates that the mean diameter of ice fog particles is small. This is connected to the size distribution of ice crystals in the model. The original Thompson scheme assumes that the ice crystals have the Marshall-Palmer distribution with mean weighted mass diameter (MWMD) ranging between 20 μm and 300 μm. N_i and the scale factor, λ in the model are adjusted by the constraint for MWMD. However, Kumai (1966) reported that most ice fog particles are between 2 μm and 15 μm in diameter with a sharp peak in the distribution near 7 μm. In our observations, ice fog particles are distributed between 1 μm and 60 μm with a peak at 7.5 μm (Fig. 10b). Furthermore, Figure 10a shows that MWMD from our observation is between 13 μm and 37 μm. Consequently, we changed the size distribution of ice crystals from the Marshall-Palmer distribution into the Gamma distribution with the shape factor, μ = 2.0, which is the average value of the size distribution observed during the ice fog episodes. In addition, the present study assumes that MWMD for ice crystals have a narrow range from 1 μm and 125 μm in diameter. Therefore the initial mass of ice crystals should be fixed. This study prescribes the initial mass of ice crystals as 1.7×10^{-16} kg, which is equivalent to the mass of the sphere with the diameter of 1 μm and the density of 330 kg m^{-3}, which is the average density of our observed ice crystals.

Gravitational Settling

The gravitational settling is a very specific characteristic for each ice fog particle. Ice fog particles are considered as the suspended particles in analogy to fog droplets. In general, terminal velocity is expressed by the power law as a function of the particle diameter (Straka, 2009). The original Thompson scheme employs the power law as the terminal velocity from the study. Figure 10d shows the terminal velocity from the original Thompson scheme and our observed velocities. For ice crystals smaller than 10 μm in diameter, terminal velocities from the observations are much slower than those from the original Thompson scheme. The slow terminal velocity makes the simulated ice crystals be suspended longer in the air. We replace the terminal velocity for the gravitational settling with the following equation (10).

$$v(D) = \alpha \times D^{\beta}, \quad (10)$$

where $\alpha = 0.647 \times 10^{7}$, $\beta = 1.73$, D is diameter (m) for an individual ice crystal and v is terminal velocity (m s^{-1}). Note that the terminal velocity as described in equation 10 is different to the terminal velocity in equation 8, which is only used to estimate N_i from the measurement by Ohtake (1970).

Thus, the present study corrects the ice microphysical processes for the successful simulation of ice fog case. The corrections are summarized as follows:

1) the ice nucleation formulation is updated;
2) the initial mass of newly nucleated ice crystals and ice density are changed;
3) The size distribution was changed to a gamma distribution from the previously used Marshall-Palmer distribution;
4) MWMD was corrected to be between 1 μm and 125 μm in diameter for ice crystals;
5) The terminal velocity was reduced for ice crystals to be suspended significantly longer in the air.

NUMERICAL MODELING

Parameterization of water vapor emissions

A primary goal of this study is to modify the ice microphysics with a given observation data to evaluate the influence of water vapor emission on the formation of ice fog. To accomplish this, water vapor emission is added from the local source, which is the Eielson HPP and its cooling pond (64.67 ^{o}N, 147.09 ^{o}W). The emission rate of water vapor at HPP is set according to the established baseline emissions as 30 tons h^{-1}. Water vapor, emitted from the HPP, is dispersed by the wind field, is diffused by the turbulence, and is transferred to the ice crystal due to the nucleation process. Figure 11 presents the flow chart to generate the ice crystals with the dispersion of emitted water vapor from the local sources. If the mixing ratio of emitted water vapor (q_{ve}) at a certain grid point is higher than 0.01 g kg^{-1} after the dispersion of water vapor, it is added to water vapor (q_{vn}), which naturally exists. This study sets the same activation condition by the supersaturation as the original Thompson scheme, i.e., ice crystal is generated when the water vapor mixing ratio exceeds 25% supersaturation with respect to ice. The total water vapor mixing ratio ($q_v = q_{ve} + q_{vn}$) enables the ice crystals to be generated when the activation condition is met.

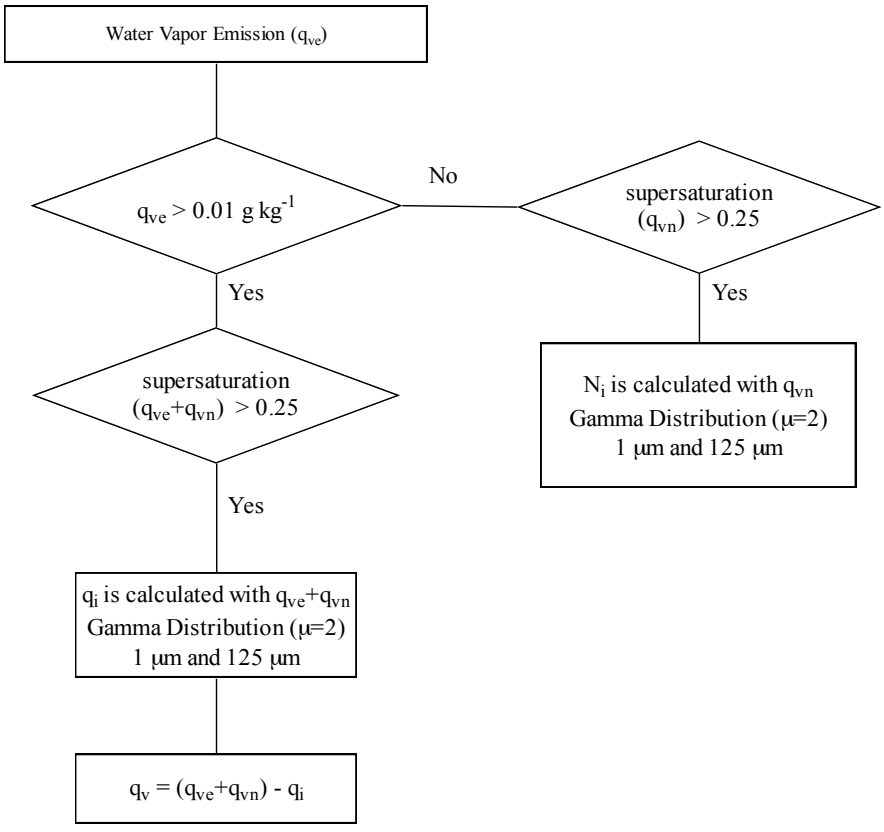

Figure 11. Flow chart for the ice nucleation process with the emission of water vapor.

Numerical experiment setup

Figure 12 shows the domain setting for the WRF simulation with the horizontal resolution of 500 m, which is centered on the location of the HPP at the Eielson Air Force Base. The entire grid system has 50 vertical layers with the top level at 600 hPa since the focus of this study is restricted to near surface boundary layer phenomena. The Moderate Resolution Imaging Spectroradiometer (MODIS) land-cover classification is selected as the land use categories, and then 'Evergreen Needleleaf Forest' is changed into 'Snow and Ice' because the domain area is covered with snow in the middle of winter. The three-hourly data from the North American Regional Reanalysis (NARR) produced by the National Center for Environment Prediction (NCEP) are used as the initial and boundary conditions.

The model configuration of WRF is summarized in detail in Table 1. There are five experiments to attain the primary goal of the present study. The experiments of 'MOD' and 'ORG' indicate the numerical simulation with the modified ice microphysics, and with the original Thompson scheme, respectively. In order to evaluate the effects of water vapor emissions as an anthropogenic source, the experiment of 'NOE' is performed without the emission and with two point sources, respectively. Finally the experiment of 'FRS' is made to test the sensitivity of land-use to the formation of ice fog. The simulation in each experiment is executed from 06 UTC 28 to 18 UTC 29 January 2012 and the first 12 h is treated as spin-up.

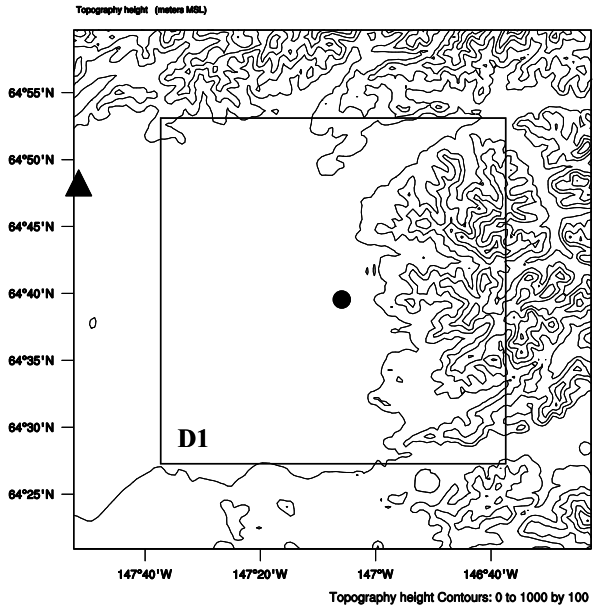

Figure 12. The WRF domain setting (inner box) with elevation contour lines in meters (a.s.l.). The closed circle and triangle indicate the location of the Eielson Air Force Base (HPP) and the Fairbanks International Airport, respectively.

Table 1: Numerical experiment design.

	MOD	ORG	NOE	FRS	2EMI
Grid spacing (m)	500	500	500	500	500
Timestep (s)	3	3	3	3	3
IC/BC	NARR	NARR	NARR	NARR	NARR
PBL	YSU	YSU	YSU	YSU	YSU
Shortwave Radiation	RRTMG	RRTMG	RRTMG	RRTMG	RRTMG
Longwave Radiation	RRTMG	RRTMG	RRTMG	RRTMG	RRTMG
Microphysics	Original	Modified	Modified	Modified	Modified
Water vapor emission	HPP	HPP	-	HPP	HPP + CTL
Land use	Snow and Ice	Snow and Ice	Snow and Ice	Evergreen Needleleaf Forest	Snow and Ice

RESULTS

Modification of ice microphysics

N_i in the experiment MOD is comparable to those from the observation even if there are occasionally large differences (03 UTC and 11 UTC 29 January). The difference in L_i between the OBS and the MOD experiment is larger than that in N_i. The decreasing span in N_i and L_i from 07 UTC to 13 UTC 29 January 2012 is of interest and it will be discussed below. For N_i and L_i, however, the ORG experiment simulates the lowest value, comparing to the other experiments. This makes sense since the nucleation rate of ice crystal in the ORG experiment is much lower than that in the MOD and NOE experiments (Fig. 10c).

Of the modifications in this present study, most noticeable is the size distribution of ice crystals to be changed into the Gamma distribution with MWMD between 1 μm and 125 μm. For comparison, Fig. 10b shows the size distributions of the ice crystals from the experiment MOD and ORG. Note that the right axis is only used for the ORG experiment. Total N_i are 34.1 cm^{-3}, 48.0 cm^{-3} and 0.199 cm^{-3} for the OBS, the MOD and ORG experiment, respectively. The particle size distribution for 1.0 μm bandwidth in the MOD experiment is given by the Gamma distribution with the assumption with shape factor, μ=2, and scale factor, λ=0.30 μm^{-1}. The peak value in the MOD experiment is at 6.5 μm, which is almost consistent with the diameter at the peak in the OBS. The number concentration of ice crystals, which have diameters higher than 20 μm, is higher in the OBS than that in the MOD experiment, implying that the size distribution in the model should be prescribed to be broader. Meanwhile, as expected, the Marshall-Palmer distribution is given in the ORG experiment. Even if the total N_i is largely different between the OBS, the MOD and ORG experiment, the comparison of the relative frequency in each distribution is meaningful. For the ice crystals larger than 15 μm, the relative frequencies are

28.7%, 12.3% and 42.1% for the OBS, the MOD and ORG experiment, respectively, indicating that the Marshall-Palmer distribution overestimates N_i for the larger ice crystals while the Gamma distribution overestimates N_i for the smaller ice crystals. However, the Gamma distribution is more suitable for the simulation of ice fog episode because most ice fog particles typically are smaller than 15.0 μm.

Sensitivity tests

Effect of water vapor emission: NOE experiment

As introduced, Benson (1970) referred to an ice fog event as low temperature air pollution. Emitted water vapor from the power plant and combustion product from cars are a crucial source for the formation of ice fog particles because the saturation vapor pressure with respect to ice is as low as 12.85 Pa at –40^{o}C, which is equivalent to the mixing ratio of 0.079 g kg^{-1} at 1013 hPa. The emission rate of water vapor is 30 ton h^{-1} at the HPP. With the horizontal resolution, 500 m, the emission rate is converted to 5.46 x 10^{-3} g kg^{-1} s^{-1}, assuming that the air density is 1.22 kg m^{-3}. From the above theoretical calculation, the time scale is just 15 s for water vapor saturation with respect to ice to be achieved. The present study attempts to evaluate the effect of water vapor emission on the ice fog formation with no emission case, the NOE experiment

Figure 13 shows the horizontal distributions of L_i from the MOD, the 2EMI, and the NOE experiment at 06 UTC 29 January 2012. Ice fog forms as the water vapor is emitted from the HPP in the MOD experiment. However, the emitted water vapor is not dispersed widely since it is nucleated into the ice fog particles for a short time. Ice fog, which is divided into two cells at the Tanana River, is dispersed. In contrast to the above experiment, MOD, there are just a few ice fog patches in the NOE experiment although the saturation vapor pressure is low. The traditional and the modified model parameterization schemes reveal that ice fog is the product of water vapor emissions as an anthropogenic activity. Significant increased ice fog forms during the 2EMI experiment with the water vapor emissions from the CTL (Fig. 13, right panel).

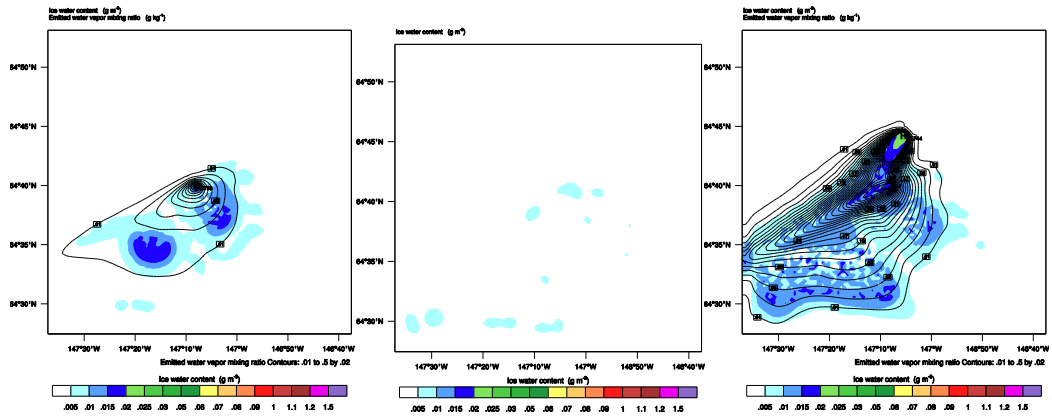

Figure 13. Horizontal distribution of ice water content (shaded) and emitted water vapor mixing ratio (contour) at 06 UTC 29 January 2012 from the MOD (left) and NOE (middle) and 2EMI (right) experiments.

Land use: FRS experiment

The present study changes the land use from 'Evergreen Needle leaf Forest' into 'Snow and Ice'. Figure 14 represents the land use for the MOD and FRS experiment. Most of the domain area is covered with the evergreen needle leaf forest but snow cover prevails in the middle of winter.

According to equation 7, the ice nucleation is dependent on the temperature T. The prediction of T at the lowest level is a good indicator to evaluate the performance of the numerical model. The time series of T at the lowest level from the MOD and the FRS experiment are given in Fig. 15 with the observation. Both experiments, MOD and FRS, show that T gradually increases until 00 UTC 29 January and then decreases. The MOD experiment represents the better performance for the prediction of T even if T is not as low as the observation during cooling span. Moreover, T at peak is higher by 7 ^{o}C in the FRS experiment than the OBS. Figure 15b shows that the difference of T between two experiments is due to the difference of sensible heat flux from the land surface. Therefore, these characteristics results in that relatively warm air in the FRS generates the ice fog particles less, comparing to the MOD experiment.

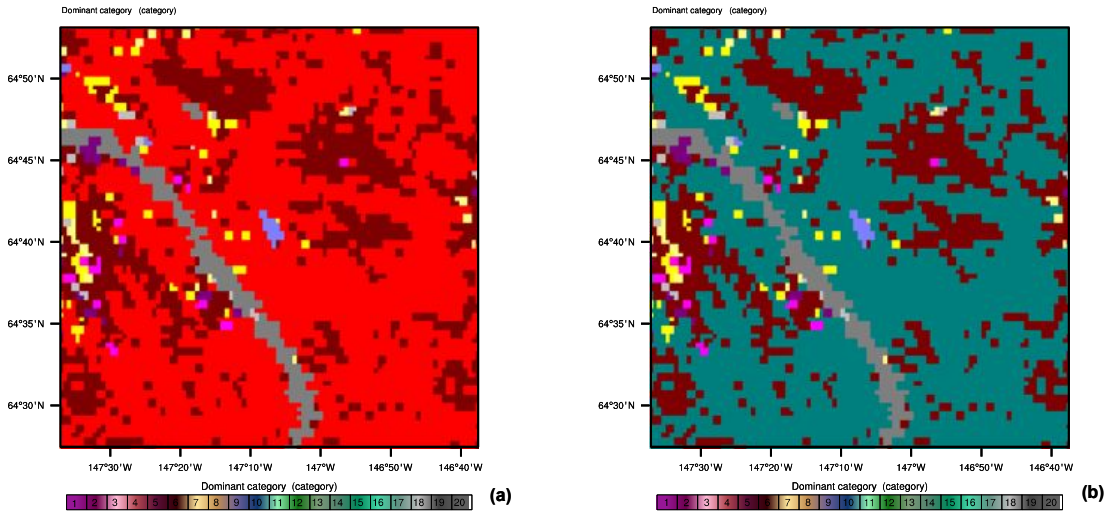

Figure 14. Land use category used in the FRS (a) and MOD (b) experiment. The number '1' and '15' indicates the 'Evergreen Needle leaf Forest' and 'Snow and Ice', respectively.

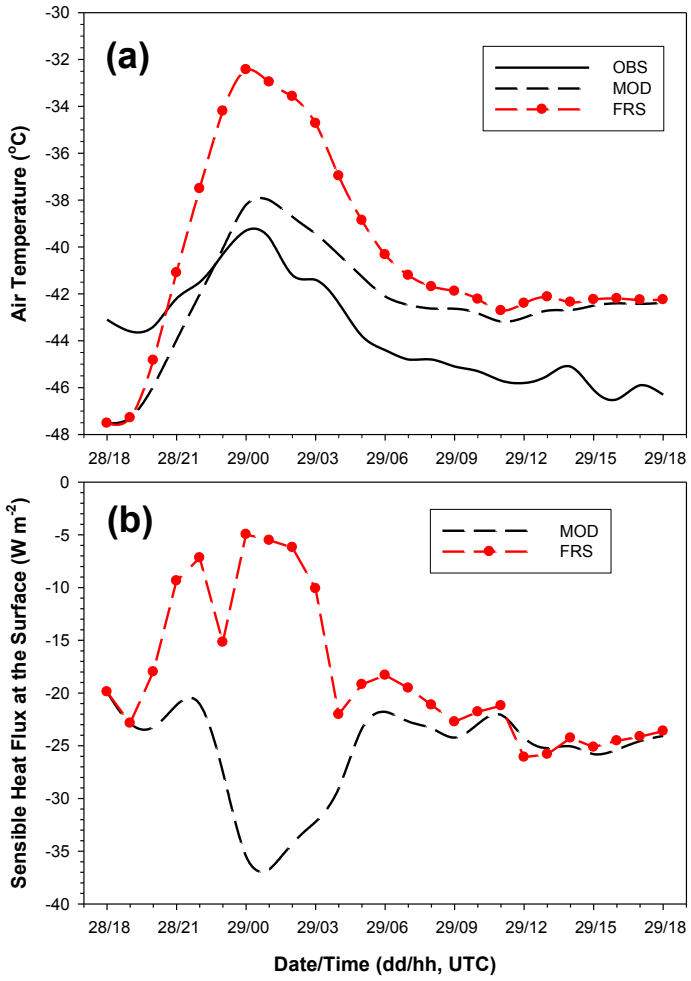

Figure 15. Time series of the air temperature (a) and sensible heat flux at the surface (b) from the OBS (solid line), MOD (dashed line) and FRS (dashed line with closed circle) experiment.

DISCUSSION

There are two largest differences of N_i (03 UTC and 14 UTC 29 January) in Fig. 10a: the MOD experiment underestimates N_i at 03 UTC 29 January whereas ice fog particles at 11 UTC 29 January are more produced by the MOD experiment than the OBS. In Fig. 15a, T at 03 UTC 29 January is overestimated by 2°C in the MOD, comparing to the observation. In this condition, the ice fog particles are less generated by the equation 7. This is why N_i is lower in the MOD than the OBS. Meanwhile, N_i increases gradually in the MOD while the opposite is true in the observation from 03 UTC to 11 UTC 29 January. Figure 16 shows that N_i from the MOD is highly correlated to T. This makes sense since modified ice nucleation process in the present study is defined as the function of T. In contrast to the MOD, the observed N_i is reduced even if T decreases (Fig. 16). Ice fog particles are generated and then grown by the vapor diffusion (Rogers and Yau, 1989). L_i from the NOE experiment is similar to that from the OBS, implying that the water vapor mixing ratio, which is not enough to generate ice fog particles, results in the low N_i at low T. In the present study, water vapor emission rate is set as constant for 24 hours

after spin-up ends and then emitted water vapor mixing ratio is satisfied with the activation condition, which is defined as 25% supersaturation with respect to the ice. This is why the MOD experiment can generate ice fog particles from 07 UTC to 13 UTC 29 January.

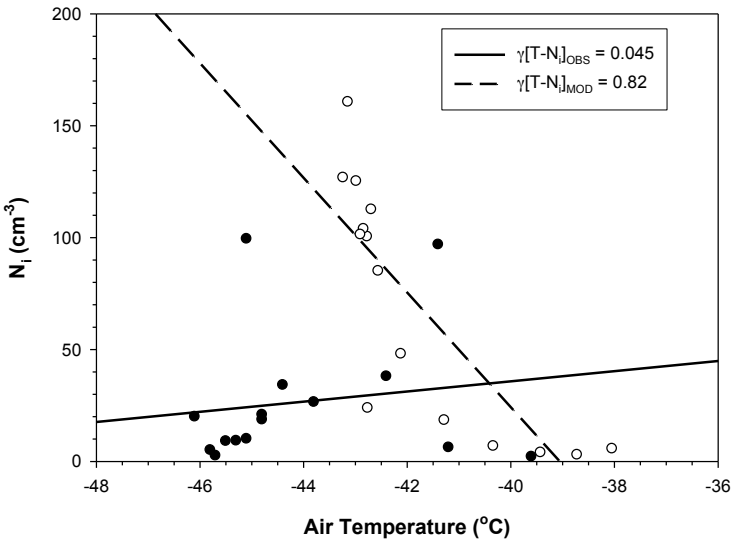

Figure 16. Scatter plots for air temperature (T) and number concentration of ice fog particles (Ni) in the MOD experiment and OBS. Correlation coefficients are given in the plot.

The time series of ice water content at 2 m altitude from the MOD experiment show significant differences when compared to the 2EMI (including the HPP and a CTL) experiments (Fig. 17 left). Ice water content is higher in the 2EMI than the MOD since the increased water vapor emission may be satisfied with the activation condition. Air temperature between two experiments is similar but that from the 2EMI is slightly higher, implying the latent heat release as a result from the deposition heating the air. We present the horizontal distribution of ice water content at 20 UTC 26 January 2012 at which ice water content is highest in both experiments. As illustrated in the figures, ice fog is dispersed with the emission of water content from the HPP and CLP. In the 2EMI experiment, ice fog is stronger and wider distributed than the MOD. As a result of the higher N_i, the visibility is significantly reduced during the 2EMI (CTL) case. Figure 18 shows the visibility differences for the MOD and 2EMI experiments during the 26 (Fig. 18 above) and 28 January 2012 (Fig. 18 bottom).

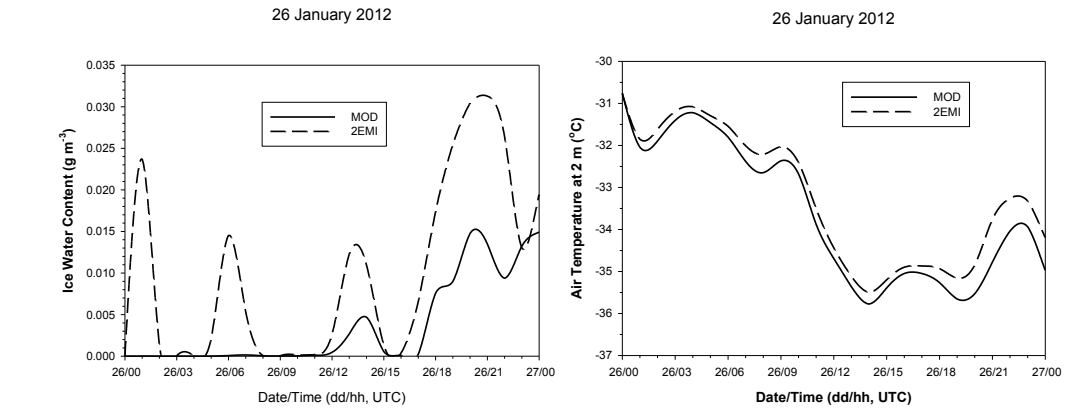

Figure 17: Modeled ice water content (left) and air temperature (right) during the 26 January 2012. The 2EMI experiment refers to water vapor emissions from the Eielson and HPP, while the MOD experiments includes anthropogenic background and HPP emissions only.

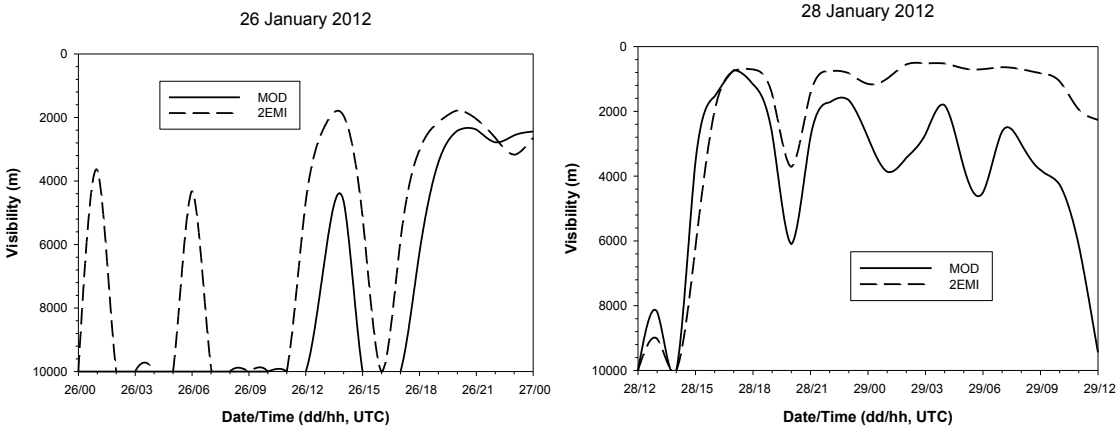

Figure 18: The modeled visibility during a less cold day (26 January 2012) with moderate ice particle concentration and no ice fog conditions (above), and during strong ice fog conditions the 28 January 2012. Note the MOD experiment refers to anthropogenic background and HPP water vapor emissions only, while the 2EMI experiment includes potential CTL water vapor emissions.

SUMMARY AND CONCLUSIONS

A major goal of this project was to develop an ice fog forecasting tool in order to better predict the impact water vapor emissions from a CTL facility at Eielson Air Force Base on air quality (specifically ice fog) during arctic winter conditions. In order to do this, we modified the Weather Research Forecast (WRF) model, a model used by the Air Force Weather Agency, National Weather Service offices and atmospheric scientists all over the world for research and operational weather prediction. However, in order to modify the WRF model for this purpose, the causes and microphysics of ice fog formation needed to be better understood. The microphysical characteristics of ice fog are different from those of ice clouds. However, to date

there were no dedicated tools available to accurately model the generation and atmospheric dispersion of ice fog.

For the first time in several decades, ice fog particle observations have been made at the Eielson AFB and in Fairbanks. Ice fog microphysical characteristics were derived with a Video Ice Particle Sampler (VIPS) during strong ice fog cases in January and February 2012. New technology enabled us to collect ice fog particles with glass slides coated with thin layers of Formvar (polyformalvinyl). The Formvar was liquefied immediately before exposure to the fog particles. Ice fog crystals that impacted on the Formvar were encapsulated by the Formvar which then hardened leaving a perfect and permanent replica of the crystal. Analysis of the VIPS and the Formvar measurements revealed ice fog property evolution as well as particle density, size, and shape characteristics. Measured particle sizes were generally very small (less than 20 microns) during the heavy ice fog events while during lighter events, larger crystals up to 100 microns were observed. Most particles smaller than 10 microns were quasi-spherical droxtal shaped crystals while larger crystals were more likely to be plate-shaped with irregular crystals becoming more common at sizes larger than 30 microns. Column-shaped ice crystals were rarely observed. This information was used to calculate cross sectional areas and the mass of the ice particles for derivation of ice water densities and the vertical settling velocities.

We used the observational data to model the microphysics of water vapor emissions from anthropogenic sources as well as from open water surfaces. The Thompson microphysics scheme available within the WRF model estimates water vapor phase changes as a function of temperature. However the scheme was developed for natural ice clouds occurring in the upper troposphere and lower stratosphere, which typically consist of ice particles with lesser density. Preliminary modeling experiments underestimated ice fog particle densities by one to two magnitudes. We modified the original Thompson scheme with a new ice nucleation process accounting for higher number concentrations of ice crystals. The crystal size distribution was changed into a Gamma distribution according to the observed size distribution. Furthermore, gravitational settling was adjusted for the ice crystals to be suspended since the crystals in ice fog do not precipitate in similar manner when compared to the ice crystals of cirrus clouds. The slow terminal velocity plays a role in increasing the time scale for the ice crystal to take to settle to the surface. As a consequence, the improved particle concentrations, diameters and residence times allowed calculation of improved visibility values.

WRF model experiments with different water vapor emission scenarios showed clearly the ice fog dispersion and the related visibility effects of the various water vapor sources. The treatment of water vapor within the modified WRF microphysics scheme allowed quantifying visibility during days with strong ice fog as well as during days with moderate ice particles present within the atmospheric boundary layer. Ice fog extinction is calculated from the cumulative projected area over the WRF particle size distribution. The modeled visibility values compared well with visibility measurements at the Eielson AFB runway. The modeling experiments further confirmed previous studies of expected visibility restrictions due to ice fog with additional water vapor sources from a potential CTL plant.

CHAPTER 8: ENERGY PROJECT OPTIONS FOR FAIRBANKS--A COMPARATIVE ECONOMIC ANALYSIS

by Antony Scott, Dennis Witmer, Ed King and Brent Sheets

INTRODUCTION

Energy prices in Fairbanks are high. This directly affects disposable household income. It may also affect economic development.

It is in this context that the potential for a coal-to-liquids project to provide reduced-cost energy to Fairbanks has been raised. Assessing the economics of coal-to-liquids, however, needs to be done in context. A large number of "magic bullets" have been proposed over the years to reduce Fairbanks energy costs. These include:

- Converting coal to liquids
- Making and trucking liquefied natural gas (LNG) from the North Slope
- A small-diameter (12") natural gas pipeline from the North Slope to Fairbanks
- A 250 MMcf/day natural gas "bullet line" from the North Slope to Cook Inlet, with a lateral to Fairbanks
- 500 to 1,000 MMcf/day "bullet lines" from the North Slope to meet Railbelt gas needs and provide for gas export with a lateral to Fairbanks
- A 3 Bcf/day Major Gas Sale (MGS) natural gas pipeline from the North Slope to export LNG at tidewater, with a natural gas lateral to Fairbanks
- A small-diameter (18-24") pipeline from Cook Inlet to Fairbanks
- Using electricity from the proposed Susitna dam to generate heat
- Using HVDC to transport electricity generated from North Slope gas to Fairbanks, Railbelt communities, and other communities.

The economics of each of these projects have been evaluated at different times and by different proponents. Assessments have used different assumptions for financing, government subsidies, consumer demand, the cost of gas, etc. This has muddied understanding of the comparative value of different projects for Fairbanks consumers and hindered policy and commercial decision-making.

This study seeks to systematically compare this multitude of proposed energy projects on an apples-to-apples basis. Common assumptions were imposed across all projects. This allows a less obstructed view of the comparative ability of different projects to deliver household energy cost savings.

It also allows for a comparative assessment of the vulnerability of projects to various risks. Any informative comparative assessment of project economics must critically assess the risks that the project faces should "baseline" projections turn out to be incorrect. After all, baseline projections are *always* based on assumptions that are unlikely to be completely correct. Future commodity price uncertainty, capital cost

uncertainty, demand uncertainty, and the rate of future escalation in project capital costs are key risks assessed in this study.

By putting the projects on a common analytical footing, the relative importance and effectiveness of possible state financing and subsidies can be understood. State support can make a large difference to the cost of infrastructure. However, it turns out that changes in infrastructure costs do not necessarily translate into changes in energy prices that Alaskans will pay.

ANALYTICAL FRAMEWORK

Five elements particularly shape this analysis and deserve comment. The next section reviews these five key elements, including: the choice of projects included, and not included, in this study; the philosophical approach or "meta-method" that guides analysis; the approach and analytical results associated with commodity pricing; how project costs are modeled in light of resource constraints; the importance of and approach to modeling customer demand of the different projects' services.

Project Universe

The projects modeled in this study have all had some level of political or commercial support or interest, and in the last 6 years or so, each has developed cost estimates that are publicly available.

One project that has *not* been modeled, but has enjoyed a past level of political support, is the manufacture and distribution of North Slope propane. The Alaska Natural Gas Development Authority (ANGDA) pursued a propane project for some time. ANGDA was unsuccessful in securing contracts for propane supply. For whatever reason the commercial reality is that propane cannot be purchased at an acceptable price. Given practical hurdles in making it real, therefore, the analysis did not cover this project.

Another project that was excluded from analysis is a major gas sale (MGS) project that would send North Slope gas to Alberta, where it could interconnect and access the broader North American market. As originally proposed, the "overland" MGS pipeline would be a 48" diameter, 2500 psi line that would transport roughly 4.5 Bcfd. For the foreseeable future that project, which as recently as two years ago boasted two distinct commercial sponsors, now appears to be uneconomic. Natural gas prices in Alberta, at the AECO Hub, trade today at about $3/MMBtu; the pipeline tariff to transport the gas to the hub would exceed this by perhaps $1/MMBtu. An important signal against the medium term prospects of an overland MGS is that the same commercial sponsors that originally pursued it have in the last year redirected their attention towards pursuing a version of the MGS LNG project modeled here.

Meta-methods

This study embodies some overarching methodological approaches that are cross cutting and that affect results. These "meta-methodology" decisions are critical to understanding the overall approach of this analysis. Elements of the methodology have been chosen to help level the playing field to allow for comparative project economics.

First, the analysis substantially relies upon published results concerning potential projects. The study team has not attempted to design new concepts, nor re-engineer or "optimize" existing ones. Instead, the authors have relied upon existing cost estimates and project designs. Where necessary the primary author supplemented these with interviews to elicit necessary detailed information required for modeling.

Second, to perform "apples-to-apples" economic comparisons and avoid idiosyncratic financing or subsidy strategies for particular projects as proposed by project champions, the team modified some financing assumption. For example:

- The Alaska Gasline Development Corporation (AGDC) has suggested that the state might provide free royalty gas for "line pack". This would somewhat reduce the project's capital cost, as line pack is a "capital asset" that must otherwise be purchased by a pipeline project and becomes part of the rate base.
- The Fairbanks Pipeline Company has advocated that its project be significantly owned by citizens of the State. Although details are somewhat unclear from publicly available documents, this ownership structure appears to be chosen by the proponent to ensure profits from pipeline ownership materially remain within the state.
- The Susitna-Watana dam project, as modeled by AEA, presumes cost contributions from the state that do not earn compound interest during the lengthy project development and construction period, but which are "rate based" and earn a return to the State once project operation begins. This reduces the overall per-kWh charges to customers. There is nothing integral to the infrastructure itself of such an approach.

There is nothing necessarily inappropriate about any of the mechanisms as originally proposed by the project champions. However, because the combinations of the nature, type, and degree of Government support are essentially infinite, it is necessary to shun "designer" approaches in favor of generic ones that are imposed on all projects for the purpose of analysis.

Third, and consistent with the foregoing point, projects have been abstracted from the original proposals as set forth by their respective proponents. At least three different entities have been potential project sponsors for an LNG trucking project. In modeling projects, no distinction has been made between them, and instead this study considers only a singular generic sponsor. At some level the identity of the project sponsor can clearly matter, of course. It is hard to imagine a Major Gas Sale, for example, being

successful without the creditworthiness of some very large private entities such as the North Slope's major producers. .[1]

This assumption sometimes affects the modeling of the overall project schedule. The time estimates used here may be at variance with a particular project sponsor's estimates. In particular, this study assumes that no major construction, procurement, or right of way clearing occurs until all critical permits are in hand. Successful projects can, and often do, proceed with developers taking risks and making large, irrevocable procurement expenditures prior to all major hurdles being cleared. Sometimes this bet pays off. In other cases it does not.[2] Because projects are abstracted from their proponents, similar risk preferences for the generic developers are assumed.

Fourth, non-favored access to commodity markets, infrastructure technology, and cost structures, are assumed. Some examples:

- While recognizing that in the real world one project entity might do a better job negotiating a gas supply agreement for itself than another, this analysis assumes that all projects that rely upon stranded North Slope gas acquire that gas for the same wellhead price. Similarly, all projects that access North Slope gas that has been unstranded do so at the same price value to the producer.
- It is assumed that the capital costs of gas treatment plants for two similarly sized projects are the same, even if project proponents have developed different estimates for what is essentially the same plant.
- It is assumed that the local distribution system for all of the projects providing gas to Fairbanks consumers will have the same design and cost, and provide service to the same volumes for the same number of customers. This assumption would not perfectly hold true in practice, of course. At a minimum, projects that deliver gas to Fairbanks later in time will have a different customer base.

Commodity Prices

Although pipeline transportation rates, or "tariffs", are regulated by the Federal Energy Regulatory Commission (FERC) and the Regulatory Commission of Alaska (RCA), gas prices are not. This analysis assumes that each project purchasing gas within the same market will secure the same pricing terms.

For the projects considered herein, there are three relevant gas markets, and three distinct pricing alternatives: North Slope gas prices that are linked to the Asian-Pacific LNG market; North Slope gas that is "stranded" from Outside markets; and Cook Inlet gas serving Southeast Alaska.

---

[1] As an aside we note that to our knowledge all of the cost estimates for all of the projects were put together assuming experienced and professional project management. Deviations from this assumption would generally impose significant risks to both cost and project schedule.

[2] On TAPS, for example, the project's steel pipe was ordered, paid for, and delivered several years before construction was ultimately allowed to begin.

Table 1: The commodity markets, or pricing regimes, as modeled as applicable to projects considered in this study.

	Asian-Pacific LNG	ANS Stranded Gas	Cook Inlet Gas
ASAP 250 MMcf/d		X	
ASAP 500 & 1,000 MMcf/d	X		
Beluga to Fairbanks			X
Trucking from the ANS		X	
12" fit for purpose pipeline		X	
Spur-line off a MGS[3]	X		
HVDC transmission		X	

The first two gas markets (Asia-Pacific LNG and ANS Stranded Gas), as well as fuel oil prices in Fairbanks, can be directly and empirically linked with North Slope crude oil prices on the West Coast. Therefore, projects can be compared on an "apples to apples" basis using crude oil prices as the common denominator. Projects across real oil prices from $50/Bbl to $140/Bbl were modeled. The "base case" is $100/Bbl. (The coal-to-liquids project modeling assumes that coal is purchased within Alaska at a fixed, long term price; this is consistent with market data. (US DOE (2007b).) Pricing terms of each separate market are described, below.

Fairbanks Heating Oil Market

As one might expect, heating oil and crude oil prices are highly correlated. (Figure 1)

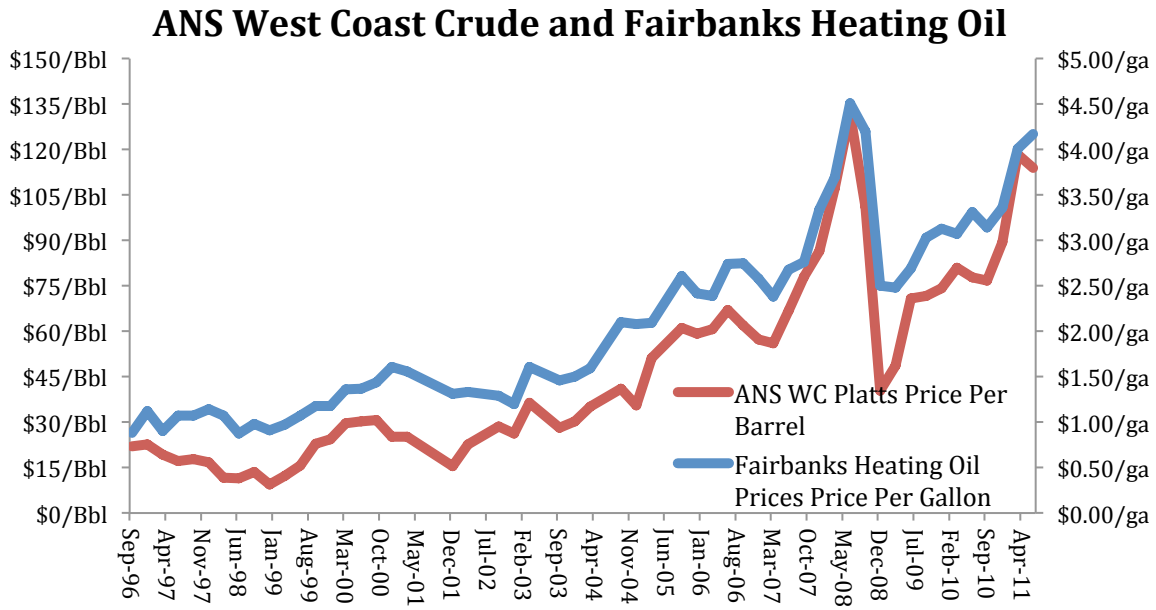

[3] For an overland MGS in-state gas would be priced off of the interconnected North American grid.

Figure 1: History of ANS West Coast crude and Fairbanks retail heating oil prices

The correlation between ANS crude and Fairbanks retail fuel oil prices can be estimated on the basis of publicly available data.[4] The statistical relationship is estimated by simple linear regression:[5]

$$Fuel\ Oil\ Price/gallon = \alpha + \beta(Crude\ Oil\ Price/Bbl)$$

The regression of crude oil price on fuel oil price explains more than 95% of the variation in Fairbanks fuel oil prices. The estimated parameters are .5888 and .0315 for α and β, respectively, and are statistically significant.[6] Translating fuel oil heat content per gallon to MMBtu, we obtain:

$$\$/MMBtu \approx 4.20 + .225\times(ANS\ WC\ \$/Bbl)$$

In other words, a $1/Bbl change in ANS crude oil prices translates to a $.225/MMBtu change in the cost of fuel oil.

Alaska North Slope (ANS) Stranded Gas market

The ANS stranded gas market prices used in this study are based on published contracts for gas supply, published reports of project delivered prices at various oil prices, public royalty data on gas value, and analysis of the Gas Royalty Settlement Agreements between the major North Slope producers and the State of Alaska. While full discussion is beyond the scope of this report, there is strong support for the conclusion that North Slope gas is generally priced with reference to the following formula[7]:

$$\$/MMBtu = .0464\times(ANS\ WC\ \$/Bbl)$$

Better or worse pricing terms may be secured. Public statements from GVEA suggest they may have secured better pricing terms. (GVEA, 2012; p.5) Nevertheless, for comparative modeling purposes this formula should work reasonably well.

---

[4] Fairbanks heating oil data from each quarter can be downloaded from Extension's Food Cost Survey web site, at http://www.uaf.edu/ces/hhfd/fcs/.

[5] Daily ANS crude prices are taken from Platts' corresponding *Oil Daily* assessments.

[6] Adjusted R^2 = .958, standard errors of .0513 and .0009 for α and β, respectively. Additional confidence in the regression's validity comes from two directions. First, plotting the residuals of predicted versus actual heating oil prices against ANS actual prices indicates no observable pattern, suggesting an absence of heteroskedacity. Second, and perhaps more tellingly, we ran an analogous regression of ANS crude prices on EIA-reported national average heating oil prices. The coefficients are very similar (α = .5907 (.0175), β=.0301 (.00033)), suggesting that the Fairbanks regression results reflect underlying fundamentals of the broader heating oil market. As well, to the extent that they differ, they do so as one might expect (the β coefficient for the national market regression is smaller, suggesting that Fairbanks heating oil prices rise more in response to a hike in oil prices than do heating oil prices nationally; this is consistent with the smaller degree of refinery competition in Alaska than in Outside markets).

[7] The formula exactly captures some contract pricing; other contracts use but modify the formula. Available evidence suggests that other transactions are priced consistent with its general provisions.

The ANS stranded market pricing formula is based on a "net forward" approach. Untreated gas is purchased on the North Slope. Transportation costs to get it to market are then "added in" to determine a final delivered price to Alaskan consumers. Part of this transportation cost is the amount of gas consumed in the transportation chain – *e.g.*, gas treatment plant, pipeline compression, North Slope gas liquefaction – from the point of sale forward. What separates those projects accessing the stranded ANS gas market is their comparative project costs and risks.

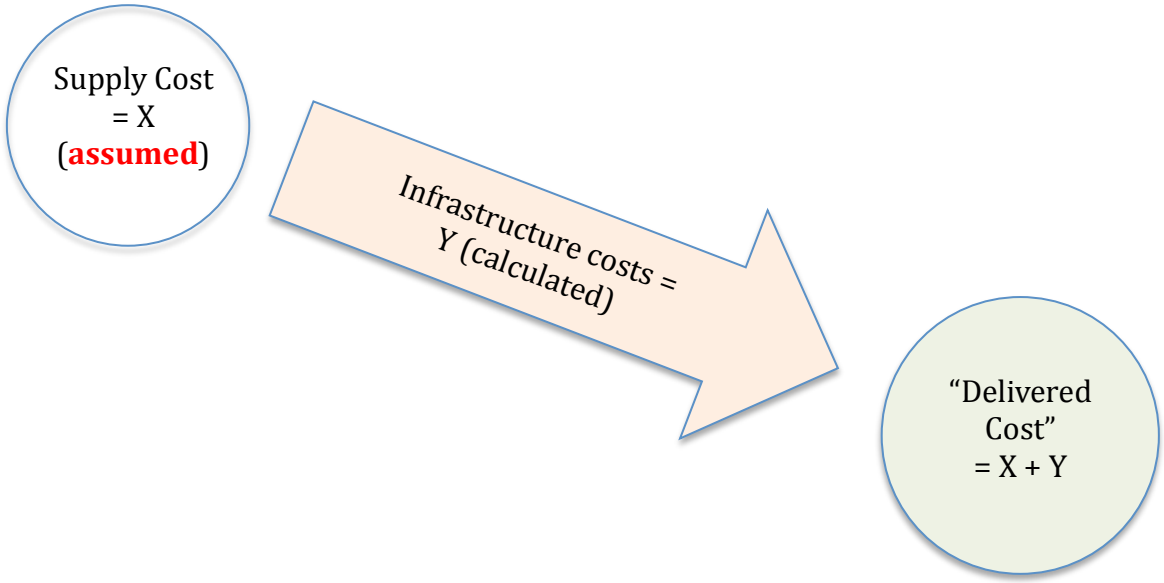

Figure 2: An example of "net forward" pricing.

Asian Pacific LNG Pricing

The Asian Pacific LNG market assessment relies on the broad consensus between three publicly available expert consultant reports.[8] These reports rely on market intelligence concerning existing long-term LNG contracts and modeling of the likely supply-demand LNG balance that will give rise to new contract terms. For modeling purposes, the mid-point of the three assessments is used, and it is assumed that landed prices in Asia take the form[9]:

$$\$/MMBtu_{Asia,CIF} = .90 + .1485 \times JCC$$

Where JCC = Japanese Crude Cocktail, or Japan Customs-cleared Crude (JCC), is the average price of customs-cleared crude oil imports into Japan (formerly the average of the top twenty crude oils by volume) as reported in customs statistics.

[8] See AGDC (2011b), Gas Strategies (2008), and Wood Mackenzie (2011).

[9] The abbreviation "CIF" stands for "Cash, Insurance, Freight" and refers to LNG cargoes where seller has responsibility to delivery to the buyer, generally at a regasification facility.

Recent trends in the Asian LNG spot market, and a few reports of recent long term contracts, suggest that these terms may be softening somewhat;[10] specific contract terms remain confidential. The cause for the price softening is the significant disconnect between historical Asian LNG pricing terms (which tend to be relatively similar to the above) and the significant and sustained plunge of North American gas prices. However, whether this new pricing regime becomes the new norm for contract deliveries that are eight to twelve years into the future remains to be seen. World class LNG projects are highly capital intensive, relatively "lumpy" in the size of their deliveries, and require long-term contracts to be financed. Without adequate compensation, producers may find the project risks simply too great to proceed. (Iwata, 2012) Indeed, absent pricing terms that are broadly in line with what is modeled herein, it seems unlikely that the Alaska LNG projects considered here would be built because transport and liquefaction costs would create unreasonable risks. Nevertheless, given the volumes contemplated for the MGS project, such pricing terms may be aggressive.

In the wake of a major gas sale Fairbanks, prices will be determined on a "netback" basis from the Asian LNG market. Costs of transportation downstream of the Fairbanks off-take point are subtracted from the Asian LNG long term contract price. These include the gas consumed by pipeline compression downstream of Fairbanks and used to run the liquefaction plant at tidewater.

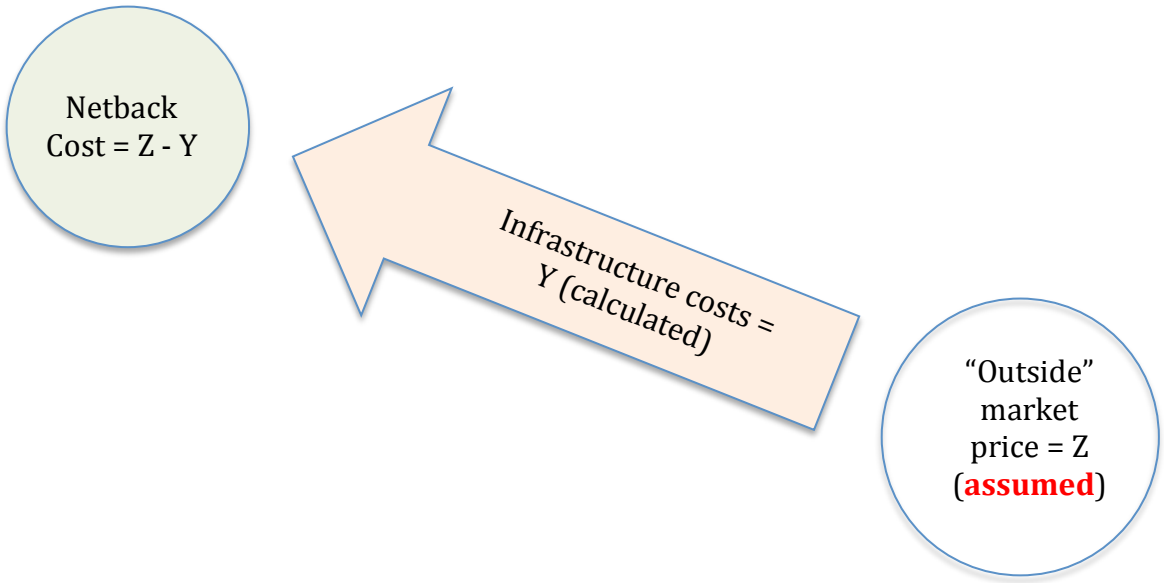

Figure 3: An example of "netback" pricing.

Costs for final transport of natural gas from the MGS mainline to the Fairbanks citygate, and costs of distribution to consumers, are then added back in. The costs for local gas storage, which may be significant, are ignored in this analysis because no party has estimated what these might be.

[10] See, e.g., Dow Jones (2012); Terazono (2012).

The "netback" pricing approach is adopted for this analysis based upon the assumption that the Asian LNG market will be fully saturated by gas coming from a 3 Bcfd MGS project. In such circumstances, in-state sales are not made at the expense of export sales in Asia; rather, they are in addition to such LNG sales. Accordingly, for the producer, the wellhead netback (from Asia) determines their view of the value of the gas, and costs of transportation from wellhead to Fairbanks offtake are just additional costs that Fairbanks must bear.

"Opportunity cost" pricing is used to assess Fairbanks prices for the two larger ASAP project configurations of 500 MMcfd and 1 Bcfd. Both of these projects critically access LNG export markets.[11] Meanwhile, their ability to supply the Asian market is significantly smaller than Asian market demand and would not saturate Asian market demand. Accordingly, short-haul (in-state market) sales necessarily preclude long-haul (LNG export market) sales. Thus, in-state sales can engender an "opportunity cost" associated with foregoing LNG sales. The profit maximizing Producer will address this cost when pricing instate gas. "Opportunity cost" adjustments to Fairbanks netback pricing can be affected by three downstream netback elements.

- *Shipping*. Producers can avoid maritime shipping expense if Fairbanks consumes "short haul" gas. Whether the full costs of shipping could be avoided, and savings passed to Fairbanks consumers, would depend critically on Fairbanks being able to nominate sufficiently large volumes sufficiently early. Only by doing so could the number of projected ships under long-term charter be adjusted downwards. If not, then only the variable portion of shipping costs – about $.50/MMBtu – could be saved. (AGDC, 2011b). The modeling assumes that Fairbanks is able to avoid full increment of shipping costs.

- *Pipeline*. For the bullet line, Producers cannot avoid pipeline tariffs "downstream" of the Fairbanks offtake point. Fairbanks consumers therefore will not see savings associated with downstream tariffs. This potentially counter-intuitive result stems from engineering realities: the volumes that Fairbanks need are too small to affect pipeline sizing and the need for compressor stations on a bullet line. If Fairbanks takes volumes from the ASAP project, then the effective tariff on all "downstream" sales increases, and profits on Asian LNG sales decrease. A Producer can only prevent Fairbanks sales from reducing overall profitability, therefore, by including downstream pipeline costs in the commodity price that is charged to Fairbanks entities.

- *Liquefaction*. Liquefaction costs at tidewater may, or may not, be avoidable. If Fairbanks' offtake volumes enable the liquefaction plant's capital costs to be reduced because of smaller volumes of gas to convert to LNG, then there is a slight chance that the savings associated with the reduced capital could be realized by Fairbanks consumers. Given that liquefaction is generally constructed in

[11] Our conclusion that these projects "must" access LNG export markets is based on the AGDC's work, which shows that the economics of LNG exports are more favorable than either NGL or GTL exports. (AGDC, 2011) Other "anchor tenants" are theoretically possible, but we see no economic basis, nor commercial customers, to realize this possibility.

modular "trains", and train size tends not to be infinitely variable, such construction saving may not materialize. It is a matter of efficient engineering.[12] Assuming the prerequisite were satisfied, Fairbanks entities would need to commit to taking their volumes sufficiently early for the project if they were to avoid design and construction costs of the liquefaction plant.[13] Finally, because in-state volumes would reduce liquefaction plant economies of scale, Producers have every incentive to charge Fairbanks for their increased per-unit liquefaction costs. Potential Fairbanks savings will be less than the full MMBtu costs of a larger liquefaction plant.

Of course, just because a producer can avoid shipping or liquefaction costs do not mean that the full increment of savings would be passed to Fairbanks consumers. The level of competition between the three North Slope entities will influence the extent that they pass such savings along. Recent analysis has shown that the gas market in Alaska, both on the North Slope and in Cook Inlet, is marked by imperfect competition; sellers at least partially exercise market power to increase shareholder profits. (Scott, 2012). Nevertheless, for simplicity this model assumes that Producers refrain from exercising market power.

Cook Inlet pricing

The commodity price of Cook Inlet gas, which would be needed for any Beluga to Fairbanks project, would depend centrally on several factors, none of which can be well predicted:

- New gas discoveries in the Cook Inlet
- Access to LNG export markets
- Market power of Cook Inlet sellers

In this modeling we are guided by recent contracts in Cook Inlet. Lately these contracts have taken a variety of forms: a floor price, a price ceiling, and some price indexing mechanism. Under the assumption that a Beluga to Fairbanks pipeline would be supported only if sufficient local discoveries were made (which would put downwards pressure on a pricing floor), we suggest a formula something like:

$$\$/MMBtu \;=\; \max\{5.60, .07\times(ANS\ WC\$/Bbl)\}$$

Project costs

Cost of service methods

[12] If Fairbanks volumes were coordinated with potential demand from the Anchorage market it appears considerably more likely that size of the tidewater liquefaction plant might be reduced and associated capital costs avoided.

[13] Given ramp-up risks associated with uncertain Cook Inlet production declines, as well as the possibility of successful Cook Inlet exploration, it would be unsurprising if utilities were not prepared to make sufficiently large and irrevocable commitments to an ASAP project to allow such cost avoidance.

This analysis relies upon a regulated "cost of service" methodology for determining transportation and processing costs. Some projects in their entirety – such as a coal-to-liquids facility – are not subject to cost of service regulation. Other projects have subcomponents, such as LNG liquefaction, that are also almost certainly not subject to either FERC or RCA regulation.[14] Nevertheless, the goal of a cost of service regulatory framework is to establish service rates that reflect all costs, including costs of capital. It therefore provides a reasonable lens for assessing potential, if not actual, consumer cost differences. Although we calculate "traditional" declining cost of service rates, only levelized cost of service rates are reported as these facilitate project comparisons.

Within the cost of service framework, two different "business models" are run for each project. (The MGS is an exception; it is too large to be financed as a state enterprise.) Critically, both business models assume a world reasonably close to the current one with regard to the cost of debt.

In the first model, "normal" private enterprise assumptions are adopted. Modeled projects are financed with 30 percent assumed equity, which generates an after-tax return to investors of 12 percent; the cost of project debt is assumed to be 6 percent. These are relatively favorable terms, but may be feasible given financially strong project proponents and currently favorable debt markets. With only a few exceptions, all gas project subcomponents are depreciated for book purposes over 25 years. It seems unlikely that gas supply agreements would be available for longer terms than this, and such agreements are generally essential to project financing. Benefits from accelerated tax depreciation schedules are returned to users on a straight-line basis. Property, state, and Federal income taxes are assumed at maximum statutory rates.

The second business case differs by assuming that projects are financed 100 percent with state-backed debt.[15] The cost of this debt is assumed to be 4 percent; in essence, debt service coverage is included in this figure. This assumption may be overly aggressive. For the larger projects, such indebtedness could stress the state's credit rating and debt capacity (see, e.g., AGDC 2011a, p. 4-9). Absent private ownership, it is assumed that the project pays no property taxes or payments in lieu of taxes. Similarly, there is no state or Federal income taxes, and thus no return of tax depreciation benefits to project users.

Projects are conceptually divided into project "development" and "execution" stages. "Development" encompasses project planning, permitting, and most engineering; the

[14] For discussion of the regulatory regime concerning liquefaction projects supporting LNG export see Minesinger and Green (2008). We note that the Alaska Pipeline Acts, AS 42.06, does not appear to grant authority for the RCA to regulate a liquefaction plant that is not integral to a pipeline system, thereby precluding regulation of an in-state LNG liquefaction scheme.

[15] As a practical matter the development stage of each project would have to be financed with state appropriations from the general fund, or (what amounts to the same thing) general obligation bonds. By assuming debt financing prior to construction we in essence assume that the state "loans" the project money through appropriations in the early years, and the project subsequently pays this money back through rates, with interest that compounds over the entire period.

"execution" stage begins with irrevocable commitments to the project and involves the order of long lead items, land clearing and actual construction. For all project schedules, we assume common developer risk preferences and that project execution does not begin until the development stage has concluded. In a couple of instances this assumption has lengthened total project schedule. As well, the conceptual division between "development" and "execution"will be useful in our discussion of state cash subsidy scenarios.

Project capital and operating costs

Given the significant effort required to generate cost estimates for major projects, this study mostly relies upon project proponents' latest and best capital and operating cost estimates, as well as project schedule estimates. Appendix A lists primary sources upon which analysis of project costs and schedule are based.[16] Appendix B shows the key cost and schedule input for each project. Given that all project estimates lack precise project definition, "cost overrun" and "cost underrun" sensitivities of +/-30 percent are elements of the model developed as part of this analysis. This band is generally consistent with project proponent assessment of the range of cost uncertainty, although some projects (e.g., CTL) have wider bounds. In practice project costs are more likely to "overrun" than "underrun".

For some projects, the proponents' original assessments were adjusted to ensure inter-project comparability, especially in cases where project proponents have excluded some cost categories included by others. And, because most project capital and operating cost estimates were made in earlier years, all estimates are adjusted to current-year dollars.

Abstracting Projects from Project Proponents

To facilitate "level playing field" comparisons across projects, an analogue of the "efficient markets" hypothesis is assumed: For a given project size and concept the best engineering and commercial ideas will eventually be applied. Where two different projects have subcomponents that are similarly sized for similar throughput requirements, we apply a common subcomponent cost estimate to both. This allows projects to be abstracted from their proponents. It should not matter who the sponsor is *so long as they are competent*. This approach particularly affects analysis of four of the projects:

ASAP 250 MMcfd and 1 Bcfd "bullet line" projects
In 2010, the Governor's office published results of an "Alternatives Analysis" that addressed project throughput variations of 250 MMcfd, 500 MMcfd and 1 Bcfd from the

[16] Two of the projects – the LNG trucking project, and the HVDC project – have not previously published adequate detail of all of their project subcomponents. LNG trucking project proponents generously provided us their assumed capital costs for critical subcomponents, as well as their assumed operating costs for hiring trucks. The HVDC proponents not only shared their cost assumptions but "re-designed" their conceptual project for using HVDC to provide electricity and heating by wire to Fairbanks residents after we explained that their assumed Fairbanks heating needs were vastly higher what we are using for local gas distribution.

"Base Case" throughput level of 500 MMcfd that was adopted by the AGDC. (State of Alaska, 2010). The cost estimates for the 500 MMcfd case were significantly updated and refined by the AGDC in 2011. (AGDC, 2011a) This reports use AGDC's more recent (AGDC, 2011a) work to similarly "update" the earlier cost assessments for the other cases by factoring project subcomponent assessments, where appropriate.[17]

The 12" diameter, "fit for purpose" pipeline

The "level playing field" approach particularly affects how this study models this project. Fairbanks Pipeline Company (FPC) reasons, based on comparative market value of gas produced in the lower-48, that the North Slope producers will sell cleaned, treated and high-pressure gas into a 12" pipeline at the prevailing price of gas at the Henry Hub. Their analysis of "reasonable" pricing could well be correct. But "reasonable" does not equate to "feasible". Nothing compels the North Slope producers to sell at any particular price, and especially nothing compels them to make investments in gas treatment that would facilitate the sale terms that FPC contemplates.

Using publicly available data, this analysis unbundles the commodity and services that FPC has bundled together. One example is the commodity price for untreated North Slope natural gas. The same price for gas is applied to all projects that involve the purchase of gas that is "stranded" on the North Slope.[18] Also departing from FPC, this study uses factored estimates of the capital, operating and fuel use costs of gas treatment and compression, which rely on base estimates determined by the LNG trucking project's estimates.[19] Together, these determine the cost of gas delivered into the community.

---

[17] The pipeline base design – 24", high-pressure pipeline – is invariant across throughput variations. (State of Alaska, 2010) AGDC's updated compression costs were scaled for the 1,000 Bcfd case's additional compression needs (the 250 MMcfd case requires no compressor stations). GTP and Cook Inlet straddle-plant costs for the variations were taken by applying the AGDC estimates to the ratio of costs for these subcomponents established under the Alternatives Analysis. Some of the base data generated by the Alternatives Analysis was not published in the Governor's original report. The AGDC, after receiving assurance from the DNR that the data was not confidential, kindly provided us with the underling cost data used for their report.

[18] FPC's assessment might be correct. However, given that a particular commercial transaction underpins their results we urge that their project should first obtain a gas supply agreement consistent with their assumptions. If this can be done then their project can be put together on this basis. (We note, for example, that LNG trucking project proponents have obtained gas sales agreements with the North Slope producers.)

[19] Jim Dodson and Steve Haagenson kindly provided their estimates of gas treatment plant, liquefaction, and North Slope storage costs for the LNG trucking project. These estimates were factored from other data, but reviewed with commercial parties who had done engineering for similar concepts and found to be "in the ballpark". To confirm this, the National Energy Technology Lab helped us solicit cost assessments from a third-party vendor for a gas treatment plant that could handle relevant project throughput. The estimates used here indeed appear to be generally adequate. We note that our calculated "tariff" for North Slope gas treatment and liquefaction (about $4/MMBtu, in 2016 dollars) meshes with public assertions by GVEA, who in partnership with Flint Hills Resources have performed engineering cost analysis of the plant. (GVEA, 2012).

FPC's initial project schedule has also been extended. FPC assumed that its project was of a sufficiently small diameter that it could obtain an easement within the Dalton Highway, which could permit construction within the Highway itself. Because the Dalton Highway is owned by the state this might allow the project to avoid the need for any Federal permits and thereby bypass the National Environmental Policy Act process. However, it turns out that the Dalton Highway grant of land from the Bureau of Land Management to the State expressly forbids the land from being used for anything other than a road. (Allison Iverson, Joint Pipeline Office, personal communication; 11/7/2012). FPC confirms BLM's view that a right-of-way will need to be acquired and the EIS process fully engaged. (Christian Gou-Leonhardt, Energia Cura, personal communication; 11/13/2012) Because much of the required data has been gathered by the AGDC, the project development stage has been (somewhat arbitrarily) shortened by nine months compared with the ASAP schedule.

FPC's pipeline capital cost estimate was adopted, but note that FPC's costs are about 25 percent of the AGDC project's pipeline to Dunbar, a line of twice the diameter but similar length. FPC explains that the small bore of their project permits construction techniques that are faster and cheaper. Implicit is that such techniques, and greater worldwide competition among providers of small-bore pipe, reduce FPC's capital costs by about 50 percent per diameter-inch mile. Given the potential cost savings associated with this project, and (critically) its potential ability to be extended to supplement Cook Inlet gas supply in Anchorage, a transparent and thorough assessment of project construction costs using the techniques suggested by FPC appears deserving of further research.

"Beluga to Fairbanks pipeline"

Landing on a cost assessment for this project was challenging. At present the project does not have a sponsor, private or public. This study includes the project in its anaysis, in part because political interest periodically resurfaces. (See discussion at Alaska State Senate Resource Committee meeting on 3/26/2012, for one example.) There are at least four different public cost estimates of pipeline projects – with different diameters, compression needs, and directions of flow – connecting Cook Inlet and Fairbanks.[20]

All of the projects involve designs of at least 20" diameter that are clearly "oversized" for the Fairbanks market.[21] A larger diameter might be justified given the advisability of retaining the option of extending a Beluga to Fairbanks pipeline to the North Slope, reversing flow, and delivering volumes to Fairbanks. However, even a 20" diameter line may be oversized. A historical J-curve analysis suggests that an 18" diameter pipeline operating at 2500 psi pipeline would, generally, more cost-effectively transport volumes between 250-400 MMcf/d than larger alternatives. (US DOE, 2007; p. ix). Because engineering a project "from scratch" is beyond the scope of this study, existing larger diameter designs are used as a basis for developing cost estimates. After normalizing

[20] See US DOE (2007a); State of Alaska (2009); ANGDA (2009); AGDC (2011a).

[21] FPC's hydraulic analysis that concludes that a 12" pipeline would be sufficient to meet foreseeable Fairbanks needs clearly shows this. (Fairbanks Pipeline Company, 2011)

costs by adjusting for pipeline diameter and distance, and then adjusting cost estimates to current day dollars, we find that the US DOE and AGDC estimates are within 6% of each other. The average of the two was adopted.

Updating (and projecting forward) historical cost estimates

Cost estimates for different projects have been generated at different times. Therefore, costs need to be brought to the level playing field of today's dollars, reflecting changes in the construction and operating cost environment as compared to when the estimates were generated by the project sponsor.

Broader measures of consumer inflation, such as the CPI-U or the GDPIP, do not reflect changes in the pipeline construction sector. The IHS/CERA Upstream Construction Cost Index (UCCI) was used to adjust historical project cost estimates here.[22] Many of the same inputs are needed for both plants and pipelines. As well, reported changes in pipeline project costs, as reported in the *Oil and Gas Journal*,[23] suggest that the UCCI reasonably tracks reported project costs.

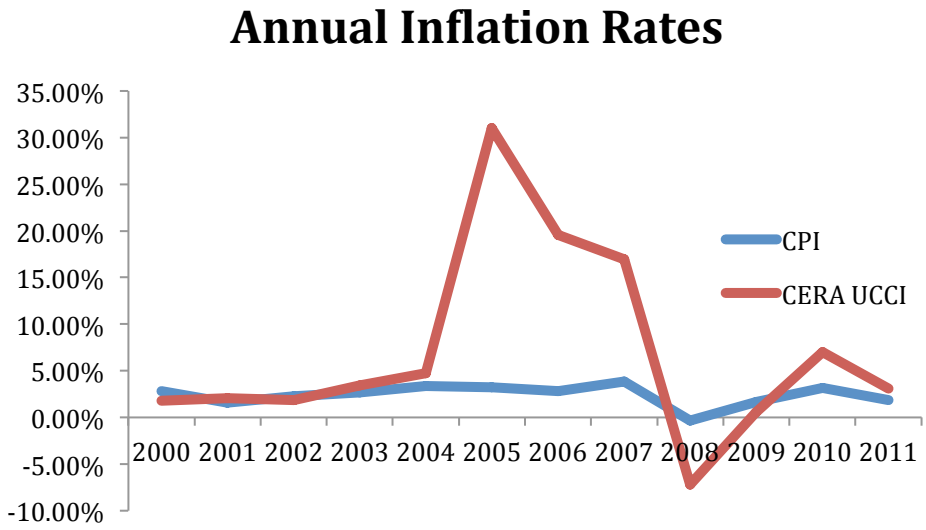

Figure 4: The middle of last decade saw explosive upstream cost escalation. Commodity prices and attendant upstream activity were then hit hard by the worldwide recession in 2008. Recovering commodity prices have reestablished pressure on upstream costs.

[22] The IHS/CERA Upstream Construction Cost index, and its companion Upstream Operating Cost Index, can be found online at http://www.ihs.com/info/cera/ihsindexes/index.aspx.

[23] These data should be approached with caution. For any given region since 2000 there are several years in which no pipelines in the 12"-24" range were constructed. Thus, a given project may disproportionately affect cost trends. Additional noise (bias) is introduced by the *Journal*'s diameter-inch mile reporting basis: total costs do not generally increase linearly with pipe diameter. Nevertheless broad correlation between reported pipeline construction costs and IHS/CERA upstream construction costs supports using the UCCI index.

Because expenditures will be made in future years, project costs must be projected forward as well. For the electric projects, this is calculated based on spend profiles (percent spend per unit of time) derived from historical published estimates for the Susitna Watana project. (AEA, 2009; Appendix D) For the gas and CTL projects, spend profiles are taken from the AGIA Finding (State of Alaska, 2008). A 3 percent annual project cost escalation for the base case is assumed, and run sensitivities of 2 and 4 percent escalation.

Billing Determinants

Larger pipelines and plants tend to exhibit economies of scale. The projects analyzed are capital intensive. Further, they generally need to be built "all at once", with comparatively limited opportunity for gradually adding capacity towards "optimal" design.[24] The major portions of each project's operating expenses are fixed.

What is not always appreciated is that economies of scale are a two-edged sword.[25] For projects modeled, the per-unit cost of infrastructure falls as demand approaches 100 percent project utilization, meaning also that per-unit costs rise if demand is less than 100 percent. These risks of project "underuse" can be substantial.

Three demand risks (i.e., risk that "billing determinants" will be less than anticipated) are considered. First, local gas distribution projects, as well as new electricity projects from which homes could be "heated by wire", have "ramp up" periods during which the new option is adopted. All else being equal, if initial savings are smaller, then ramp-up will be slower and temporarily higher per-unit delivered costs will result.

Second, actual space heating needs for Fairbanks homes and businesses is uncertain. Heating oil, wood and coal purchases are unregulated, and not made from a single source. No entity collects comprehensive heating oil purchase data. Accordingly, demand can be estimated only indirectly. In a study for the Fairbanks North Star Borough, heating demand was estimated on the basis of ENSTAR's gas sales data in Anchorage. (Northern Economics, 2012) Measured heating needs per square foot in Anchorage were "normalized" and applied to Fairbanks by adjusting for Fairbanks' colder weather. Total square footage to be heated was estimated from Borough property tax records. The implicit working presumption is that Fairbanks homes have the same energy efficiency as Anchorage homes, despite Fairbanks having greater heating needs and significantly higher costs.

A separate study for the Cold Climate Housing Research Center (CCHRC) estimated Fairbanks heating needs from data collected on local housing stock by the Alaska Housing Development Corporation (AHFC). (Information Insights, 2009). Data from

[24] A particularly clear example is "base" pipeline infrastructure. Setting aside compression, all of the costs of the pipeline itself must be undertaken up front.

[25] Another key aspect of this two-edged sword is that some economies of scale can only be realized through infrastructure large enough to access Outside markets. Once accessed, Outside market realities can then discontinuously affect in-state commodity markets, overwhelming the benefits of lower infrastructure costs.

AHFC's energy conservation retrofit program. It finds that Fairbanks housing is more energy efficient than Anchorage housing. Total space heating needs are estimated at about 82% the level developed for Fairbanks North Star Borough. However, the AHFC data is not comprehensive, nor obtained from a random sample of housing stock.[26]

The Fairbanks North Star Borough estimates are adopted as the "base case" potential demand, with slight modification. (Moving forward, Fairbanks heating demand is assumed constant at today's levels, whereas Northern Economics assumed that demand and population would continue to grow in lock-step.)[27] As a sensitivity case, the model also assesses project costs associated with the demand estimates developed for CCHRC.

Third, this study uses DNR's Cook Inlet production decline curve. Cook Inlet production is a major risk for each of the three ASAP bullet line projects' ability to reach 100 percent capacity. In AGDC's list of key project risks, this issue is foremost. (AGDC, 2011a; p. 4-2)

The success of the ASAP project hinges on the substantial failure of Cook Inlet gas development and exploration. If "new gas" is developed in existing fields to stem or slow decline, then a 250 MMcfd North Slope project will not start at or near full capacity. Larger configurations of the ASAP project could potentially start at full capacity should they secure sufficient export contracts, but in such circumstances a bullet line would be unable to economically deliver North Slope gas to Cook Inlet customers.

The chance for new discoveries and developments is significant. The US Geological Survey estimate that mean technically recoverable undiscovered conventional gas resource in Cook Inlet exceeds 12 Tcf. (Stanley et al, 2011) Meanwhile, the State DNR estimates wellhead gas prices of less than $10/MMBtu could be sufficient to provide a real return on investment of over 20% and support gas production from existing fields through 2020. (Gibson et al, 2011; 21) Discoveries from new fields would further extend this date.

Of course, nothing guarantees that sufficient exploration investment will be made. For companies operating in Cook Inlet, robust rates of return may by themselves matter little. If projects with large levels of net present value matter materially more, then adequate investment might not occur. (Gibson et al, 2011; 22)

---

[26] A reasonable hypothesis is that the CCHRC results overstate total Fairbanks heating needs, because one might expect that only the least energy efficient houses would participate in the AHFC program.

[27] On the one hand this is unreasonably conservative, as price relief should lead to higher levels of energy consumption. (Joutz and Trost, 2007) On the other, given that some are already transitioning from heating oil to wood or coal, and that high costs may be depressing Fairbanks population and economic activity, rising levels of total Fairbanks demand between now and when an energy relief occurs, may also be unreasonable.

Four different Cook Inlet decline scenarios are modeled, (Figure 5) DNR's P90 and P10 assessments of potential gas production from existing fields.[28]. Two less favorable scenarios, with exponential decline of 14 percent beginning in 2016 and 2018, are also modeled. These assume no new material fields are developed. Reasonably likely futures, in which Cook Inlet cannot fully satisfy local demand in the medium term but discoveries extend the aggregate production tail, are not modeled.

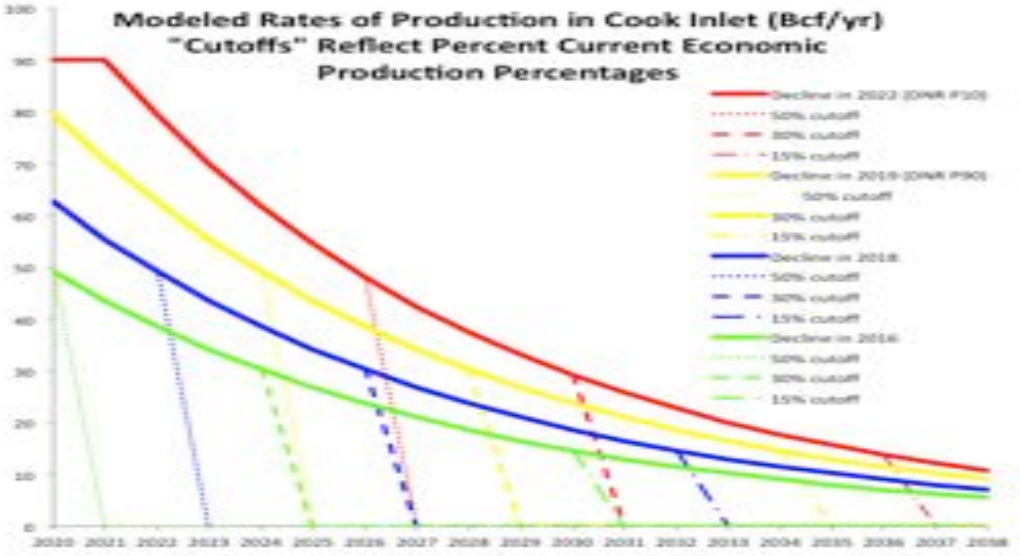

Figure 5: Modeled Cook Inlet decline rates, with different levels of minimum production necessary to keep Cook Inlet production economics viable.

This model does not assume that Cook Inlet gas production would necessarily continue to be economically produced and delivered into Anchorage at a tiny fraction of existing utility demand, because there may be a minimum level of production needed to support the costs of continuing to operate operating local production and transportation infrastructure. Absent studying what the minimum level might be, the figures shows decline "cutoffs" at 50, 30, and 15 percent of existing production levels.

RESULTS

Comparative project results are presented first. A brief discussion of results noteworthy to specific projects follows.

Comparative results

The cost of delivered energy for the various projects is a function of ANS WC (ANS-West Coast) oil prices. Assuming the private ownership business model, delivered energy

[28] The "P90" assessment reflects 90 percent likelihood that the fields will produce at least the level of gas forecasted, conditional on adequate investment. It is at the "conservative" end of DNR's assessed range. The "P10" assessment reflects 10 percent likelihood that fields will produce at least the level of gas forecasted.

costs for nearly all projects can be either higher or lower than the existing cost of heating oil (dashed black line, Figure 6).

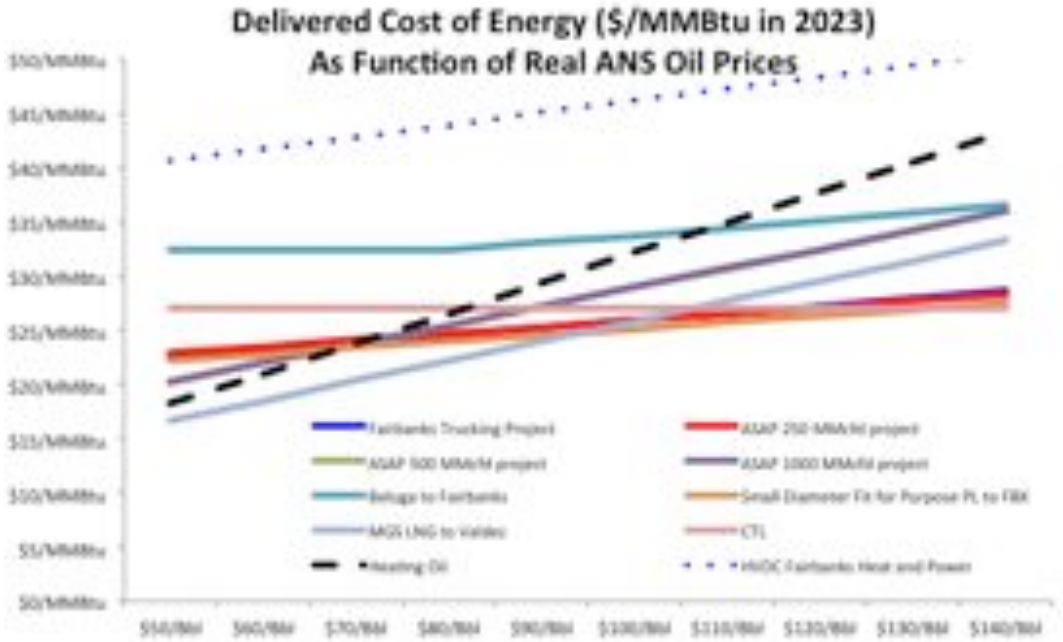

Figure 6: Private developer business model. Real (2012$) ANS WC oil prices are along the X-axis, while the Y-axis measures money of the day (2023$) energy prices. Susitna results at $80/MMBtu not shown as doing so compresses the figure's scale.

The projects delivering otherwise "stranded" North Slope gas tend, coincidentally, to lie very close together. At real crude oil prices of about $70/Bbl and above, the larger ASAP configurations deliver higher-cost energy than the smaller 250 MMcfd configuration; delivered energy costs from the ASAP 500 MMcfd and 1 Bcfd projects are essentially identical owing to "opportunity cost" pricing.

For nearly all projects, the delivered cost of energy under the private model can be above heating oil at modest, but realistic, crude oil prices. Accordingly, there is non-material price risk for a private project developer. The CTL project is particularly interesting in this regard.

Absent price regulation, a private CTL developer could sell product at competitive fuel oil prices, and the CTL project would not offer price relief. But given the high project risk, regulating prices dooms the business model. When oil prices are less than about $80/Bbl the developer would be unable to recover costs, regardless of the regulated rate: the market heating oil price would be below the cost of manufacture. Conversely, under price controls, the developer would be unable to charge market rates for oil prices greater than $80/Bbl, else consumer price relief is voided.

Project ramp-up risks are also acute for the private business model case. (Figure 7)

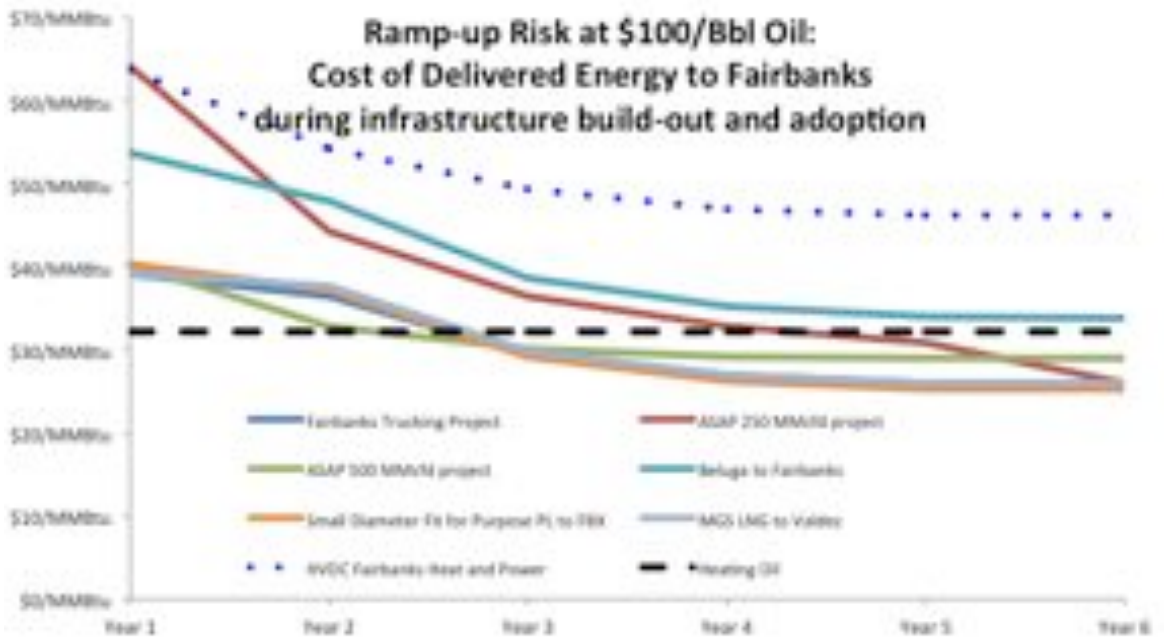

Figure 7: Delivered Fairbanks energy costs in first 6 years after project start-up at real ANS WC oil price of $100/Bbl, private ownership model. DNR P90 decline rate for Cook Inlet production assumed.

All projects with demand ramp-up start with unsubsidized energy costs that are materially greater than the cost of heating oil. Absent the project developer taking significant project losses for the first several years, such that consumers see "final" plateaued energy savings, no customers will sign up for service. This study does not address increased return on project equity that a developer might demand as a reward for taking on such risk.[29]

The state ownership business model, not surprisingly, materially reduces energy costs for nearly all projects by reducing the cost of capital. (Figure 8) Even the HVDC project can deliver savings at real oil prices greater than about $100/Bbl. Projects for which capital costs loom larger in the overall cost structure benefit more. For example, of the three projects marketing "stranded gas", LNG trucking is now the most expensive owing to the actual trucking expense – here modeled as an operating cost – being unaffected.

[29] Ramp-up risks will be attenuated if certain infrastructure, such as gas treatment and liquefaction, can be added in "trains" as demand builds to better match ultimate demand. Lacking this granularity in subcomponent project costs, no attempt has been made to do this.

Figure 7: State ownership business model. Real (2012$) ANS WC oil prices are along the X-axis, while money of the day (2023$) energy prices are along the Y-axis. Susitna project results (over $48/MMBtu) not shown.

Over most of the oil price range, the CTL project boasts a cost of service that is less than all other options (save a MGS). Further, business risks on the CTL project are now materially reduced, such that a price-regulated commodity could be contemplated. Real ANS crude oil prices would need to be below $50/Bbl, in real terms, before the state began making losses.

However, a state-owned, cost-of-service CTL project would engender a host of complex regulatory and market issues. Most obviously, it would provide enormous incentive for commercial entities to purchase heating oil from the state at the regulated rate, and sell it to the general public at competitive market rates. Marketing entrepreneurs would be enriched at the expense of intended project beneficiaries. This is a problem that, with adequate policing and regulatory resources, might be kept to a dull roar, but is inextricably fraught with complication.

At these sorts of delivered costs, consumer savings in Fairbanks would appear large enough to encourage ready adoption of the new heating technologies. We have calculated the "average household's" internal rate of return that is necessary for consumers to invest in new heating technologies. At the baseline level of assumed demand, it appears that for the representative household, the conversion cost investment may pay handsomely for gas sourced from the stranded gas projects. The household's initial cost of conversion will matter significantly. (Table 2)

Table 2: Representative household Internal Rate of Return and years to payback as a function of initial household capital expenditure level ($3, $10, and $20 thousand dollars). Nominal-dollar oil prices of $100 assumed.

Scenario	Year of first gas	Gross Fuel Cost Savings from 2012-2035	$3,000		$10,000		$20,000	
			IRR	Years to Payback	IRR	Years to Payback	IRR	Years to Payback
Fairbanks Trucking	2016	$49,102	207%	1	27%	4	11%	9
ASAP 250 MMcfd	2020	$38,511	390%	1	31%	4	11%	8
ASAP 500 MMcfdd	2020	$14,318	45%	3	5%	11	0%	0
ASAP 1000 MMcfdd	2020	$14,262	45%	3	5%	11	0%	0
Beluga to Fairbanks	2019	$0	0%	0	0%	0	0%	0
Small Diameter	2019	$46,619	830%	1	37%	3	14%	7
MGS LNG to Valdez	2023	$8,735	26%	4	0%	0	0%	0

State ownership also helps, but does not eliminate, ramp up risk at $100/Bbl crude oil prices. (Figure 9) The ASAP projects all start with energy costs above the heating oil benchmark, as do the Beluga and HVDC projects. While the LNG trucking, 12" pipeline, and MGS projects all can initially deliver energy at less than the cost of heating oil, project savings may be insufficient to induce consumers to switch at the rates modeled here.

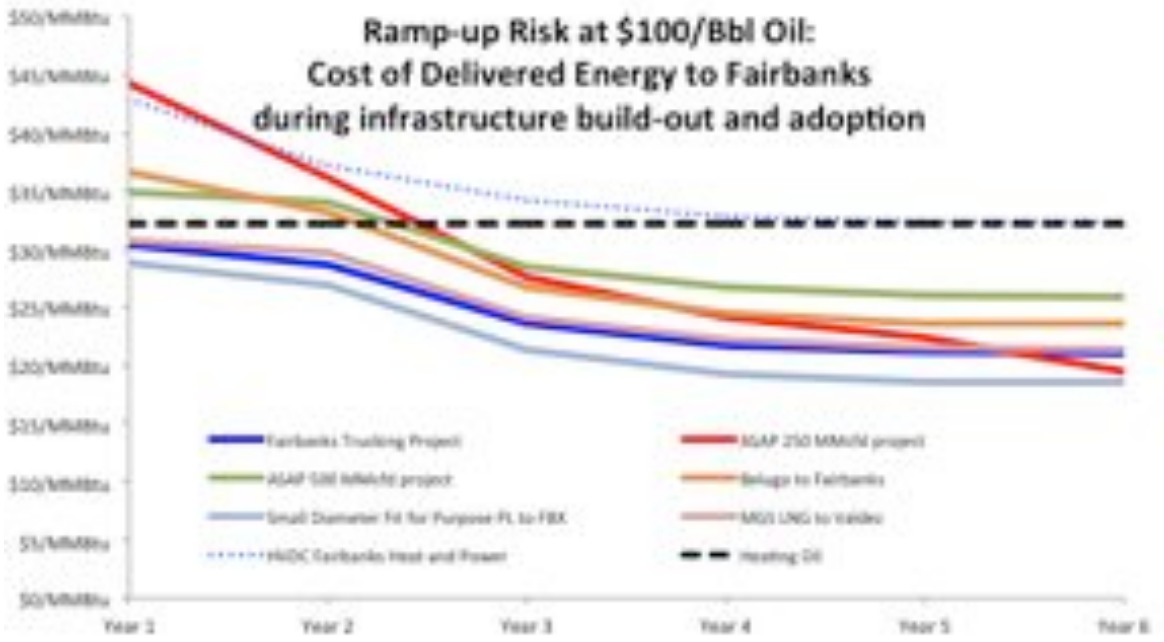

Figure 8: Delivered Fairbanks energy costs in first 6 years after project start-up at real ANS WC oil price of $100/Bbl, state ownership model; DNR P90 decline rate for Cook Inlet production assumed.

At $100/bbl oil, the ASAP 250 MMcfd project can ultimately deliver energy at significantly less cost than the larger ASAP configurations. However, for the first several years this project's ramp-up risk is particularly acute; the ASAP 250 MMcfd project's cost of energy is greater than the 500 MMcfd and 1 Bcfd cases. This is because for the smaller ASAP project the unused capacity – which is determined by the decline rate in Cook Inlet – is initially a greater percentage of total project capacity. Fairbanks, which ultimately benefits from the economies of sale associated with stranded gas shipments to Anchorage under the smallest ASAP project configuration, shoulders its portion of this largely unused project capacity.

Ramp up risk due to Cook Inlet production decline is a function of the start and pace of that decline. If Cook Inlet steep and irrevocable production decline begins as early as 2016, and Cook Inlet is no longer economic at fifty percent of current utility needs, then the "ramp up" cost of energy will be significantly attenuated. Conversely, if Cook Inlet production does not begin exponential decline for another decade then the ramp up costs would substantially outstrip the cost of LNG imports. (Figure 10)

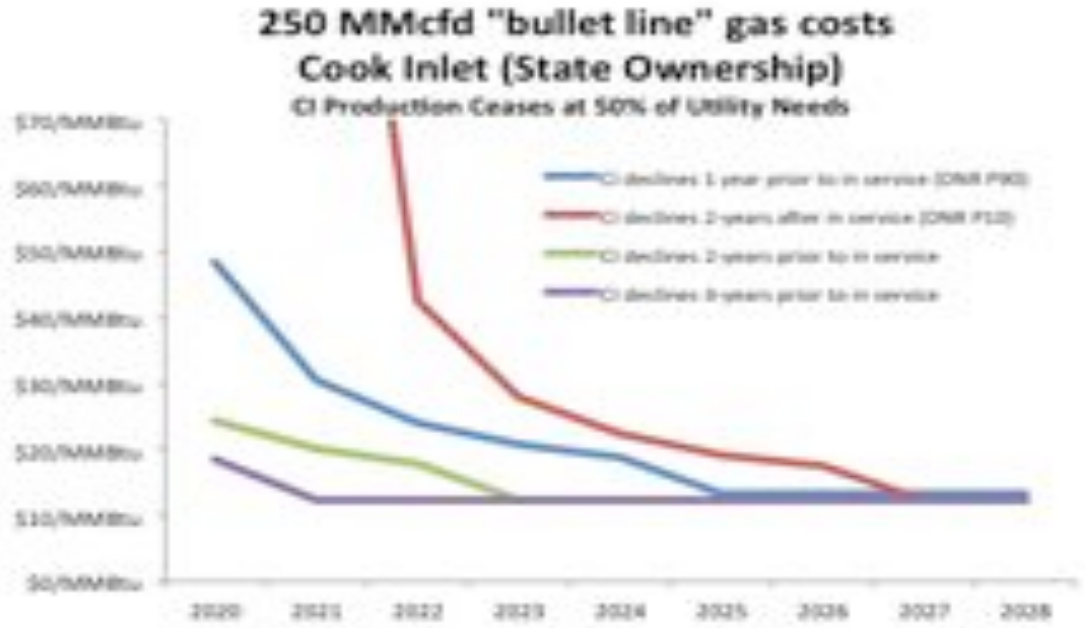

Figure 9: Ramp-up risks for Cook Inlet delivered costs of energy from ASAP 250 MMcfd project as a function of production decline. All curves assume Cook Inlet production ceases at 50% of current production.

At day's end some mechanism would be needed to pay for the ramp-up risk associated with Cook Inlet production declines. Subsidy needs may be substantial. For the 250 MMcfd case the net present value of ramp up subsidy needs could exceed $2 billion (Figure 11). Ramp-up subsidy needs decline as ASAP project size rises. This is ironic: the project promising lowest-cost energy (the 250 MMcfd case) also comes with the largest subsidy risk.

Subsidy needs also decline with delays in Cook Inlet production decline. The state might be better off waiting to launch a bullet line project until the Cook Inlet production picture becomes somewhat clearer. Finally, ramp-up subsidies fall as the Cook Inlet minimum production threshold rises. For the 250 MMcfd ASAP project the net present value (discount rate of 5%) of the difference between 50% and 15% thresholds exceeds $500 million. The general magnitude of the Cook Inlet production threshold could be reasonably estimated given data on field production and transportation costs.

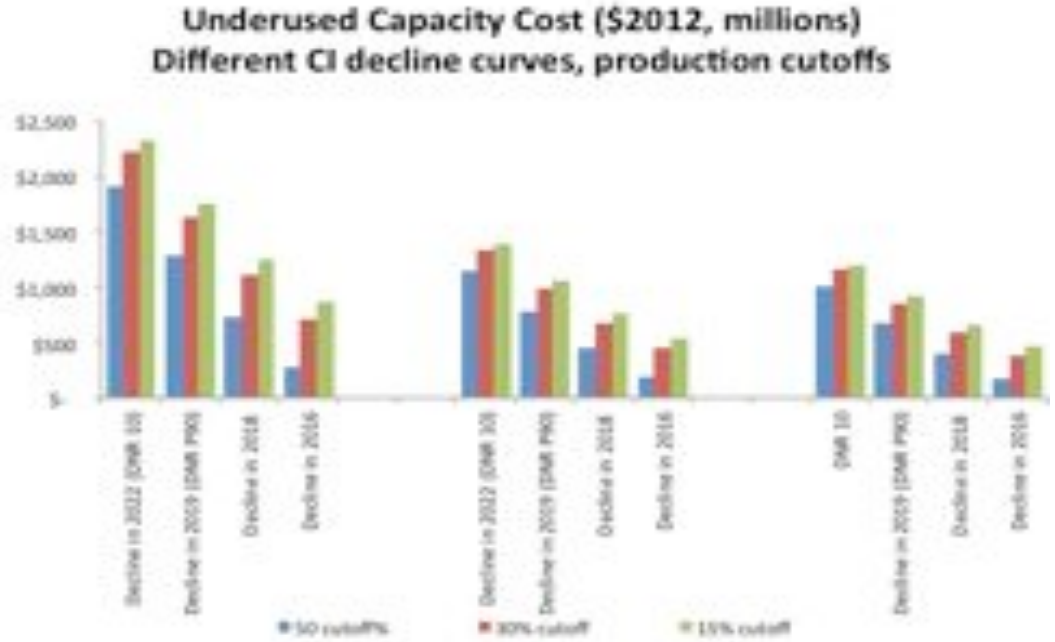

Figure 10: Net present value (NPV5%), in millions, of subsidy needs for ASAP "bullet line" projects associated with Cook Inlet production decline.

Demand risk is also caused by uncertainty in the rate at which Fairbanks customers might adopt the new energy offering. The assessment of risk is further compounded by uncertainty regarding Fairbanks' current heating needs. Both affect the magnitude of ramp up risk as modeled. The cost of service of only the local gas distribution system – an infrastructure component of all gas projects considered here – could potentially swing by $8/MMBtu depending upon the level of existing heating need and the rate of gas service adoption. (Figure 12)

Figure 11: Evolution in the cost of local distribution service only, as a function of existing Fairbanks demand and rate of market penetration.

If Fairbanks heating needs are closer to those estimated by CCHRC (the red lines in Figure 12) then the cost of local distribution service will be initially be roughly $2/MMBtu to $4/MMbtu greater. If ramp up proceeds more gradually than our base case (solid lines rather than dashed ones) then initial costs of distribution service would jump by nearly $5/MMBtu. Clearly, initial system rates must somehow be covered (*e.g.*,rolled into long term rates, or subsidized) to reduce these risks and ensure that consumers join the system.

The overall level of subsidy ultimately required will depend importantly on whether some customers to the LDC system can be brought online before the system is fully built out. The approach used here regarding capital expenditures follows that of Northern Economics: there are two "stages" to the LDC build-out, serving "high" and "medium" density areas of Fairbanks, respectively. As modeled here, a given "stage" of the LDC does not begin billing customers until its entire portion has been constructed. However, if some customers can be brought online prior to the conclusion of that "stage's" construction, then this can reduce ramp-up risk.

In addition to risks caused by commodity price and demand uncertainty, projects are also marked by uncertainty in construction costs and future escalation rates of those costs. In the following multi-page chart, ten sets of "tornado diagrams" are stacked. Each shows the effects on delivered energy costs of each of these variables, and of oil price uncertainty. This facilitates comparison of the effects of each variable across business models (state ownership on the left, private ownership on the right), and across projects.

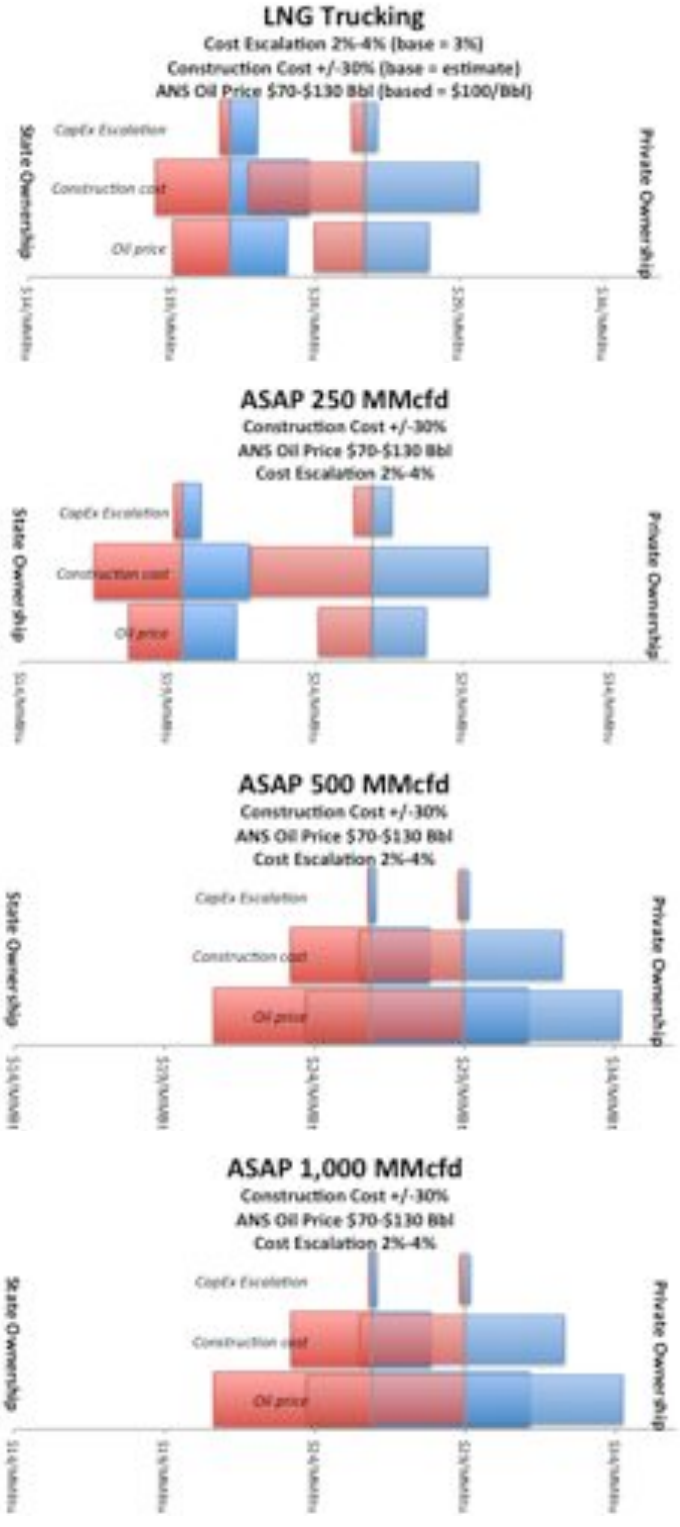
LNG Trucking
Cost Escalation 2%-4% (base = 3%)
Construction Cost +/-30% (base = estimate)
ANS Oil Price $70-$130 Bbl (based = $100/Bbl)
State Ownership
Private Ownership
CapEx Escalation
Construction cost
Oil price
ASAP 250 MMcfd
Construction Cost +/-30%
ANS Oil Price $70-$130 Bbl
Cost Escalation 2%-4%
State Ownership
Private Ownership
CapEx Escalation
Construction cost
Oil price
ASAP 500 MMcfd
Construction Cost +/-30%
ANS Oil Price $70-$130 Bbl
Cost Escalation 2%-4%
State Ownership
Private Ownership
CapEx Escalation
Construction cost
Oil price
ASAP 1,000 MMcfd
Construction Cost +/-30%
ANS Oil Price $70-$130 Bbl
Cost Escalation 2%-4%
State Ownership
Private Ownership
CapEx Escalation
Construction cost
Oil price

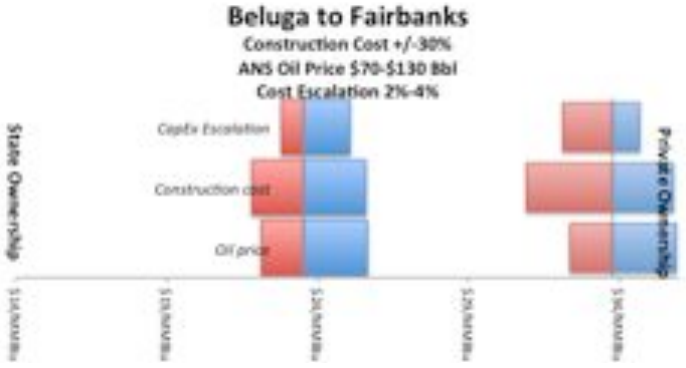
Beluga to Fairbanks
Construction Cost +/-30%
ANS Oil Price $70-$130 Bbl
Cost Escalation 2%-4%
CapEx Escalation
Construction cost
Oil price
State Ownership
Private Ownership


12" ANS to Fairbanks
Construction Cost +/-30%
ANS Oil Price $70-$130 Bbl
Cost Escalation 2%-4%
CapEx Escalation
Construction cost
Oil price
State Ownership
Private Ownership


MGS (LDC Only)
Construction Cost +/-30%
ANS Oil Price $70-$130 Bbl
Cost Escalation 2%-4%
CapEx Escalation
Construction cost
Oil price
State Ownership
Private Ownership

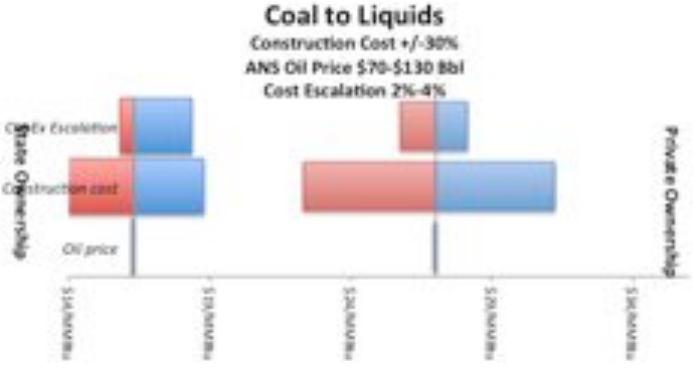
Coal to Liquids
Construction Cost +/-30%
ANS Oil Price $70-$130 Bbl
Cost Escalation 2%-4%
CapEx Escalation
Construction cost
Oil price
State Ownership
Private Ownership

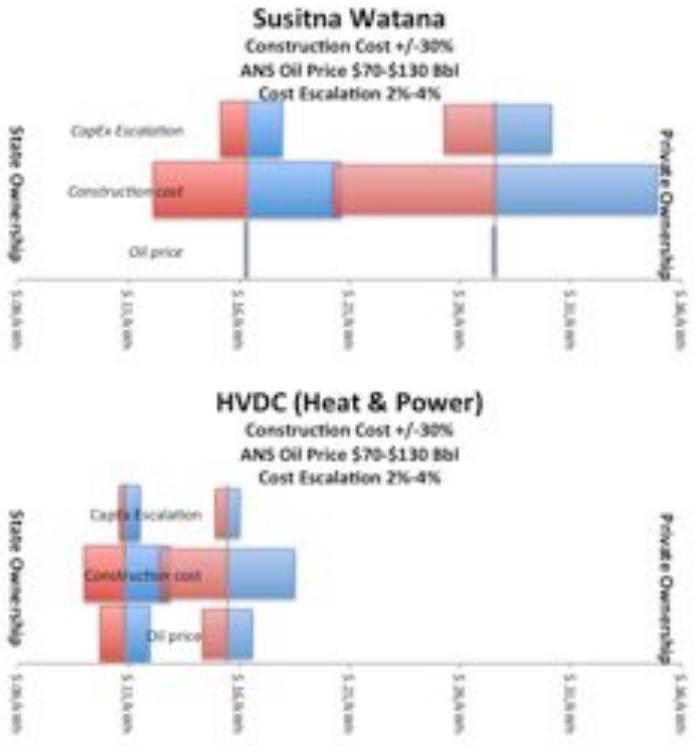

Figure 12: Comparative sensitivity of delivered energy cost to oil price, construction cost, and construction cost escalation rate uncertainty. State and ownership cases are centered at $100/Bbl oil price, "base" construction cost estimates, and 3% capital cost escalation rates. MGS results reflect "state" and "private" ownership only for the Fairbanks LDC.

A few patterns are noted:

- The larger ASAP and MGS projects are particularly susceptible to oil price swings. This is largely due to the commodity portion of the delivered energy price being determined by the Asian LNG export market.
- The uncertainty bands for the 500 and 1,000 MMcfd ASAP projects are identical. This is a function of "opportunity cost" pricing.
- Construction cost uncertainty is most important for the projects that deliver gas whose commodity price is in the "stranded gas" market.
- Capital cost escalation rates ("CapEx Escalation" in Figure 13) are always least important within a project, but across projects are most important for the largest projects with the greatest lead times.
- Assuming that adequate demand exists, the HVDC project offers more economical electricity and at less project risk than does the Susitna project. While the chart does not explicitly show this, transmission lines could be "twinned" to provide redundancy and the HVDC project would still delivery lower cost power.
- Both the Susitna and CTL projects are largely immune to oil price risk.

Project specific results

A few results specific to individual projects deserve to be mention.

CTL Project

Private ownership of a CTL project would engender significant risks for the project developer. If successful, such a venture would nevertheless fail to reduce energy prices in Alaska because produced liquids would need to be sold at market rates to compensate for extant price risks. Public financing and ownership of a CTL plant could, conceivably, permit heating oil deliveries at reduced costs.

Pursuing such a CTL scheme would be complicated, however. Product output would need to be economically regulated to offer consumer benefits. A two-tiered scheme, in which CTL-produced heating oil was sold at regulated rates but refinery-based heating oil was sold at market rates, would create enormous incentives for fraud and market manipulation. These could potentially be addressed, at least in theory.

The intrinsic and financial risks associated with a CTL project are considerable. While the base cost estimate is roughly $8 billion, that estimate is quite preliminary and uncertain; error bounds are +/- 40%. As a practical matter the upper end of the range would be more likely to occur than the lower end. The likelihood is enhanced given that the state, as a public entity, has no experience managing +$10 billion construction projects.

Finally, the environmental permitting hurdles facing a CTL project engender potentially severe risks. The energy and security act of 2007, Section 526, would effectively prohibit sale of CTL fuels to federal government consumers; new EPA rules on CO_2 emissions from coal fired power plants are problematic, and there is long term uncertainty over green house gas emission regulations and costs. All could make this plant difficult to finance.

This is not to say that pursuing a CTL project is necessarily inadvisable. Rather, because the risks are material given the scale, technical complexity, and the fact that such projects are outside the state's core competency, policy makers would do well to approach such a project with considerable deliberation and caution.

Beluga to Fairbanks (B2F)

Under certain conditions – sufficiently high oil prices, the ability to acquire Cook Inlet gas at relatively modest terms (compared with the current long-term contracting environment) – this project has potential to deliver cost savings to Fairbanks consumers. However, even if the project were to be fully financed by the State, it generally offers materially reduced savings compared with other alternatives (Figure 8). The reason is two-fold. First, like the 12" fit-for-purpose project, the B2F concept involves building a long pipeline carrying quite modest volumes. Second, based on existing contracting data

and the fact that new gas from Cook Inlet will require significant additional investment, it seems likely that Cook Inlet prices will need to be higher than prices demanded for "stranded" North Slope gas that is currently being produced.

The main value of a B2F project appears to lie in its ability to deliver gas to Fairbanks while providing the "option" of eventual extension to the North Slope and a reversal of its flow to serve Anchorage. As a practical matter it appears that a project along the lines contemplated by the Fairbanks Pipeline Company makes more sense. Although a south-flowing line entails additional expense of gas treatment, the more moderate North Slope pricing regime could offset these costs.

Bullet line projects

There are two main surprises concerning bullet-line results. First, for the range of oil prices modeled, smaller natural gas throughput configurations often provide greater consumer savings than do larger throughput configurations. Second, Fairbanks' delivered commodity prices are invariant between the larger (500 MMcfd and 1 Bcfd) bullet line project configurations. Both of these results stem from how commodity prices associated with the project are modeled.

250 MMcfd Bullet Line

Because it does not export gas to the Pacific Rim, this project enjoys the benefits of stranded gas pricing. This project could deliver gas to Fairbanks and the Cook Inlet at lower cost than other alternatives. For this to happen, two conditions must be met.

- The project needs to be wholly or substantially owned and financed by the state. Absent state ownership there is essentially no meaningful difference between this and the LNG trucking and fit-for-purpose projects' cost of delivered energy (Figure 8).
- The project needs to essentially obtain full capacity from the beginning of operations.

The first factor is largely within the state's control; the second is not.

The State's potential exposure associated with the gradual decline of Cook Inlet production is substantial. Especially as prices in Cook Inlet rise, it would appear that the possibility is substantial for significant new discoveries in the Cook Inlet. Increased Cook Inlet volumes will serve to delay the time when an ASAP line is needed to serve the Anchorage market. This creates real danger that the State might commit to a North Slope gas project before it is actually needed.

Unlike the illustrative decline scenarios presented here (Figure 5), Cook Inlet production decline could see a long tail rather than a steep drop. This could occur if investments continue to be made in Cook Inlet but at a rate insufficient to fully meet all of Cook Inlet's needs.

Such cash outlays would follow on a project that would require over $7 billion of project financing and likely stress the state's credit capacity (AGDC, 2011a). Because for the first years the underlying business case appears underwater, the state's credit would seem especially subject to pressure unless sufficient cash reserves were set aside to address the eventuality of potential shortfalls in Cook Inlet gas need from the project.

500 MMcfd and 1,000 MMcfd Bullet Lines

Depending on oil prices, both of these projects may deliver gas to Alaskans at a less affordable rate than a smaller bullet line. This counter-intuitive result flows from the fact that larger lines require LNG exports. Once the generally more lucrative LNG export market is reachable via a "medium-sized" project, and because the export market is larger than the capacity of either line to feed it, then if a Producer would sell into the Alaska market it would give up sales into the Asian export market. Accordingly, these "larger" project configurations would price in-state Alaska sales at the same level as LNG export prices so as not to lose any profit by selling locally.

The state ownership model does effect Fairbanks consumer costs through its favorable financing terms for LDC distribution and straddle plant costs, and would similarly effect Anchorage consumer costs through reduction in the Cook Inlet straddle plant cost of service. To the extent that the State does not desire simply to subsidize profits associated with LNG exports, therefore, it would do well to avoid providing benefits to the gas treatment plant and pipeline subcomponents of any project that exports gas.

Major Gas Sale

A major gas sale has potential to provide gas to Fairbanks less expensively than the other gas projects when real oil prices are under roughly $75/Bbl. This is owing to superior economies of scale upstream of Fairbanks, and the clear ability to save on pipeline tariffs, liquefaction costs, and shipping downstream of Fairbanks. As oil prices rise the project tends to lose its relative advantage.

However, the major gas sale gas offers considerable savings compared with Fairbanks heating oil across a very wide range of crude oil prices. It is, in this respect, a less risky "bet" on realized savings compared with other project alternatives. Of course, a major gas sale may never transpire. Worse, there is very little that the state can do to force it to occur. Accordingly, the major gas sales option involves considerable risk in that it may fail to provide energy price relief in any timely manner.

12" Fit for purpose pipeline project

This project appears to offer slightly favorable consumer benefits compared with either the trucking or 250 MMcfd bullet line options over the full range of oil prices. Because all three projects are modeled as accessing untreated gas at Prudhoe Bay at the same price, cost savings for the full project is necessarily due to a lower cost of transportation.

The 12" line also is subject to reduced ramp up risk (Figure 9). This is a simple function of the project having lower modeled capital costs. Whether capital costs can be driven as low as FPC suggests could matter a great deal. It may be worth examining the issue further.

HVDC project

Modeled results for this project suggest too much and reveal too little. Results indicate that the project would not make sense for delivering "heat by wire" to Fairbanks given other alternatives. Meanwhile, there are problems with real-world installation that this modeling has ignored. Modeling assumes only a single set of transmission lines connecting the North Slope to Fairbanks. Given the load contemplated, the risk to system reliability would be intolerable. The Railbelt electricity system strives for reliability levels in excess of 99%, which a single set of transmission lines cannot provide. Reliability is all the more critical if customers use electricity for space heating; an outage of hours could potentially result in a house freezing up. Accordingly, modeled billing determinants are too high and system costs (which would need to be bolstered with redundant transmission line, material costs of maintaining existing spinning reserve, and other measures) are too low.

However, the results also suggest that given adequate load to spread the fixed costs of HVDC transmission over a large number of kWh, some version of the HVDC project might be able to deliver electricity more cost effectively than the Susitna-Watana project. We note, for example, the modeled costs per kWh of power to Fairbanks is composed of:

Generation costs:	4 cents/kWh
Transmission costs:	3 cents/kWh
Gas costs:	3 cents/kWh

Even if transmission lines were twinned there would appear to be the possibility for an HVDC project to deliver electricity cost effectively. Loads, however, would need to come from new sources rather than existing space heating needs. Mines could be good candidates. Indeed, the viability of HVDC may depend on reaching commercial agreements with mining interests. Mining needs are potentially significant, suggesting material downward pressure on the per-kWh cost of transmission. Were mining offtake contracts secured, then the resulting economies of scale might be sufficient to allow HVDC infrastructure to reduce electricity costs in many parts of the state, even including the Railbet. It is an area deserving closer scrutiny.

Susitna-Watana Project

Modeled kWh results here are similar to those most recently developed by AEA (AEA, 2012). We stress that given exactly the same financing inputs, interest compounding assumptions, and business model approaches, the results of this analysis essentially match those of AEA. Differences between the two approaches are not disagreements, but reflect assumptions made for this study that are necessary to "normalize" the projects for comparison.

POLICY IMPLICATIONS

Perspectives will differ on the results presented. Here we offer what we hope are uncontroversial insights that have policy relevance. They are divided into mitigating consumer energy cost risks and prioritizing state subsidies.

Risks to consumer energy costs

A key goal shared by all projects is to reduce delivered energy costs to Alaskans. Commodity price and the level of consumer demand both significantly affect such costs. Fortunately, there are measures that can be taken to mitigate these risks. Policy makers can insist that such mitigation takes place before considerable resources are expended.

One of the easiest ways the state could reduce energy project risks statewide would be to pursue legislative measures that require fuel oil purchases to be reported. Lack of clear understanding of community heating needs can have a material affect on project risks. Many possible mechanisms could be used to ensure fuel oil purchases are comprehensively reported by geographic location. Sellers would no doubt be unhappy to have to report such data, but doing so could generate important public benefits and help guide prudent investment of state resources.

A key uncertainty affecting project energy costs is the commodity price that sellers will require. Fortunately, securing long term gas (or coal, in the case of CTL) supply contracts are something that can be done today by the relevant commercial parties. Because such pricing terms are integral to the energy savings sought, policy makers can insist on access to all relevant pricing terms before they make large appropriations. Without this information they cannot know whether state monies are being efficiently directed. This is especially the case given the potential, on larger bullet line projects, for state subsidies to be substantially, if not wholly, directed in a way that underwrites export profits while doing little to relieve Alaskans' high energy costs.

It is often assumed that favorable in-state commodity prices can be secured in exchange for generous state infrastructure subsidies. And it is at least possible that such a bargain might be secured, leading to commodity pricing very different from what we have modeled. However, if such bargained pricing is integral to project benefits it makes sense for policy makers to ensure that the "bargain" be struck early, before significant resources are expended. The further along the state goes in supporting a project, the more leveraged it will be in seeing that project to completion regardless of its benefits. At a minimum, an

explicit plan for when, how, and who will negotiate that bargain should be made transparent along with agreement on acceptable and unacceptable terms.

Some risks associated with consumer demand can and should be addressed before problems arise. Fairbanks ramp up costs are inevitable. Initial loans and grants to reduce consumer capital costs of switching to new heating technologies will help. They may not be sufficient. As we have seen, early consumers may need to be sheltered from the full transportation system cost or they are unlikely to ever join the system. Shelter might be accomplished in a number of ways, by a number of parties, but it is going to require planning and real expenditures. Various options need to be considered and a preferred method selected.

The bullet-line projects engender substantial risks associated with Cook Inlet production and decline. Given the enormous capital costs, the state cannot afford to "build it" and hope that customers come. Projects must be underwritten by capacity commitments.

To obtain such commitments some have focused on the need to improve capital cost estimates. However, a cheaper, quicker and potentially more important course of action may be available. Gas supply contracts go hand-in-glove with pipeline capacity commitments; no rational entity would make capacity commitments without having secured gas supply contracts at acceptable prices. Contract pricing terms can swamp the uncertainty in the ultimate costs of service. Very substantial costs, likely to be borne by the State, will be involved in refining project engineering cost estimates. It may make more sense to insist that Anchorage-based utilities secure North Slope gas supply contracts, potentially subject to conditions precedent. This would provide critical information as to whether securing pipeline capacity makes sense.

Subsidies

All of the projects considered here, with the exception of a MGS, appear to require state subsidy of some sort. They are also all expensive (Figure 14).

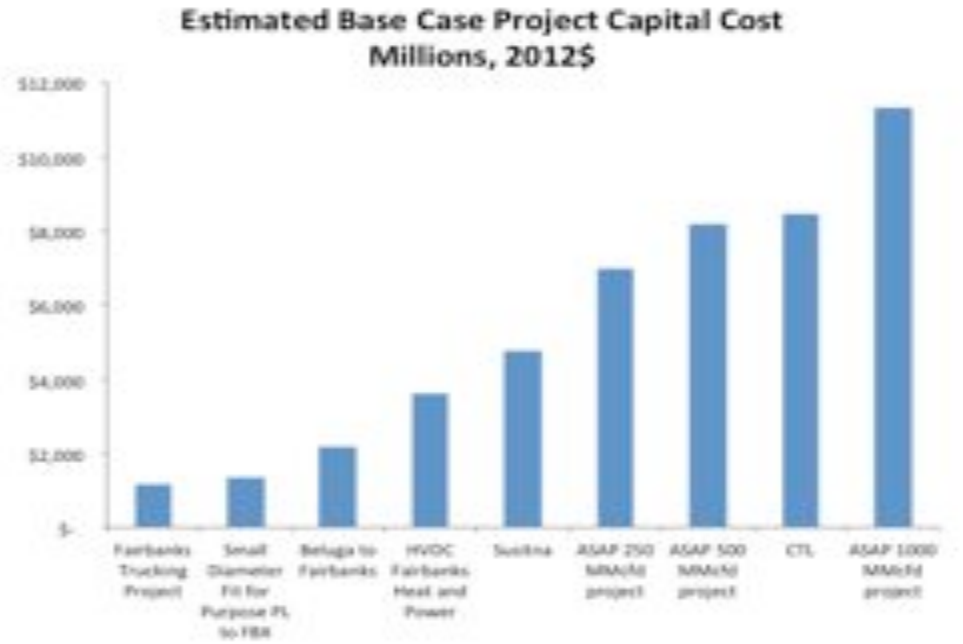

Figure 13: Capital costs, base case, in millions of dollars. The MGS project is excluded, but its total base case capital cost exceeds $53 billion.

Clearly, the state cannot support all of these projects, nor should it. A clear next step is for project evaluation to be undertaken in the context of comprehensive medium-term fiscal planning to clarify what the state can afford to pursue in light of available savings, tight budgets, and competing needs. Addressing this question would require coupling a model of revenue and spending forecasts for the next ten years or so, with an assessment of the available capital that would need to be devoted to any particular project in each year.

Priorities may also be clarified by addressing state priorities in light of the fact that different projects serve different in-state customers, have different inherent and commercial risks, proceed on different timelines, and offer different opportunities. The Susitna and HVDC projects, for example, appear to be of roughly similar sizes. The first promises a sizeable quantity of price-stable, renewable energy for Railbelt customers. The second *may* – if sufficient demand can be assembled under long term contract – provide "wires to resources" transmission infrastructure. That infrastructure could unstrand otherwise stranded renewable resources, unlock opportunities for expanded mining, reduce rural energy costs and power value-added manufacturing. Given limited state budgets, clarifying and ranking priorities for the state's future may be worthwhile.

At minimum, attention should be trained on deploying state subsides towards projects, and project subcomponents, that will be effective in reducing in-state energy costs. Only some supply markets will be successful candidates for thinking about consumer energy costs as the sum of a commodity price plus all infrastructure costs. Buying down the cost of infrastructure will do little to help Alaskan consumers if the project does not access the right market. Projects that involve "net forward" pricing – the smaller-configuration

bullet line, a 12” fit-for-purpose line to Fairbanks, LNG trucking, HVDC – will benefit from subsidies at any point in the transportation chain. Projects involving net-back pricing may not. Policy makers can ensure that the mechanisms they establish are not unintendedly used to subsidize export profits.

CHAPTER 9: A STOCHASTIC MULTI-ATTRIBUTE ASSESSMENT OF ENERGY OPTIONS FOR FAIRBANKS, ALASKA

by Laura Read[1], Soroush Mokhtari[2], Kaveh Madani[2], Mousa Maimoun[2], Catherine Hanks[3]

INTRODUCTION

Interior Alaskan residents and industries in Fairbanks, the rail belt, and bush communities face economic and accessibility challenges in delivering affordable energy for heating and electricity. Of the nine major energy projects proposed by both private and public entities to develop a new energy source for Fairbanks (Table 1), each one varies in social and political support, economic costs, and environmental impacts. An analysis that evaluates multiple criteria can inform decision makers (DMs) as to the trade-offs involved in selecting between projects. This is a multi-criteria multiple decision maker (MC-MDM) problem because the final decision is affected by the input from stakeholders from different areas with various concerns. This work uses a suite of multi-criteria decision-making, social-choice, and fallback bargaining methods to demonstrate how different methods can lead to different project selection outcomes, and also provides a robust solution by aggregating the results from each method into a single score. This chapter discusses the collaborative process to develop performance measures and criteria in section one, the formulation of methods employed in this multi-attribute analysis in section two, the modeling procedures in section three, results in section four, and implications in section five.

Table 1. Proposed energy projects

Alternative	Description
A1	Large diameter pipeline Edmonton → Chicago
A2	LNG export North Slope to Valdez
A3	Bullet line to Anchorage, spur to Fairbanks
A4	Small diameter pipeline: North Slope to Fairbanks
A5	Liquid Natural Gas trucking project
A6	Big Lake gas pipeline: Beluga to Fairbanks
A7	High Voltage DC line from North Slope
A8	Coal to liquids power plant in Fairbanks
A9	Susitna Dam

[1] Department of Civil and Environmental Engineering, Tufts University, 300 Anderson Hall, Medford, MA 02155; 617-627-6200, email: laura.read@tufts.edu
[2] Department of Civil, Environmental and Construction Engineering, University of Central Florida; 4000 Central Florida Blvd, Orlando, FL, 32816; 407-823-2317; emails: s.mokhtari@knights.ucf.edu, kaveh.madani@ucf.edu, mousamaimoun@knights.ucf.edu
[3] [3]Geophysical Institute and Department of Petroleum Engineering, University of Alaska – Fairbanks; 1000 University Ave, Fairbanks, AK, 99709; 909-474-7211; email: chanks@gi.alaska.edu

COLLABORATIVE PROCESS

An important aspect of this analysis is the collaborative process that the active project investigators engaged in for collecting information and determining the inputs for the model. The research project leaders participated in open communication sessions for several months to develop the desired performance measures for assessing the projects as a group. Following the development of performance criteria, experts on the project assumed roles to represent the range of social and political responses expected by decision-makers.

Decision criteria matrix and performance measures

The initial phase of this project began with conversations among project investigators to determine the relevant criteria for assessing the performance of the energy projects. Based on the local knowledge and field expertise of economists, environmental specialists, and natural resource engineers, involved in this research project, a set of criteria were developed. Each expert was asked to submit a list of criteria from their field so that a final list could be compiled. The decision making research, led by the University of Central Florida, then helped with facilitating discussion among the research team experts over the prioritization and categorization of the suggested criteria. Over several weeks these criteria were combined into three main categories – environment, economics, and socio-political – with sub-categories for specific metrics. In the environmental category, air quality has two sub-criteria to include both particulate matter and water vapor. The social criterion of "social acceptability" contains three sub-criteria to assess how each project interacts with the personal views and values of residents. The political criteria are evaluated in four sub-criteria to include the major elements of how politics affect project selection. Table 2 summarizes the criteria and their descriptions as defined collectively by the group.

Table 2. Criteria descriptions for project evaluation

Major Category	**Criteria**	**Description**
Environment	Net Carbon Footprint	The carbon footprint of each project including construction and operation
	Air Quality: *Particulate Matter*	The level of PM 10 and PM 2.5 emitted by each project
	Air Quality: *Water Vapor*	The amount of water vapor released for each project
	Ecological/Land footprint	The land area affected by the construction and operation of each project
	Water footprint	The amount of water used to construct and operate each project
Economics	Project levelized cost	The levelized cost of each project including development, capital, and operations and maintenance costs
	Capital cost	Immediate cost burden
	Commodity price reliance	Price volatility; the degree to which the price of the sale is expected to change with the given markets
Socio-political	Social acceptability: *Infrastructure/access*	How the projects' scheduled impacts on land use and accessibility affect the personal view of the resident

	Social acceptability: *Job creation*	The likelihood of a project to create local jobs and whether the resident sees this as a positive addition (long-term jobs) or potentially negative (transient, short-term jobs)
	Social acceptability: *Address energy needs*	Projects receive higher rankings according to whether the respondent believes the project will address their personal energy concerns
	Political support by legislator: *By region and subsidy*	Viewpoints of politicians divided by location, since a Fairbanks politician has a different agenda than one from Anchorage or the Bush communities. For this sub-category, each project is ranked based on how it meets the needs of the local political constituent from that region; the subsidy sub-category refers to whether the project will rely heavily on a government subsidy (lower rank) versus externally funded (higher rank)
	Sponsor credibility	Projects are ranked according to the credibility (and existence) of a sponsor – taking into consideration both funding and status
	Local materials and labor	Ranks projects on their reliance on local resources versus bringing in external resources, crediting projects that rely more on local supplies
	Timing	Projects receive higher rankings if they are expected to be operational earlier

The performance evaluation tree matrix is provided in Figure 1, where criteria and sub-criteria are chosen and used as inputs to the model. Experts determined the criteria categories through discussion of the level of detail necessary to assess the projects and the data available for evaluation. Following criteria identification, the descriptions and measurable outcomes from each were agreed upon and scripted as a group.

An important step in designing the evaluation tree matrix, which combines multi-objective assessment and decision tree concepts, was to determine the importance level of each criterion. Based on the importance level of each criterion the decision criteria were organized into levels and sub-levels. This organization has three main objectives: 1) A systematic multi-attribute evaluation at each level to determine the overall performance value at that level; 2) Transferring/mapping performance uncertainty from lower level to higher-level decision making within the tree; and 3) Preventing biasing the results toward a main decision attribute (i.e., environmental, economic, social-political) in cases where evaluating one attribute required using multiple criteria (e.g. water footprint, carbon footprint, land footprint, etc. for environmental performance). Step-wise comparisons are made at the sub-criteria level and moving left on the evaluation tree matrix to the higher levels. Uncertainty at each step-wise evaluation is carried through to the higher level analysis using Monte Carlo simulations of the probability distribution for project performance.

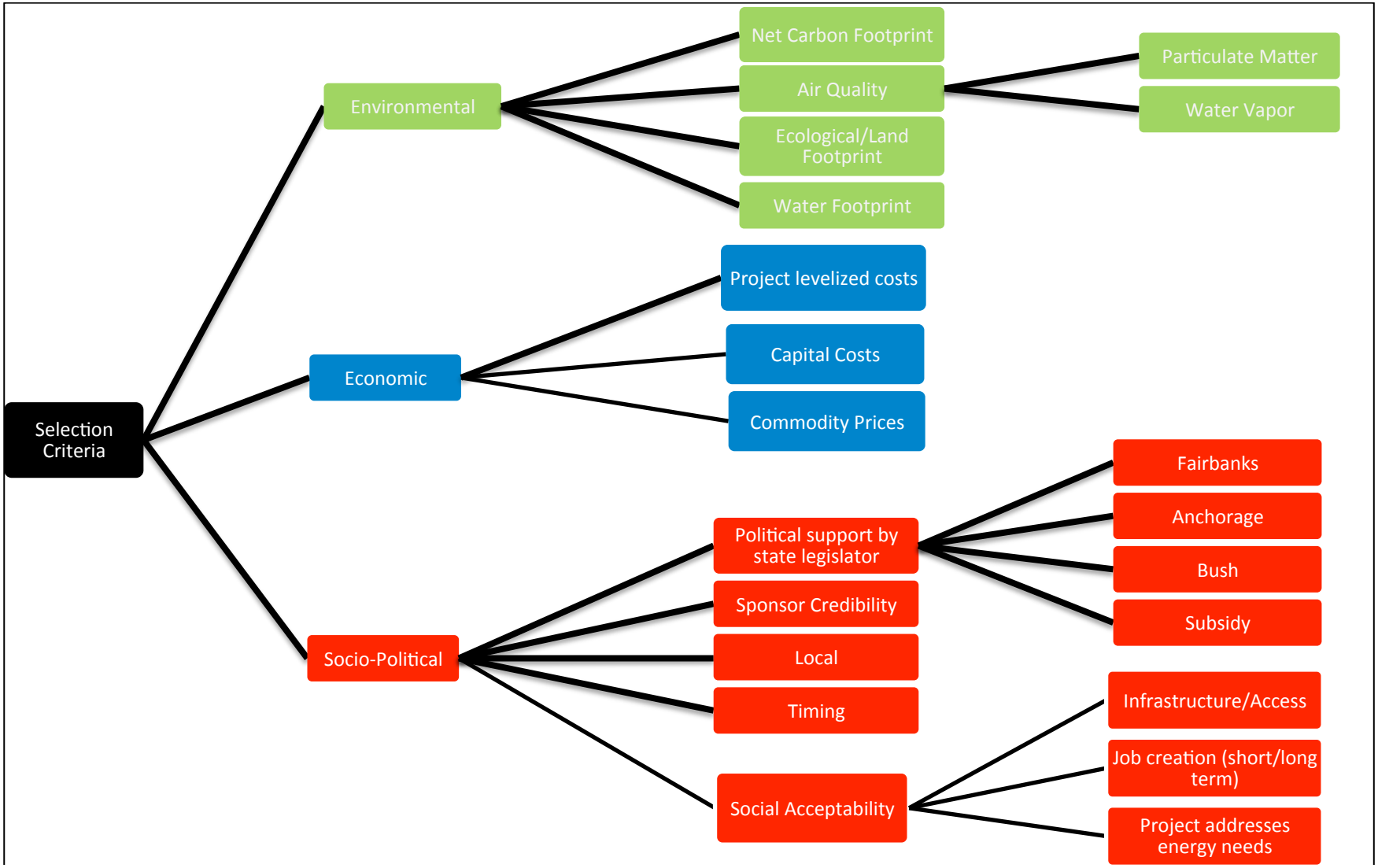
Selection Criteria
Environmental
Net Carbon Footprint
Air Quality
Particulate Matter
Water Vapor
Ecological/Land Footprint
Water Footprint
Economic
Project levelized costs
Capital Costs
Commodity Prices
Socio-Political
Political support by state legislator
Fairbanks
Anchorage
Bush
Subsidy
Sponsor Credibility
Local
Timing
Social Acceptability
Infrastructure/Access
Job creation (short/long term)
Project addresses energy needs

Data collection and role playing

Once the criteria and decision tree were defined for DMs, the environmental and economic experts were asked to provide quantitative values for their criteria. Uncertainty in the estimated quantitative and qualitative data derived from the range of values for each category and the differences in opinions expressed in the performance data and were reported in ranges for inputs to the model.

The environmental performance data values (Table 3) were derived from reports published by the supporters of each project and by the State. Quantitative data was converted into qualitative rankings for each category. Values for the net carbon footprint were estimated using the emissions from the pipeline volumetric flow rate over the expected lifetime of the project. Carbon emissions from liquefaction were based on the expected BTU productivity for the delivery of gas to Fairbanks for the proposed project. The HVDC and Susitna Dam electric line carbon footprints were estimated from the expected kWh delivery over the project lifetime. All environmental values for the coal-to-liquids power plant were taken from the Hatch report, which assesses the environmental impacts of the plant (Hatch Ltd, 2008). Air quality impacts from particulate matter and water vapor were estimated from the emission rates for the proposed capacity for each project. Since not all projects have completed an environmental impact assessment, the ecological/land footprints were calculated by assuming a 100 foot of right-of-way for each pipeline and multiplying by the total length (TransCanada Alaska Company, 2011). The water footprints for the gas pipelines were estimated from State resource assessment documents that include water-use of the production processes; rankings in this category also reflect the potential risk for contamination if safety measures fail.

Table 3. Environmental Criteria Performance Values

Alternatives	Net Carbon Footprint	Air Quality		Ecological/Land Footprint	Water Footprint
		Particulate matter	Water Vapor		
A1	7	3	3 to 6	7	6
A2	6	4	7	6	5
A3	5	5 to 7	3 to 6	5	7
A4	4	5 to 7	3 to 6	1	2 to 4
A5	8	8	8	2	1
A6	3	5 to 7	3 to 6	3	2 to 4
A7	2	2	2	4	2 to 4
A8	9	9	9	9	9
A9	1	1	1	8	8

The economic values (Table 4) used in this analysis are derived from work by Antony Scott, an economist at the Alaska Center for Energy and Power (Chapter 8, this report). The model incorporates development costs, capital costs, and operating expenses over the expected lifetime of the project. Costs for a distribution infrastructure to deliver gas to Fairbanks are estimated;

however, household level conversions costs from oil to gas or electricity for heating are not included. The analysis does not account for uncertainties in the interest rates or market fluctuations in materials pricing, but does incorporate the reliance of gas and electric prices on market oil prices to give a correlation cost.

Table 4. Economic Criteria Performance Values

Alternatives	Cost	Commodity prices	Capital costs
	$/mm btu		
A1	7.00	7	9
A2	16.02-16.38	8-9	8
A3	12.47-14.45	8-9	6
A4	15.63-19.16	3-6	2
A5	17.15-19.41	3-6	1
A6	18.56-26.87	3-6	4
A7	26.39 - 35.19	3-6	3
A8	18.77-26.76	1-2	7
A9	8.21 - 61.59	1-2	5

Project performance in the socio-political criteria (Table 5) was determined through surveys in which participants ranked each project based on their own personal preferences to the social sub-categories. Survey participants were members of the active expert project team and thus were all well informed on the specifics and impacts of each proposed project. The political performance and ranking for each project were assessed by interviewing political experts on the project as well as attending a local forum where politicians spoke in detail on Fairbanks' energy and stated their support for the proposed projects.

Table 5. Socio-political Criteria Performance Values

Alternatives	Infrastructure /Access	Job creation (long & short term)	Project will address my energy needs
A1	3-5	2-5	6-9
A2	2-4	2-5	4-7
A3	1-6	4-6	4-6
A4	1-3	6-8	2-4
A5	4-7	6-9	1-4
A6	5-7	4-7	4-5
A7	5-9	4-7	3-5
A8	6-9	8-9	6-8
A9	7-9	1	7-9

MULTI-ATTRIBUTE ANALYSIS METHODS

Studies in the natural resources and operations research literature have applied multi-criteria decision making methods to solve similar problems, where there is either a single (MC-SDM) person with power to decide the final selection (Figueira, Greco, & Ehrgott, 2005; Hajkowicz & Collins, 2007), or multiple decision makers (MC-MDM), where inputs from several stakeholders influence the decision (Madani & Lund, 2011). Since MC-MDM problems rely on interactions between stakeholders for agreement on a final decision, this work applies MCDM methods, social-choice, and game theory techniques to provide a robust set of solution ranking methods that view the problem from a different approach. MCDM methods solve the problem considering full cooperation ("high cooperation") among parties to achieve the optimal decision, whereas social-choice methods inform the socially optimal selection ("medium cooperation), and fallback bargaining, as game theoretic methods provide the best solution based on bargaining in a non-cooperative mode ("low cooperation") toward an acceptable agreement. Game theory is particularly informative for MC-MDM problems since these methods consider the behavior and self-interests of stakeholders in selecting an alternative (Madani, 2010; Madani and Lund, 2012). Table 6 summarizes the methods selected for this analysis and provides a brief description.

Table 6. MC-MDM Analysis Methods used in this study

Category	Method	Description
MCDM	Dominance	Makes pair-wise comparisons across all combinations of criteria; the best alternative is the project that wins most often.
	Maximin	Ranks the projects based on maximizing the worst performance; represents a pessimistic or "best of the worst" case perspective.
Social Choice Rules	Borda Count	Scores the projects according to preference order of alternatives for each criterion, with the top choice receiving N points, second receiving N-1, etc. Sums the values to select the best project as the one with the highest overall score.
	Plurality	For each criterion, the most preferred alternative is selected. Winner is the alternative with majority of votes. Ties are allowed by this method.
	Median Voter Rule	If an alternative receives the majority of votes for most criteria (from the majority of decision makers), it is selected; otherwise each criterion (decision-maker) will vote for the second most preferred alternative. The procedure continues until a unique alternative receives the majority votes.
	Condorcet Practical Method	Ranks projects according to majority support; works by the same logic as dominance.

	Majoritarian Compromise	Similar to Median Voter Rule except when ties exist in the rankings, winner is the alternative with the greatest number of supporters.
Fallback Bargaining (Brams and Kilgour, 2001)	Unanimity	Selects the project that receives all stakeholder support as bargainers fall back to agree on an outcome; this solution is always Pareto optimal because it chooses at least the middle preference of each bargainer.
	Q-Approval	Selects the project that is preferred by "*q*" parties, where *q* (minimum threshold of persons required for consensus) can be set by the bargainers.

Modeling procedures

Stochastic MC-MDM analysis

In classical MC-MDM problems, a finite set of criteria evaluates a finite set of alternatives, and the performance measures of these alternatives are unique deterministic values. In this space, payoffs correspond to points instead of regions, and MCDM procedures aim to single out one point as the optimal solution of the problem. However, in this study performance values were associated with uncertainty, making the MC-MDM problem stochastic, where performances were reported as ranges instead of single values. In applying deterministic MC-MDM methods to stochastic problems, the discretization of each alternative's feasible performance region is required. Following Madani and Lund (2011) such discretization can be performed using a Monte-Carlo selection through which a single point from each feasible performance region is randomly selected according to a probability distribution of values over these regions. At this point, a MC-MDM procedure is implemented for the selected points, where additional points are included in the analysis by repeating the procedure. This process is similar to repeating a random event, for as the number of trials approaches infinity, the ratio of the number of an event's occurrence to the total number of trials approaches the values of a distribution function. This process ensures that all points within the feasible regions have been included in the analysis with respect to their probability of occurrence.

In practice, the analysis iterates for a large number of repetitions sufficient enough so that the results converge on a constant value, i.e. the winning probabilities are determined and the results converge. Different characteristics of the problem can alter the number of required cycles for converge, such as the number of alternatives and criteria, therefore the number of simulations should be estimated on a case by case basis (10,000 iterations for this analysis). The results of MC-MDM analysis based on each decision making method (Table 6) in each round of selection are recorded and the aggregated results determine the merit and ranking of each alternative. Examples of stochastic MC-MDM through Monte-Carlo selection include Madani and Lund (2011), Madani et al. (2011), Shalikarian et al. (2011), Rastgoftar et al. (2012), and Hadian et al. (2012).

Results yield two probability distributions that provide different information about the decision outcomes. Winning probabilities are useful measures in identifying the most probable optimal solution of the problem, but they do not provide further information about other less probable situations in which the selected solution is not optimal. Therefore, to assess the reliability of an alternative, the method selects the optimal project, eliminates it, and repeats the process with the rest of the options. From this, a ranking of all projects is determined and the overall performance score can be calculated.

Performance scores

Based on the Borda concept, the results are converted into a single score to inform DMs on the relative performance of each project, computed by:

$$Score = 100 - \frac{100 * \frac{\sum_i^9 C_i * i}{N} - 1}{m - 1}$$

Where *N* is the number of Monte-Carlo simulations, *m* is the number of methods applied, and *C* is the count for every *i* ranking. The score communicates two important pieces of information about the performance:

(1) the performance of the project on a 100-point scale, indicating the risk or imperfection involved in selecting this project; a project that scores 100% is expected to perform perfectly in each defined criteria, an impossibility given the competing trade-offs, the uncertainties involved, and the difference in notion of "best alternative" under each decision making method;

(2) the relative quantitative performance of projects to one another; DMs can use the scores to help determine the difference (relative risk) in choosing two projects that are ranked sequentially, and also see how the best project compares to the worst. A higher value indicates a project that meets more of the DMs identified needs.

RESULTS

Baseline results

Results are shown in Figure 2 with the socio-political, environmental, and economic criteria as the three major criteria categories. The small diameter pipeline (A4) receives the highest score, followed by the HVDC (A7), LNG trucking (A5) and Big Lake (A6) projects. The scores indicate three levels, where A4 is the winner, and A5-A7 are relatively tied for second, with A1-A3 and A9 as the third tier of scores.

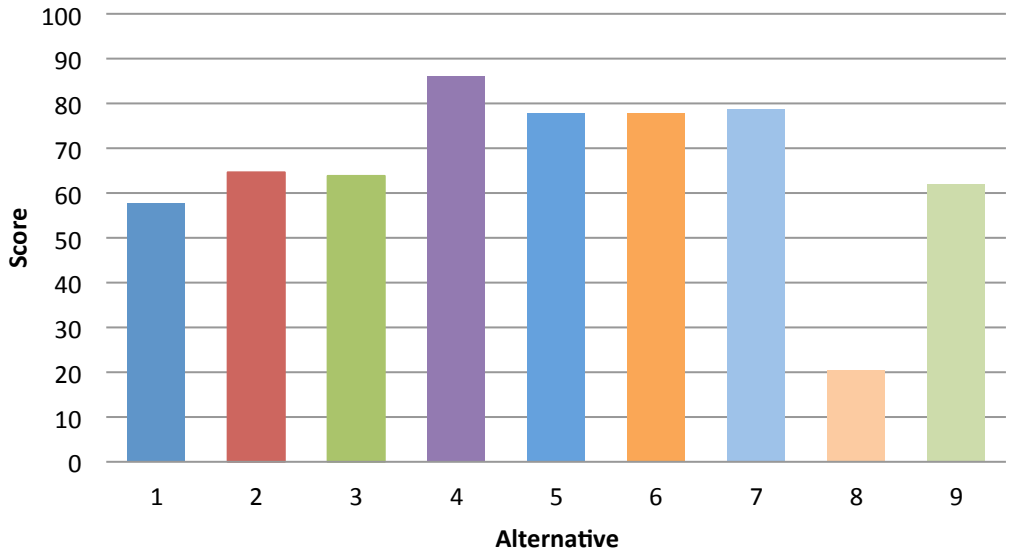

Figure 2. Overall project score results summary (baseline case)

Figure 3 shows the score of each alternative under the three different selection method categories (MCDM, social-choice, and fallback bargaining) used in this study. Results show clearly that the selection method impacts the overall performance score of the projects. Alternatives 1-4 show a relatively homogeneous performance regardless of method, whereas the latter alternatives show more heterogeneity, especially between MCDM and social choice. This indicates that a socially-optimal decision made through social choice methods may not represent an optimal decision selected by MCDM, or a stable (reachable) decision selected through fallback bargaining.

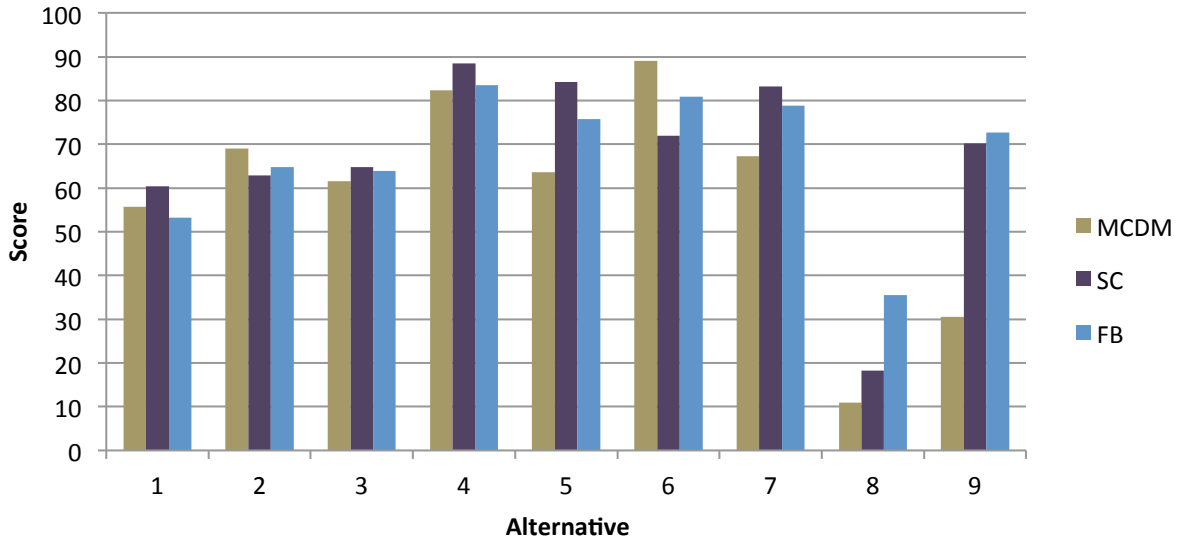

Figure 3. Performance results by analysis method type (MCDM=Multi-Criteria Decision Making, SC=Social Choice making, FB=Fallback Bargaining)

Sensitivity analysis

In order to test the sensitivity of the rankings and identify which criteria are driving the results, the model was run with each major criterion (i.e. environment) eliminated once; the rankings by score are displayed in Figures 4-6. Since all criteria are considered to have equal importance to the decision makers, a sensitivity analysis is insightful for understanding the impact of over-valuing or de-valuing criteria. The environmental and socio-political criteria results are presented in Figure 4, where the economics are left out of the analysis. In this case A2 – LNG export project outperforms the overall winner (A4). Without economics, most projects have higher scores overall, indicating that economics is an important factor in risk of project selection. Figure 5 shows the case without socio-political criteria included, where scores are more heterogeneous overall; and, A4 is again the winner. The LNG export project performs worst (A2) due to the high cost and impact on the environment. The analysis without environmental assessment is presented in Figure 6, where the LNG trucking project (A5) performs best followed by Big Lake (A6) and Bullet Line (A3) tied for third best.

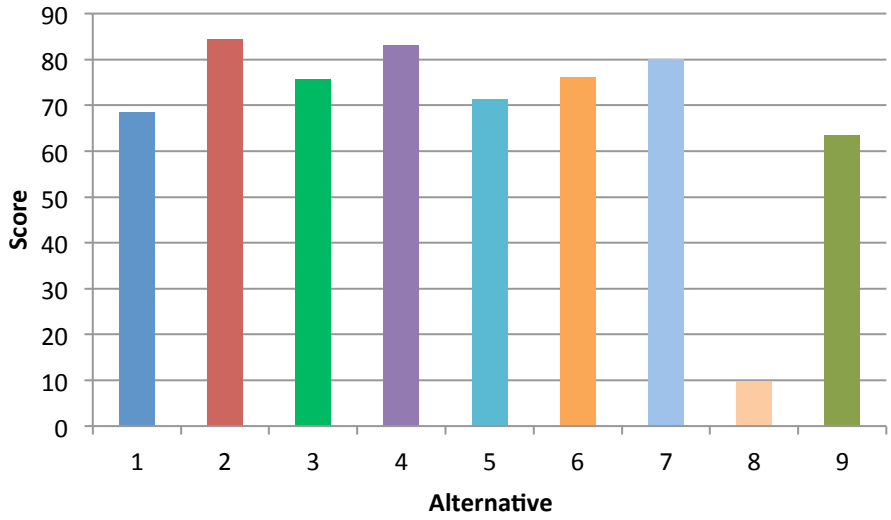

Figure 4. Environmental and Socio-Political criteria scores

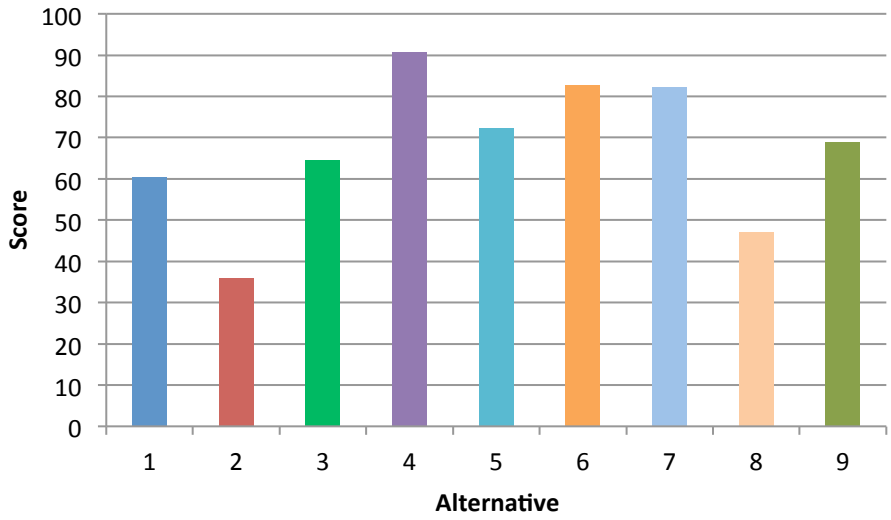

Figure 5. Environmental-Economic criteria scores

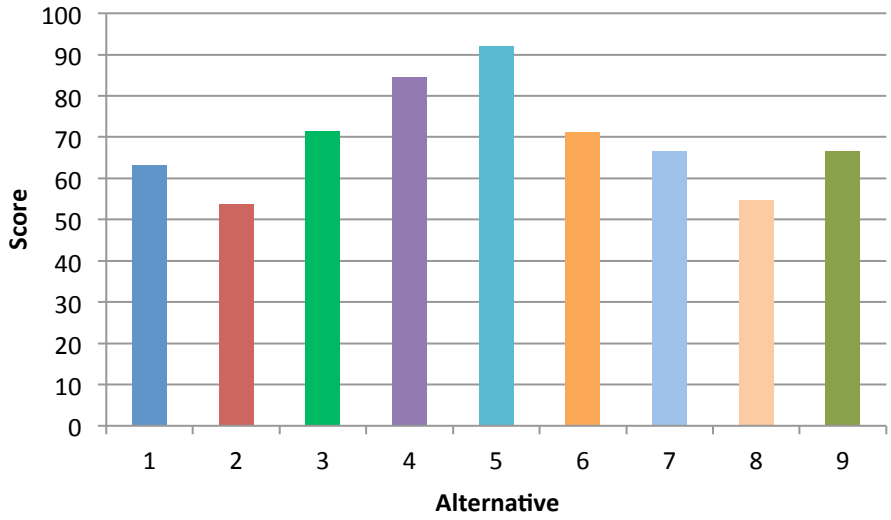

Figure 6. Economic and Socio-Political criteria scores

Political and social separation case

Due to the importance and subjectivity of social and political opinions regarding energy projects in Alaska, a second sensitivity analysis case was developed to explore the changes in project selection if social and political performance measures were given equal weight with economics and the environment. Thus, for this case the evaluation matrix tree is re-defined according to Figure 7 and the analysis follows from sub-criteria up to the main level criteria. Scores for the overall results aggregated across all methods are shown in Figure 8, where the small diameter pipeline (A4) is ranked as the best overall selection, followed by the liquid-natural gas trucking project (A5), and with the coal-to-liquids plant (A8) as the worst choice. A summary table of the scores is provided in Table 4, showing how the scores change when political and social criteria

are considered as equal main categories. From this comparison, the LNG trucking project (A5) receives a higher ranking when social and political are separated due to the increased weight placed on both these categories, and the project's relatively high performance. The HVDC line (A7) drops in ranking when the categories are separated, indicating that it performs better when political and social criteria are given less weight, and environmental and economic are more dominant. Projects that maintain the same score regardless of the political/social separation are more robust in these categories and thus less volatile to changes in the socio-political structure influencing the decision. These projects may be considered more reliable in these categories and include A1, A3, A4, A8, and A9 according to Table 7.

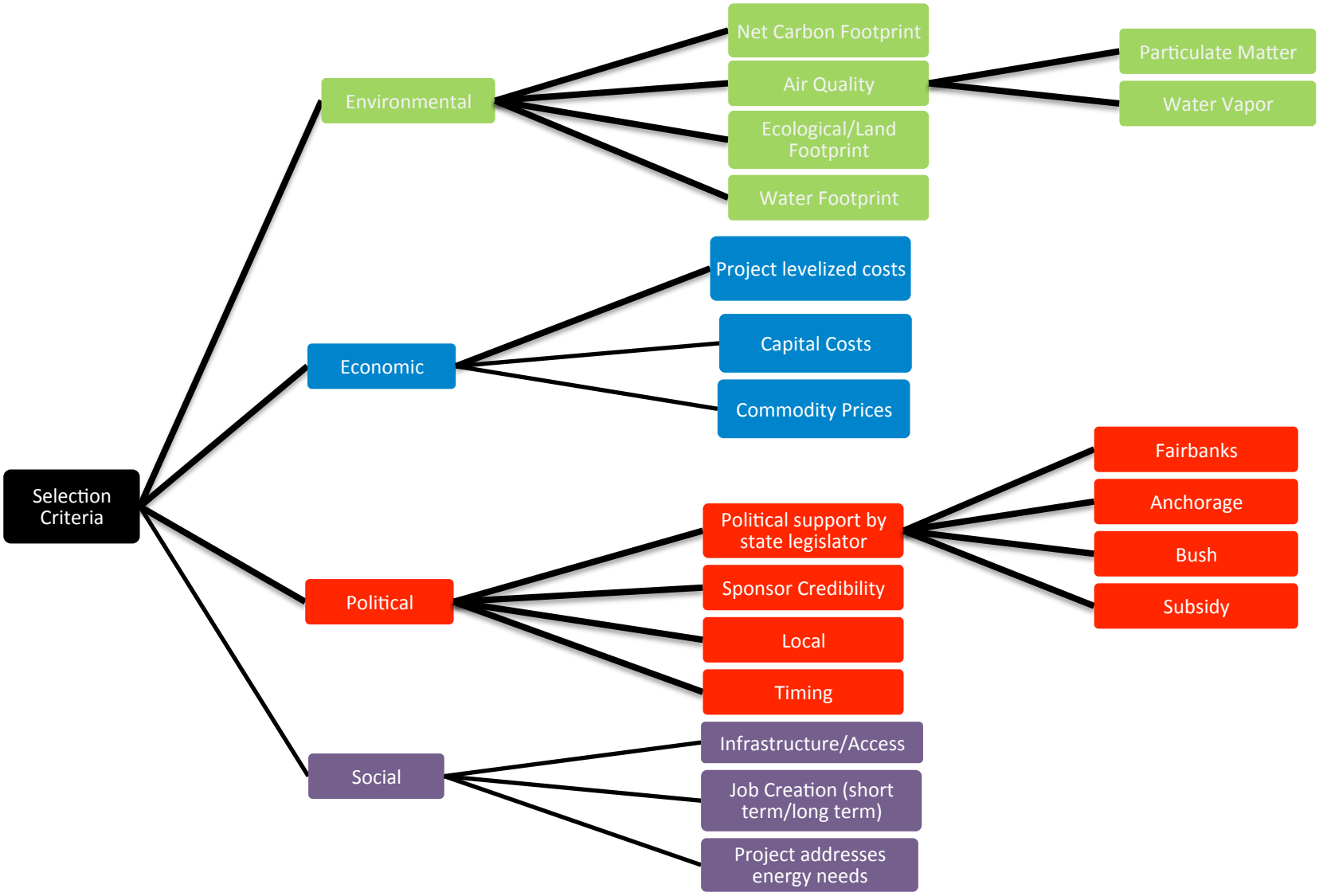
Selection Criteria
Environmental
Net Carbon Footprint
Air Quality
Particulate Matter
Water Vapor
Ecological/Land Footprint
Water Footprint
Economic
Project levelized costs
Capital Costs
Commodity Prices
Political
Political support by state legislator
Fairbanks
Anchorage
Bush
Subsidy
Sponsor Credibility
Local
Timing
Social
Infrastructure/Access
Job Creation (short term/long term)
Project addresses energy needs

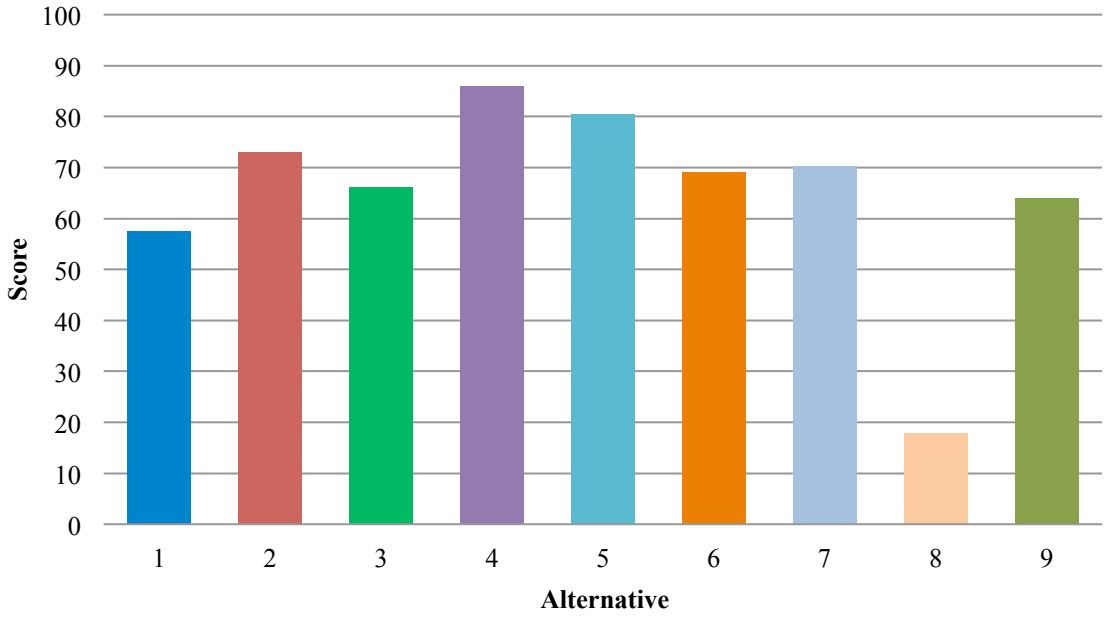

Figure 8. Overall results when political and social criteria are separated into major categories

Table 7. Score comparison of baseline and political-social separation (case 1)

Alternative	Description	Baseline	Case 1
A1	Large diameter pipeline Edmonton → Chicago	58	57
A2	LNG export North Slope to Valdez	65	73
A3	Bullet line to Anchorage, spur to Fairbanks	64	66
A4	Small diameter pipeline: North Slope to Fairbanks	86	86
A5	Liq. Natural Gas trucking project	78	81
A6	Big Lake gas pipeline: Beluga to Fairbanks	78	69
A7	High Voltage DC line from North Slope	79	70
A8	Coal to liquids power plant in Fairbanks	20	18
A9	Susitna Dam	62	64

The ranking results are separated by each set of methods (MCDM, social choice, and fallback bargaining) in Figure 9, showing the differences in performance according to method selection. The best results for MCDM (assuming perfect cooperation) are A6, A2, A4 and A5. For social choice rules (assuming partial cooperation) A4 and A5 perform best; and, for fallback bargaining (low cooperation) A4, A5, and A9 are the optimal projects. Table 4 lists the scores by method, showing how the scores under each method vary. For example for MCDM, A4 has a score of 99 under the Dominance method, but only a 52 under Maximin. This is an example of how methods vary even within the MCDM category, where Maximin is more conservative, and under these conditions A4 may not be as good a selection. By including nine methods, this analysis is able to provide a robust ranking outcome rather than relying on a single method.

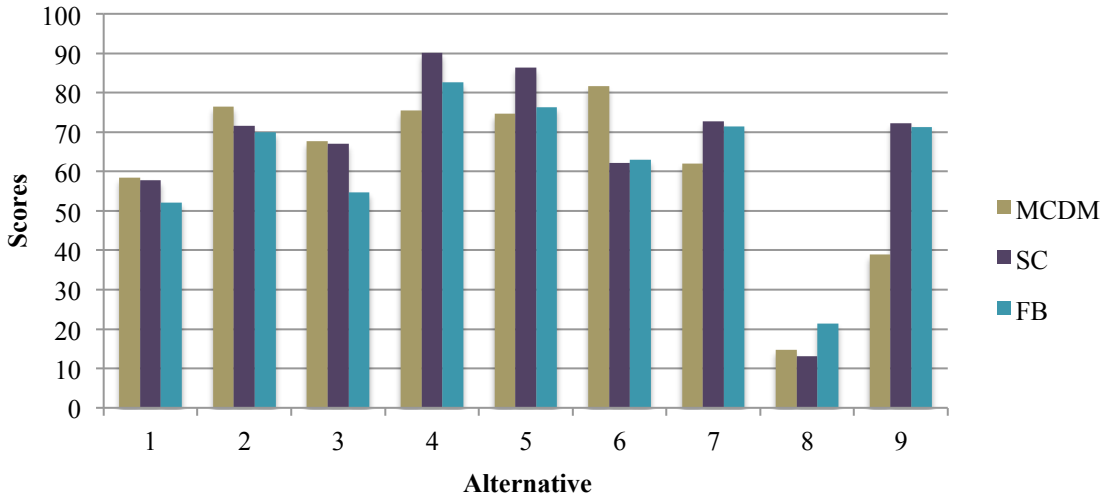

Figure 9. Results by analysis method type (MCDM=Multi-Criteria Decision Making, SC=Social Choice making, FB=Fallback Bargaining) when political and social criteria are separated into major categories

Sensitivity analysis

A sensitivity analysis is also completed for the case where political and social criteria are separated into main criteria categories (Figures 10-13). When economics are eliminated, the liquid natural gas (LNG) export to Valdez (A2) project ranks first. This is due to the relatively high levelized and capital costs of the project being eliminated from considering the decision. The Susitna dam (A9) project also performed better when economics were left out, while the coal fired power plant (A8) had a lower score compared to the aggregated case. When social criteria were eliminated, the LNG trucking project (A5) had the best score, likely due to poor responses in the category of job creation. The large diameter pipeline performed worse than the base case in line with the slightly negative public opinion expressed openly about the project. When politics are eliminated, the small diameter pipeline (A4) reports a score of 95, indicating it would be a very low risk selection and be reliable in meeting the performance criteria. Leaving politics out of the analysis also helps the Big Lake (A6) and HVDC line (A7) projects as both rank low in sponsor credibility and use of local resources. Finally, eliminating the environmental criteria selects the LNG trucking project (A5) as the best project selection since its low rankings in air quality and carbon footprint are not considered.

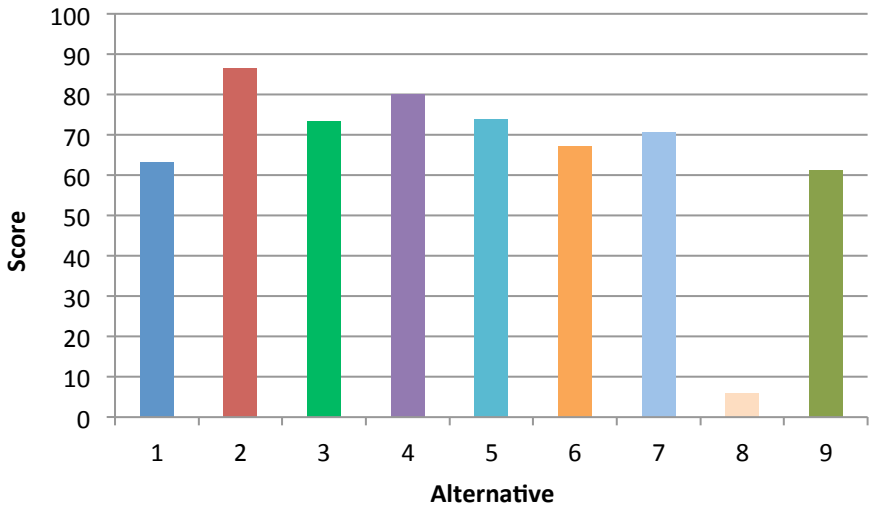

Figure 10. Environmental-Social-Political scores when political and social criteria are separated into major categories

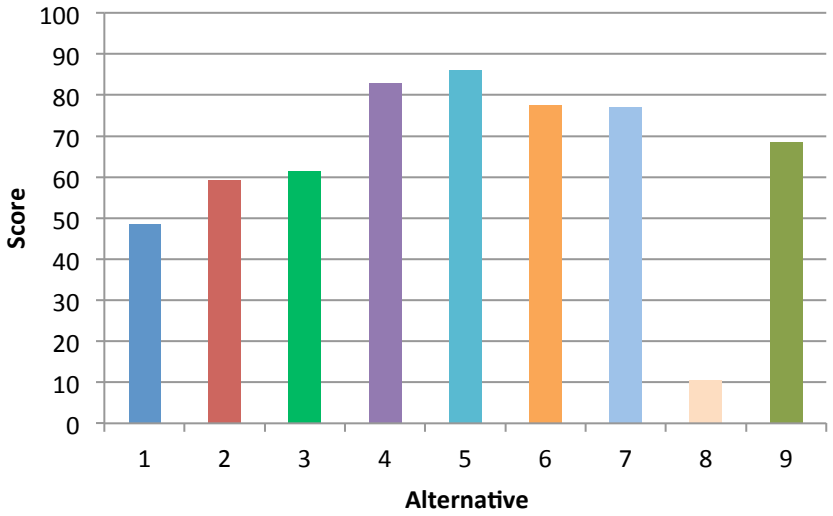

Figure 11. Economic-Environmental-Political scores when political and social criteria are separated into major categories

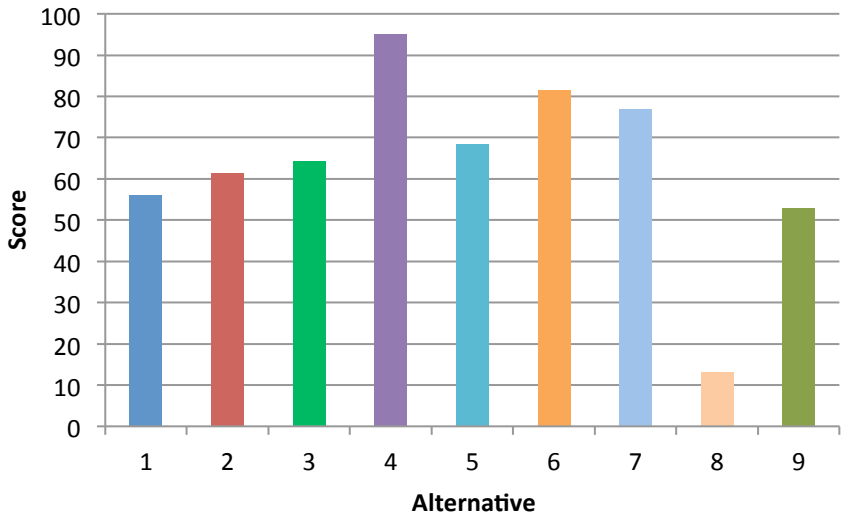

Figure 12. Economic-Environmental-Social scores when political and social criteria are separated into major categories

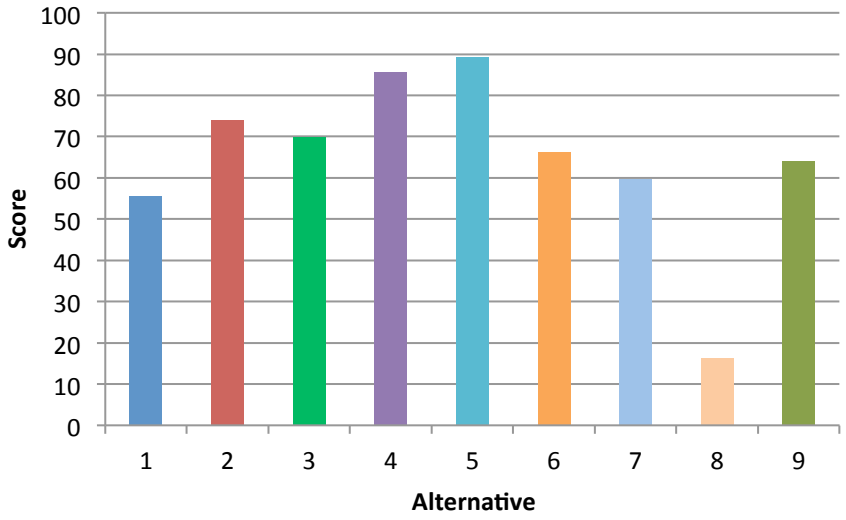

Figure 13. Economic-Political-Social scores when political and social criteria are separated into major categories

CONCLUSIONS

Based on the results of this analysis, the small diameter pipeline (A4) and LNG trucking project (A5) have the best scores overall and according to each method type. The coal-to-liquids power plant and Susitna dam projects have reliably low scores across all methods, suggesting that these two projects are risky for DMs to invest in since they will not perform well under the developed criteria. The case studies provide an example of the sensitivity of classifying a criteria as a main or sub level, where certain projects perform better when more or less emphasis is placed on a given category. Projects whose scores change when the social and political criteria are combined

(A2, A6, A7) are more volatile to changes in these categories. This can help DMs understand the reliability of projects and select which to move forward with given the current social and political situations.

The methods applied in this work communicate uncertainty and risk to the decision makers starting from the input data through to the final decision outcome. In order to maintain the uncertainty given in the input data, a stochastic MC-MDM analysis was needed to be able to combine data at different levels. Since each analysis method under the three categories – MCDM, social choice, and fallback bargaining – approach the problem with different assumptions regarding cooperation, this work includes a range of methods which add robustness to the ranking solutions. Another way this methodology produces a robust solution is the ability to maintain the stochasticity of the inputs throughout the model instead of converting to a deterministic problem. Effectively, this allows for mapping the uncertainty from the input to the output and thus makes the ranking more robust and the risks more understandable to DMs. A sensitivity analysis for each case offers a rationale for which criteria drove the ranking results, and suggests that if decision makers are more concerned with one criterion over another, the optimal project may be different than if all criteria are weighted the same. This is helpful for DMs in understanding how their stated priorities and concerns align with how the model processes information. In cases where the stakeholders are not cooperative but willing to bargain, the game theory methods are more suited to solve the problem; on the other hand, if the DMs are only concerned with the optimal solution, then MCDM methods provide this decision.

This study collected data from project experts to compile the evaluation tree matrix and its contents. Future studies may expand the scope of the data collection process and open the qualitative responses to a wider audience for a larger sample size. To take this study one step further, DMs could engage in this same collaborative process and further indicate which projects have social and political support given the economics and environmental data.

CHAPTER 10. CONCLUSIONS

by Catherine Hanks

This project used a variety of approaches to augment our understanding of how specific geologic, engineering, environmental and economic factors in Interior Alaska may impact decisions regarding implementation of alternative energy sources available to the community. The specific alternative energy source under investigation, a coal-to-liquids plant proposed for Eielson Air Force base outside of Fairbanks, drove the direction of several of the detailed studies, but the overall methodology and results are also applicable to any isolated community where multiple decision makers are trying to reach a consensus on an alternative energy solution.

Results of this study specific to the proposed CTL plant

To address the goals of the project, the study was subdivided into three parts--environmental issues related to the proposed CTL plant and how those could be mitigated or eliminated; the economic viability of the CTL plant as compared to other options; and developing a methodology that incorporates all of this information into the form that decision makers can use to help in determining the best alternative energy sources for Interior Alaska.

Environmental concerns

Two major environmental concerns related to the proposed CTL plant are CO2 emissions and the creation of ice fog due to water emissions during Interior winter conditions. The proposed plant, operating at 40,000 barrels/day, would generate CO2 at ~1200 tons/hr or 10,512,000 tons/year (Dover, 2008).

Results of detailed studies of the southern Nenana basin (Ch. 2) suggest that 4.368 billion metric tons of CO2 could be sequestered in deep coal seams via enhanced coal bed methane production. The amount of CO2 that could be sequestered significantly increases if the northern Nenana basin (which is significantly deeper) is included in the estimate. The CO2 sequestration potential of the Nenana basin is thus significant, and could make a significant contribution to reducing green house gases emissions from a coal-to-liquids plant (CTL) or coal-fired power plant near Fairbanks, Interior Alaska. However there is not sufficient detail available at this time regarding the depth, distribution and thickness of specific target horizons and the presence of sealing rocks to pinpoint where in this fairly large basin one would drill and safely inject and store CO2.

Using CO2 as an Enhanced Oil Recovery (EOR) mechanism in depleted oil fields is an established technology. In this study, we evaluated the potential EOR CO2 sequestration capacity of a single field, the West Sak oil field. Simulations indicate that 48 million tons of CO2 can be sequestered in the West Sak Core area using this method with an added benefit of producing 112 million barrels of additional petroleum (Chapter 3). However, CO2 emitted at a CTL plant based in Eielson would have to be transported ~400 miles

north to North Slope oil fields, adding additional economic expense.

Co-firing a CTL plant with locally grown biomass has the potential to reduce CO2 emissions while regrowth of the biomass could sequester the CO2. However, prior to this study, little data existed on the growth rates of local biomass that could be used as a sustainable fuel source or how much carbon would be permanently stored once local biomass was harvested. This study developed equations that allowed estimation of the amount of harvestable biomass available in a standing short rotation crop of local plant species (Chapter 4). Based on our studies, it is estimated that approximately 2,100 to 2,300 kg/ha of carbon (~1-1.1 ton/acre) were removed from the atmosphere per year during the first seven years of growth of the short rotation crop. This suggests that over 10 million acres would have to be cultivated to compensate for the yearly CO2 emitted by the proposed CTL plant.

Low rank Alaska coal is currently a feedstock for coal-fired power generators in the Interior and would be the feedstock for the proposed CTL plant. Ash content in these coals has a detrimental effect on gasification units, reducing their lifespan and increasing costs. This study (Chapter 6) suggests that ash levels can be brought down to very low levels if necessary by ultra-cleaning the coal prior to gasification. However, ultra-cleaning the coal to total ash levels of 0.5% or below will require significant effort including gravity cleaning, grinding, and leaching with both nitric acid and hydrofloric acid.

This study also simulated the quality of the produced gas and the behavior of trace elements using Alaska coal and two possible gasification technologies - moving bed gasification and entrained flow gasification (Chapter 6). The results indicate a significant difference in both the quality of the product gas stream and how trace elements would leave the gasifier. Moving bed gasification resulted in a product gas stream with a synthesis gas proportion ($CO+H_2$) of 60.5% and significant methane (8.4%), CO_2 (28.8%) and tars. Entrained flow gasification yielded much cleaner product gas, with a synthesis gas proportion ($CO+H_2$) of 91-93%, low CO_2 and negligible tars and methane. Regardless of the type of coal gasified (raw coal or leached coal), mercury products would be in gas phase for both moving bed and entrained flow technologies and would depart the gasifier along with product gases with the potential for causing harm downstream. In contrast, vanadium products would be in solid/liquid phase and thus leave with ash/slag and not be harmful to downstream processes. However, for leached coal gasification, arsenic products will be in gas phase and end up in the product gas stream; for raw coal gasification, arsenic products will probably end up in the ash/slag. Thus the choice of gasifier and the degree of coal cleaning prior to gasification will have a large impact on the amount of CO2 and trace elements emitted.

Another environmental concern that is unique to Interior Alaska is ice fog. Ice fog increases in frequency with decreasing temperature until it is almost always present at air temperatures below -40°C in the vicinity of a source of water vapor. Ice fog can have a serious impact on local populations by keeping daytime temperatures low, decreasing visibility, affecting airport operations and limiting vehicle travel. The proposed CTL

facility will generate significant additional water vapor, leading to the potential of limited visibility during severe weather conditions. A major goal of this project was to develop an ice fog forecasting tool in order to better predict the impact water vapor emissions from the proposed CTL facility (Chapter 7). New, high quality microphysical information on ice fog particles was collected and used to improve model representation of ice fog the Weather Research Forecast (WRF) model, a model used world wide for research and operational weather prediction. Subsequent modeling experiments confirmed that additional water vapor from the proposed CTL plant will lead to additional visibility restrictions due to ice fog during the arctic winter.

Economics

The economic viability of a coal-to-liquids plant (or any energy alternative) is a major consideration. Will the CTL project successfully meet the goal of reducing energy costs for the average Interior Alaska resident? Is it the most economic option available? To what extents should it, or any project, be subsidized by the state?

This study evaluated the economics of a proposed CTL facility along with a range of other proposed projects that included several gas pipelines from gas fields on the North Slope or Cook Inlet, a large hydropower project and a HVDC line from the North Slope. The study first developed a cost analysis of all the projects using the same assumptions for construction costs, etc. This allowed us to compare the effect of the scale of the project, changing commodity prices, 100% private ownership vs 100% state ownership and implementation time on the overall cost of the product that would be produced by each project.

The results of the study indicated that some form of state subsidy would be necessary in order for any project to be economically viable. Because the state then becomes involved in the decision-making process, this opens up a wide range of questions that policy makers will have to address, including what form the subsidy should take, who will be the consumers of the product, and how to ensure that the project will yield a lower cost of energy to the consumer.

Multicriteria multidecision maker analysis

The preceding studies of both environmental and economic issues related to the proposed CTL plant or any alternative energy option highlight both the lack of scientific and technical information regarding resources in the Interior, and the significant economic and technical obstacles that exist to move the situation off of the status quo. These studies also highlight that, in order to be implemented, any project will require a consensus between what is economically best, what is technically feasible, and what is socially and politically desirable. Consequently, there will several entities making this decision, making the decision-making process potentially complex and contentious.

In order incorporate multiple decision makers with varying concerns and definitions of a 'successful' project, we conducted a stochastic multi-attribute assessment of energy

options for Fairbanks, Alaska. This assessment utilized existing multicriteria multidecision maker (MCDM) and game theory concepts to incorporate and communicate relative uncertainty and risk of the projects to the decision makers starting from the input data through to the final decision outcome.

The study collected data from project experts to compile an evaluation tree. Criteria were developed that addressed the environmental, economic, political and social concerns that would need to be addressed by any of the proposed projects. Project experts then ranked the alternative energy projects according to criteria in each of these 4 categories. These rankings were used as input into the analysis. In order to maintain the uncertainty given in the input data, a stochastic method was developed in order to combine data at different levels.

Three types of analysis were used: MCDM, social choice, and fallback bargaining. Each type of analysis approaches the problem with different assumptions regarding cooperation-- where the stakeholders are not cooperative but willing to bargain, the game theory methods are more suited to solve the problem; on the other hand, if decision makers are only concerned with the optimal solution, then MCDM methods help in making this decision. Including a range of methods adds robustness to the final ranking solutions. Maintaining the uncertainty of the inputs throughout the model had the additional benefit of makes the final rankings more robust and the risks more understandable to decision makers. In addition, a sensitivity analysis was conducted to shed light on which criteria drove the ranking results.

Based on the results of this analysis, the small diameter pipeline and LNG trucking project have the best scores overall and according to each type of analysis. The coal-to-liquids power plant and Susitna dam projects have reliably low scores across all methods, suggesting that these two projects are risky for decision makers to invest in since they will not perform well under the criteria. Scores of some of the other projects, specifically the LNG export line to Valdez, the Beluga to Fairbanks gas pipeline, and the high voltage DC line from the North Slope, change when the social and political criteria are combined, suggesting that they are more volatile to changes in criteria in these categories. This can help decision makers understand the reliability of these projects and select which to move forward with given the current social and political situations.

This analysis was conducted using input from project experts; future studies should expand the scope of the data collection process and open the qualitative responses to a wider audience for a larger sample size. However, it is interesting to note that while this analysis was being conducted at UAF, all of these projects were being considered in the public arena. Independent of this study, decision makers appear to be coalescing behind the LNG trucking option as an immediate alternative energy solution.

Broader implications of this work

This study, while focused on one particular community, highlights the complex issues surrounding development of alternative energy resources. Energy resources vary in ease and practicality of implementation, based on the maturity of the technology, the actual knowledge of the available resource, the economics of individual projects, and the environmental, social and political impacts of individual projects. This lack of knowledge and multiplicity of criteria for picking a project may preclude short term implementation of what otherwise may be an attractive energy alternative.

It is important to note that economics alone may not always determine which project is most likely to succeed in garnering support from all parties involved with or impacted by the decision. Environmental concerns, technology maturity, and social and political factors all play a role in what project/s are ultimately deemed feasible.

While stochastic multi-criteria, multi-decision maker analysis cannot identify the 'right' project or projects, it can provide insights into the likelihood of the ‘success’ of a particular project in meeting the criteria of the various stakeholders and thus the likelihood that a consensus can be reached regarding the project. The approach developed in this study utilizes a broad range in analytical methods, which adds robustness to the analysis by assuming different degrees of cooperation between the decision makers. The rankings produced by the overall MCDM analysis thus provide an indication of the level of risk associated with individual projects and what conditions may need to change in order for a previously nonviable project to become attractive.

REFERENCES

Ajit, Das, D. K., Chaturverdi, O. P., Jabeen, N. and Dhyani, S. K. 2011. Predictive models for dry weight estimation of above and below ground biomass components of Populus deltoides in India: Development and comparative diagnosis. *Biomass & Bioenergy*, 35, 1145-1152.

Akenergyauthority.org, 2012. Alaska Wood Energy Development Task Group: http://www.akenergyauthority.org/biomasswoodenergygrants.html

Al-Meshari, A.A. and McCain, W.D., 2005. New Strategic Method to Tune Equation-of-State for Compositional Simulation. SPE Technical Symposium of Saudi Arabia Section, Dhahran, Saudi Arabia, 14-16 May 2005.

Alaska Department of Commerce Community and Economic Development, 2012. Current Community Conditions Alaska Fuel Price Report, Division of Community and Regional Affairs. URL: http://www.bbna.com/ak%20state/FuelWatch_2012_January.pdf.

Alaska Energy Authority (AEA), 2009. Susitna Hydroelectric Project, Project Evaluation, Interim Memorandum, FINAL. Prepared for the Alaska Energy Authority, by HDR Alaska, Inc. Available at: http://www.akenergyauthority.org/SusitnaFiles/031609EvaluationWOappen.pdf

Alaska Energy Authority (AEA), 2010. Railbelt Large Hydro Evaluation; Preliminary Decision Document. November 23, 2010. Available at: www.akenergyauthority.org

Alaska Energy Authority (AEA). 2010. Alaska Energy plan: A Guide for Alaskan Communities to Utilize Local Energy Resources. URL: http://www.akenergyauthority.org/alaska-energy-plan.html.

Alaska Energy Authority (AEA), 2012. Presentation to AEA Board of Directors, August 14, 2012.

Alaska Energy Wiki, 2012. Energy Flow: http://energy-alaska.wikidot.com/energy-flow

Alaska Gasline Development Corporation, 2011a. Alaska Stand Alone Gas Pipeline/ASAP Project Plan. July 1, 2011. Alaska Gasline Development Corporation. Currently available at: http://www.agdc.us/wp-content/uploads/2011/07/ASAP-Project-Plan_1July2011_WEB1.pdf

Alaska Gasline Development Corporation, 2011b. Greenfield Liquified Natural Gas (LNG) Economic Feasibility Study. Report prepared for the Alaska Stand Alone Gas Pipeline/ASAP. June 8, 2011. Currently available at: http://www.agdc.us/gas-studies/

Alaska Natural Gas Development Authority, 2009. Beluga to Fairbanks, Natural Gas Pipeline System Project Description. Available at:

http://www.angda.state.ak.us/B2F/20091221_Proj_Desc.pdf

Alaska State Legislature, 2012. Minutes of the Senate Resources Committee, 3/26/2012, concerning SB 215. Available at: http://w3.legis.state.ak.us

Arenas, A., G. 2004. Development of gas production curves for coalbed methane reservoirs. MS Thesis, West Virginia University, Morgantown, West Virginia.

Arevalo, C. B. M., Volk, T. A., Bevilacqua, E. & Abrahamson, L. 2007. Development and validation of aboveground biomass estimations for four Salix clones in central New York. *Biomass & Bioenergy*, 31, 1-12.

Aspen Tech, 2010. ASPEN Plus Model for Moving Bed Gasifier. http://www.aspentech.com/

Athey, J.E, Newberry, R.J., Werdon, M.B., Freeman, L.K., Smith, R.L., and Szumigala, D.J. 2006. Bedrock geologic map of the Liberty Bell area, Fairbanks A-4 Quadrangle. Bonnifield Mining District, Alaska. Alaska Division of Geological & Geophysical Surveys Preliminary Interpretive Report 2006-2, 1 sheet, scale 1:50,000.

Bachu, S., 2000. Sequestration of CO2 in Geological Media: Criteria and Approach for Site Selection in Response to Climate Change. Energy Conversion and Management, 41(9): 953-970.

Ballard, B. D., Stehman, S. V., Briggs, R. D., Volk, T. A., Abrahamson, L. P. and White, E. H. 2000. Aboveground biomass equation development for five Salix clones and one Poplulus clone. New York Center for Forestry Research and Development (NYCFRD-99-01). Syracruse, NY: SUNY-ESF.

Bakshi, A.K., 1991. Computer Modeling of CO2 Stimulation in the West Sak Reservoir, University of Alaska Fairbanks, MS Thesis.

Barnes, D.F., 1972. Notes on processing and presentation of U. S. Geological Survey Alaskan gravity data: U. S. Geological Survey Open-File Report 72-16: 25.

Beeson, D.M. and Ortloff, G.D., 1959. Laboratory Investigation of the Water-Driven Carbon Dioxide Process for Oil Recovery. Journal of Petroleum Technology, 11(4): 63-66.

Bemis, S., and Wallace, W.K. 2007. Neotectonic framework of the north-central Alaska Range. In: Ridgway, K.D., Trop, J.M., Glen, J.M.G., and O'Neill, J.M. (Eds.), Growth of a Collisional Continental Margin: Crustal Evolution of Southern Alaska. GSA Special Paper 431, pp.549–572.

Benson, C. S. 1970. ICE FOG, *Weather*, *25*(1), 11-18.

Benson, S.M., 2006. Benson Lab. Department of Energy Resources Engineering, Stanford University, URL: http://pangea.stanford.edu/research/bensonlab/relperm/index.html.

Biagini, E., Bardi, A., Pannocchia, G. and Tognotti, L. 2009. Development of an Entrained Flow Gasifier Model for Process Optimization Study. Industrial & Engineering Chemistry Research. 48(19): p. 9028-9033.

Bibber, L.V., Thomas, C. and Chaney, R. 2007. Alaskan Coal Gasification Feasibility Studies-Healy Coal-To-Liquids Plant. Final Report for Task 41817.333.01.01, Submitted to US DOE Arctic Energy Office, DOE/NETL 2007/1251.

Brams, S.J., & Kilgour, D.M., 2001. Fall Back Bargaining. *Group Decision and Negotiation,* 287-316.

Breon, F-M, and Dubrulle B. 2004. Horizontally oriented plates in clouds, *J. Atmos. Sci*., 61: 2888-2898.

Brock, W.R. and Bryan, L.A., 1989. Summary Results of CO2 EOR Field Tests, 1972-1987. Low Permeability Reservoirs Symposium, Denver, Colorado, 6-8 March 1989.

Broiles, Randy, Trond-Erik Johansen, John Minge, and Tony Palmer. Letter to Governor Sean Parnell, October 1, 2012. Currently available online at: http://gasline.alaska.gov/gasline-documents/ProducerLtr10032012.pdf

Brogan, G.E., Cluff, L.S., Korringa, M.K., and Slemmons, D.B., 1975, Active faults of Alaska: Tectonophysics, v. 29, pp. 73–85.

Caudle, B.H. and Dyes, A.B., 1958. Improving Miscible Displacement by Gas-Water Injection. 32nd Annual Fall Meeting of Society of Petroleum Engineers Dallas, Texas, Oct. 6-9, 1957.

Chaney, R. and Bibber, L.V. 2006. Beluga Coal Gasification Feasibility Study. Final Phase I Report to US DOE, Task 41817.333.01.01, July.

Chang, Y.-B., Coats, B.K. and Nolen, J.S., 1998. A Compositional Model for CO2 Floods Including CO2 Solubility in Water. SPE Reservoir Evaluation & Engineering, 1(2): 155-160.

Chang, Y.B., 1990. Development and Application of an Equation of State Compositional Simulator, University of Texas at Austin, PhD Dissertation.

Cole, R. B., Nelson, S.W., Layer, P.W., and Oswald, P. J.2006. Eocene volcanism above a depleted slab window in southern Alaska. GSA Bulletin; Vol. 118, pp 140-158.

Couch, G.R. 1990. Lignite upgrading, IEA Coal Research, IEACR/23, May, 72 pp.

Curry, J. A., Meyer F. G., Radke L. F., Brock C. A., and Ebert E. E. 1990. Occurrence and characteristics of lower tropospheric ice crystals in the arctic, *Inter. J. Climatology*, *10*(7): 749-764.

Diaz-Somoano, M. and Martinez-Tarazona, M.R. 2003. Trace Element Evaporation During Coal Gasification Based On A Thermodynamic Equilibrium Calculation Approach. Fuel, 82 (2003) 137–145.

DOE National Energy Technology Laboratory, 2007. Conceptual Engineering/Socioeconomic Impact Study - Alaska Spur Pipeline. http://www.jpo.doi.gov/SPCO/DOESpurlineDocuments/SpurLineFinalReport.pdf

Donelick, A.A., O'Sullivan.P.B., and Ketcham, R.A., 2005. Apatite-fission track analysis. Reviews in Mineralogy and Geochemistry, Vol. 58, pp.49-94

Dover, B. 2008. Fairbanks Economic Development Corporation Coal-to-Liquids FEL1 Study. Final Report to Fairbanks Economic Development Corporation, October.

Dow Jones, 2012. Total Agrees to 20-Year Deal to Buy LNG From Cheniere's Export Project. Dow Jones Business News, December,17 2012.

Doyon, 2012. Nenana oil and gas: AAPG Pacific Section Meeting, Anchorage Alaska

eia Beta, 2012, U.S. States: State Profiles and Energy Estimates: http://www.eia.gov/beta/state/#/series/12

Enick, R.M. and Klara, S.M., 1992. Effects of CO2 Solubility in Brine on the Compositional Simulation Of CO2 Floods. SPE Reservoir Engineering, 7(2): 253-258.

Fairbanks Pipeline Company, 2010a. 1/6/11 Presentation to Governor's Office. Available online at: http://www.fairbankspipelinecompany.com/pdf/1-6-11_Presentation_to_the_Governor's_Office.pdf

Fairbanks Pipeline Company, 2010b. FPC Revenues, Expenses and Organization - Presentation for the Alaskan Banking and Accounting Community, 1/11/11. Available online at: http://www.fairbankspipelinecompany.com/pdf/1-11-11_Presentation_to_Bankers-3.pdf

Fairbanks Pipeline Company, 2011. Pipeline Hydraulic Simulations. Available at: http://www.fairbankspipelinecompany.com/technical.html

Fang, S., Xu, X., Lu, S. and Tang, L. 1999. Growth dynamics and biomass production in short-rotation poplar plantations: 6-year results for three clones at four spacings. *Biomass and Bioenergy*, 17, 415-425.

Felix, E., Tilley, D. R., Felton, G. and Flamino, E. 2008. Biomass production of hybrid poplar (Populus sp.) grown on deep-trenched municipal biosolids. *Ecological Engineering*, 33, 8-14.

Figueira, J., Greco, S., & Ehrgott, M. (2005). Multiple criteria decision analysis: state of the art surveys. New York: Springer.

Finn, T. M., and Pawlewicz, M.J., 2002. Vitrinite reflectance data for the Greater Green River Basin, southwestern Wyoming, northwestern Colorado and northeastern Utah. U.S. Geological Survey Open File Report, 02-339.

Flores, R.M, Stricker G.D., and Kinney, S.A. 2004. Alaska coal geology, resources and coal bed methane potential. U.S. Geological Survey, Digital Data Series 77.

Frost, G.M., Barnes, D.F., and Stanley, R.G., 2002. Geologic and isostatic map of the Nenana Basin area, central Alaska. U.S. Geological Survey Report I-2543; pp. 16 , 1 sheet.

Ganguli, R. and Wash, D.E. 2010. Investigation of Pre-Combustion Processing of Coal to Improve Coal Quality," Final Report to United States Air Force through Jacobs Engineering, Alaska Center for Energy and Power, University of Alaska Fairbanks, 30 pp.

Garber-Slaght, R., Sparrow S.D., Masiak D.T. and Holdmann, G. 2009. Opportunities for Woody Biomass Fuel Crops in Interior Alaska, University of Alaska Fairbanks, School of Natural Resources and Agricultural Sciences. URL: https://www.uaf.edu/files/snras/MP_08_09.pdf.

Garn.com, 2012, How a GARN Works: http://garn.com/how-garn-works-full/

Gas Strategies, 2008. Potential LNG Production from North Slope Gas. Report for the State of Alaska by Gas Strategies: Rob Shepherd, Rob Fenton, Salmon Wasti, Peter Thompson, Prajakta Munshi. Appendix of the Findings and Determination by the Commissioners of Natural Resources and Revenue for Issuance of a License under the Alaska Gasline Inducement Act. Currently available at: http://gasline.alaska.gov/Findings/findings.html

Gibson, K.K., Dykstra, J.R., Williamson, J., Issaev, Y.V., Hobbs, G.S., Kremer, M.C., Heumann, M.P., Gregersen, L.J., Krouskop, D.L., Wilson, S., Sachivichik, N., 2011. Cook Inlet Natural Gas Production Cost Study: Alaska Division of Oil and Gas report, 24 p., currently available online at: http://www.dog.dnr.alaska.gov/

Glen, J.M.G., 2004, A kinematic model for the southern Alaska orocline based on regional fault patterns, Geological Society of America, Special Publication 383, Ch. 11, 1pp.61-172.

Golden Valley Electric Association (GVEA), 2012. GVEA White Paper: State Assistance for Trucking Liquefied Natural Gas (LNG) From the North Slope. 5 pps.

Goodrich, J.H., 1980. Review and Analysis of Past and Ongoing Carbon Dioxide Injection Field Tests. SPE/DOE Enhanced Oil Recovery Symposium, Tulsa, Oklahoma, 20-23 April 1980.

Govind, R. and Shah, J. 1984. Modeling and simulation of an entrained flow coal gasifier. AIChE Journal. 30(1): p. 79-92.

Guillemette, T. & Desrochers, A. 2008. Early growth and nutrition of hybrid poplars fertilized at planting in the boreal forest of western Quebec. *Forest Ecology and Management*, 255, 2981-2989.

Guler, B., Wang, P., Delshad, M., Pope, G.A. and Sepehrnoori, K., 2001. Three- and Four-Phase Flow Compositional Simulations of CO2/NGL EOR. SPE Annual Technical Conference and Exhibition, New Orleans, Louisiana, 30 September-3 October 2001.

Hadian, S., Madani, K., Rowney, C., Mokhtari, S., 2012. "Toward more efficient global warming policy solutions: the necessity for multi-criteria selection of energy sources." World Environmental and Water Resources Congress, pp. 2884-2892, ASCE, Albuquerque, New Mexico, Edited by Loucks, E.D.

Hand, K., Carvitti, J., Rectanus, M., Boczek, B., and Diltz, B.,2011. Study of the feasibility of coal-to-liquids plant in Interior Alaska. NDIA, E2S2 conference, New Orleans, LA.

Hanks, C., and Holdmann, G. (Eds.). 2012. CO2 sequestration options and other environmental issues related to the proposed coal-to-liquids facility at Eielson Air Force Base: Phase 2. Prepared for the U.S. Air Force by the Geophysical Institute and the Alaska Center for Energy and Power, University of Alaska Fairbanks, pp. 207

Hajkowicz, S., & Collins, K., 2007. A review of multiple criteria analysis for water resource planning and management. *Water Resources Management*, 1553-66.

Hatch, 2008. Fairbanks Biomass/Coal to Liquids Energy Prefeasibility Study; FEL I. Prepared for the Fairbanks Economic Development Corporation. Final Report.

HDR., 2009. Sustina Hydroelectric Project Evaluation. Anchorage: Alaska Energy Authority. http://www.akenergyauthority.org/SusitnaFiles/031609EvaluationWOappen.pdf

Henry, R.L. and Metcalfe, R.S., 1983. Multiple-Phase Generation During Carbon Dioxide Flooding. Society of Petroleum Engineers Journal, 23(4): 595-601.

Heymsfield, A. J., and Westbrook C. D. 2010. Advances in the Estimation of Ice Particle Fall Speeds Using Laboratory and Field Measurements. *J. Atmos. Sci*., 67: 2469-2482.

Heymsfield, A. J., Schmitt C., and Bansemer A. 2012. Ice cloud particle size distributions and pressure dependent terminal velocities from in situ observations at temperatures from 0 to -86C, *J. Atmos. Sci*., in press.

Higman, C. and van der Burgt, M. 2003. Gasification. Elsevier Publication, 391 pp.

Holm, L.W., 1976. Status of CO2 and Hydrocarbon Miscible Oil Recovery Methods. Journal of Petroleum Technology, 28(1): 76-84.

Hwang, C.L., Yoon, K., 1981. Multiple Attribute Decision Making: Methods and Applications: A State-of-the-Art Survey, Springer-Verglag.

Information Insights, Inc., 2009. Alaska Housing Assessment. Report prepared for Cold Climate Housing Research Center and Alaska Housing Finance Corporation. Technical Report Number TR 2009-02. Available online at: http://www.cchrc.org/docs/reports/TR_2009_02_2009_AK_Housing_Assessment_Final.pdf

Inventory of U.S. Greenhouse Gas Emissions and Sinks: 1990 – 2010, 2012. U.S. Environmental Protection Agency.

Iwata, Mari, 2012. Chevron: Most LNG Prices to Remain Linked to Oil. *The Wall Street Journal*. December 5, 2012.

Johnsson, M.J., Howell, D.G., and Bird, K.J., 1993, Thermal maturity patterns in Alaska: Implications to tectonic evolution and hydrocarbon potential: American Association of Petroleum Geologists Bulletin, v. 77, p. 1874–1903.

Johansson, T. & Karacic, A. 2011. Increment and biomass in hybrid poplar and some practical implications. *Biomass & Bioenergy*, 35, 1925-1934.

Joutz, Federick and Robert P. Trost, 2007. An Economic Analysis of Consumer Response to Natural Gas Prices. Published by the American Gas Association, 400 North Capitol Street, NW, Suite 450 Washington, DC 20001. www.aga.org

Kajikawa, M. 1973. Laboratory measurements of falling velocity of individual ice crystals. *J. Meteorol. Soc. Japan,* 51: 263-271.

Karacic, A., Verwijst, T. and Weih, M. 2003. Above-ground woody biomass production of short-rotation Populus plantations on agricultural land in Sweden. *Scandinavian Journal of Forest Research*, 18, 427-437.

Khan, S.A., Pope, G.A. and Sepehrnoori, K., 1992. Fluid Characterization of Three-Phase CO2/Oil Mixtures. SPE/DOE Enhanced Oil Recovery Symposium, Tulsa, Oklahoma, 22-24 April 1992.

Khataniar, S., Kamath, V.A., Patil, S.L., Chandra, S. and Inaganti, M.S., 1999. CO2 and Miscible Gas Injection for Enhanced Recovery of Schrader Bluff Heavy Oil. International Thermal Operations/Heavy Oil Symposium, Bakersfield, California, 17-19 March 1999.

Kooten, G., Richter, M., and Zippi, P., 2012. Alaska's interior rift basins: A new frontier for discovery: Oil and Gas Journal, Vol. 110, Issue-1.

Koschmieder H. 1924. Theorie der horizantalen sichtweite, *Beitr. Phys. Atmos.* 12, 33-55: 171-181.

Kotelnikova S. 2002. Microbial production and oxidation of methane in deep subsurface. Earth-Science Reviews, Vol.58, pp. 367-395.

Kulkarni, M., and Ganguli, R. 2012. Moving Bed Gasification of Low Rank Alaska Coal. Journal of Combustion. Volume 2012 (2012), Article ID 918754, 8 pages. doi:10.1155/2012/918754

Kumai, M. 1966. Electron Microscopic Study of Ice-Fog and Ice-Crystal Nuclei in Alaska, *Journal of the Meteorological Society of Japan. Ser. II*, *44*(3): 185-194.

Lang, R.J., and Neavel, R.C. 1982. Behavior of calcium as a steam gasification catalyst. Fuel, 61, 620–626.

Laureysens, I., Pellis, A., Willelms, J. and Ceulemans, R. 2005. Growth and production of a short rotation coppice culture of poplar. III. Second rotation results. *Biomass & Bioenergy*, 29, 10-21.

Lee, H., Choi, S. and Paek, M. 2011. A simple process modelling for a dry-feeding entrained bed gasifier. Proceedings of the Institution of Mechanical Engineers, Part A: Journal of Power and Energy, 2011. 225(1): p. 74-84.

Lesh, M.E., and Ridgway, K.D. 2007, Geomorphic evidence of active transpressional deformation in the Tanana foreland basin, south-central Alaska. Geological Society of America Special Paper 431, pp. 573–592

Lim, M.T., Khan, S.A., Sepehrnoori, K. and Pope, G.A., 1992. Simulation of Carbon Dioxide Flooding Using Horizontal Wells. SPE Annual Technical Conference and Exhibition, Washington, D.C., 4-7 October 1992.

Lohrenz, J., Bray, B.G. and Clark, C.R., 1964. Calculating Viscosities of Reservoir Fluids From Their Compositions. Journal of Petroleum Technology, 16(10): 1171-1176.

Madani K., 2010, "Game Theory and Water Resources", Journal of Hydrology, Vol. 381 (3-4): 225- 238,

Madani, K., Shalikarian, S., Naeeni, T.O., 2011. Resolving hydro-environmental conflicts under uncertainty using Fallback bargaining procedures. *Proceedings of the International Conference on Environment Science and Engineering.*

Madani K., Hipel K. W., 2011, "Non-Cooperative Stability Definitions for Strategic Analysis of Generic Water Resources Conflicts", Water Resources Management, Vol. 25: 1949–1977.

Madani K.**,** Lund J. R., 2012, "California's Sacramento-San Joaquin Delta Conflict: from Cooperation to Chicken", ASCE Journal of Water Resources Planning and Management, Vol. 138 (2): 90-99.

Madani K., Lund J.R. 2011. A Monte-Carlo game theoretic approach for Multi-Criteria Decision Making under uncertainty, *Advances in Water Resources,* 607-616.

Matmon, A., Schwartz, D.P., Haeussler, P.J., Finkel, R., Lienkaemper, J.J., Stenner, H.D. and Dawson, T.E., 2006. Denali fault slip rates and Holocene–late Pleistocene kinematicsof central Alaska. Geology 34, pp. 645–648.

McFarquhar, G. M., and Heymsfield A. J. 1997. Parameterization of tropical cirrus ice crystal size distributions and implications for radiative transfer: results from CEPEX. *J. Atmos. Sci*., 54: 2187-2200.

McGuire, P.L. and Moritz Jr., A.L., 1992. Compositional Simulation and Performance Analysis of the Prudhoe Bay Miscible Gas Project. SPE Reservoir Engineering, 7(3): 329-334.

McGuire, P.L., Redman, R.S., Jhaveri, B.S., Yancey, K.E. and Ning, S.X., 2005. Viscosity Reduction WAG: An Effective EOR Process for North Slope Viscous Oils. SPE Western Regional Meeting, Irvine, California, Mar 30 - Apr 01, 2005

Merritt, R.D. 1985. Coal Atlas of the Nenana Basin, Alaska. Alaska Division of Geological & Geophysical Surveys Public-data File 85-41, 197 pp., scale 1: 250,000, 5 sheets.

Merritt, R.D. 1986a. Alaska Coal Fields and Seams. Alaska Division of Geological & Geophysical Surveys, Public-data File 086-67, 41pp.

Merritt, R.D. 1986b. Coal Geology and Resources of the Nenana Basin, Alaska. Alaska Division of Geological & Geophysical Surveys, Public-data File 086-74, 71 pp.

Merritt, R.D., and Hawley, C.C., compilers, 1986, Map of Alaska's coal resources: Fairbanks, Alaska Division of Geological and Geophysical Surveys, scale 1:2,500,000.

Mery. J., 2009. Nenana basin: Interior Alaska, natural gas exploration. Alaska Miners Association Fairbanks Chapter.

Meyer, J.F.Jr, 2008. Bouguer Gravity Anomaly Map of the Nenana Basin, Alaska, Div. of Natural Resources Oil and Gas Consevation Commission, Sheet 3 of 4.

Meyer, J.F.Jr, 2008. Total Intensity Magnetic Anomaly Map of the Nenana Basin, Alaska, Div. of Natural Resources Oil and Gas Consevation Commission, Sheet 4 of 4.

Meyers, M. P., DeMott P. J., and Cotton W. R. 1992. New Primary Ice-Nucleation Parameterizations in an Explicit Cloud Model, *J. Appl. Meteor.*, *31*(7): 708-721.

Minesinger, Kenneth and Richard C. Green; 2008. Lack of Open Access for LNG Export Terminals. Appendix R3 of the Findings and Determination by the Commissioners of Natural Resources and Revenue for Issuance of a License under the Alaska Gasline

Inducement Act. Currently found at: http://gasline.alaska.gov/Findings/findings.html

Mokhtari, S., Madani, K., Chang, N.B., 2012. Multi-Criteria Decision Making under Uncertainty: Application to the California's Sacramento-San Joaquin Delta Problem. In: D.E. Loucks, ed. World Environmental and Water Resources Congress, 20-24 May 2012 Albuquerque, New Mexico. Reston, VA: ASCE, 2339-2348.

Ning, S.X., Jhaveri, B.S., Jia, N., Chambers, B. and Gao, J., 2011. Viscosity Reduction EOR with CO2 & Enriched CO2 to Improve Recovery of Alaska North Slope Viscous Oils. SPE Western North American Region Meeting, Anchorage, Alaska, USA, 7-11 May 2011.

Northern Economics, Inc., 2012. Fairbanks North Star Borough Gas Distribution System Analysis. Prepared for the Fairbanks North Star Borough. June 29, 2012. FNSB Project number: 11- PWDPRJ-02.

Northwest Geophysical Associates, Inc. 2004. GM-SYS Users guide, Ver. 4.9:01

Nourpour Aghbash, V. and Ahmadi, M., 2012. Evaluation of CO2-EOR and Sequestration in Alaska West Sak Reservoir Using Four-Phase Simulation Model. SPE Western Regional Meeting, Bakersfield, California, USA, 21-23 March 2012.

Nussbaumer, T., 2003. Combustion and Co-combustion of Biomass: Fundamentals, Technologies, and Primary Measures for Emission Reduction. *Energy & Fuels*, 1510-1521.

Ohtake, T., and Huffman P. J. 1969. Visual range in ice fog. *J. Appl. Meterol.*, 8: 499-501.

Ohtake, T. 1970. Studies on Ice Fog, *Geophysical Institute, University of Alaska Fairbanks Rep. UAG R-211*, 177 pp.

Orr Jr., F.M., Yu, A.D. and Lien, C.L., 1981. Phase Behavior of CO2 and Crude Oil in Low-Temperature Reservoirs. Society of Petroleum Engineers Journal, 21(4): 480-492.

Ozdemir, E. 2009. Modeling of coal bed methane (CBM) production and CO_2 sequestration in coal seams. International Journal of Coal Geology, Vol. 77, pp. 145-152 .

Packer, D., Brogan G., and Stone D. 1975. New data on plate tectonics of Alaska. Tectonophysics. Vol.29, pp. 87-102 .

Page, R., Plafker, G., and Pulpan, H., 1995. Block rotation in east-central Alaska: a framework for evaluating earthquake potential. Geology, Vol. 23, No. 7, pp.629-632 .

Panda, M.N., Zhang, M., Ogbe, D.O., Kamath, V.A. and Sharma, G.D., 1989. Reservoir Description of West Sak Sands Using Well Logs. SPE California Regional Meeting, Bakersfield, California, 5-7 April 1989.

Peichl, M., Thevathasan, N., Gordon, A. M., Huss, J. and Abohassan, R. A. 2006. Carbon sequestration potentials in temperate tree-based intercropping systems, southern Ontario, Canada. *Agroforestry Systems*, 66, 243-257.

Peng, D.Y. and Robinson, D.B., 1976. A New Two-Constant Equation of State. Industrial & Engineering Chemistry Fundamentals, 15(1): 59-64.

Potas, T.A., Anderson, C.M., and Malterer, T.J. 1989. Continuous Production of Deep-Cleaned Low-Rank Coal. Proceedings of the 14th International Conference on Coal and Slurry Technology, Clearwater, FL, April 24–27.

Ranz, W. E., and Wong J. B. 1952. Impaction of dust and smoke particles on surface and body collectors. *J. Ind. Eng. Chem*., 44: 1371–1381.

Rao, P.D. and Walsh, D.E. 1991. Characterization of Coal Properties from High Temperature Processing of Usibelli Low Rank Coal. MIRL report No.92.

Rao, P.D., Walsh, D.E., and Willson, W. 1999. Ash characterization for two Alaskan low-rank coals. Coal Preparation, 20, 161–178.

Rasmussen, P. and L.B. Pedersen, 1979. End correction in potential field modeling. Geophys. Prospecting, 27: 749-760.

Rastgoftar, H., Imen, S., Madani, K., 2012. "Stochastic fuzzy assessment for managing hydro-environmental systems under uncertainty and ambiguity." World Environmental and Water Resources Congress, pp. 2884-2892, ASCE, Albuquerque, New Mexico, Edited by Loucks, E.D.

Ratchkovski, N.A., and Hansen, R.A. New constraints on tectonics of Interior Alaska: Earthquake locations, source mechanisms and stress regime. Bulletin of the Seismological Society of America. Vol. 92, No. 3, pp.998-1014.

Richle, J.R., Fleming, M.D., Moliniam B.F., Dover, J.H., Keley, J.S., Miller, M.L., Nokleberg, W.J., Plafker, G., and Till, A. B. 1997. Digital-shaded relief image of Alaska: U.S. Geological Survey Miscellaneous Investigations Map I- 2585, Scale: 1:250,000.

Ridgway, K.D., Thoms, E.E., Layer, P.W., Lesh, M.E., White, J.M., and Smith, S.V., 2007. Neogene transpressional forland basin developement on the north side of the Central Alaska Range, Usibelli Group and Nenana Gravel, Tanana Basin, Geological Society of America, Special Paper 431.

Ridgway, K.D., Trop, J.M., Knollenberg, W.J., Davidson, C.M., and Eastham, K.R. 2002. Mesozoic and Cenozoic tectonics of the eastern and central Alaska Range: Progressive basin development and deformation in a suture zone. GSA Bulletin 114(12): 1480–1504.

Rizzo, A., J. and Hanks C., L. 2012. Fracture character and distribution in the Nenana Basin, Alaska. AGU Fall Meeting 2012, T31A-2573.

Ryan, B., and Richardson, D. 2004. The potential for CO_2 sequestration in British Columbia coal seams. Resource Development and Geoscience Branch, B.C. Ministry of Energy and Mines.

Rytter, L. and Stener, L. G. 2005. Productivity and thinning effects in hybrid aspen (Populus tremula L. x P. tremuloides Michx.) stands in southern Sweden. *Forestry*, 78, 285-295.

Schmitt, C.G., and Arnott W.P 1999. Infrared emission (500-2000 cm-1) of laboratory ice clouds. *J. Quant. Spec. Rad. Trans.*, 63: 701-725.

Schmitt, C. G., and Heymsfield A. J. 2009. The size distribution and mass-weighted terminal velocity of low-latitude cirrus crystal populations. *J. Atmos. Sci*., 66: 2013-2028.

Schmitt, C. G., and Heymsfield A. J. 2010. Dimensional characteristics of ice crystal aggregates from fractal geometry. *J. Atmos. Sci*., 67: 1605-1616.

Schnabel, W. E., Munk, J., Abichou, T., Barnes, D., Lee, W. & Pape, B. 2012. Assessing the Performance of a Cold Region Evapotranspiration Landfill Cover Using Lysimetry and Electrical Resistivity Tomography. *International Journal of Phytoremediation*, 14, 61-75.

Schön, R., Schnaiter M., Ulanowski Z., Schmitt C., Benz S., Mohler O., Vogt S., Wagner R., and Schurath U. 2011. Particle Habit Imaging Using Incoherent Light: A First Step toward a Novel Instrument for Cloud Microphysics. *J. Atmos. Oceanic Technol.*, 28: 493–512

Scott, Antony, 2012. A Consideration of the Role of Commodity Prices In Project Solutions to Fairbanks' Energy Cost Problem; Final report prepared for the Fairbanks-North Star Borough. Unpublished.

Serio, M.A, Solomon, P.R., Heninger, S.G. 1986. Coal pyrolysis in high pressure entrained flow reactor. ACS Division of Fuel Chemistry, Preprints, Volume 31, Issue 3, 1986, Pages 210-221.

Shalikarian, L., Madani, K., Naeeni, S.T.O., 2011. "Finding the socially optimal solution for California's Sacramento-San Joaquin Delta Problem," Proceeding of the 2011 World Environmental and Water Resources Congress, pp. 3190-3197, ASCE, Palm Springs, California, Edited by: Beighley II R.E. and Kilgore, M.W.

Sharma, G., 1990. Development of Effective Gas Solvents Including Carbon Dioxide for the Improved Recovery of West Sak Oil, University of Alaska Fairbanks, Fairbanks, AK.

Sheikhmohammady, M., Madani, K., Moradi, M., Behmanesh, I., 2011. "Finding the best legal governanace regime for the Caspian Sea through Multi-Criteria Decision-Making methods," Proceeding of the 2011 IEEE International Conference on Systems, Man., And

Cybernetics (SMC), pp. 3029-3034, IEEE, Anchorage, Alaska.

Sheikhmohammady, M. & Madani, K., 2008. "Sharing a multi-national resource through bankruptcy procedures," Proceeding of the 2008 World Environmental and Water Resources Congress, Honolulu, Hawaii, ASCE, Edited by: Babcock R.W. and Walton R..

Shelton, J.L. and Yarborough, L., 1977. Multiple Phase Behavior in Porous Media During CO2 or Rich-Gas Flooding. Journal of Petroleum Technology, 29(9): 1171-1178.

Simon, R. and Graue, D.J., 1965. Generalized Correlations for Predicting Solubility, Swelling and Viscosity Behavior of CO2 -Crude Oil Systems. Journal of Petroleum Technology, 17(1): 102-106.

Stanley, Richard G., Ronald R. Charpentier, Troy A. Cook, David W. Houseknecht, Timothy R. Klett, Kristen A. Lewis, Paul G. Lillis, Philip H. Nelson, Jeffrey D. Phillips, Richard M. Pollastro, Christopher J. Potter, William A. Rouse, Richard W. Saltus, Christopher J. Schenk, Anjana K. Shah, and Zenon C. Valin. 2011. Assessment of Undiscovered Oil and Gas Resources of the Cook Inlet Region, South-Central Alaska, 2011. *National Assessment of Oil and Gas Fact Sheet*. Available at: http://pubs.usgs.gov/fs/2011/3068/

State of Alaska, 2010. Alaska Stand Alone Gas Pipeline Project Update and FY 2010 Deliverables; submitted to Alaska Gasline Development Corporation. Available at: www.legis.state.ak.us

State of Alaska, 2009. Stand Alone Gas Pipeline Route Alternatives Analysis. Prepared by Michael Baker Jr., Inc. with support from ASRC Energy Services and Northern Economics, Inc. for the In-State Gas Program by the Office of the Governor.

State of Alaska, 2008. Findings and Determination by the Commissioners of Natural Resources and Revenue for Issuance of a License under the Alaska Gasline Inducement Act. Currently found at: http://gasline.alaska.gov/Findings/findings.html

Steel, K.M., and Patrick, J.W. 2001. The production of ultra-clean coal by chemical demineralization. Fuel, 80, 2019–2023.

Steckler, M.S., and Watts, A. B. Subsidence of Atlantic type continental margin off New York. Earth and Planetary Science letters, Vol. 41, pp. 1-13

Straka, J. 2009. *Cloud and Precipitation Microphysics: principles and parameterization*, Cambridge University Press, pp. 406

Suuberg, E., Peters, W. and Howard, J. 1978. Product Composition and Kinetics of Lignite Pyrolysis. Industrial & Engineering Chemistry Process Design and Development 17, no. 1: 37-46.

Tahvanainen, L. 1996. Allometric relationships to estimate above-ground dry-mass and height in

Salix. *Scandinavian Journal of Forest Research*, 11, 233-241.

Takahashi, T., and Fukuta N. 1988. Ice crystal replication with common plastic solutions, *J. Atmos. Ocean. Tech.,* 5: 129-15.

Talwani, M.Worzel, J.L., and Landisman, M.1959. Rapid gravity computations for two dimensional bodies with application to Mendicino submarine fracture zone. Geophys. Res. 64, pp. 49-59

Tamon, H., Ogawa, Y., and Mukai, S.R. 2003. Adsorption characteristics of carbon dioxide and methane on coal; Coal and Safety, Japan Coal Energy Centre, v23, p44-49.

Targac, G.W., Redman, R.S., Davis, E.R. et al., 2005. Unlocking the Value in West Sak Heavy Oil. SPE/PS-CIM/CHOA International Thermal Operations and Heavy Oil Symposium, Calgary, Alberta, Canada, 1-3 November 2005.

Terazono, Emiko, 2012. Japan's LNG in crucial pricing shift. *Financial Times*. December 18, 2012.

Tomsich, C.S., Hanks, C.L., McCarthy, P.J . and Coakley, B.J., 2012, Geologic Co2 Sequestration Potential Of Tertiary Coal Basins In Interior Alaska: *in* Hanks, C. and Holdmann, G. (Eds.). 2012. CO_2 sequestration options and other environmental issues related to the proposed coal-to-liquids facility at Eielson Air Force Base: Phase 2. Prepared for the U.S. Air Force by the Geophysical Institute and the Alaska Center for Energy and Power, University of Alaska Fairbanks, 207 pp.

Thompson, G., Rasmussen R. M., and Manning K. 2004. Explicit forecasts of winter precipitation using an improved bulk microphysics scheme. Part I: Description and sensitivity analysis, *Mon. Wea. Rev.*, *132*(2): 519-542.

Thompson, G., Field P. R., Rasmussen R. M., and Hall W. D. 2008. Explicit Forecasts of Winter Precipitation Using an Improved Bulk Microphysics Scheme. Part II: Implementation of a New Snow Parameterization, *Mon. Wea. Rev.*, *136*(12): 5095-5115.

Thuman, W. C., and Robinson E. 1954. Studies of Alaskan ice-fog particles, *J. Meteor.,* 11: 151-156.

Telenius, B. F. 1999. Stand growth of deciduous pioneer tree species on fertile agricultural land in southern Sweden. *Biomass and Bioenergy*, 16, 13-23.

TransCanada Alaska Company, 2011a. Alaska Pipeline Project - Water Use and Quality. Fairbanks: TransCanada.

TransCanada Alaska Company, 2011b. Alaska Pipeline Project Draft Resource Report 1 - Rev 0 . Fairbanks: TransCanada.

Trop, J., and Ridgway, K. 2007. Mesozoic and Cenozoic tectonic growth of southern Alaska: a sedimentary basin perspective. The Geological Society of America, Special Paper 43, pp.55-86 .

Truax, B., Gagnon, D., Fortier, J. and Lambert, F. 2012. Yield in 8 year-old hybrid poplar plantations on abandoned farmland along climatic and soil fertility gradients. *Forest Ecology and Management*, 267, 228-239.

Turek, E.A., Metcalfs, R.S., Yarborough, L. and Robinson Jr., R.L., 1984. Phase Equilibria in CO2 - Multicomponent Hydrocarbon Systems: Experimental Data and an Improved Prediction Technique. Society of Petroleum Engineers Journal, 24(3): 308-324.

Twu, C.H., 1984. An Internally Consistent Correlation for Predicting the Critical Properties and Molecular Weights of Petroleum and Coal-Tar Liquids. Fluid Phase Equilibria, 16(2): 137-150.

US Department of Energy, 2007a. Conceptual Engineering / Socioeconomic Impact Study – Alaska Spur Pipeline. DOE-NETL Contract Number: DE-AM26-05NT42653. Available at: http://www.netl.doe.gov/technologies/oil-gas/NaturalGas/Projects_n/TDS/TD/T%26D_42653AlaskaSpur.html

US Department of Energy, 2007b. Alaska Coal Gasification Feasibility Studies– Healy Coal-to-Liquids Plant. DOE/NETL-2007/1251. Available at: http://www.netl.doe.gov/technologies/coalpower/gasification/pubs/pdf/FINAL-Healy%20FT%201251%2007062007.pdf

Wahrhaftig, Clyde, 1987, The Cenozoic section at Suntrana, Alaska, *in* Hill, M.L., ed., Cordilleran section of the Geological Society of America: Boulder, Colo., Geological Society of America, Centennial Field Guide, v. 1, p. 445–450.

Wahrhaftig, Clyde, Bartsch-Winkler, Susan, and Stricker, G.D., 1994, Coal in Alaska, *in* Plafker, George, and Berg, H.C., eds., The geology of Alaska: Geological Society of America, The geology of North America, v. G–1, p. 937–978.

Wahrhaftig, Clyde, and Hickcox, C.A., 1955, Geology and coal deposits, Jarvis Creek coal field, Alaska: U.S. Geological Survey Bulletin 989–G, p. 353–367, plates 10–12.

Wallenius, J., Dyer, J. S., Fishburn, P. C., Steuer, R. E., Zionts, S., & Deb, K., 2008. Multiple criteria decision making, multiattribute utility theory: recent accomplishmanets and what lies ahead. *Management Science*, 1336-49.

Wang, G.C. and Locke, D.C., 1980. A Laboratory Study of the Effects of CO2 Injection Sequence on Tertiary Oil Recovery. Society of Petroleum Engineers Journal, 20(4): 278-280.

Wang, X. and Strycker, A., 2000. Evaluation of CO2 Injection with Three Hydrocarbon Phases.

International Oil and Gas Conference and Exhibition in China, Beijing, China, 7-10 November 2000.

Wen, H.C, and Onozaki, M. 1982. User's Manual for Computer Simulation and Design of the Moving-Bed Coal Gasifier. Final Report. DOE/MC/16474-1390, 1982.

Wendler, G. 1969. Heat balance studies during an ice-fog period in Fairbanks, Alaska, *Mon. Weather Rev.*, 97: 512-520.

Werner, M., 1987. Tertiary and Upper Cretaceous Heavy Oil Sands, Kuparuk River Unit Area, Alaskan North Slope. Exploration for Heavy Crude Oil and Natural Bitumen: American Association of Petroleum Geologists Studies in Geology(25): 537-548.

WHPacific, 2012, Alaska Energy Authority End Use Study: 2012: http://www.akenergyauthority.org/PDF%20files/EndUseStudy2012/AlaskaEndUseStudy2012.pdf

Won, I. J. and Bevis, M. 1987. Computing the gravitational and magnetic anomalies due to a polygon: Algorithms and Fortran subroutines, Geophysics, 52, pp. 232–238.

Wood, G.H., Kehn, T. M., Carter,M.D., and Culbertson,W.C. 1983.*Coal Resource Classification System of the U.S. Geological Survey.*U.S. Geological Survey Circular 891, Washington D.C.: U.S. Department of the Interior; 65 pp.

Wood Mackenzie, 2011. Alaskan LNG Exports Competitiveness Study. Alaska Gasline Port Authority (AGPA). July 27, 2011. Currently available at: http://www.allalaskagasline.com/featuredarticlesanddocuments/

Yan, W. and Stenby, E.H., 2009. The Influence of CO2 Solubility in Brine on CO2 Flooding Simulation. SPE Annual Technical Conference and Exhibition, New Orleans, Louisiana, 4-7 October 2009.

Yarie, J., Kane, E., and Mack, M. 2007. Aboveground biomass equations for the trees of interior Alaska. AFES Bulletin 115. University of Alaska Fairbanks Agricultural and Forestry Experiment Station. URL: http://www.lter.uaf.edu/pdf/1271_Yarie_Kane_2007.pdf.

Yarie, J. and Mead, B. R. 1988. Twig and foliar biomass estimation equations for major plant species in the Tanana River basin of interior Alaska. Res. Prp. PNW-RP-401. U.S. Department of Agriculture, Forest Service: Pacific Northwest Research Station.

Zianis, D. and Mencuccini, M. 2004. On simplifying allometric analyses of forest biomass. *Forest Ecology and Management*, 187, 311-332.

PUBLICATIONS RESULTING FROM THIS STUDY

Aghbash, V.N. and Ahmadi, M., 2012, Evaluation of CO2-EOR and Sequestration in Alaska West Sak Reservoir Using Four-Phase Simulation Model: SPE Western Regional Meeting, 21-23 March 2012, Bakersfield, California, USA, paper 153920.

Dixit, N., Hanks, C., and Tomsich, C., 2012, Tectonic evolution and subsidence history of the Nenana Basin, Interior Alaska: Preliminary results from seismic-reflection, electric logs and gravity data: 2012 AGU Fall meeting.

Kim, Chang Ki, Stuefer, Martin, and Schmitt, Carl, in review, Improved ice microphysics for numerical studies of ice fog using the Weather Research and Forecasting (WRF) model: Submitted to Journal of Geophysical Research

Kim, Chang Ki, Stuefer, Martin and Schmitt, Carl G., 2012, Improved ice microphysics for numerical studies of ice fog using the Weather Research and Forecasting (WRF) model: 2012 annual meeting of the American Geophysical Union.

Kulkarni, Mandar and Ganguli, Rajive, 2012, Gasification of Alaska Coal," Alaska Miners Association Biennial Conference, March 2012, Fairbanks.

Kulkarni, Mandar and Ganguli, Rajive, 2012, Moving Bed Gasification of Low Rank Alaska Coal: Journal of Combustion, vol. 2012, Article ID 918754, 8 pages, 2012. doi:10.1155/2012/918754

Read L., Mokhtari S., Madani K., Hanks C. L., Maimoun M., 2012, "A Stochastic Multi-Criteria Analysis of Energy Options for Fairbanks, Alaska", American Geophysical Union (AGU) Annual Meeting 2012, San Francisco, California.

Read L., Mokhtari S., Madani K., Maimoun M., Hanks C. L., in press, A Multi-Participant Multi-Criteria Analysis of Energy Supply Sources for Fairbanks, Alaska", American Society of Civil Engineers 2013 World Environmental and Water Resources Congress

Read L., Mokhtari S., Madani K., Hanks C. L., (in press), "A Stochastic Multi-Criteria Multi-Decision Maker Analysis of Energy Resources of Fairbanks, Alaska".

Rizzo, A., Hanks, C., 2012, Fracture character and distribution in the Nenana basin, Alaska: 2012 AGU Fall meeting

Schmitt, Carl G., Stuefer, Martin, Heymsfield, Andy, and Kim, Chang Ki, in review, New measurements of the microphysical properties of ice fog particles: Submitted to Journal of Geophysical Research

Schnabel, W., J. Munk, D. Barnes, and W. Lee (2012). "Four-year performance evaluation of a pilot-scale evapotranspiration landfill cover in Southcentral

Alaska." Cold Region Science and Technology, DOI: 10.1016/j.coldregions.2012.03.009

Tomsich, C. S., Hanks, C. L., Coakley, B. J., 2011, Basement Depth and Stratigraphic Thickness Solutions from Modeled Gravity Data for the Tanana and Nenana Basins and Implications for CO2 Sequestration: in Program with Abstracts 2011 joint AAPG Pacific Section/SPE Western Regional meetings, Anchorage, Alaska.

Umekwe, P., Mongrain, J., Ahmadi, M., and Hanks, C., 2012, An assessment of the CO2 sequestration capacity of Alaska's North Slope: Natural Resources Research, 14 pp.

Theses/Dissertations supported by this project

Aghbash, V.N., 2013,

Byrd, A., 2013, In Progress, Biomass Production And Carbon Sequestration Of Short Rotation Coppice Crops In Alaska: M.S. thesis, University of Alaska Fairbanks.

Dixit, N., in progress, CO2 sequestration potential of the Nenana basin: Ph.D. dissertation, University of Alaska Fairbanks.

Kulkarni, Mandar, 2012, Potential Application Of Alaskan Coal Gasification Technology To Produce Synthetic Fuels For The Interior ", Ms (Petroleum Engineering) Project Report, University Of Alaska Fairbanks.

King, E.,

Mokhtari, S., in progress, Decision Making under Uncertainty: A New Framework for Analyzing Probabilistic Dominance in Multi-Criteria Multi-Decision Maker Problems", Ph.D. in Civil Engineering, University of Central Florida (Expected Graduation: Fall 2013).

Mokhtari, S., in progress, "Developing a Group Decision Support System (GDSS) for Decision Making under Uncertainty", M.Sc. Water Resources Engineering, University of Central Florida (Expected Graduation: Spring 2013).

Read, L., in progress,

Rizzo, A., in progress, Fracture character and distribution in the Nenana basin, Alaska. M.S. thesis, University of Alaska Fairbanks.

Umekwe, P., 2011, Assessment of CO_2 sequestration potential through enhanced oil recovery in oil fields on the North Slope of Alaska: M.S. thesis, University of Alaska Fairbanks.

APPENDIX A: PROJECT COST SOURCES

12" Fit-for-purpose pipeline
Project capital costs were taken from FPC (2010a, 2010b). In addition, the Fairbanks Pipeline Company provided numerous emails and interviews to clarify their numbers and approach. They also provided updated cost estimates for the pipeline since their project materials were first published.

ASAP Bullet Line Projects
We relied on published work by entities of the state that have been conducting initial development work on various configurations of the project (AGDC, 2011a; AGDC, 2011b; State of Alaska, 2010.) In addition, AGDC kindly provided source data generated by Energy Project Consultants that underlies results generated within the 2010 Project Update. AGDC also generously provided data on assumed heat content and fuel use data for the project described in their 2011 Project Plan.

Beluga to Fairbanks Project
We relied upon previous work by the US Department of Energy (US DOE, 2007a) and the State of Alaska (State of Alaska, 2009; ANGDA, 2009; AGDC, 2011a). The US DOE and AGDC were particularly important.

Coal to Liquids
Input data were taken from Hatch (2008).

Fairbanks LNG trucking
For this project we relied substantially on personal communications of cost inputs with Jim Dodson of the Fairbanks Economic Development Coporation, and Steve Haagenson, formally chairman of the Alaska Energy Authority. They shared an excel spreadsheet model, which was a particularly good source for inputs. To our knowledge this model has not yet been published.

HVDC
Although public presentations were the starting point, these lacked requisite detail for our modeling purposes. Accordingly, we worked directly with Robert Jacobsen, who is with Marsh Creek, LLC and kindly provided the inputs shown in Appendix B.

Local Distribution System (LDC)
The LDC would be required for all projects bringing gas to Fairbanks. Project capital costs and schedule were estimated using inputs provided by Northern Economics (2012). Operating expenses for the system as a whole were estimated from ENSTAR operating statistics, as adjusted by the smaller Fairbanks system size, taken from ENSTAR's most recent rate case as filed with the RCA.

Major Gas Sale
All input data was taken and adapted from the Commissioners' Findings and Determinatino in Support of Award of a License Under the Alaska Gasline Inducement Act (State of Alaska,

2008). We particularly relied upon Appendix F, Part II which consists in Technical contractor reports.

Susitna Watana Dam Project

We relied on project documents prepared for the Alaska Energy Authority (AEA, 2009; AEA, 2010) as well as more recent cost and billing determinant updates (AEA, 2012). We benefited from conversations with AEA's technical staff, Nick Szymoniak.

APPENDIX B: COST INPUTS

	Development Duration	Execution Duration	Development Spend	Spend Execution	Operating Expense per year		Economic Life
	(Months)	**(Months)**	**2012$ MM**	**2012$ MM**	**2012$ MM**	**(% plant)**	**Years**
Fairbanks LDC Phase 1	18	18	11.55	219.28		6.0%	30
Fairbanks LDC Phase 2	15	18	8.50	164.71		6.0%	30
Pipeline – 12-inch Fairbanks Lateral, Straddle, offtake	45	39	14.05	269.57	5.18	5.4%	25
ASAP 250 MMcf/d, GTP	45	39	64.65	1228.33	42.29		25
ASAP 250 MMcf/d, PL to Dunbar	45	39	139.19	2644.58	38.59		25
ASAP 250 MMcf/d, PL Dunbar to CI	45	39	89.65	1703.39	24.85		25
ASAP 250 MMcf/d, CI NGL extraction	45	39	5.83	409.81	9.52		25
ASAP 500 MMcf/d, GTP	45	39	96.80	1839.14	65.56		25
ASAP 500 MMcf/d, PL to Dunbar	45	39	155.19	2948.56	43.09		25
ASAP 500 MMcf/d, PL Dunbar to CI	45	39	99.96	1899.18	27.75		25
ASAP 500 MMcf/d, CI NGL extraction	45	39	21.57	409.81	26.43		25
ASAP 1,000 MMcf/d, GTP	45	39	149.04	2831.82	101.50		25
ASAP 1,000 MMcf/d, PL to Dunbar	45	39	219.34	4167.40	63.02		25
ASAP 1,000 MMcf/d, PL Dunbar to CI	45	39	141.28	2684.24	40.59		25
ASAP 1,000 MMcf/d, CI NGL extraction	45	39	36.49	409.81	46.52		25
Beluga to Fairbanks	24	43	89.43	1699.12		1.5%	25
Energy Curia - Case 1, 12"	36	32	175.43	614.56	3.82		25
Energy Curia - Case 2A, 18", ANS to FBX	36	32	175.43	1244.57	6.99		25
Energy Curia - Case 2A, 18", FBX to CI	36	32	175.43	1334.57	11.86		25
LNG liquifaction (on ANS)	18	22	19.08	381.66	12.59		25
LNG storage, regas and "other plant" (in FBX)	10	19	8.50	354.01	4.00		25
CTL	43	42	402.69	8053.89	662.01		30
MGS to LNG - GTP	77	60	125.45	9873.64	124.74		25
MGS to LNG - AK pipeline to Delta	77	60	184.34	9632.82	29.58		25
MGS to LNG - AK pipeline Delta to Valdez	77	60	102.41	5298.05	16.27		25
MGS to LNG - Liquifaction	77	60	358.43	27092.30	210.03		25
Susitna-Watana (low case)	78	80	367.61	4395.39	16.87		30
HVDC Fairbanks Heat and Power – turbines	40	30	274.62	1450.80	225.16		25
HVDC Fairbanks Heat and Power – lines & transformer	40	30	295.98	1563.60	578.00		25

APPENDIX C: ABBREVIATIONS

AEA	Alaska Energy Authority.
AGDC	Alaska Gasline Development Corporation. Created by the Legislature to pursue an in-state "bullet line" from the ANS to tidewater, with capacity at or under 500MMcf/d.
ASAP	Alaska Stand Alone Project.
AGIA	Alaska Gasline Inducement Act. The provisions of this Act are contained in Alaska Statute 43.90
ANGDA	Alaska Natural Gas Development Authority
ANS	Alaska North Slope
ANS WC	Alaska North Slope, West Coast. Refers to crude oil sold on the West Coast of the United States that is produced on the ANS.
Bbl	Barrel (of oil). Typically 42 gallons.
Bcf	Billion Cubic Feet (of natural gas).
Btu	British Thermal Unit.
CCHRC	Cold Climate Housing Research Center.
CIF	Cash, Insurance and Freight. Refers to LNG cargoes where seller has responsibility to delivery to the buyer, generally at a regasification facility
CPI-U	Consumer Price Index, all urban customers. Inflation index maintained and published by the US Bureau of Labor Statistics.
CTL	Coal to liquids. A technology for converting coal to liquid petroleum products.
DNR	Alaska Department of Natural Resources
DOR	Alaska Department of Revenue
FERC	The Federal Energy Regulatory Commission. In this context the FEC regulates rates on interstate pipelines under the Natural Gas Act.

FPC	Fairbanks Pipeline Company. Launched by Energia Cura, a Fairbanks private company, the FPC would build and operate a fit-for-purpose pipeline from the ANS to Fairbanks.
GDPIP	Gross Domestic Price Implicit Price deflator. An index of price inflation that is developed with reference to total economic growth.
GVEA	Golden Valley Electric Association. The electric utility that provides electricity service in Fairbanks.
LDC	Local distribution company. LDC's distribute gas to end users through a network of small-diameter pipelines.
LNG	Liquefied Natural Gas
MBtu	Thousand Btu
Mcf	Thousand Cubic Feet (of natural gas)
MMcf	Million Cubic Feet (of natural gas)
MMBtu	Million Btu
MGS	Major gas sale. Typically understood to be a gas sale off the North Slope of at least 2 Bcf/d.
NGL	Natural Gas Liquids. Hydrocarbons in liquid form at atmospheric pressure, and generally include ethane, propane, butanes, and pentanes.
NPV	Net Present Value. "NPV5" means the NPV calculated using a 5 percent discount rate.
PBU	Prudhoe Bay Unit
US DOE	United State Department of Energy
RCA	Regulatory Commission of Alaska, charged with carrying out requirements of Alaska's Pipeline and Utility Acts (AS 42.06 and AS 42.05, respectively), which generally require pipeline and gas utility rates to be "just and reasonable".
UCCI	Upstream Construction Cost Index. Developed and published by consulting firms IHS and Cambridge Energy Research Associates.